AD_____

Award Number: DAMD17-99-1-9553

TITLE: Mechanisms of Neuronal Apoptosis In Vivo

PRINCIPAL INVESTIGATOR: Lee J. Martin, Ph.D.

CONTRACTING ORGANIZATION: The Johns Hopkins University
                          Baltimore, Maryland 21205

REPORT DATE: July 2000

TYPE OF REPORT: Annual

PREPARED FOR: U.S. Army Medical Research and Materiel Command
               Fort Detrick, Maryland 21702-5012

DISTRIBUTION STATEMENT: Approved for public release;
                        Distribution unlimited

The views, opinions and/or findings contained in this report are
those of the author(s) and should not be construed as an official
Department of the Army position, policy or decision unless so
designated by other documentation.

20001019 103

REPORT DOCUMENTATION PAGE

OMB No. 074-0188

1. AGENCY USE ONLY (Leave blank)	2. REPORT DATE July 2000	3. REPORT TYPE AND DATES COVERED Annual (1 Jul 99 – 30 Jun 00)	

4. TITLE AND SUBTITLE
Mechanisms of Neuronal Apoptosis In Vivo

5. FUNDING NUMBERS
DAMD17-99-1-9553

6. AUTHOR(S)
Lee J. Martin, Ph.D.

7. PERFORMING ORGANIZATION NAME(S) AND ADDRESS(ES)
The Johns Hopkins University School of Medicine

Baltimore, Maryland 21205

E-MAIL: lmartin@jhmi.edu

8. PERFORMING ORGANIZATION REPORT NUMBER

9. SPONSORING / MONITORING AGENCY NAME(S) AND ADDRESS(ES)

U.S. Army Medical Research and Materiel Command
Fort Detrick, Maryland 21702-5012

10. SPONSORING / MONITORING AGENCY REPORT NUMBER

11. SUPPLEMENTARY NOTES
Report contains color graphics.

12a. DISTRIBUTION / AVAILABILITY STATEMENT
Approved for public release; distribution unlimited

12b. DISTRIBUTION CODE

13. ABSTRACT *(Maximum 200 Words)*

Understanding the mechanisms of neuronal apoptosis in the central nervous system (CNS) has broad significance for military personnel and civilians. Neuronal apoptosis can occur after exposure to neurotoxins, radiation, and viruses and as a result of seizure activity, trauma, limb amputation, and hypoxia-ischemia caused by cardiac arrest, stroke, and increased intracranial pressure. The goal of this research project is to identify mechanisms of neuronal apoptosis. During the first year of funding, we found that neuronal apoptosis in the adult CNS occurs in association with activation of the oncosuppressor protein p53 and caspase-3. Furthermore, we discovered that neuronal apoptosis in the CNS is mediated by both p53-dependent and p53-independent cell death pathways and requires the programmed cell death protein Bax. In the immature brain, neuronal apoptosis is preceded by elevated levels of the cell membrane death receptor Fas and Bax, abnormalities in mitochondria, and activation of caspase-8 and caspase-3. Thus, the *in vivo* mechanisms for neuronal apoptosis in the adult and immature CNS may be dissimilar. We also employed a new technique (single-cell gel electrophoresis) to study mechanisms of neuronal apoptosis. We identified oxidative stress-induced, DNA single-strand breaks as a possible early upstream signal for neuronal apoptosis.

14. SUBJECT TERMS

Apoptosis, neurodegeneration, mitochondria, oxidative stress, Alzheimer's disease, amyotrophic lateral sclerosis, brain trauma, cerebral ischemia

15. NUMBER OF PAGES
265

16. PRICE CODE

17. SECURITY CLASSIFICATION OF REPORT Unclassified	18. SECURITY CLASSIFICATION OF THIS PAGE Unclassified	19. SECURITY CLASSIFICATION OF ABSTRACT Unclassified	20. LIMITATION OF ABSTRACT Unlimited

FOREWORD

Opinions, interpretations, conclusions and recommendations are those of the author and are not necessarily endorsed by the U.S. Army.

N/A Where copyrighted material is quoted, permission has been obtained to use such material.

N/A Where material from documents designated for limited distribution is quoted, permission has been obtained to use the material.

N/A Citations of commercial organizations and trade names in this report do not constitute an official Department of Army endorsement or approval of the products or services of these organizations.

√ In conducting research using animals, the investigator(s) adhered to the "Guide for the Care and Use of Laboratory Animals," prepared by the Committee on Care and use of Laboratory Animals of the Institute of Laboratory Resources, national Research Council (NIH Publication No. 86-23, Revised 1985).

N/A For the protection of human subjects, the investigator(s) adhered to policies of applicable Federal Law 45 CFR 46.

N/A In conducting research utilizing recombinant DNA technology, the investigator(s) adhered to current guidelines promulgated by the National Institutes of Health.

N/A In the conduct of research utilizing recombinant DNA, the investigator(s) adhered to the NIH Guidelines for Research Involving Recombinant DNA Molecules.

N/A In the conduct of research involving hazardous organisms, the investigator(s) adhered to the CDC-NIH Guide for Biosafety in Microbiological and Biomedical Laboratories.

PI — Signature _____ Date 7/24/00

3

Table of Contents

5. INTRODUCTION

Neuronal degeneration causes many neurological disorders that effect humans. Chronic neurodegeneration occurs in Alzheimer's disease, amyotrophic lateral sclerosis, Huntington's disease, and Parkinson's disease. Trauma, hypoxia-ischemia (stroke and cardiac arrest), neurotoxins, radiation, and seizures cause acute neurodegeneration in the brain and spinal cord. Apoptosis, an organized form of cell death that is mediated by active, intrinsic mechanisms, is believed to participate in the pathogenesis of abnormal neuronal death in chronic and acute neurodegenerative disorders (Martin et al., 1998a,b; Martin et al., 2000a; Martin, 2000; Appendix). The purpose of the research supported by the USAMRMC is to understand the molecular regulation of neuronal apoptosis, because it is relevant not only to neurodegeneration in pathological conditions, but also to the pathobiology of cell death in general. By using animal models of experimental neuropathology and techniques in molecular and cell biology we are identifying the mechanisms of neuronal apoptosis within the mammalian central nervous system (CNS).

6. BODY

Hypothesis 1: Neuronal apoptosis in the mammalian CNS has molecular characteristics of programmed cell death (PCD).

Apoptosis is thought to be executed by PCD mechanisms involving the expression or activation of p53, Bax, and caspases (Martin et al., 1998a,b; Martin et al., 2000a; Appendix). The tumor-suppressor protein p53 commits to death cells that have sustained DNA damage from reactive oxygen species (ROS) and other genotoxic agents. Bax is a member of the *bcl-2* protooncogene family (Merry and Korsmeyer, 1997) that functions by forming channels in mitochondrial membranes (Antonsson et al., 1997). When active, these channels may allow the release of cytochrome c from mitochondria to the cytosol, thereby initiating a cascade that leads to caspase activation and cell death. Caspases are cysteine-containing, aspartate-specific proteases that exist as dormant proenzymes in healthy cells and are activated through regulated proteolysis.

These proteins function in the execution phase of apoptosis, with "initiator" caspases activating "effector" caspases which subsequently cleave a variety of proteins, thereby causing the molecular and structural changes of apoptosis.

We have developed and characterized an injury model of unequivocal neuronal apoptosis within the rodent brain. In this model, occipital cortex ablation reliably causes neuronal apoptosis in the dorsal lateral geniculate nucleus (LGN) of thalamus (Al-Abdulla et al., 1998; Al-Abdulla and Martin, 1998). Originally, this model was developed in rat, over the past year, we have adapted this lesion to the mouse brain. We used this model in rat and mice to test the hypothesis that cortical injury-induced apoptosis of neurons in the adult brain is controlled by p53 and Bax (Martin et al., submitted; Appendix). This work is summarized below.

Unilateral ablation of the occipital cortex in rat and mouse results in unequivocal neuronal apoptosis in the dorsal LGN at 6-7 days postlesion (Al-Abdulla et al., 1998; Al-Abdulla and Martin, 1998; Martin et al., submitted; Appendix). We tested the hypothesis that p53 and Bax regulate this retrograde neuronal apoptosis. We found using immunocytochemistry that p53 accumulates in the nucleus of neurons destined to undergo apoptosis. By immunoblotting, p53 levels increase (~150% of control) in the LGN by 5 days after occipital cortex ablation. In nuclear-enriched subcellular fractions, p53 is activated (~3-fold) in the ipsilateral LGN at 5 days postlesion, as shown by DNA binding assay. The levels of procaspase-3 increase at 4 days postlesion, and caspase-3 is activated prominently at 5 days postlesion. To identify if neuronal apoptosis in the adult brain is dependent on p53 and Bax, cortical ablations were done on genetically engineered mice. In $p53^{-/-}$ mice, the severity of neuronal apoptosis is significantly attenuated (~34%) compared to wildtype mice, and in $bax^{-/-}$ mice neuronal apoptosis in the dorsal LGN is completely blocked. From these experiments we conclude that: 1) neuronal apoptosis in the adult thalamus after cortical injury is PCD; 2) neuronal apoptosis in the adult CNS requires Bax, and 3) p53 modulates neuronal apoptosis in the adult brain, but apoptosis can occur independent of p53-mediated mechanisms (Martin et al., submitted; Appendix).

We extended this work to examine whether LGN neurons in adult and immature brain die similarly after cortical injury (Natale and Martin, in press, Neurosci Abstr; Appendix). We hypothesized that the process of neuronal apoptosis is accelerated in the immature brain compared to the adult brain. Occipital cortex lesions were made in C57BL6 mice at 10 days of age and 6-8 weeks of age. In 10-day-old mice, nuclear p53 accumulation and internucleosomal fragmentation of DNA coincided at 24 hours postlesion, and maximal neuronal apoptosis occurred at 36 hours postlesion. These findings contrast sharply with the progression of neuronal apoptosis in the adult brain. We conclude that neuronal PCD is induced more rapidly in the immature brain compared to adult brain (which occurs over 6-7 days), although p53-dependent mechanisms may participate in both the adult and newborn brain.

Apoptosis of thalamic neurons can occur in different CNS injury paradigms (Martin et al., 1998a). We determined if the mechanisms of neuronal apoptosis are similar in different types of CNS insults. We found that thalamic neuron apoptosis in the neonatal rat brain after hypoxia-ischemia is structurally identical to the apoptosis of thalamic neurons after occipital ablation (Northington et al., 2000; Appendix). Hypoxia-ischemia in the neonatal rat causes a large loss of cerebral cortex, and we speculated that this thalamic neuron apoptosis is caused by target deprivation, as in our occipital cortex lesion model (Northington et al., 2000). However, we found that the mechanisms of thalamic neuron apoptosis in our different models have some components that are different and some components that are common, although both are PCD. The apoptosis in thalamic neurons after hypoxia-ischemia in neonatal rat is associated with a rapid increase in the levels of the Fas death receptor and caspase-8 activation (Northington et al., submitted; Appendix). Concurrently, the levels of Bax in mitochondrial-enriched cell fractions increase. Increased levels of Fas death receptor and Bax and activation of caspase-8 in the thalamus precede the marked activation of caspase-3 and the occurrence of neuronal apoptosis. Thus, as in nonneural tissues, the mechanisms for neuronal apoptosis in different *in vivo* settings can differ in

upstream signals, but they converge on common downstream mechanisms (i.e., the participation

of Bax and caspase-3).

We believe that our models of neuronal death in the thalamus provide a structural,

biochemical, and molecular "gold standard" for induced neuronal apoptosis *in vivo* that occurs by

PCD mechanisms. These models allow us to define the structural, molecular, and genetic criteria

for neuronal apoptosis *in vivo*. Therefore, our experience with these models places our laboratory

in a unique position to address reliably and accurately the contribution of neuronal apoptosis to

neurodegeneration in other models of CNS injury. We studied cerebral hypoxia-ischemia because

we believe that the role of neuronal apoptosis after cerebral ischemia is not understood and is

highly controversial (Martin et al., 1998a,b) and needs to be clarified soon as possible in animals

models, before antiapoptotic therapies are introduced into human clinical trials (Schulz et al.,

1999).

The goal of these experiments was to identify the contribution of apoptosis to

neurodegeneration after cerebral ischemia and the possible molecular mechanisms. In models of

complete global ischemia in cat (Martin et al., 1998a,b) and incomplete global ischemia in dog

(Martin et al., 2000b; Appendix) the degeneration of neocortical pyramidal neurons, hippocampal

CA1 neurons, and cerebellar Purkinje neurons in adult brain is not consistent with apoptosis. In

piglets the degeneration of striatal neurons is categorically necrosis (Martin et al., 2000c;

Appendix). Our data demonstrate that the degeneration of selectively vulnerable neurons

following global ischemia is cellular necrosis rather than apoptosis or a hybrid of apoptosis and

necrosis (Martin et al., 2000b; Martin et al., 2000c; Appendix). This conclusion is consistent with

that of other groups (Deshpande et al., 1992; Colbourne et al., 1999).

In models of global ischemia, the degeneration of granule neurons in hippocampus and

cerebellum sharply contrasts with the degeneration of CA1 neurons and Purkinje neurons.

Granule neuron death after ischemia closely resembles apoptosis and is associated with an

upregulation of Bax (Martin et al., 2000b). Thus, granule neuron death provides an internal

standard for classical apoptosis to which CA1 pyramidal neuron and cerebellar Purkinje cell degeneration can be compared after ischemia to demonstrate that the death of these latter neurons is not apoptosis. This apoptosis of granule neurons may possibly explain the contradictory evidence for apoptosis in hippocampal pyramidal neurons found in homogenate-based biochemical experiments. Granule neuron death may be a direct consequence of the ischemia, or it may be secondary to necrotic degeneration of hippocampal pyramidal neurons and cerebellar Purkinje cells and thus is a form of target deprivation-induced apoptosis, similar to thalamic neuron death after cortical lesions (Martin et al., 1998a,b; Al-Abdulla et al., 1998; Martin et al., submitted). The targets of dentate granule neurons include hippocampal pyramidal neurons and the targets of cerebellar granule neurons are Purkinje cells. We conclude that neuronal death after global ischemia exists as at least two distinct, temporally overlapping forms in hippocampus and cerebellum: necrosis of pyramidal neurons and Purkinje cells and apoptosis of granule neurons (Martin et al., 2000b; Appendix).

Hypothesis 2: Mitochondria accumulate and release cytochrome c within neurons during apoptosis.

Mitochondria are thought to have important roles in apoptosis (Zamzami et al., 1996). Changes in mitochondrial morphology and membrane potential precede caspase-3 activation in *in vitro* model systems. Mitochondria also serve as generators of ROS that cause DNA damage and can trigger apoptosis through p53-dependent mechanisms. Furthermore, mitochondria serve as reservoirs for apoptotic protease activating factors such as cytochrome c. We have hypothesized that mitochondria accumulate in the cell bodies of neurons at an early stage during the progression of neuronal apoptosis.

We have shown that mitochondrial accumulation occurs early during the progression of thalamic neuron apoptosis (Northington et al., submitted; Appendix) and motor neuron apoptosis (Martin et al., 1999; Appendix). These mitochondria accumulate in a perinuclear location. We conclude that mitochondria redistribute in neurons early during apoptosis. Some groups claim

that in nonneuronal cell systems *in vitro* this redistribution is an active part of cell signaling mechanisms for apoptosis (Li et al., 1998). Although we have made similar observations in neurons, it is not yet clear whether this redistribution is part of the signaling mechanisms or a consequence of early events during neuronal apoptosis. One extension of Hypothesis 2 is that changes in mitochondrial trafficking are part of the signaling mechanisms for neuronal apoptosis (Al-Abdulla and Martin, 1998). A sustained accumulation of active mitochondria in the vicinity of the nucleus may provide a source of ROS or apoptotic protease activating factors. In future experiments we will evaluate the role of cytoskeletal motor proteins in neuronal apoptosis.

We have made major technical advances during the first year of this project. We have developed a quantitative method to measure cytochrome c release from mitochondria using immunogold electron microscopy. First, we identified by western blotting reliable antibody reagents for the detection of cytochrome c in brain (Martin et al., 2000c; Appendix). We then developed an immunostaining method for the detection of cytochrome c using 1-nm colloidal gold particles (Martin and Barksdale, unpublished observations; Appendix). With this method we can quantify simultaneously in neurons the number of mitochondria and the relative amount of cytochrome c at mitochondrial and cytoplasmic sites. We will use this technique determine whether cytochrome c is released from mitochondria during apoptosis of thalamic neurons.

Hypothesis 3: Neuronal apoptosis *in vivo* evolves in association with oxidative stress.

Oxidative stress is a potent signal for cell death. We are investigating the role of oxidative stress in the induction of neuronal cell death using several models of neurodegeneration. We found that oxidative stress occurs in injured neurons before the emergence of the apoptotic structure (Martin et al., 1999, Appendix).

A marker for oxidative damage is protein nitration. Protein nitration can be detected by the formation of nitrotyrosine. Nitrotyrosine is a maker of peroxynitrite-mediated oxidative damage to proteins. Peroxynitrite is formed by the combination of nitric oxide and superoxide.

Prominent nitrotyrosine formation is detected in motor neurons during the progression of apoptosis. This nitrotyrosine immunolabeling of neuronal cell bodies and axons of motor neurons is transient, occurring primarily at 4 to 7 days postlesion, before the onset of apoptosis (Martin et al., 1999; Appendix).

In axotomy paradigms, hydroxyl radical damage to DNA was detected immunocytochemically with two different antibodies to hydroxyl-deoxyguanosine (OhdG). Intense nuclear labeling occurs only in neurons undergoing apoptosis. The most prominent OHdG immunolabeling between lesioned and unlesioned sides of spinal cord (based on the intensity of immunoreactivity) occurs at 4 to 7 days after avulsion (Martin et al., 1999; Appendix).

Our work implicates the formation ROS and oxidative damage to nucleic acids and proteins during neuronal apoptosis in the adult CNS. Our experiments demonstrate, for the first time, the formation of hydroxyl radical-modified DNA and RNA as well as nitrotyrosine-modified proteins during the progression of neuronal apoptosis in an *in vivo* setting.

DNA damage can initiate apoptosis. ROS can directly damage genomic DNA and are involved in the pathogenesis of neuronal apoptosis in animal models and in patients with Alzheimer's disease, amyotrophic lateral sclerosis, Parkinson's disease, and Huntington's disease. DNA single-strand breaks (SSB) are a major form of early DNA damage caused by oxidative stress. We tested the hypothesis that DNA-SSB occur in adult motor neurons subjected to oxidative stress *in vitro* and axotomy *in vivo*. We used single-cell gel electrophoresis (comet assay) that detects mainly DNA-SSB under alkaline elution conditions. We developed and characterized a motor neuron enriched cell suspension from adult rat spinal cord ventral horns. This cell suspension is ~84% neurons (determined by immunophenotyping with the neuronal nuclear protein NeuN), ~86% of these neurons are motor neurons (determined by choline acetyltransferase immunoreactivity), and ~72% of these motor neurons are α-motor neurons with axons in the sciatic nerve (determined by retrograde tracing). The viability of adult motor neurons in suspension was ~61% after 12 hours incubation. Exposure of these cells to nitric oxide (NO)

donor sodium nitroprusside (SNP), H_2O_2, or SNP plus H_2O_2 induced very rapid DNA damage that was dose- and time-related, as represented by comet formation and cell loss. H_2O_2 at a nontoxic concentration potentates the toxicity of SNP. Different forms of ROS left different DNA damage fingerprints, indicating different target domains of chromatin and different severities of DNA damage. By applying the comet assay to an *in vivo* model of motor neuron apoptosis (unilateral sciatic nerve avulsion), we found that DNA-SSB accumulate very slowly in injured motor neurons *in vivo* and that the comet fingerprint is similar to that caused by NO toxicity (Liu and Martin, submitted; Appendix).

Oxidative stress can also destroy neurons through pathways causing neuronal necrosis. Therefore we evaluated the possible mechanisms of neuronal necrosis *in vivo* to compare with the mechanisms of neuronal apoptosis *in vivo*. This comparison provides valuable information on the mechanisms dictating neuronal cell death pathways. We believe this comparison will also aid in the validation and understanding of the concept of the neuronal cell death continuum that we have proposed (Portera-Cailliau et al., 1997a,b).

We found that neuronal necrosis induced by hypoxia-asphyxia in piglets evolves with oxidative stress and selective organelle damage (Martin et al., 2000c; Appendix). Necrosis of striatal neurons progresses over 3-24 hours, with ~80% of putaminal neurons dead by 24 hours after the insult. By agarose gel electrophoresis striatal DNA is digested randomly at 6-12 hours. By electron microscopy, damage to the Golgi apparatus and rough endoplasmic reticulum occurs at 3-12 hours, while most mitochondria appear intact until 12 hours. Mitochondria undergo an early suppression of activity, then a transient burst of activity at 6 hours after the insult, followed by mitochondrial failure (determined by cytochrome c oxidase assay). Cytochrome c is depleted at 6 hours after hypoxia-ischemia and thereafter. Damage to lysosomes occurs within 3-6 hours. By 3 hours recovery, glutathione levels are reduced, and peroxynitrite-mediated oxidative damage to membrane proteins, determined by immunoblots for nitrotyrosine, occurs at 3-12 hours. The Golgi apparatus and cytoskeleton are early targets for extensive tyrosine nitration.

Striatal neurons also sustained hydroxyl radical damage to DNA and RNA within 6 hours after hypoxia-ischemia. This work suggests that neuronal necrosis in the striatum after hypoxia-ischemia is caused by early glutathione depletion and oxidative stress between 3-6 hours recovery that promote damage to membrane and cytoskeletal proteins, DNA and RNA, as well as damage to most organelles.

The range in neuronal death phenotypes is likely to be influenced by many factors. For example, the mechanistic rate of evolving injury may influence the cell death cascade. Oxidative stress evolves slowly in target deprivation/axotomy, and the neurodegeneration is apoptosis caused by PCD mechanisms. In contrast, oxidative stress evolves acutely with hypoxia-ischemia injury, and the majority of neurodegeneration in selectively vulnerable regions is necrosis. Neuronal death may be mediated by common upstream mechanisms that differ mechanistically in the rate (days versus hours) and severity of cellular stress.

Hypothesis 4: Antioxidant and caspase inhibitor treatments prevent neuronal apoptosis *in vivo*.

We hypothesize that oxidative damage to DNA is an upstream signal for neuronal apoptosis *in vivo*. This hypothesis is supported by our earlier work and the experiments conducted during the first year of this project. For example, thalamic neurons (Al-Abdulla and Martin, 1998) and motor neurons (Martin et al., 1999, Appendix) sustain hydroxyl radical damage to DNA during apoptosis. Furthermore, using single-cell gel electrophoresis, we have identified recently that DNA single-strand breaks occur very early in the progression of neuronal apoptosis (Liu and Martin, in press, Neurosci Abstr; Liu and Martin, submitted, Appendix). This DNA damage found *in vivo* has the same fingerprint as the DNA damage caused by prooxidants (Liu and Martin, in press, Neurosci Abstr; Liu and Martin, submitted, Appendix). We therefore

believe that oxidative damage to DNA is an upstream signal in the mechanisms for neuronal apoptosis *in vivo*.

We performed experiments to evaluate whether Trolox attenuates neuronal apoptosis in rat thalamus after cortical injury. Trolox (6-hydroxy-2,5,7,8-tetramethylchroman-2-carboxylic acid) is a cell-permeable, water-soluble derivative of vitamin E with potent antioxidant properties. Trolox blocks oxidative stress-induced apoptosis in rat thymocytes (Forrest et al., 1994). Adult male rats received occipital cortex ablations and were treated daily with either Trolox (50 mg/kg, ip, n=10) or vehicle (ethanol/bicarbonate, ip, n=10) from the day of cortical injury to the day of sacrifice at 7 days postlesion. This dosage of Trolox was chosen because we have found that it is tolerated and provides modest protection against motor neuron apoptosis *in vivo* (Martin et al, unpublished observations). Trolox did not protect against thalamic neuron apoptosis (Appendix).

We also performed experiments to evaluate whether vitamin C (ascorbate) attenuates neuronal apoptosis in rat thalamus after cortical injury. Adult male rats were treated daily with either vitamin C (50 mg/kg, ip, n=10) or vehicle (saline, ip, n=10) seven days prior to occipital cortex damage, after which injections continued from the day of injury to the day of sacrifice at 7 days postlesion. Ascorbate did not provide significant protection from apoptosis in thalamus after cortical lesions (Appendix).

7. KEY RESEARCH ACCOMPLISHMENTS

- Neuronal apoptosis in the adult brain occurs by PCD mechanisms
- Neuronal apoptosis in the adult brain requires Bax
- Neuronal apoptosis in the adult brain occurs through both p53-dependent and p53-independent cell death pathways
- The progression of neuronal apoptosis in the immature brain is accelerated compared to the adult brain

- The mechanisms for neuronal apoptosis in different *in vivo* CNS injury paradigms can differ in upstream signals, but they can converge on common downstream mechanisms

- The degeneration of neurons that are selectively vulnerable to global cerebral hypoxia-ischemia is not classical apoptosis

- Neuronal death after cerebral ischemia exists as at least two distinct, temporally overlapping forms in distinct populations of neurons

- Mitochondria accumulate at perinuclear sites early during the progression of neuronal apoptosis

- It is technically feasible to measure cytochrome c release in neurons *in vivo*

- Oxidative stress occurs in injured neurons before the emergence of apoptosis

- We have employed a new technique (single-cell gel electrophoresis or comet assay) to detect very early DNA damage in neurons

- The formation of DNA single-strand breaks is an early upstream signal for neuronal apoptosis

- Neuronal death pathways (apoptosis versus necrosis) may be mediated by common upstream mechanisms that differ mechanistically in the rate (days versus hours) and severity of cellular stress

8. REPORTABLE OUTCOMES

Martin LJ, Kaiser A and Price AC (1999) Motor neuron degeneration after sciatic nerve avulsion in adult rat evolves with oxidative stress and is apoptosis. J Neurobiol 40:185-201.

Martin LJ, Price AC, Kaiser A, Shaikh AY and Liu Z (2000a) Mechanisms for neuronal degeneration in amyotrophic lateral sclerosis and in models of motor neuron death. Int J Mol Med 5: 3-13.

Martin LJ, Sieber FE and Traystman RJ (2000b) Apoptosis and necrosis occur in separate neuronal populations in hippocampus and cerebellum after ischemia and are associated with alterations in metabotropic glutamate receptor signaling pathways. J Cereb Blood Flow Metab 20: 153-167.

Martin LJ, Brambrink AM, Price AC, Kaiser A, Agnew DM, Ichord RN and Traystman RJ (2000c) Neuronal death in newborn striatum after hypoxia-ischemia is necrosis and evolves with oxidative stress. Neurobiol Disease 7:169-191.

Northington FJ, Ferriero DM, Graham EM, Traystman RJ and Martin LJ (2000) Early neurodegeneration after hypoxia-ischemia in neonatal rat is necrosis while delayed neuronal death is apoptosis, Neurobiol Disease, in press.

Liu Z-P and Martin LJ (2000) DNA single-strand breaks occur rapidly in motor neurons in vitro and in vivo after oxidative stress and axotomy. Neurosci Abstr, in press.

Lesuisse C and Martin LJ (2000) Neuronal maturity influences the progression of neuronal apoptosis induced by DNA damage. Neurosci Abstr, in press.

Al-Abdulla NA and Martin LJ (2000) Target-deprived lateral geniculate projection neurons in the adult rat undergo DNA damage and apoptosis while interneurons transiently atrophy. Neurosci Abstr, in press.

Natale JE and Martin LJ (2000) Ablation of occipital cortex in immature mouse brain induces p53 and neuronal apoptosis in the lateral geniculate nucleus. Neurosci Abstr, in press

Martin LJ, Kaiser A, Yu JW, Natale JE and Al-Abdulla NA: Injury-induced apoptosis of neurons in adult brain is mediated by p53-dependent and p53-independent pathways and requires Bax. Submitted for publication.

Liu Z and Martin LJ: DNA single-strand breaks occur rapidly in motor neurons after in vitro oxidative stress and in vivo axotomy as demonstrated by the comet assay. Submitted for publication.

Martin LJ (2000) Neurodegenerative disorders of the human brain and spinal cord. In: Encyclopedia of the Human Brain. VS Ramachandran (ed), Academic press, in press.

Northington FJ, Ferriero DM, Flock DL and Martin LJ: Delayed neurodegeneration in neonatal rat thalamus after hypoxia-ischemia is programmed cell death. Submitted for publication.

9. CONCLUSIONS

We have made progress in each of the four original hypotheses outlined in our proposal funded by the USAMRMC. During the first year of funding our major emphasis was on Hypothesis 1, addressing the questions of when neuronal apoptosis occurs after CNS injury and whether it has molecular characteristics of PCD.

We found that axotomy/target deprivation causes unequivocal neuronal apoptosis in the adult and immature CNS. The neuronal apoptosis induced by axotomy/target deprivation is PCD.

This neuronal PCD requires Bax and occurs through p53-dependent and p53-independent cell death pathways. Our work is the first demonstration that neuronal apoptosis in the adult CNS requires the death protein Bax. The upstream signal for the induction of neuronal apoptosis may be DNA damage. This DNA damage appears to be induced by oxidative stress. The oxidative damage to DNA occurs in the form of hydroxyl radical modification and DNA single-strand breaks.

Based on our experiments, we also introduced the concept that neuronal death mechanisms in the adult and immature CNS may be dissimilar, particularly in the timing of the death process and the upstream signals; however, neuronal apoptosis in the adult and immature CNS appear to share some common dowstream mechanisms (Bax and caspase-3).

This work has implications for the treatment of neurological disorders that involve neurodegeneration through apoptotic pathways. Thus, this work is relevant to Alzheimer's disease, amyotrophic lateral sclerosis, Huntington's disease, Parkinson's disease, and traumatic brain injury. The identification of downstream mechanisms (p53, Bax, caspases) and upstream mechamisms (DNA damage and Fas death receptor) provides direction and rationale for the future development of antiapoptotic therapies.

It is difficult to identify the mechanisms of neuronal apoptosis in *in vivo* model systems. The introduction of genetically altered mice into our research projects has allowed us the show that neuronal apoptposis in the brain is controlled or modulated by Bax and p53, respectively. We have also identified DNA damage early during the progression of neuronal apoptosis, and we believe this DNA damage may be a possible upstream signal in the mechanims of neuronal apoptosis. However, we need to better characterize the role and position of DNA damage in the signaling cascade of neuronal apoptosis. *In vitro* model systems of neuronal apoptosis will help us better address the mechanisms of DNA damage-induced neuronal apoptosis. We have recently developed an *in vitro* model system of DNA damage-induced neuronal apoptosis to further

understand the molecular mechanisms of neuronal apoptosis (Lesuisse and Martin, in press,

Neurosci Abstr; Appendix).

10. REFERENCES

Al-Abdulla NA, Portera-Cailliau C and Martin LJ (1998) Occipital cortex ablation in adult rat causes retrograde neuronal death in the lateral geniculate nucleus that resembles apoptosis. Neuroscience 86: 191-209.

Al-Abdulla NA and Martin LJ (1998) Apoptosis of retrogradely degenerating neurons occurs in association with the accumulation of perikaryal mitochondria and oxidative damage to the nucleus. Am J Pathol 153: 447-456.

Antonsson B, Conti F, Ciavatta A, Montessuit S, Lewis S, Martinou I, Bernasconi L, Bernard A, Mermod J-J, Mazzei G, Maundrell K, Gambale F, Sadoul R and Martinou J-C (1997) Inhibition of bax channel-forming activity by bcl-2. Science 277: 370-372.

Colbourne F Sutherland GR, Auer RN (1999) Electron microscopic evidence against apoptosis as the mechanism of neuronal death in global ischemia. J Neurosci 19: 4200-4210.

Deshpande J, Bergstedt K, Linden T, Kalimo H, Wieloch T (1992) Ultrastructural changes in the hippocampal CA1 region following transient cerebral ischemia: evidence against programmed cell death. Exp Brain Res 88: 91-105.

Forrest VJ, Kang YH, McClain DE, Robinson DH and Ramakrishnan N (1994) Oxidative stress-induced apoptosis prevented by Trolox. Free Radic Biol Med 16: 675-684.

Lesuisse C and Martin LJ (2000) Neuronal maturity influences the progression of neuronal apoptosis induced by DNA damage. Neurosci Abstr, in press.

Li H, Zhu H, Xu C-J and Yuan J (1998) Cleavage of Bid by caspase 8 mediates the mitochondrial damage in the Fas pathway of apoptosis. Cell 94: 491-501.

Liu Z-P and Martin LJ (2000) DNA single-strand breaks occur rapidly in motor neurons in vitro and in vivo after oxidative stress and axotomy. Neurosci Abstr, in press.

Martin LJ, Al-Abdulla NA, Brambrink AM, Kirsch JR, Sieber FE and Portera-Cailliau C (1998a) Neurodegeneration in excitotoxicity, global cerebral ischemia, and target deprivation: a perspective on the contributions of apoptosis and necrosis. Brain Res Bull 46: 281-309.

Martin LJ, Portera-Cailliau C, Ginsberg SD and Al-Abdulla NA (1998b) Animal models and degenerative disorders of the human brain. Lab Animal 27: 18-25.

Martin LJ, Kaiser A and Price AC (1999) Motor neuron degeneration after sciatic nerve avulsion in adult rat evolves with oxidative stress and is apoptosis. J Neurobiol 40:185-201.

Martin LJ, Price AC, Kaiser A, Shaikh AY and Liu Z (2000a) Mechanisms for neuronal degeneration in amyotrophic lateral sclerosis and in models of motor neuron death. Int J Mol Med 5: 3-13.

Martin LJ, Sieber FE and Traystman RJ (2000b) Apoptosis and necrosis occur in separate neuronal populations in hippocampus and cerebellum after ischemia and are associated with alterations in metabotropic glutamate receptor signaling pathways. J Cereb Blood Flow Metab 20: 153-167.

Martin LJ, Brambrink AM, Price AC, Kaiser A, Agnew DM, Ichord RN and Traystman RJ (2000c) Neuronal death in newborn striatum after hypoxia-ischemia is necrosis and evolves with oxidative stress. Neurobiol Disease 7:169-191.

Merry DE and Korsmeyer SJ (1997) Bcl-2 gene family in the nervous system. Ann Rev Neurosci 20: 245-267.

Northington FJ, Ferriero DM, Graham EM, Traystman RJ and Martin LJ (2000) Early neurodegeneration after hypoxia-ischemia in neonatal rat is necrosis while delayed neuronal death is apoptosis, Neurobiol Disease, in press.

Portera-Cailliau C, Price DL and Martin LJ (1997a) Excitotoxic neuronal death in the immature brain is an apoptosis-necrosis morphological continuum. J Comp Neurol 378: 70-87.

Portera-Cailliau C, Price DL and Martin LJ (1997b) Non-NMDA and NMDA receptor-mediated excitotoxic neuronal deaths in adult brain are morphologically distinct: further evidence for an apoptosis-necrosis continuum. J Comp Neurol 378: 88-104.

Schulz JB, Weller M and Moskowitz MA (1999) Caspases as treatment targets in stroke and neurodegenerative diseases. Ann Neurol 45: 421-429.

Zamzami N, Susin SA, Marchetti P, Hirsch T, Gómez-Monterrey I, Castedo M and Kroemer G (1996) Mitochondrial control of nuclear apoptosis. J Exp Med 183: 1533-1544.

11. APPENDIX

Figure 1: Localization of cytochrome c in neurons by immunogold electron microscopy. Black gold deposits (silver-intensified 1-nm gold particles) are sites of cytochrome c immunoreactivity. Many of these particles decorate mitochondria.

Figure 2: The antioxidant Trolox does not protect against neuronal apoptosis in the rat LGN after occipital cortex lesions. Values are mean ± standard deviation (n= 10 rats/group).

Figure 3: Ascorbate (vitamin C) does not protect against neuronal apoptosis in the rat LGN after occipital cortex lesions. Values are mean ± standard deviation (n= 10 rats/group).
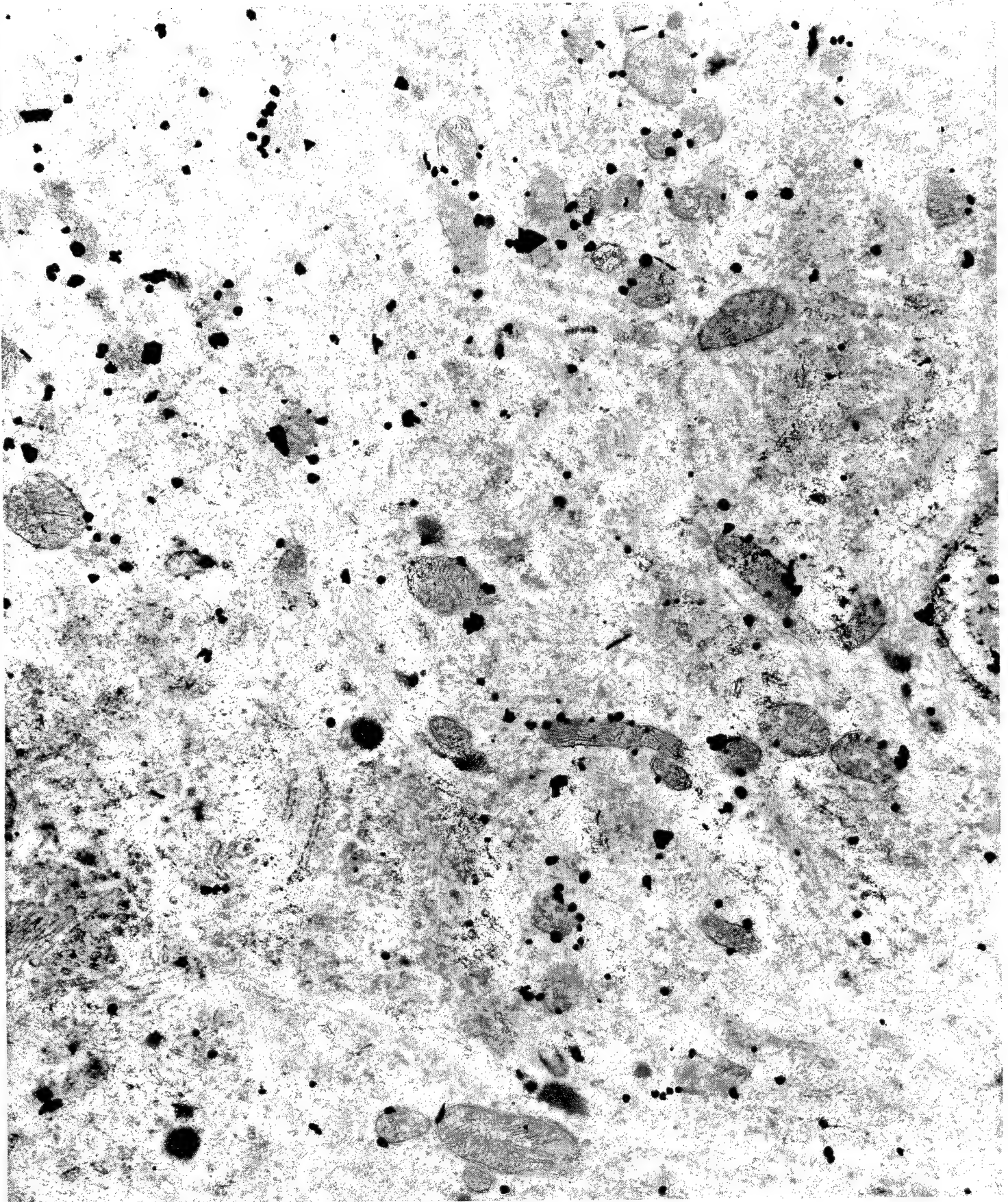
Figure 4: Identification of corticopetal projection neurons in the mouse LGN.

Figure 5: Occiptial cortex ablation in 10-day-old mice causes corticopetal projection neurons in the LGN to undergo apoptosis.
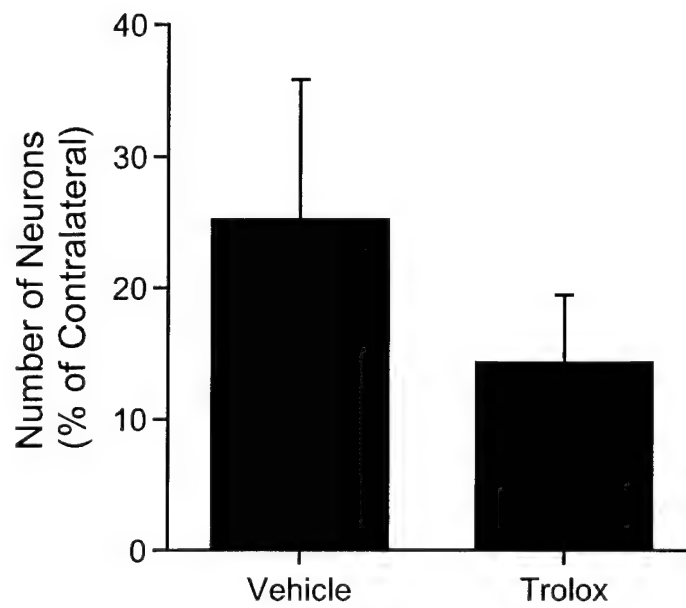
Figure 6: Internucleosomal fragmentation of DNA is detected in the ipsilateral LGN in mouse brain after occipital cortex ablation.

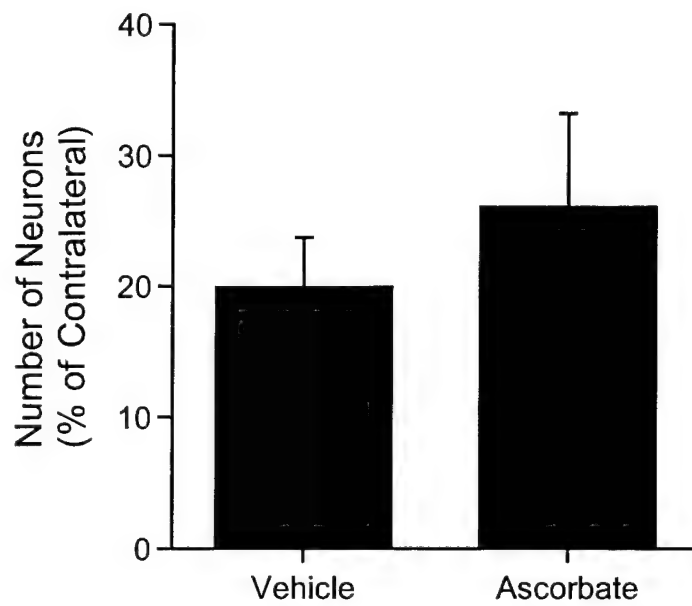**Figure 7:** Progression of neuronal apoptosis in the mouse LGN.

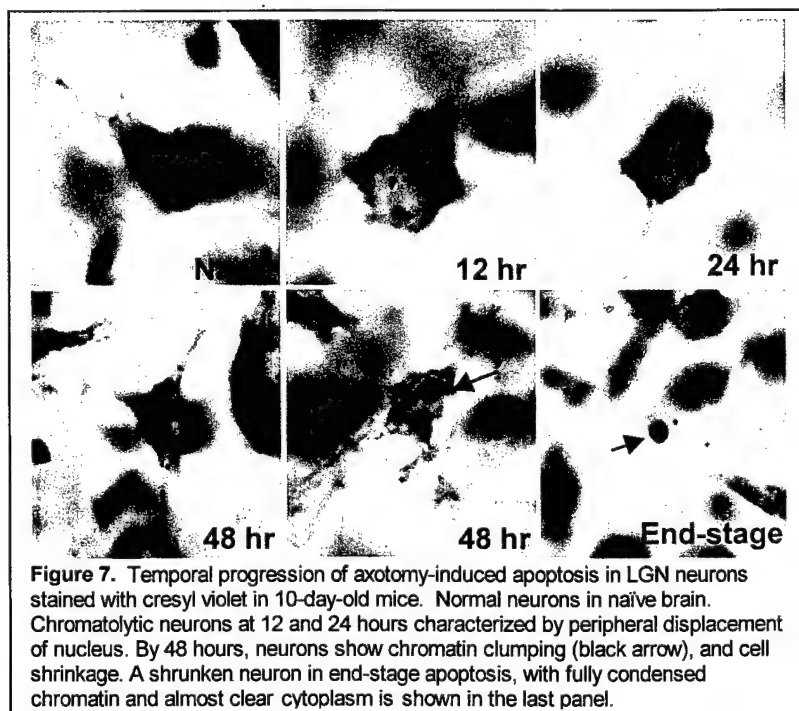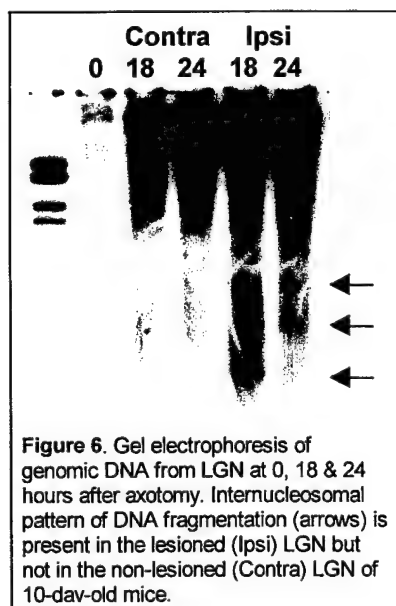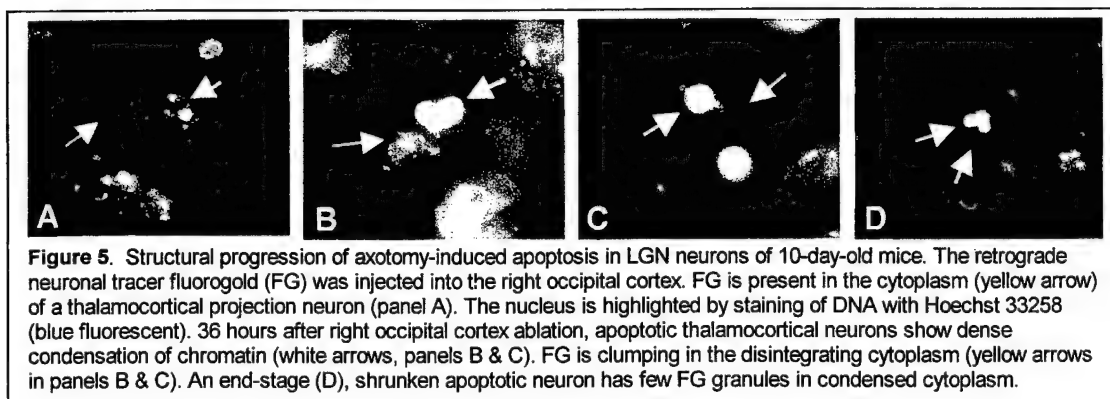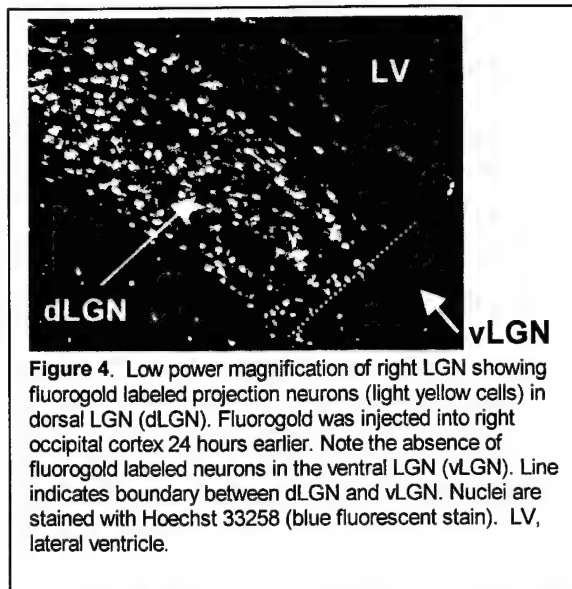**Reported Outcomes (copies of reprints, submitted manuscripts, and abstracts)**

Trolox Does Not Prevent Neuronal Apoptosis in the Adult Brain After Cortical Ablation

Ascorbic Acid (Vitamin C) Does Not Prevent Neuronal Apoptosis in the Adult Brain After Cortical Damage

Figure 4. Low power magnification of right LGN showing fluorogold labeled projection neurons (light yellow cells) in dorsal LGN (dLGN). Fluorogold was injected into right occipital cortex 24 hours earlier. Note the absence of fluorogold labeled neurons in the ventral LGN (vLGN). Line indicates boundary between dLGN and vLGN. Nuclei are stained with Hoechst 33258 (blue fluorescent stain). LV, lateral ventricle.

Figure 5. Structural progression of axotomy-induced apoptosis in LGN neurons of 10-day-old mice. The retrograde neuronal tracer fluorogold (FG) was injected into the right occipital cortex. FG is present in the cytoplasm (yellow arrow) of a thalamocortical projection neuron (panel A). The nucleus is highlighted by staining of DNA with Hoechst 33258 (blue fluorescent). 36 hours after right occipital cortex ablation, apoptotic thalamocortical neurons show dense condensation of chromatin (white arrows, panels B & C). FG is clumping in the disintegrating cytoplasm (yellow arrows in panels B & C). An end-stage (D), shrunken apoptotic neuron has few FG granules in condensed cytoplasm.

Figure 6. Gel electrophoresis of genomic DNA from LGN at 0, 18 & 24 hours after axotomy. Internucleosomal pattern of DNA fragmentation (arrows) is present in the lesioned (Ipsi) LGN but not in the non-lesioned (Contra) LGN of 10-day-old mice.

Figure 7. Temporal progression of axotomy-induced apoptosis in LGN neurons stained with cresyl violet in 10-day-old mice. Normal neurons in naïve brain. Chromatolytic neurons at 12 and 24 hours characterized by peripheral displacement of nucleus. By 48 hours, neurons show chromatin clumping (black arrow), and cell shrinkage. A shrunken neuron in end-stage apoptosis, with fully condensed chromatin and almost clear cytoplasm is shown in the last panel.

Motor Neuron Degeneration after Sciatic Nerve Avulsion in Adult Rat Evolves with Oxidative Stress and Is Apoptosis

Lee J. Martin,[1,2] Adeel Kaiser,[1] Ann C. Price[1]

[1] Department of Pathology, Division of Neuropathology, Johns Hopkins University School of Medicine, 558 Ross Building, 720 Rutland Avenue, Baltimore, Maryland 21205-2196

[2] Department of Neuroscience, Johns Hopkins University School of Medicine, Baltimore, Maryland 21205-2196

ABSTRACT: The mechanisms for motor neuron degeneration and regeneration in adult spinal cord following axotomy and target deprivation are not fully understood. We used a unilateral sciatic nerve avulsion model in adult rats to test the hypothesis that retrograde degeneration of motor neurons resembles apoptosis. By 21 days postlesion, the number of large motor neurons in lumbar spinal cord was reduced by ~30%. The death of motor neurons was confirmed using the terminal transferase-mediated deoxyuridine triphosphate-biotin nick-end labeling method for detecting fragmentation of nuclear DNA. Motor neuron degeneration was characterized by aberrant accumulation of perikaryal phosphorylated neurofilaments. Structurally, motor neuron death was apoptosis. Apoptotic motor neurons undergo chromatolysis followed by progressive cytoplasmic and nuclear condensation with chromatin compaction into uniformly large round clumps. Prior to apoptosis, functionally active mitochondria accumulate within chromatolytic motor neurons, as determined by cytochrome c oxidase activity. These dying motor neurons sustain oxidative damage to proteins and nucleic acids within the first 7 days after injury during the progression of apoptosis, as identified by immunodetection of nitrotyrosine and hydroxyl-modified deoxyguanosine and guanosine. We conclude that the retrograde death of motor neurons in the adult spinal cord after sciatic nerve avulsion is apoptosis. Accumulation of active mitochondria within the perikaryon and oxidative damage to nucleic acids and proteins may contribute to the mechanisms for apoptosis of motor neurons in the adult spinal cord. © 1999 John Wiley & Sons, Inc. J Neurobiol 40: 185–201, 1999

Keywords: amyotrophic lateral sclerosis; neuronal cell death; axotomy; target deprivation; mitochondria

Retrograde degeneration and neuronal apoptosis may participate in the mechanisms for motor neuron death in amyotrophic lateral sclerosis (ALS) (Price et al., 1992; Martin et al., 1998a; Martin, 1999). Degener-ating motor neurons in ALS undergo chromatolysis and then progressive cytoplasmic and nuclear conden-sation (Martin, 1999), with affected neurons demon-strating evidence of cytoskeletal pathology in the form of neurofilament accumulation within the neu-ronal cell body and axon (Manetto et al., 1988; Munoz et al., 1988). The degeneration of neurons in ALS is structurally a form of apoptosis that may be mediated by a caspase-dependent programmed cell death (PCD) mechanism (Martin, 1999). In ALS, a variety of ab-

© 1999 John Wiley & Sons, Inc. CCC 0022-3034/99/020185-17

normalities in the molecular regulators of cell death have been identified, including increased caspase-3 activity and abnormalities in the expression of the antiapoptotic protein Bcl-2 and the proapoptotic proteins Bax and Bak, as well as abnormalities in the interactions of these proteins (Martin, 1999). These observations in the human disease underscore the necessity of developing animal models of apoptotic retrograde neuronal death for identifying mechanisms of motor neuron degeneration in the adult central nervous system (CNS), because ALS is an adult-onset neurodegenerative disease, and brain maturity may influence the structure of neuronal death (Clarke, 1990; Portera-Cailliau et al., 1997a; Martin et al., 1998a,b; Li et al., 1998).

The likelihood of neuronal death or of regeneration and survival after injury to motor neurons is influenced by age at the time of injury and location of axonal trauma in relation to the soma (Ramón y Cajal, 1928; Lieberman, 1971; Price and Porter, 1972; Fry and Cowan, 1972; Torvik, 1976). Axotomized motor neurons in the immature CNS die rapidly, whereas axotomized motor neurons in the mature CNS are more likely to recover or persist in some altered form (Romanes, 1946; Lieberman, 1971; Torvik, 1976). Avulsion of spinal cord ventral roots in adult rodents, however, induces retrograde degeneration and apparent elimination of neurons (Wu, 1993; Koliatsos et al., 1994; Li et al., 1995, 1998). An inadequate supply of neurotrophic factor support contributes to this neurodegeneration (Ramón y Cajal, 1928; Hamburger, 1975), because glial cell line–derived neurotrophic factor (Li et al., 1995) and brain-derived neurotrophic factor (Novikov et al., 1995, 1997) promote the survival of avulsed spinal motor neurons in adult rodents. However, the mechanisms for retrograde degeneration of motor neurons in adult spinal cord are poorly understood, notably with regard to the signals that govern neuronal responses to injury and, if neuronal death occurs, the structural and molecular pathways leading to the elimination of motor neurons.

Cell death has been classified generally as necrosis or apoptosis (Kerr and Harmon, 1991), although structural hybrids of neuronal cell death may also occur (Portera-Cailliau et al., 1997a,b; Martin et al., 1998a,b; Li et al., 1998). Necrosis and apoptosis are classified differently because they are believed to differ structurally and biochemically (Kerr and Harmon, 1991; Sen, 1992). Necrosis is always pathological cell death, induced by departures from physiological conditions, involving perturbations in plasma membrane structural and functional integrity and abormalities in intracellular Na^+, Ca^{2+}, and water homeostasis and subsequent dissolution of the cell. In

contrast, apoptosis is generally regarded as physiological cell death and is considered to be an organized PCD that is mediated by active, intrinsic mechanisms through which certain molecular pathways are activated to initiate apoptosis (Kerr and Harmon, 1991; Sen, 1992; Gerschenson and Rotello, 1992). In *in vitro* settings, trophic factor deprivation of neurons results in apoptosis (Pittman et al., 1993) that is mediated by a caspase-dependent PCD mechanism (Milligan et al., 1995; Deshmukh et al., 1996). Trophic factor deprivation appears to contribute to the mechanisms for avulsion-induced degeneration of motor neurons in the adult spinal cord (Li et al., 1995; Novikov et al., 1995, 1997), possibly involving a nitric oxide pathway for cell death (Wu and Li, 1993). Therefore, we hypothesized that motor neuron degeneration in the adult spinal cord after avulsion is apoptosis and evolves in association with oxidative stress.

MATERIALS AND METHODS

Lesion Paradigm to Study Motor Neuron Degeneration

A unilateral sciatic nerve avulsion served as the model for producing degeneration of motor neurons in adult rats. Male Sprague–Dawley rats (Charles River, Wilmington, MA) (*n* = 40), weighing ~150–200 g, were housed in a colony room with a 12:12-h light/dark cycle and access to food and water ad libitum. The animal protocol was approved by the Animal Care and Use Committee of the Johns Hopkins University School of Medicine. Rats were anesthetized deeply with a mixture of enflurane/oxygen/nitrous oxide (1:33:66). A midline incision was made in the lateral aspect of the left pelvis and upper hindlimb. The sciatic nerve was located by blunt retraction of biceps femoris and gluteus muscles and was tracked proximally to an extravertebral location deep within the pelvis. A steady, moderate traction was applied to the sciatic nerve with forceps until the nerve separated from the spinal cord, resulting in a mixed motor-sensory root avulsion [Fig. 1(A)]. Muscle retraction was released and the overlying skin was sutured. Postlesion survival times following sciatic nerve avulsion were 4, 7, 14, and 21 days. Sham control rats (*n* = 5) were subjected to the anesthesia, muscle retraction, and sciatic nerve visualization, but the nerve was not avulsed.

Retrograde Labeling of Spinal Motor Neurons

Unilateral injections of the retrograde tract tracer Fluorogold (FG) (Fluorochrome, Inc., Englewood, CO) were made into the gastrocnemius muscle of deeply anesthetized adult rats (*n* = 10). Approximately 1 μL of a 5% solution of FG
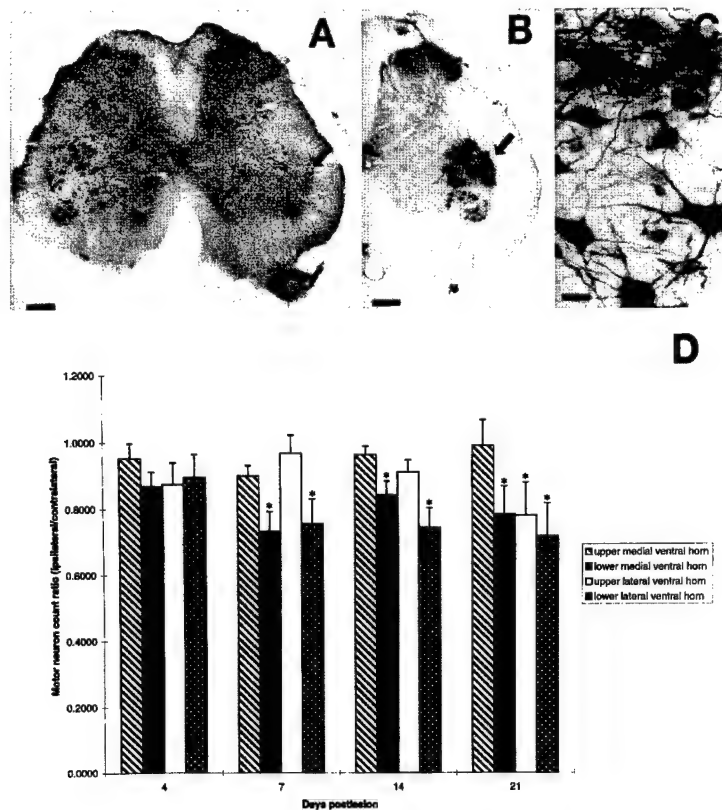
Figure 1   Sciatic nerve avulsion causes selective degeneration of spinal motor neuron pools. (A) Nissl-stained transverse section of spinal cord at about an L5 level shows the apparent loss of large motor neurons in the ventral horn (arrow) ipsilateral to the avulsion at 21 days postlesion. The apparent loss of motor neurons is greatest at L5 and is less prominent in other segments of lumbar cord. The inflammatory scar tissue (asterisk) identifies the remaining part of the ventral root. Scale bar = 287 μm. (B) Injection of FG into the gastrocnemius muscle retrogradely labels the group IX motor neuron pool (arrow), corresponding to the population of large motor neurons that degenerates after sciatic nerve avulsion [compare with (A)]. Scale bar = 267 μm. (C) FG-labeled cells are α-motor neurons. Scale bar = 31 μm. (D) Numbers of remaining motor neurons in lumbar spinal cord ventral horn at different times after sciatic nerve avulsion. Motor neurons were counted in more than one level of lumbar spinal cord (L4–6), because motor neurons within other lumbar levels (in addition to L5) project to the gastrocnemius (Nicolopoulos-Stournaras and Iles, 1983). Large multipolar motor neurons and small (possibly shrunken) motor neurons were counted. The values are mean ± standard error of the mean and reflect averages based on neuron counts in multiple levels of lumbar spinal cord. Asterisks indicate significant difference ($p < .05$) from control and 4 days postlesion.

in deionized-distilled H_2O was infused slowly over 10 min using a Hamilton syringe. Three days later, some rats (n = 4) were anesthetized and perfused for light microscopic analysis, while other rats (n = 6) underwent a unilateral sciatic nerve avulsion (on the same side of the FG injection) as described above. FG-injected rats with sciatic nerve avulsions recovered for 7 or 14 days before being perfused for light microscopic analysis. Identification of retrogradely labeled motor neurons was done by antibody detection of FG as described (Al-Abdulla et al., 1998; Al-Abdulla and Martin, 1998).

Light Microscopic Evaluation of Spinal Motor Neuron Degeneration

At 4, 7, 14, and 21 days postlesion, rats (n = 4–6/time point) were anesthetized with an overdose of chloral hydrate and perfused intraaortically with ice-cold phosphate buffered saline (PBS) (100 mM, pH 7.4) delivered by a perfusion pump, followed by 4% paraformaldehyde/1% glutaraldehyde in ice-cold PBS. After perfusion-fixation, spinal cords were allowed to remain *in situ* for 1 h before they were removed from the vertebral column. The lower tho-

racic and lumbar-upper sacral segments were removed from the spinal cord and were cryoprotected in 20% glycerol-PBS prior to freezing in isopentane chilled by dry ice. Frozen, transverse, symmetrical sections (40 μm) through the lower thoracic and lumbosacral cord were cut serially using a sliding microtome, collected serially in 96-well plates, and stored in antifreeze buffer at $-20°C$. Sections were either stained with Cresyl violet or used for the terminal transferase-mediated deoxyuridine triphosphate-biotin nick-end labeling (TUNEL) assay for nuclear DNA fragmentation (Gavrieli et al., 1992), with modifications for frozen sections; the immunocytochemical detection of phosphorylated neurofilaments, FG, and oxidative injury markers (Al-Abdulla et al., 1998; Al-Abdulla and Martin, 1998); or for the enzyme histochemical detection of cytochrome c oxidase activity (Wong-Riley, 1979).

Quantification of Motor Neurons

Cresyl violet–stained sections were used to count motor neurons in spinal cords of rats at 4, 7, 14, and 21 days postlesion. Profile counts were made at $\times 400$ magnification by an observer unaware of treatment. Motor neurons were counted in ventral horns ipsilateral and contralateral to the sciatic nerve avulsion. Motor neurons were counted in lower thoracic levels, lumbar levels (L4–6), and sacral levels (S1–3). At lumbosacral levels, the ventral horn was consistently divided into four quadrants (upper medial, upper lateral, lower medial, and lower lateral), with the upper medial quadrant corresponding primarily to cell group (layer) VII, the lower medial quadrant corresponding to cell group VIII, and the lower and upper lateral quadrants corresponding to cell group IX. Neurons were distinguished from glia and inflammatory cells by strict criteria based on perikaryal and nuclear morphology. The criterion for inclusion was any multipolar cell with granular cytoplasmic staining of Nissl and nucleus with nucleolus, regardless of size. Cells were excluded if they had a nonneuronal nucleus typical of astrocytes, oligodendrocytes, or microglia. Cell counts were expressed as a ratio of motor neuron number in spinal cord ventral horn ipsilateral and contralateral to the lesion.

Statistical analysis of neuronal numbers per postlesion time point was performed on pooled sets. Neuronal numbers per rat were averaged and a weighted standard deviation was calculated for a more reliable estimate of the neurons per time point. Comparisons of the time points were performed using a one-way analysis of variance with Student t test using the appropriate degrees of freedom.

Immunocytochemistry

A peroxidase-antiperoxidase detection method was used for the immunocytochemical staining of free-floating spinal cord sections with diaminobenzidine as chromogen. To confirm that degenerating cells were motor neurons, phosphorylated neurofilaments were detected with a mouse monoclonal antibody (SMI-31; Sternberger Monoclonals,

Jarrettsville, MD) at a dilution of 1:10,000, and FG was detected with rabbit polyclonal antibodies (diluted 1:10,000; Chemicon, Temecula, CA). To determine if degenerating motor neurons undergo oxidative stress, peroxynitrite-mediated damage to proteins was detected with monoclonal and polyclonal antibodies to nitrotyrosine (Upstate Biotechnology, Lake Placid, NY), and hydroxyl radical damage to DNA was detected with monoclonal antibodies to 8-hydroxy-2′-deoxyguanosine (QED Bioscience and PharMingen, San Diego, CA). For competition controls, sections were reacted with antibody to 8-hydroxy-2′-deoxyguanosine (OHdG) that was incubated at 4°C for 24 h with 1000-fold concentrations of OHdG, 8-hydroxyguanosine, or guanosine (Cayman Chemical, Ann Arbor, MI). As additional controls, sections were digested with DNase (5–10 mg/mL) or RNase (11–50 mg/mL) prior to incubation with OHdG antibody.

Electron Microscopic Analysis of Motor Neuron Death after Sciatic Nerve Avulsion

At 1 day and 3, 8, 14, 18, and 21 days postlesion, rats ($n = 2$–3 animals/time point) were anesthetized with chloral hydrate and perfused intraaortically with 1% paraformaldehyde/0.1% glutaraldehyde in ice-cold PBS followed by 2% paraformaldehyde/2% glutaraldehyde in ice-cold PBS. After perfusion-fixation, spinal cords were allowed to remain *in situ* for 1 h before they were removed from the vertebral column. After further fixation overnight, lumbar and upper sacral segments (ipsilateral and contralateral to the avulsion) were microdissected from each rat, rinsed in phosphate buffer, placed in 2% osmium tetroxide for 2 h, dehydrated, and embedded in plastic. Semithin sections (1 μm) stained with 1% Toluidine blue were screened for motor neurons of interest, and then thin sections (gold interference color) were cut on an ultramicrotome (Sorvall, Norwalk, CT), contrasted with uranyl acetate and lead citrate, and viewed with a Jeol 100S electron microscope.

RESULTS

Peripheral Nerve Avulsion Causes Loss of Motor Neurons in Adult Spinal Cord

A unilateral sciatic nerve avulsion in adult rat induces a loss of motor neurons in lumbosacral spinal cord (Fig. 1). At 21 days postlesion, the apparent death of motor neurons is revealed in Nissl-stained sections of L5 levels of spinal cord [Fig. 1(A)]. The loss of motor neurons occurred most prominently in the lateral-most motor neuron cell group of lower lumbar and sacral spinal cord, corresponding to motor neuron cell column IX [Fig. 1(A,D)]. This pool of α-motor neurons projects to the gastrocnemius muscle via the tibial branch of the sciatic nerve (Nicolopoulos-Stournaras

and Iles, 1983), as demonstrated by the retrograde transport of FG [Fig. 1(C,D)]. In this model, the majority of motor neuron loss occurred by 7 days postlesion [Fig. 1(D)]. Throughout the time course, many motor neurons in the lateral quadrants were shrunken (i.e., reduced cytoplasmic volume) and the perikaryon was pale by Nissl staining. As a control, motor neurons were counted in lower thoracic segments of spinal cord. Motor neuron number in thoracic spinal cord was not reduced by this lesion (data not shown).

Motor Neurons Die after Sciatic Nerve Avulsion

Tunel–positive cells were detected within the lumbosacral spinal cord ipsilateral to the avulsion at 4–14 days postlesion [Fig. 2(A,B)]. No labeling was seen in the lumbosacral spinal cord contralateral to the lesion or in the thoracic cord at any time. TUNEL-positive cells in ventral horn were identified as motor neurons based on perikaryal and nuclear morphology, size, location, and postlesion time of appearance. Interestingly, the frequency occurrence of TUNEL-positive motor neurons did not appear to be commensurate with the loss of motor neurons as predicted by cell counts in Nissl-stained sections. TUNEL-positive neurons were present primarily in the lateral quadrants of the ventral horn. In degenerating motor neurons, DNA cleavage preceded nuclear condensation as detected in Nissl sections. This fragmentation of DNA in dying motor neurons emerged compartmentally within the nucleus, with the earliest DNA fragmentation occurring at perinucleolar sites [Fig. 2(A)].

Retrogradely Degenerating Spinal Motor Neurons Accumulate Phosphorylated Neurofilaments

Aberrant accumulation of perikaryal phosphorylated neurofilament confirmed the neuronal identity of injured motor neurons [Fig. 2(C–G)]. Normal spinal motor neurons do not have immunocytochemically detectable phosphorylated neurofilaments within their perikarya [Fig. 2(C)] (Cork et al., 1988). However, by 4 days postlesion, phosphorylated neurofilament immunoreactivity increases within the proximal processes of subsets of motor neurons in the ipsilateral lumbosacral cord [Fig. 2(D)], relative to the contralateral spinal cord and nonlesioned controls [Fig. 2(C)]. Motor neurons in the ipsilateral thoracic cord were not immunolabeled. By 7–14 days, the cell bodies of

subsets of motor neurons in group IX of lumbosacral cord were enriched with phosphorylated neurofilaments [Fig. 2(E)]. Their perikarya developed an irregular shape and became shrunken compared to uninjured neurons [Fig. 2(C,E)]. Neurofilament immunoreactivity also accumulated in axons and dendrites that were distorted, distended, and convoluted [Fig. 2(E)]. At 7 and 14 days after injury, some motor neurons with perikaryal accumulations of phosphorylated neurofilament transformed from multipolar cells to round cells that had thin processes [Fig. 2(F)]. Many of the phosphorylated neurofilament-enriched motor neurons appeared structurally similar to degenerating motor neurons found in ALS (see Fig. 3 in Munoz et al., 1988). After 14 days postlesion, neurofilament immunoreactivity began to dissipate as the degenerating motor neurons underwent shrinkage [Fig. 2(G)], so that by 21 days, the perikaryon of most remaining motor neurons on the lesioned side were not immunopositive for phosphorylated neurofilament.

Motor Neuron Death after Sciatic Nerve Avulsion Resembles Apoptosis

The morphology of avulsion-induced motor neuron degeneration was examined by light microscopy to determined if it resembled apoptosis, as found in *in vivo* paradigms of neuronal apoptosis (Chu-Wang and Oppenheim, 1978; Clarke, 1990; Portera-Cailliau et al., 1997a,b; Martin et al., 1998b; Al-Abdulla et al., 1998). Criteria for identifying cells as motor neurons included, size, shape, and aggregates of Nissl. Using Nissl-stained sections of lumbosacral spinal cord from rats at 4, 7, and 14 days postlesion, a staging scheme was formulated for the structural progression of motor neuron death (Fig. 3). This staging arrangement revealed that the death of motor neurons had a distinctive structural phenotype that was apoptosis. This progression occurred over 7–14 days. As in apoptosis in other systems, both the cytoplasm and the nucleus underwent condensation [Fig. 3(D–H)]. After an initial preapoptotic chromatolytic stage [Fig. 3(B,C)], motor neurons progressively underwent shrinkage of the cell body and dendrites [Fig. 3(D–F)] that culminated in apoptosis [Fig. 3(G,H)]. At the transition between chromatolysis and apoptosis, the normal multipolar cell body [Fig. 3(A)] transformed and became round [Fig. 3(D)]. Motor neurons with round cell bodies then separated from the surrounding neuropil, as the cell surface appeared scalloped [Fig. 3(E,F)]. The cytoplasm was initially depleted of Nissl bodies [Fig. 3(C,D)] and appeared mostly homogeneous, and progressively became hypochromic and then translucent in Nissl-stained sections [Fig.
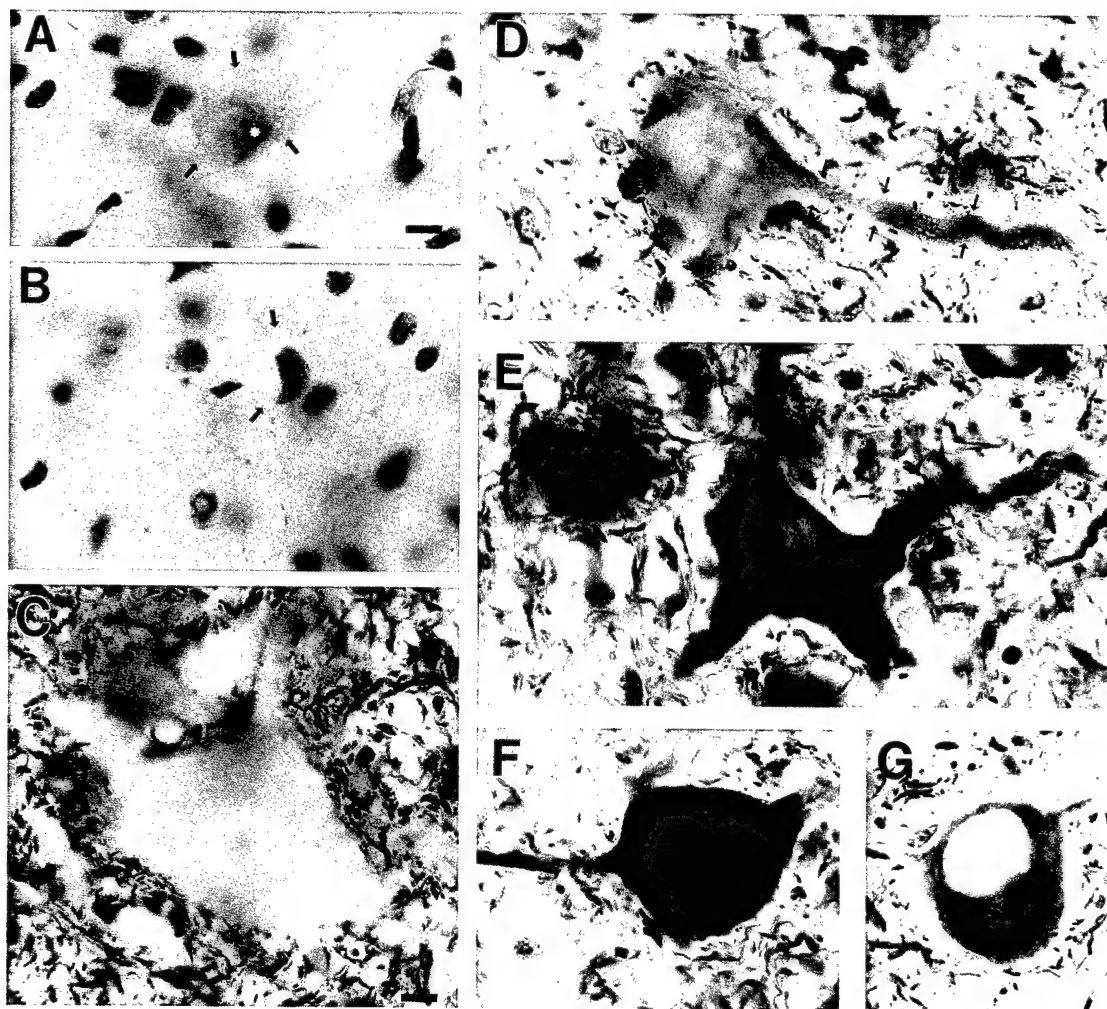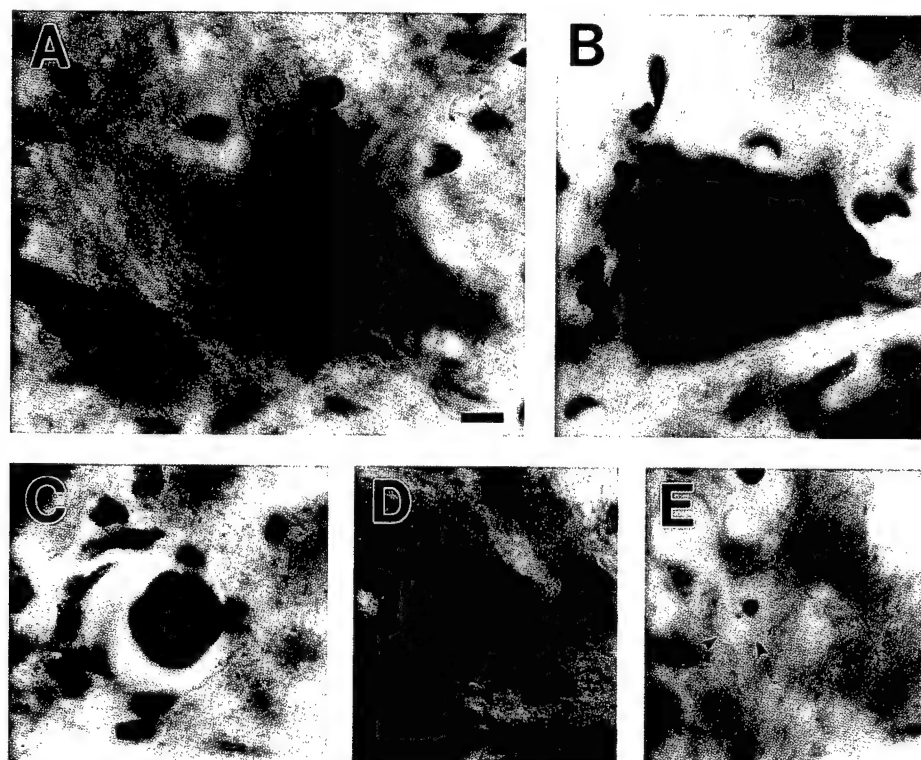
Figure 2

Figure 7

3(G,H)]. Within the nucleus, the chromatin initially aggregated into several, small round minimasses [Fig. 3(D)] and then condensed into a few sharply delineated, uniformly dense, smooth, round masses within the nucleus [Fig. 3(E,F)]. Prelabeling experiments with FG demonstrated that these neurons with structural features of apoptosis projected to the gastrocnemius muscle and thus were motor neurons (data not shown). At end-stage apoptosis, the cellular debris within the neuropil usually existed as two closely apposed, small, round nuclear fragments surrounded by a thin rim of translucent cytoplasm [Fig. 3(H)]. Often, this cellular debris was apposed by cells with nuclei typical of phagocytes [Fig. 3(H)]. This structural progression of motor neuron death is similar to the morphological progression of neuronal apoptosis found in other *in vivo* paradigms (Martin et al., 1998b; Al-Abdulla et al., 1998).

Ultrastructure of Spinal Motor Neuron Death after Avulsion Is Apoptosis

By electron microscopy, cellular alterations within degenerating motor neurons evolved into classic apoptosis, as revealed by the progressive cytoplasmic and nuclear condensation with chromatin compaction into uniformly large round clumps, while the morphologic integrity of mitochondria was preserved until late in the progression of neuronal degeneration. Subcellular changes within the perikaryon of dying motor neurons included the classic chromatolytic response with redistribution of the rough endoplasmic reticulum and dispersion of free ribosomes, followed by fragmentation of the rough endoplasmic reticulum, and accumulation of mitochondria [Fig. 4(A)]. Dying motor neurons at 8 and 14 days postlesion were found at various stages of apoptosis. Some neurons had a very dark, shrunken perikaryon that contained small vacuoles and numerous mitochondria within a dense cytoplasmic matrix [Fig. 4(A)]. Some mitochondria that accumulated in the condensing perikaryon underwent swelling and disintegration of the inner membrane, whereas other mitochondria remained intact [Fig. 4(A), inset]. At midapoptotic stages, the nucleus of dying motor neurons was eccentrically located (typical of chromatolysis), dark, and shrunken, and it contained small compact clumps of chromatin. In other dying cells, still recognizable as motor neurons owing to their size and the presence of vacated postsynaptic densities, the nuclear condensation had progressed until large, round chromatin clumps were present within a homogeneously dense nuclear matrix

Figure 2   Spinal motor neurons die and accumulate phosphorylated neurofilaments after avulsion. (A,B) TUNEL preparations counterstained with Cresyl violet demonstrating motor neurons (the cell bodies are delineated by the arrows) undergoing nuclear DNA fragmentation (brown labeling) at 7 (A) and 14 (B) days after avulsion. Fragmented DNA highlights the nucleolus [white asterisk in (A)]. Surrounding glial nuclei are unlabeled. Scale bars (A,B) = 5 μm. (C) Immunocytochemical preparation counterstained with Cresyl violet showing that phosphorylated neurofilament immunoreactivity (brown labeling) is absent within the cell body and proximal dendrites of normal motor neurons. Scale bars (C–G) = 4 μm. (D) Dendrites (one dendrite is delineated by small arrows) of injured motor neurons begin to accumulate phosphorylated neurofilament immunoreactivity by 4 days postlesion. (E–G) The cell bodies and proximal dendrites of injured motor neurons are enriched with phosphorylated neurofilaments by 7–14 days postlesion. The perikarya of injured motor neurons initially become irregular in shape with distorted, thick proximal dendrites (E), and then degenerating motor neurons become round with thin, regressing processes (F). Subsequently, neurofilament immunoreactivity dissipates as degenerating motor neurons shrink (G).

Figure 7   Functionally active mitochondria accumulate in motor neurons undergoing apoptosis after avulsion, as shown in histochemical preparations for cytochrome c oxidase that were counterstained for Nissl. (A) Normal large motor neurons have only faint histochemically detectable cytochrome c oxidase activity within their cell bodies, although the surrounding neuropil is enriched in activity. Scale bars (A–E) = 4 μm. (B) Injured motor neurons at preapoptotic, chromatolytic stages accumulate intense cytochrome c oxidase activity within their perikaryon. (C) Apoptotic motor neurons (indicated by the round cell body detaching from the neuropil and the chromatin that is condensed into several, small, round masses) maintain high levels of cytochrome c oxidase activity within the cell body. (D) Eventually, mitochondrial metabolic activity diminishes in motor neurons advancing toward end-stage apoptosis (delineated by small arrowheads), coinciding with the loss of ultrastructural integrity of mitochondria [see Fig. 4(A), inset]. (E) Cytochrome c oxidase activity is low within apoptotic cellular debris (delineated by small arrowheads).
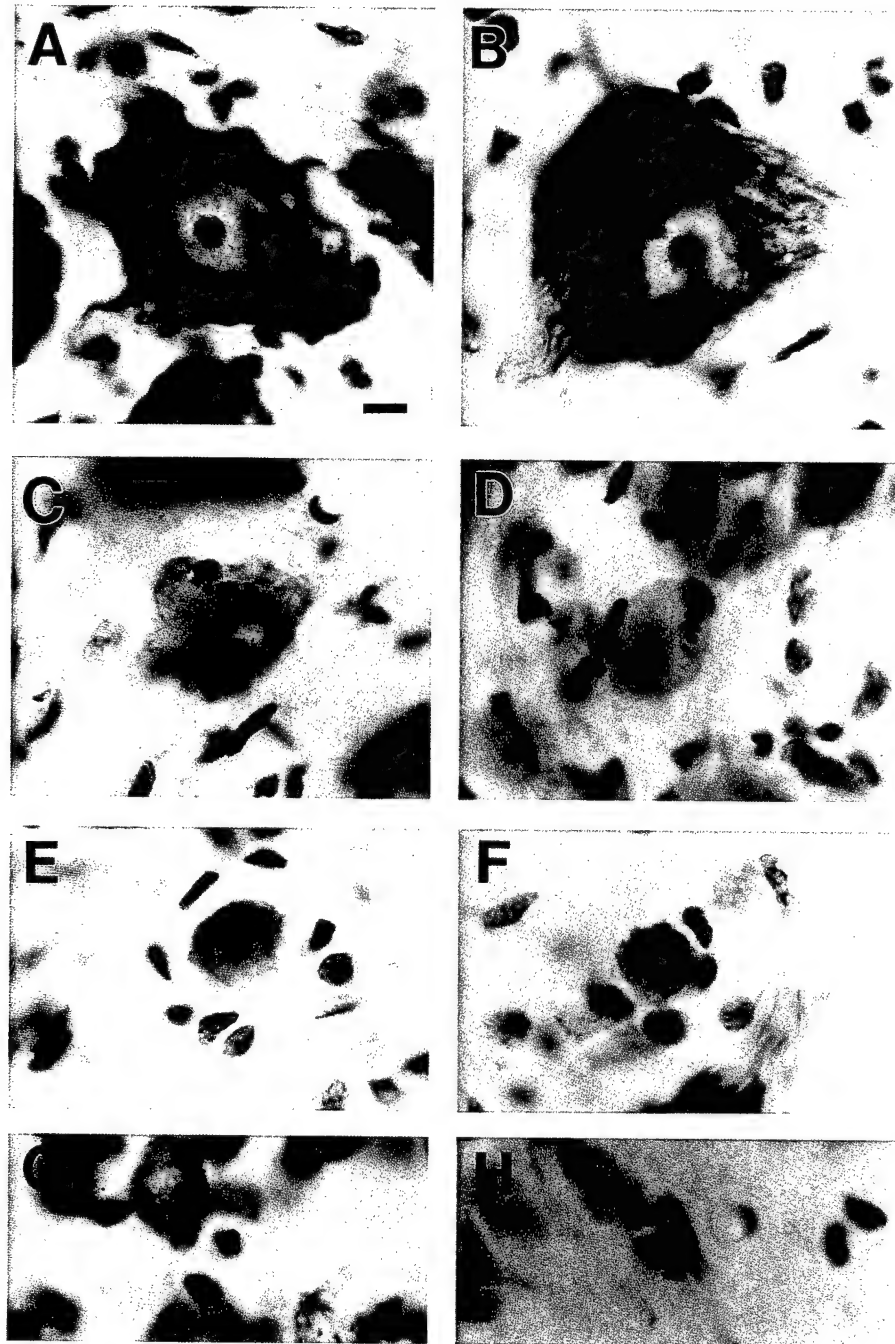
Figure 3

that was surrounded by a ruffled nuclear envelope [Fig. 4(A)]. In these motor neurons, the nucleus was surrounded by either an intact or disrupted nuclear envelope. Motor neuron debris was engulfed by phagocytes [Fig. 4(B)]. The ultrastructure of this death of motor neurons after sciatic nerve avulsion was similar to the morphological progression of neuronal apoptosis found by electron microscopy in other *in vivo* paradigms (Martin et al., 1998b).

Oxidative Stress Occurs in Injured Motor Neurons before the Emergence of the Apoptotic Structure

We determined by immunocytochemistry whether abnormal nitration of proteins occurs in motor neurons after avulsion. Nitrotyrosine immunoreactivity was detected above background levels in motor neurons and axons after sciatic nerve avulsion (Fig. 5). Using

two different antibodies, prominent nitrotyrosine immunoreactivity was found selectively within subsets of group IX motor neurons ipsilateral to the lesion [Fig. 5(B,D)]. The same group of motor neurons in the unlesioned side was not immunoreactive for nitrotyrosine [Fig. 5(A,C)]. Nitrotyrosine immunoreactivity was also detected within subsets of large distorted axons in the ventral horn neuropil and in ventral root stumps exiting the spinal cord [Fig. 5(B)]. This prominent nitrotyrosine immunolabeling of neuronal cell bodies and axons of motor neurons was transient, occurring primarily at 4 and 7 days postlesion, before the onset of apoptosis.

Hydroxyl radical damage to DNA was detected immunocytochemically with two different antibodies to OHdG (Fig. 6). Immunoreactivity for OHdG was detected in motor neurons within both ipsilateral and contralateral ventral horns and dorsal horns [Fig. 6(A)]; however, the immunolabeling was most intense in motor neurons on the lesioned side [Fig. 6(A)]. The patterns of cellular labeling were very different in motor neurons in lesioned versus unlesioned ventral horns. Motor neurons on both sides had cytoplasmic labeling suggestive of an RNA pattern, although the intensity of cytoplasmic immunoreactivity was much greater in avulsed motor neurons [Fig. 6(B,C)]. In contrast, intense nuclear labeling occurred only in motor neurons that underwent avulsion [Fig. 6(B,C)]. The most prominent differences in OHdG immunolabeling between lesioned and unlesioned sides of spinal cord (based on the intensity of immunoreactivity) occurred at 4 and 7 days after avulsion. Because of both nuclear and Nissl-like cytoplasmic immunoreactivity for OHdG, it was likely that these antibodies detected more than OHdG. Digestion of DNA with DNase abolished the nuclear labeling of

retrogradely degenerating motor neurons [Fig. 6(D)]. Digestion of RNA with DNase-free RNase substantially eliminated the cytoplasmic labeling [Fig. 6(E)]. Preadsorption of OHdG antibody with OHdG, 8-hydroxyguanosine, or guanosine prior to the immunocytochemistry selectively blocked the labeling in the different cellular compartments. OHdG abolished the nuclear staining in avulsed motor neurons (not shown), similar to results shown in another paradigm of axotomy (Al-Abdulla and Martin, 1998). Hydroxyguanosine and guanosine blocked the cytoplasmic immunostaining that resembled a Nissl pattern [Fig. 6(F,G)], while the nuclear immunoreactivity remained.

Mitochondrial Metabolic Activity Increases during Apoptosis of Motor Neurons

Retrograde neuronal apoptosis in other systems of axotomy/target deprivation occurs in association with increased perikaryal mitochondria and oxidative damage to DNA (Al-Abdulla and Martin, 1998). To analyze the possible mechanisms of oxidative stress in apoptotically dying motor neurons, cytochrome c oxidase enzyme histochemistry was used to assess mitochondrial localization and metabolic activity (Fig. 7). Histochemical preparations that were counterstained for Nissl showed that cytochrome c oxidase activity was localized within punctate structures and axons in the neuropil and in neuronal cell bodies [Fig. 7(A)]. Normal large motor neurons have only faint histochemically detectable cytochrome c oxidase activity, possibly because the mitochondria are dispersed within the cytoplasm and are obscured by the Nissl [Fig. 7(A)]. After avulsion, motor neurons at

Figure 3 Motor neuron death after sciatic nerve avulsion resembles apoptosis. Nissl-stained sections of spinal cord were used to construct a staging scheme for the structural progression of motor neuron death. Over 14 days, neurons pass through chromatolytic stages (B,C) and then undergo apoptosis (D–H). (A) A normal, uninjured motor neuron is shown for comparison with neurons in (B–H). Scale bar (A–H) = 5 μm. (B) During the early chromatolytic stage, the motor neuron swells, the nucleus becomes eccentric, and the Nissl disperses. (C) During the preapoptotic, chromatolytic stage, the motor neuron cell body undergoes homogenization of the Nissl (shown by the cytoplasmic pallor) and shrinks. (D) Once in apoptosis, the motor neuron transforms into a round cell. At this stage, the cytoplasm is depleted of Nissl, appearing homogeneous and hypochromic, and the nucleus condenses into several small, round aggregates. (E,F) As apoptosis progresses, the round cell body condenses and detaches from the surrounding neuropil, as the cell surface becomes ruffled. The chromatin condenses into a few sharply delineated, uniformly dense, smooth, round masses within the nucleus, and the nuclear envelope disappears. (G) At end-stage apoptosis, the chromatin condenses further into fewer uniformly round discrete masses, and the cytoplasm is reduced to a thin, translucent rim. (H) The apoptotic motor neuron debris exists as round, dense chromatin masses surrounded by translucent cytoplasm which is usually apposed by phagocytic cells [see Fig. 4(B)].
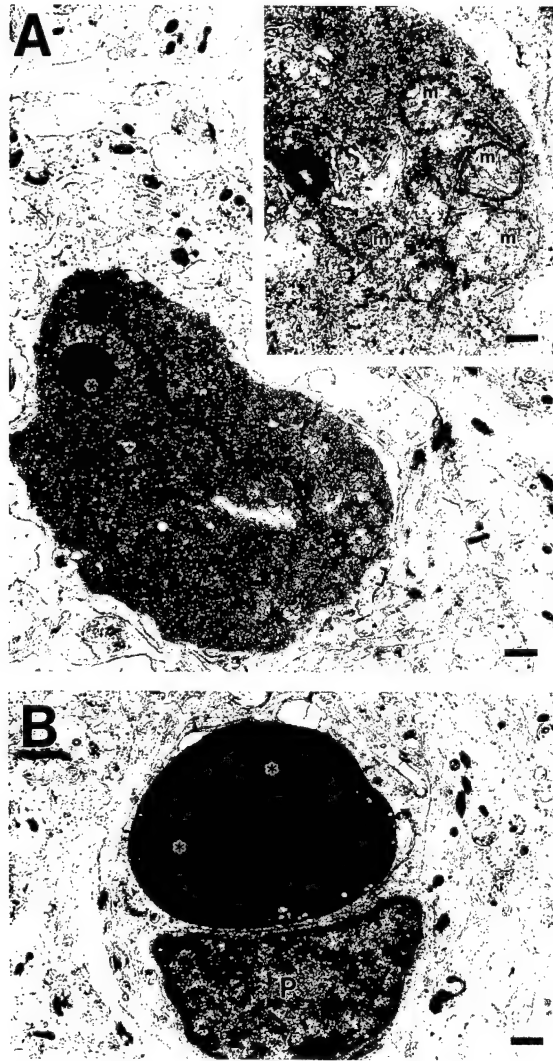
Figure 4 Avulsion-induced degeneration of motor neurons is apoptosis ultrastructurally. (A) Degenerating motor neurons become dark and shrunken. The motor neuron shown ultrastructurally corresponds to a neuron at the stage of apoptosis represented in Figure 3(D–F). The condensed cytoplasm contains small vacuoles, some of which are degenerating mitochondria [the bracketed area in (A) is shown as an inset, mitochondria (m)]. The nucleus becomes eccentrically placed and the chromatin condenses into large, round, uniformly compact chromatin masses (asterisk) embedded within a homogeneously condensed nuclear matrix. The nucleus is still surrounded partially by a nuclear membrane. The rough endoplasmic reticulum and Golgi apparatus become indiscernible within a condensed cytoplasmic matrix. Free ribosomes and rosettes are increased, resulting in a darker, granular cytoplasmic matrix. Some mitochondria are ultrastructurally intact but others are pale and swollen or overtly showing cristaeolysis (inset). Scale bar = 2.0 μm; inset scale bar = 0.5 μm. (B) At end-stage degeneration, debris of apoptotic motor neurons is engulfed by phagocytes (p). This debris consists of round or elliptical cellular fragments with one or two round, dark masses of

preapoptotic chromatolytic stages accumulated intense cytochrome c oxidase activity within their perikaryon [Fig. 7(B)] compared to contralateral uninjured neurons [Fig. 7(A)]. Motor neurons in apoptosis maintained high levels of cytochrome c oxidase activity within the cell body, as revealed by the round cell body and the chromatin condensation into several round minimasses [Fig. 7(C)]. As apoptosis progressed, cytochrome c oxidase activity within the cell body dissipated [Fig. 7(D)]. The loss of cytochrome c oxidase activity coincided with incipient mitochondrial damage as detected by electron microscopy [Fig. 4(A)]. In apoptotic motor neurons, mitochondria could appear intact or swollen and cristaeolytic [Fig. 4(A), inset] within the condensed cytoplasmic matrix. At end-stage neuronal apoptosis, cytochrome c oxidase activity was low within the cellular debris [Fig. 7(E)].

DISCUSSION

Ventral root avulsion is used as a model for retrograde degeneration of motor neurons in the adult mammalian spinal cord (Wu, 1993; Koliatsos et al., 1994; Li et al., 1995, 1998; Novikov et al., 1997). It has been assumed that this lesion in adult animals produces death of spinal motor neurons. However, these motor neurons undergo chromatolysis, loss of Nissl, and dramatic perikaryal shrinkage (Fig. 3). These responses make the counting of motor neurons difficult, particularly in the presence of reactive glial changes. In addition, nuclear DNA fragmentation, signifying cell death, has not been observed in motor neurons after this lesion in adult mice, although cell counts and electron microscopy indicate loss of motor neurons (Li et al., 1998). Thus, uncertainty still exists regarding whether avulsion causes neurodegeneration that culminates in neuronal death or only severe neuronal atrophy and apparent loss of large motor neurons. In addition, the structural and molecular mechanisms for this degeneration of spinal motor neurons are not understood, although it appears that trophic factor deprivation (Li et al., 1995; Novikov et al., 1995, 1997) and nitric oxide–mediated oxidative stress (Wu and Li, 1993) play a role in this motor neuron degeneration.

compact chromatin (asterisks) within a condensed nucleus that is surrounded by a thin rim of dark, condensed cytoplasm. This stage of apoptosis corresponds to the stage shown in Figure 3(H). Scale bar = 1.25 μm.
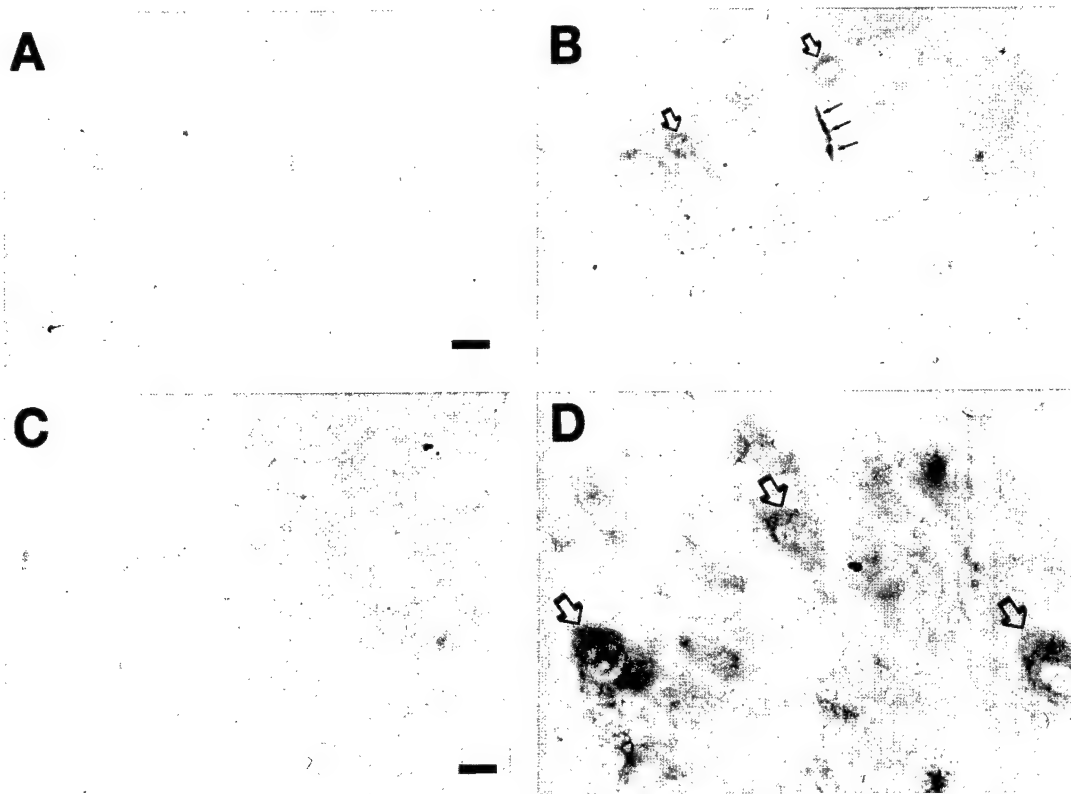
Figure 5 Peroxynitrite-mediated oxidative damage is found in motor neurons early after avulsion. (A,B) At 4 days postlesion, nitrotyrosine immunoreactivity is not detected in spinal cord contralateral to the lesion (A), but in the ipsilateral spinal cord, subsets of avulsed motor neuron cell bodies (open arrows) and axons (small thin arrows) show nitrotyrosine immunoreactivity. Scale bars (A,B) = 22 μm. (C,D) At higher magnification, nitrotyrosine immunoreactivity is enriched within the cytoplasm and nucleus of subsets of motor neurons ipsilateral to the avulsion at 7 days (D), but not in control motor neurons contralateral to the lesion (C). Scale bars (C,D) = 10 μm.

Here, we demonstrate that sciatic nerve avulsion causes motor neurons to die apoptotically in the adult spinal cord. This motor neuron apoptosis *in vivo* occurs in association with oxidative damage to nucleic acids and protein. The oxidative injury occurs in the form of hydroxyl radical damage to DNA and RNA as well as peroxynitrite damage to proteins. This oxidative stress possibly results from an abnormal accumulation of metabolically active mitochondria within the perikaryon of injured motor neurons and may participate in the signaling mechanisms for apoptosis.

Methodological Considerations

We used a peripheral nerve avulsion model because it is thought that this lesion causes loss of motor neurons, as compared to peripheral nerve transection which does not produce motor neuron elimination in the adult CNS (Lowrie and Vrbová, 1992). Avulsion injures motor neurons by axotomy, mechanical strain

(traumatic injury), and target deprivation. In addition, because the sensory root is removed, an extravertebral avulsion also partially deprives spinal motor neurons of dorsal root afferent innervation (Conradi, 1969; McLaughlin, 1972). Adult animals were used, rather than immature animals, because we sought to study degeneration of mature motor neurons to compare these findings with observations on motor neuron degeneration in ALS (Martin, 1999), which has an adult onset.

Motor neuron death in this model was established by the TUNEL method for the *in situ* detection of nuclear DNA fragmentation (Gavrielli et al., 1992). This method identifies neurons undergoing normal developmental cell death (Portera-Cailliau et al., 1997b) and induced cell death in several paradigms of experimental neuropathology (Martin et al., 1998b). The TUNEL method, however, does not distinguish between the DNA fragmentation in apoptosis and necrosis (Martin et al., 1998b); therefore, we evalu-

Figure 6 Hydroxyl radical damage occurs in motor neurons early after avulsion. (A) OHdG immunoreactivity was greater in motor neurons on the lesioned side (arrow) compared to the unlesioned side. Scale bar = 120 μm. (B) Motor neurons in the unlesioned, control side of spinal cord had cytoplasmic OHdG immunoreactivity but no OHdG immunoreactivity within the nucleus (asterisk). Scale bars (B–E) = 10 μm. (C) Avulsed motor neurons displayed intense OHdG immunoreactivity within the cytoplasm and nucleus (asterisk) at 7 days postlesion. (D) DNase treatment abolished the labeling for OHdG within the nucleus (asterisk) of degenerating motor neurons. (E) RNase digestion depleted the cytoplasmic labeling for OHdG in injured motor neurons. (F,G) Preadsorption of OHdG antibody with 8-hydroxyguanosine (F) or guanosine (G) selectively competed the cytoplasmic labeling in motor neurons but had limited effects on the nuclear labeling (asterisks). Scale bars (F,G) = 8.5 μm.

ated the structural progression of motor neuron degeneration after avulsion to determine whether it more closely resembles apoptosis, necrosis, or a hybrid of these two forms of cell death that falls along the apoptosis–necrosis continuum (Portera-Cailliau et al., 1997a,b). We further evaluated the specific type of degeneration in motor neurons by electron microscopy, because ultrastructure is the best index for defining cell death (Martin et al., 1998b). We found that adult spinal motor neurons die apoptotically after avulsion.

Spinal Motor Neurons Die after Avulsion

Studies have shown that unilateral avulsion of cervical spinal or sciatic nerves produces retrograde degeneration of motor neurons in adult rodents (Wu, 1993; Koliatsos et al., 1994; Li et al., 1995, 1998; Novikov et al., 1997). Previous quantitative analyses indicated that the number of motor neurons that appear morphologically normal after avulsion is reduced ~70% (Wu, 1993; Li et al., 1995, 1998; Novikov et al., 1997). We found in Nissl preparations that about 30% of motor neurons are lost in the lateral pool (group IX) of lumbosacral spinal cord by 7–14 days postlesion. This magnitude is lower than previous quantitative estimates of spinal motor neuron counts following ventral root avulsion. In our paradigm, the origin of the avulsion is more distal compared to previous studies. Thus, the magnitude of motor neuron loss probably depends on the type of avulsion (i.e., intravertebral ventral root avulsion vs. extravertebral peripheral nerve avulsion). In addition, previous studies focused on counts of motor neurons in L5 [where the most dramatic cell loss appears to occur; see Fig. 1(A)], whereas we counted motor neurons in multiple levels of lumbar cord, because the sciatic nerve contains axons derived from motor neurons within more than one lumbar segment (Nicolopoulos-Stournaras and Iles, 1983). Our additional results based on TUNEL show that subsets of motor neurons in the adult spinal cord undergo nuclear DNA fragmentation following sciatic nerve avulsion. Within the ventral horn, this neuronal death was selective for the group IX motor neuron pool. This location of neuronal death is dictated by the distribution of motor neuron axons within the sciatic and motor neuron–muscle connectivity, as predicted by tracing experiments (Nicolopoulos-Stournaras and Iles, 1983) (Fig. 1). Our results demonstrate that a subset of motor neurons definitely dies, rather than only shrinks or atrophies, in the adult rat spinal cord after avulsion.

Retrograde Death of Adult Motor Neurons Is Apoptosis

An important contribution of the present study is the discovery that avulsion-induced, retrograde degener-

ation of motor neurons in the adult CNS structurally resembles apoptosis. This retrograde neurodegeneration evolves from classical chromatolysis to apoptosis over 14 days. This result contrasts with experiments in adult mice showing that avulsion-induced motor neuron degeneration more closely resembles necrosis, although ultrastructural characteristics of necrosis and apoptosis may overlap in these neurons (Li et al., 1998). This important difference in the structure of avulsion-induced motor neuron degeneration in rat and mice may be related to differences in the paradigm of avulsion or to fundamental differences in the mechanisms for neuronal injury in adult mouse and rat. Support for this latter possibility is derived from experiments showing that nitric oxide synthase is induced after avulsion in motor neurons in adult rat (Wu, 1993) but not in adult mouse (Li et al., 1995).

As with apoptosis in nonneuronal tissues (Kerr and Harmon, 1991) and in naturally occurring neuronal death in developing CNS (Chu-Wang and Oppenheim, 1978; Clarke, 1990; Portera-Cailliau et al., 1997b), we found that avulsion-induced degeneration of motor neurons is characterized structurally by a progressive sequence of organized alterations in the cytoplasm and nucleus. The most prominent alterations observed by light microscopy (Fig. 3) and electron microscopy (Fig. 4) were chromatolysis and Nissl depletion followed by condensation of chromatin into large spherical clumps and progressive cellular shrinkage. We assume that degenerating motor neurons at different postlesion times *in vivo* are at different stages of a single progressive cell death process. The reliably synchronous stages of different degenerating motor neurons at the same time postlesion and the consistent and predictable time course of neurodegeneration support this assumption. This degeneration of motor neurons after sciatic nerve avulsion has many similarities to the apoptosis of other CNS neurons induced by axotomy and target deprivation in immature animals (Romanes, 1946; Chu-Wang and Oppenheim, 1978) and adult animals (Martin et al., 1998b; Al-Abdulla et al., 1998). As found here with motor neurons, the degeneration of target-deprived thalamic neurons that are destined to die is characterized morphologically by chromatolysis followed by a progressive sequence of neurofilament accumulation, cytoplasmic and nuclear condensation, and cellular shrinkage that culminates in apoptosis (Al-Abdulla et al., 1998; Al-Abdulla and Martin, 1998). Avulsion-induced death of motor neurons is distinct structurally from axotomy-induced, retrograde and transsynaptic atrophy of neurons (Ginsberg and Martin, 1998; Ginsberg et al., 1999) and is very different from *N*-methyl-D-aspartate (NMDA) gluta-

mate receptor–mediated excitotoxic neuronal necrosis (Portera-Cailliau et al., 1997a). Furthermore, based on the structural pattern of chromatin condensation seen by light and electrom microscopy, avulsion-induced death of motor neurons does not appear to be a structural hybrid of necrosis and apoptosis, similar to non–NMDA glutamate receptor–mediated neuronal death (Portera-Cailliau et al., 1997a). Therefore, we conclude that the death of motor neurons induced by sciatic nerve avulsion is apoptosis.

By light microscopy, chromatolysis and subsequent depletion of Nissl within injured motor neurons were prominent at 7–14 days postlesion.We propose that if motor neurons, which have undergone axotomy and deprivation of their major sustaining targets, cannot regain trophic support by reestablishing connectivity with muscle targets or interactions with supporting cells, then these injured neurons undergo apoptosis at about 7–14 days postlesion. Chromatolysis in axotomized motor neurons has been described thoroughly (Lieberman, 1971; Price and Porter, 1972; Torvik, 1976). However, chromatolysis does not necessarily foreshadow neuronal cell death after axotomy (Price and Porter, 1972), although specific signals during chromatolysis may be required to initiate apoptosis after axotomy. Chromatolysis following axotomy can be blocked or delayed when RNA synthesis is inhibited with actinomycin D (Torvik and Heding, 1969), thereby implicating activation of gene transcription and protein synthesis in the molecular signaling for this structural response. In the context of axotomy-induced neuronal apoptosis, this finding is important because some types of PCD can be prevented by inhibitors of RNA and protein synthesis (Sen, 1992). Thus, a regenerative–degenerative response continuum may exist after axotomy that begins as chromatolysis and evolves into either repair and survival of neurons or apoptosis of neurons.

The fate of injured motor neurons after axotomy may be determined in part by mitochondrial accumulation. In axotomized neurons destined to die apoptotically, the transition between chromatolysis and early apoptosis coincides with accumulation of metabolically active mitochondria within the perikaryon and oxidative stress (Al-Abdulla and Martin, 1998) (Fig. 7). This mitochondrial accumulation may result from an interruption in normal trafficking of mitochondria into damaged axons, as predicted by the aberrant accumulation of phosphorylated neurofilaments within the cell body and processes of motor neurons. It has been observed previously that axotomy and axonal ligation in peripheral and central nervous systems can cause accumulation of mitochondria within proximal axons and cell bodies of injured

neurons (Hartmann, 1954; Weiss and Pillai, 1965; Blümcke et al., 1966; Al-Abdulla and Martin, 1998). It has been known that the distance between the site of axonal trauma and the neuronal cell body affects the fate of axotomized neurons (Lieberman, 1971; Fry and Cowan, 1972). In this regard, distal axon transection would afford greater cytoplasmic volume and antioxidant capacity [e.g., glutathione, superoxide dismutase 1 (SOD1), and catalase] for perturbations in mitochondrial trafficking and free radical generation compared to proximal axon transection. It is possible that an abnormal accumulation of active mitochondria at perinuclear locations serves as a sensor for the severity of axonal injury and thus influences whether a neuron survives or undergoes apoptosis after axotomy.

Motor Neuron Apoptosis *In Vivo* Is Associated with Oxidative Stress

Mitochondria are thought to participate in the effector stage of apoptosis (Kroemer et al., 1995) through changes in Bcl-2 function in the outer mitochondrial membrane and antioxidant mechanisms (Hockenbery et al., 1993). The finding that oxidative stress induces neuronal apoptosis *in vitro* (Kroemer et al., 1995; Ratan et al., 1994) supports our idea that mitochondria may participate in the signaling of injured, chromatolytic motor neurons to enter apoptosis, possibly by releasing cytochrome c (Yang et al., 1997) or by generating excessive reactive oxygen species (ROS). Mitochondria generate the major source of superoxide (Boveris and Cadenas, 1997). If normal trafficking of these organelles into axonal and dendritic compartments is not reestablished or effectively buffered, a sustained accumulation of active mitochondria in the vicinity of the nucleus may provide a source for ROS or apoptotic protease activating factors. It has been suggested that hydroxyl radical production by microdialysis of hydroxyl radical generators can kill motor neurons in spinal cord (Liu et al., 1994). However, at present, it is uncertain whether mitochondrial-derived ROS can trigger apoptosis of motor neurons *in vivo*.

The present study is novel because our data implicate the formation ROS and oxidative damage to nucleic acids and proteins during motor neuron apoptosis in the adult CNS. Our experiments demonstrate for the first time the formation of hydroxyl radical-modified DNA and RNA as well as nitrotyrosine-modified proteins during the progression of motor neuron apoptosis in an *in vivo* setting. The formation of OHdG occurs as a product of oxidative injury to DNA by ROS (Kasai et al., 1984). Singlet oxygen (Devasagayam et al., 1991; Inoue and Kawanishi,

1995) as well as nitric oxide and superoxide (Inoue and Kawanishi, 1995) produce OHdG, the formation of which is inhibited by free radical scavengers (Inoue and Kawanishi, 1995). Among the ROS, hydroxyl radicals are highly reactive and are thought to be genotoxic by interacting with DNA and producing DNA strand breaks and base modifications (Kuchino et al., 1987; Fraga et al., 1990). Hydroxyl radicals are products of the transitional metal (e.g., iron)-catalyzed, Haber–Weiss- and Fenton-type reactions that use superoxide and hydrogen peroxide as substrates, respectively (Boveris and Cadenas, 1997). We found that OHdG immunoreactivity is formed within the nucleus of injured motor neurons at 4 to 7 days after avulsion prior to apoptosis. Cytoplasmic immunolabeling in a Nissl-like pattern was also observed with OHdG antibodies. The nuclear immunolabeling was competed with OHdG, and the cytoplasmic immunoreactivity was competed with hydroxyguanosine and guanosine. Furthermore, the nuclear and cytoplasmic immunoreactivities were abolished, respectively, by DNase and RNase. These experiments demonstrate that the antibodies used to detect OHdG can recognize hydoxyl-deoxyguanosine and hydroxyl-guanosine and also normal guanosine and thus detect hydroxyl radical-damaged DNA and RNA as well as normal RNA. A possible role of oxidative damage to RNA in apoptosis has not been suggested previously, but oxidative damage to DNA is known to induce apoptosis in neurons, possibly by mechanisms involving p53 (Wood and Youle, 1995). These observations suggest that hydroxyl radical-mediated damage to DNA and RNA may contribute to the mechanisms for motor neuron apoptosis in the adult CNS.

In addition, our results indicate that peroxynitrite radicals are formed in motor neurons early after avulsion at preapoptotic stages of degeneration, based on the transient detection of intense nitrotyrosine immunoreactivity within subsets of ventral root axons and motor neuron cell bodies. The appearance of this intense nitrotyrosine immunoreactivity occurred prior to structural evidence for apoptosis in avulsed motor neurons. Nitric oxide synthase is induced in motor neurons after avulsion (Wu , 1993) and in primary cultures of embryonic motor neurons deprived of brain-derived neurotrophic factor (Estévez et al., 1998). In this latter *in vitro* paradigm, motor neurons cultured in the absence of trophic factor exhibit nitrotyrosine immunoreactivity prior to the occurrence of apoptosis (Estévez et al., 1998), similar to our findings *in vivo*. Inhibition of nitric oxide synthase reduces motor neuron loss after spinal root avulsion (Wu and Li, 1993). Therefore, the accumulation of active mitochondria within neuronal cell bodies, com-

bined with nitric oxide induction (Wu , 1993), may lead to peroxynitrite formation and the induction of motor neuron apoptosis after avulsion.

Importance of This Animal Model of Motor Neuron Apoptosis to ALS

This particular model of target deprivation and axotomy in the CNS of adult rat was used to study the fate of mature spinal motor neurons undergoing retrograde neurodegeneration. These neurons die apoptotically. These results are important because no other animal model exists for studying motor neuron apoptosis in the adult CNS (Martin et al., 1998a,b), and because the degeneration of motor neurons in ALS appears to be a form of apoptosis, based on structural, biochemical, and molecular data (Martin, 1999). The degeneration of motor neurons in sporadic and familial ALS (Martin, 1999) is different structurally from the motor neuron degeneration found in transgenic mice overexpressing the familial ALS mutant forms of SOD1 (Dal Canto and Gurney, 1994). Neither morphological nor biochemical evidence for apoptotic death of motor neurons has been shown in SOD1 transgenic mouse models of ALS. Although the survival of mutant SOD1 mice is prolonged when crossed with mice overexpressing Bcl-2 (Kostic et al., 1997) or a dominant negative inhibitor of caspase-1 (Friedlander et al., 1997), the degeneration of motor neurons is not prevented (Kostic et al., 1997), suggesting that neuronal degeneration in this mouse model of motor neuron degeneration may not be apoptosis controlled by PCD mechanisms. Instead of apoptosis, the vacuolar degeneration of motor neurons in mice harboring SOD1 mutations more closely resembles excitotoxic neurodegeneration (Ikonomidou et al., 1996; Portera-Cailliau et al., 1997a; Ginsberg et al., 1999) or transsynaptic neuronal injury in response to deafferentation (Ginsberg and Martin, 1998; Ginsberg et al., 1999). Interestingly, the degeneration of motor neurons in individuals with ALS is different structurally from the excitotoxic neurodegeneration *in vivo* caused by acute activation of NMDA and non-NMDA glutamate receptors in the mature CNS and by cerebral ischemia (Martin et al., 1998b; Portera-Cailliau et al., 1997a; Ikonomidou et al., 1996; Ginsberg et al., 1999). We conclude that the motor neuron degeneration in ALS most closely resembles neuronal apoptosis induced by target deprivation/axotomy in the mature CNS.

Conclusions

Sciatic nerve avulsion in the adult rat causes apoptosis of motor neurons. The cellular changes that occur during this process progress from chromatolysis through consecutive stages associated with apoptosis. Motor neuron apoptosis involves oxidative damage to nucleic acids and protein. This oxidative stress evolves early in association with the accumulation of metabolically active mitochondria within the perikaryon of axotomized, apoptotically dying neurons. This model system will be useful for analyzing the molecular mechanisms for motor neuron death in the adult CNS and can thereby provide important information toward the understanding of motor neuron apoptosis in ALS (Martin, 1999).

REFERENCES

Al-Abdulla NA, Portera-Cailliau C, Martin LJ. 1998. Occipital cortex ablation in adult rat causes retrograde neuronal death in the lateral geniculate nucleus that resembles apoptosis. Neuroscience 86:191–209.

Al-Abdulla NA, Martin LJ. 1998. Apoptosis of retrogradely degenerating neurons occurs in association with the accumulation of perikaryal mitochondria and oxidative damage to the nucleus. Am J Pathol 153:447–456.

Blümcke S, Neidorf HR, Rode J. 1966. Axoplasmic alterations in the proximal and distal stumps of transsected nerves. Acta Neuropathol 7:44–61.

Boveris A, Cadenas E. 1997. Cellular sources and steady-state levels of reactive oxygen species. In: Biadasz Clerch L, Massaro DJ, editors. Oxygen, gene expression, and cellular function. New York: Marcel Dekker. p 1–25.

Chu-Wang I-W, Oppenheim RW. 1978. Cell death of motoneurons in the chick embryo spinal cord. I. A light and electron microscopic study of naturally occurring and induced cell loss during development. J Comp Neurol 177:33–58.

Clarke PGH. 1990. Developmental cell death: morphological diversity and multiple mechanisms. Anat Embryol 181:195–213.

Conradi S. 1969. Ultrastructure of dorsal root boutons on lumbosacral motoneurons of the adult cat as revealed by dorsal root section. Acta Physiol Scand 332(Suppl):85–115.

Cork LC, Troncoso JC, Klavano GG, Johnsen ES, Sternberger LA, Sternberger NH, Price DL. 1988. Neurofilamentous abnormalities in motor neurons in spontaneously occurring animal disorders. J Neuropathol Exp Neurol 47:420–431.

Dal Canto MC, Gurney ME. 1994. Development of central nervous system pathology in a murine transgenic model of human amyotrophic lateral sclerosis. Am J Pathol 145:1271–1280.

Deshmukh M, Vasilakos J, Deckwerth TL, Lampe PA,

Shivers BD, Johnson EM. 1996. Genetic and metabolic status of NGF-deprived sympathetic neurons saved by an inhibitor of ICE family proteases. J Cell Biol 135:1341–1354.

Devasagayam TPA, Steenken S, Obendorf MSW, Schultz WA, Sies H. 1991. Formation of 8-hydroxy(deoxy)-guanosine and generation of strand breaks at guanine residues in DNA by singlet oxygen. Biochemistry 30:6283–6289.

Estévez AG, Spear N, Manuel SM, Radi R, Henderson CE, Barbeito L, Beckman JS. 1998. Nitric oxide and superoxide contribute to motor neuron apoptosis induced by trophic factor deprivation. J Neurosci 18:923–931.

Fraga CG, Shigenaga MK, Park J-W, Degan P, Ames BN. 1990. Oxidative damage to DNA during aging: 8-hydroxy-2′-deoxyguanosine in rat organ DNA and urine. Proc Natl Acad Sci USA 87:4533–4537.

Friedlander RM, Brown RH, Gagliardini V, Wang J, Juan, J. 1997. Inhibition of ICE slows ALS in mice. Nature 388:31.

Fry FJ, Cowan WM. 1972. A study of retrograde cell degeneration in the lateral mammillary nucleus of the cat, with special reference to the role of axonal branching in the preservation of the cell. J Comp Neurol 144:1–24.

Gavrieli Y, Sherman Y, Ben-Sasson SA. 1992. Identification of programmed cell death in situ via specific labeling of nuclear DNA fragmentation. J Cell Biol 119:493–501.

Gerschenson LE, Rotello RJ. 1992. Apoptosis: a different type of cell death. FASEB J 6:2450–2455.

Ginsberg SD, Martin LJ. 1998. Ultrastructural analysis of the progression of neurodegeneration in the septum following fimbria-fornix transection. Neuroscience 86:1259–1272.

Ginsberg SD, Portera-Cailliau C, Martin LJ. 1999. Fimbria-fornix transection and excitotoxicity produce similar neurodegeneration in the septum. Neuroscience 88:1059–1071.

Hamburger V. 1975. Cell death in the development of the lateral motor column of the chick embryo. J Comp Neurol 160:535–546.

Hartmann JF. 1954. Electron microscopy of motor nerve cells following section of axones. Anat Rec 118:19–33.

Hockenbery DM, Oltavi ZN, Yin X-M, Milliman CL, Korsmeyer SL. 1993. Bcl-2 functions in an antioxidant pathway to prevent apoptosis. Cell 75:241–252.

Ikonomidou C, Qin YQ, Labruyere J, Olney, JW. 1996. Motor neuron degeneration induced by excitotoxin agonists has features in common with those seen in the SOD-1 transgenic mouse model of amyotrophic lateral sclerosis. J Neuropathol Exp Neurol 55:211–224.

Inoue S, Kawanishi S. 1995. Oxidative DNA damage induced by simultaneous generation of nitric oxide and superoxide. FEBS Lett 371:86–88.

Kasai H, Nishimura S. 1984. Hydroxylation of deoxyguanosine at the C-8 position by ascorbic acid and other reducing agents. Nucleic Acids Res 12:2137–2145.

Kerr JFR, Harmon BV. 1991. Definition and incidence of apoptosis: an historical perspective. In: Tomei LD, Cope FO, editors. Apoptosis: the molecular basis of cell death. Cold Spring Harbor, NY: Cold Spring Harbor Laboratory Press. p 5–29.

Koliatsos VE, Price WL, Pardo CA, Price DL. 1994. Ventral root avulsion: an experimental model of death of adult motor neurons. J Comp Neurol 342:35–44.

Kostic V, Jackson-Lewis V, de Bilbao F, Dubois-Dauphin M, Przedborski S. 1997. Bcl-2: prolonging life in a transgenic mouse model of familial amyotrophic lateral sclerosis. Science 277:559–562.

Kroemer G, Petit P, Zamzami N, Vayssière J-L, Mignotte B. 1995. The biochemistry of programmed cell death. FASEB J 9:1277–1287.

Kuchino Y, Mori F, Kasai H, Inoue H, Iwai S, Miura K, Ohtsuka E, Nishimura S. 1987. Misreading of DNA templates containing 8-hydroxydeoxyguanosine at the modified base and at adjacent residues. Nature 327:77–79.

Li L, Wu W, Lin LF, Oppenheim RW, Houenou LJ. 1995. Rescue of adult mouse motoneurons from injury-induced cell death by glial cell line-derived neurotrophic factor. Proc Natl Acad Sci USA 92:9771–9775.

Li L, Houenou LJ, Wu W, Lei M, Prevette DM, Oppenheim RW. 1998. Characterization of spinal motoneuron degeneration following different types of peripheral nerve injury in neonatal and adult mice. J Comp Neurol 396:158–168.

Lieberman AR. 1971. The axon reaction: a review of the principal features of perikaryal responses to axon injury. Int Rev Neurobiol 14:49–124.

Liu D, Yang R, Yan X, McAdoo DJ. 1994. Hydroxyl radicals generated in vivo kill neurons in the rat spinal cord: electrophysiological, histological, and neurochemical results. J Neurochem 62:37–44.

Lowrie MB, Vrbová G. 1992. Dependence of postnatal motoneurones on their targets: review and hypothesis. Trends Neurosci 15:80–84.

Manetto V, Sternberger NH, Perry G, Sternberger LA, Gambetti P. 1988. Phosphorylation of neurofilaments is altered in amyotrophic lateral sclerosis. J Neuropathol Exp Neurol 47:642–653.

Martin LJ. 1999. Neuronal death in amyotrophic lateral sclerosis is apoptosis: possible contribution of a programmed cell death mechanism. J Neuropathol Exp Neurol 58:459–471.

Martin LJ, Portera-Cailliau C, Ginsberg SD, Al-Abdulla NA. 1998a. Animal models and degenerative disorders of the human brain. Lab Animal 27:18–25.

Martin LJ, Al-Abdulla NA, Brambrink AM, Kirsch JR, Sieber FE, Portera-Cailliau C. 1998b. Neurodegeneration in excitotoxicity, global cerebral ischemia, and target deprivation: a perspective on the contributions of apoptosis and necrosis. Brain Res Bull 46:281–309.

McLaughlin B. 1972. Dorsal root projections to the motor nuclei in the cat spinal cord. J Comp Neurol 144:429–460.

Milligan CE, Prevette D, Yaginuma H, Homma S, Cardwell C, Fritz LC, Tomaselli KJ, Oppenheim RW, Schwartz LM. 1995. Peptide inhibitors of the ICE protease family

arrest programmed cell death of motoneurons in vivo and in vitro. Neuron 15:385–393.

Munoz DG, Greene C, Perl DP, Selkoe DJ. 1988. Accumulation of phosphorylated neurofilaments in anterior horn motor neurons of amyotrophic lateral sclerosis. J Neuropathol Exp Neurol 47:9–18.

Nicolopoulos-Stournaras S, Iles JF. 1983. Motor neuron columns in the lumbar spinal cord of the rat. J Comp Neurol 217:75–85.

Novikov L, Novikova L, Kellerth J-O. 1995. Brain-derived neurotrophic factor promotes survival and blocks nitric oxide synthase expression in adult rat spinal motoneurons after ventral root avulsion. Neurosci Lett 200:45–48.

Novikov L, Novikova L, Kellerth J-O. 1997. Brain-derived neurotrophic factor promotes axonal regeneration and long-term survival of adult rat spinal motoneurons *in vivo*. Neuroscience 79:765–774.

Pittman RN, Wang S, DiBenedetto AJ, Mills JC. 1993. A system for characterizing cellular and molecular events in programmed neuronal cell death. J Neurosci 13:3669–3680.

Portera-Cailliau C, Price DL, Martin LJ. 1997a. Non-NMDA and NMDA receptor-mediated excitotoxic neuronal deaths in adult brain are morphologically distinct: further evidence for an apoptosis-necrosis continuum. J Comp Neurol 378:88–104.

Portera-Cailliau C, Price DL, Martin LJ. 1997b. Excitotoxic neuronal death in the immature brain is an apoptosis-necrosis morphological continuum. J Comp Neurol 378:70–87.

Price DL, Martin LJ, Clatterbuck RE, Koliatsos VE, Sisodia SS, Walker LC, Cork LC. 1992. Neuronal degeneration in human diseases and animal models. J Neurobiol 23:1277–1294.

Price DL, Porter KR. 1972. The response of ventral horn neurons to axonal transection. J Cell Biol 53:24–37.

Ramón y Cajal S. 1928. Degeneration and regeneration of the nervous system. New York: Oxford University Press 769 p.

Ratan RR, Murphy TH, Baraban JM. 1994. Oxidative stress induces apoptosis in embryonic cortical neurons. J Neurochem 62:376–379.

Romanes GJ. 1946. Motor localization and the effects of nerve injury on the ventral horn cells of the spinal cord. J Anat 80:117–131.

Sen S. 1992. Programmed cell death: concept, mechanism and control. Biol Rev 67:287–319.

Torvik A. 1976. Central chromatolysis and the axon reaction: a reappraisal. Neuropathol Appl Neurobiol 2:423–432.

Torvik A, Heding A. 1969. Effect of actinomycin D on retrograde nerve cell reaction: further observations. Acta Neuropathol 14:62–71.

Weiss P, Pillai A. 1965. Convection and fate of mitochondria in nerve fibers: axonal flow as vehicle. Proc Natl Acad Sci USA 54:48–56.

Wong-Riley MTT. 1979. Changes in the visual system of monocularly sutured or enucleated cats demonstrable with cytochrome oxidase histochemistry. Brain Res 171:11–28.

Wood KA, Youle RJ. 1995. The role of free radicals and p53 in neuron apoptosis *in vivo*. J Neurosci 15:5851–5857.

Wu W. 1993. Expression of nitric oxide synthase (NOS) in injured CNS neurons as shown by NADPH diaphorase histochemistry. Exp Neurol 120:153–159.

Wu W, Li L. 1993. Inhibition of nitric oxide synthase reduces motoneuron death due to spinal root avulsion. Neurosci Lett 153:121–124.

Yang J, Liu X, Bhalla K, Kim CN, Ibrado AM, Cai J, Peng T-I, Jones DP, Wang X. 1997. Prevention of apoptosis by bcl-2: release of cytochrome c from mitochondria blocked. Science 275, 1129–1132.

Lee J. Martin, Ph.D.
DAMD17-99-1-9553

Appendix

Apoptosis and Necrosis Occur in Separate Neuronal Populations in Hippocampus and Cerebellum After Ischemia and Are Associated With Differential Alterations in Metabotropic Glutamate Receptor Signaling Pathways

*†Lee J. Martin, ‡Frederick E. Sieber, and ‡Richard J. Traystman

*Departments of *Pathology (Division of Neuropathology), †Neuroscience, and ‡Anesthesiology/Critical Care Medicine, Johns Hopkins University School of Medicine, Baltimore, Maryland, U.S.A.*

Summary: It was evaluated whether postischemic neurodegeneration is apoptosis and occurs with alterations in phosphoinositide-linked metabotropic glutamate receptors (mGluRs) and their associated signaling pathways. A dog model of transient global incomplete cerebral ischemia was used. The CA1 pyramidal cells and cerebellar Purkinje cells underwent progressive delayed degeneration. By *in situ* end-labeling of DNA, death of CA1 and Purkinje cells was greater at 7 days than 1 day after ischemia, whereas death of granule neurons in dentate gyrus and cerebellar cortex was greater at 1 than at 7 days. Ultrastructurally, degenerating CA1 pyramidal neurons and cerebellar Purkinje cells were necrotic; in contrast, degenerating granule neurons were apoptotic. In agarose gels of regional DNA extracts, random DNA fragmentation coexisted with internucleosomal fragmentation. By immunoblotting of regional homogenates, mGluR1α, mGluR5, phospholipase Cβ (PLCβ), and G$\alpha_{q/11}$ protein levels in hippocampus at 1 and 7 days after ischemia were similar to control levels, but in cerebellar cortex, mGluR1α and mGluR5 were decreased but PLCβ was increased. By immunocytochemistry, mGluR and PLCβ immunoreactivity dissipated in CA1 and cerebellar Purkinje cell/molecular layers, whereas immunoreactivities for these proteins were enhanced in granule neurons. It was concluded that neuronal death after global ischemia exists as two distinct, temporally overlapping forms in hippocampus and cerebellum: necrosis of pyramidal neurons and Purkinje cells and apoptosis of granule neurons. Neuronal necrosis is associated with a loss of phosphoinositide-linked mGluR transduction proteins, whereas neuronal apoptosis occurs with increased mGluR signaling. **Key Words:** Bax—Excitotoxicity—Glutamate receptors—Granule neuron—Phospholipase C—Programmed cell death.

The mechanisms for delayed neuronal death (DND) after global cerebral ischemia in the adult CNS are not understood. Structurally and mechanistically, cellular degeneration resulting from hypoxia–ischemia has been thought to be a form of necrosis (Laiho and Trump, 1975; Wyllie et al., 1980; Kerr and Harmon, 1991; Deshpande et al., 1992); but recently postischemic DND has been considered to be a form of apoptosis mediated by programmed cell death (PCD) mechanisms (Héron et al., 1993; MacManus et al., 1995; Nitatori et al., 1995; Krajewski et al., 1995). However, the idea that selectively vulnerable neurons undergo apoptosis after ischemia is very controversial (Deshpande et al., 1992; Martin et al., 1998; Ishimaru et al., 1999), although ischemic DND might be more easily classified according to the concept of the apoptosis–necrosis continuum (MacManus et al., 1995; Portera-Cailliau et al., 1997a,b). The accurate identification of the contributions of apoptosis and necrosis to neuronal death in the adult central nervous system after ischemia has very important therapeutic relevance.

Neuronal cell death after ischemia involves perturbations in intracellular Ca^{2+} homeostasis and impairments in protein synthesis, possibly resulting from excitotoxic activation of neuronal glutamate receptors (GluRs)

(Diemer et al., 1993). The GluRs that modulate intracellular Ca^{2+} levels within neurons are the ion channel receptors [*N*-methyl-*D*-aspartate (NMDA) and α-amino-3-hydroxy-5-methyl-4-isoxazole propionate receptors] and the G protein-coupled, phosphoinositide-linked metabotropic GluRs (mGluRs) (Nakanishi, 1992). Within the central nervous system, excitotoxic activation of GluRs delineates an apoptosis–necrosis continuum for neuronal death in which the structure of neuronal degeneration is influenced by the subtype of GluR that is activated (Portera-Cailliau et al., 1997*a,b*). A possible role for excessive activation of GluRs in the mechanisms for postischemic DND is supported by studies showing that blockade of α-amino-3-hydroxy-5-methyl-4-isoxazole propionate receptors is neuroprotective after forebrain ischemia in adult rodents (Sheardown et al., 1990), that abnormalities in phosphoinositide signaling pathways occur in hippocampus after ischemia (Kirino et al., 1992), and that mGluR antagonists are neuroprotective in *in vitro* hippocampal slice models of hypoxia–hypoglycemia (Opitz et al., 1995) and *in vivo* models of excitotoxicity and transient global ischemia (Bruno et al., 1999).

Some forms of PCD are Ca^{2+} dependent (Sen, 1992), and activation of mGluRs and heterotrimeric GTP-binding proteins (G proteins) can regulate neuronal apoptosis *in vitro* (Copani et al., 1995; Yan et al., 1995). Therefore, we evaluated whether ischemic DND is apoptosis structurally and whether DND is possibly associated mechanistically with abnormalities in phosphoinositide-linked mGluRs and their downstream intracellular signal transduction proteins, including the functionally coupled G proteins and phospholipase C (PLC). Thus, the goal of this study was to provide insight into the possible contribution of apoptosis to neurodegeneration after ischemia and the possible molecular mechanisms for this DND.

METHODS

Model of ischemia

A model of temporary global incomplete cerebral ischemia in dogs was used (Sieber et al., 1995). All animal procedures were conducted in accordance with the *NIH Guide for the Care and Use of Laboratory Animals*, and protocols were approved by the institutional animal care and use committee. Under sterile conditions, anesthetized (1 to 2% inspired halothane), mechanically ventilated, normothermic (epidural temperature at 37 to 38°C), adult beagles (n = 20) were subjected to transient incomplete global cerebral ischemia by intraventricular infusion of prewarmed sterile artificial cerebrospinal fluid into the lateral ventricle, producing an intracranial pressure of 10 mm Hg below mean arterial blood pressure (Sieber et al., 1995). The intracranial pressure was maintained, keeping cerebral perfusion pressure constant at 10 mm Hg for 20 minutes. To start reperfusion, the cerebrospinal fluid pressure reservoir was disconnected, and intracranial pressure was allowed to normalize. Six dogs were used as nonischemic sham controls.

Neuropathology, TUNEL, and electron microscopy

To evaluate neuropathology, sham control dogs (n = 3) and ischemic dogs surviving for 1 day (n = 5) or 7 days (n = 9) were anesthetized with pentobarbital, vasodilated with sodium nitrite, anticoagulated with heparin, and perfused intraaortically with phosphate-buffered saline followed by a mixture of 4% paraformaldehyde and 0.5% glutaraldehyde. The brains were divided midsagittally, and each hemisphere was cut into 1-cm-thick coronal slabs. In this model of ischemia, neuronal damage is similar bilaterally (Sieber et al., 1995). From the left hemisphere, samples of midhippocampus (containing the septal and temporal hippocampus) and cerebellum (at the level of the vermis) were used for paraffin histology. For quantification of postischemic neurodegeneration in hippocampus and cerebellar cortex (Fig. 1), sections (10 μm thick) were stained with hematoxylin and eosin or the terminal transferase-mediated biotin-dUTP nick end-labeling (TUNEL) method for *in situ* detection of nuclear DNA fragmentation as described (Portera-Cailliau et al., 1997*a,b*; Martin et al., 1997*a*; Al-Abdulla et al., 1998). The TUNEL method was used to identify dying cells after ischemia, although this technique is not specific for apoptosis (Martin et al., 1998).

Profile counting was used to estimate ischemic neuronal damage in hematoxylin and eosin-stained sections in the stratum pyramidale of CA1 (in six microscopic fields at 600×; see Fig. 1A) and in the Purkinje cell layer of the anterior vermis of cerebellar cortex (in four microscopic fields at 400×; see Fig. 1B). Because Purkinje cells are arranged in only a single layer (Fig. 1B), the cerebellar sections were counted at a lower magnification so that a greater number of Purkinje cell could be analyzed per microscopic field. The percentage of neurons with ischemic cytopathology was determined using as criteria microvacuolar change within the soma, peripheralization of Nissl substance, nuclear pyknosis, perinuclear eosinophilia, or perikaryal shrinkage with cytoplasmic eosinophilia (Sieber et al., 1995; Martin et al., 1997*a,b*, 1998). The percentage neuronal damage was estimated by identifying the fraction of neurons with ischemic cytopathology relative to the total number of neurons in microscopic fields of the CA1 and cerebellar cortex. The percentage neuronal damage in each region was averaged for each animal, and a group mean was calculated. The number of neurons per square millimeter was calculated for each region in control and ischemic dogs, and the percentage of remaining neurons following ischemia was calculated. Neuropathology scores between groups and regions at each time point were analyzed using the Mann–Whitney test.

In TUNEL preparations counterstained with cresyl violet, the densities of cells showing DNA fragmentation were determined by counting TUNEL-positive nuclei in six microscopic fields at 1,000× in the stratum pyramidale of CA1 and CA2–superior CA3, the granule cell layer of the dentate gyrus, and the Purkinje cell and granule cell layers of cerebellar cortex (Fig. 1). The TUNEL sections were counted at 1,000× so that TUNEL-positive nuclei could be easily identified and the type of cell could be recognized. The number of TUNEL-positive cells per square millimeter in each region was averaged for each animal, and a group mean was calculated. The TUNEL scores between groups and regions at each time point were analyzed using the Mann–Whitney test.

To determine whether DND has the structure of apoptosis, necrosis, or a hybrid form of degeneration, samples (3 mm³) of hippocampus and cerebellar cortex from the left hemisphere were osmicated immediately, embedded in plastic, and evaluated by electron microscopy. Ischemic DND was evaluated using ultrastructural criteria described previously in models of
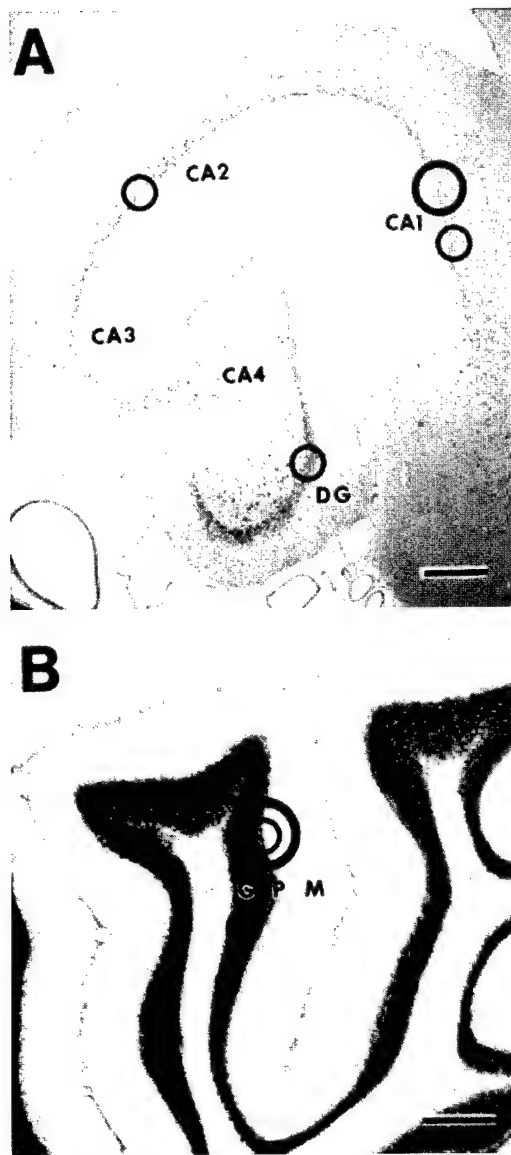
FIG. 1. Locations in hippocampus **(A)** and cerebellar cortex **(B)** where cell counts were made in hematoxylin and eosin and terminal transferase-mediated biotin-dUTP nick end-labeling (TUNEL) sections. CA1–CA4, Ammon's horn subfields 1 to 4; DG, dentate gyrus; m, molecular layer; p, Purkinje cell layer; g, granule cell layer. Bars = 12 mm. Circles with three different diameters are shown. The smallest circle (shown in A and B) corresponds to the 1,000× microscopic fields in which the counts of TUNEL-positive cells were made in CA1, CA2 and CA3, and dentate gyrus of hippocampus and in the granule cell and Purkinje cells layers of cerebellar cortex. This magnification was used to best identify TUNEL labeling in the nucleus. The intermediate circle (shown in A), corresponding to the 600× magnification fields, was used to determine in larger sample sizes the neuronal density and percentage neuronal damage in CA1. The largest circle (shown in B), corresponding to the 400× magnification fields, was used to determine the neuronal density and percentage neuronal damage in the Purkinje cell layer. For this purpose, a larger microscopic field (i.e., lower magnification) was used so that a greater number of Purkinje cells per field could be analyzed.

unequivocal neuronal apoptosis (Portera-Cailliau et al., 1997*a,b*; Al-Abdulla et al., 1998; Martin et al., 1998, 1999).

DNA isolation and agarose gel electrophoresis

Because the TUNEL method identifies DNA fragmentation independent of mechanisms (Portera-Cailliau et al., 1997*b*; Martin et al., 1998), we evaluated regional neuropathology based on DNA fragmentation patterns in agarose gels. Genomic DNA was isolated from samples of hippocampus (septal and temporal) and cerebellar cortex from control dogs (n = 2) and dogs at 1 day (n = 2) and 7 days (n = 2) after ischemia. Two additional animals were killed at 6 hours after ischemia. Tissue samples were homogenized in DNA extraction buffer containing 10 mmol/L Tris (pH 7.4), 10 mmol/L NaCl, 25 mmol/L ethylenediaminetetraacetate, 1% sodium dodecyl sulfate, and 1 mg/ml proteinase K and incubated in the same buffer overnight at 37°C. DNA was extracted with an equal volume of salt-saturated phenol/chloroform/isoamyl alcohol (10:10:1), and the recovered aqueous phase was extracted with diethyl ether. The DNA was precipitated with ethanol (2.5 volumes). The DNA pellet was dissolved in 0.1× saline–sodium citrate and incubated (37°C) with DNase-free RNase A (0.1 mg/mL) for 1 hour and then overnight (37°C) with 0.1 mg/mL proteinase K. DNA was reextracted, precipitated, and dissolved in Tris/ethylenediaminetetraacetate buffer. The DNA samples (~1.0 μg) were 3′ end-labeled with digoxigenin-11-dideoxy-uridine-5′-triphosphate using terminal transferase (Boehringer-Mannheim, Indianapolis, IN, U.S.A.), precipitated, resuspended in Tris/ethylenediaminetetraacetate buffer, fractionated by agarose gel (1.2%) electrophoresis, and transferred to nylon membrane followed by ultraviolet cross-linking. Membranes were incubated in 2% nucleic acid blocking reagent (Boehringer-Mannheim) and then in blocking reagent containing 75 mU/mL antidigoxigenin Fab fragments conjugated to alkaline phosphatase (Boehringer-Mannheim). After washing, membranes were reacted with chemiluminescent substrate for alkaline phosphatase detection reagent (Boehringer-Mannheim) and exposed to Kodak X-OMAT film to visualize DNA.

Immunoblotting

To evaluate possible mechanisms for DND, we studied by immunoblotting the expression of the proapoptotic protein Bax as well as mGluRs and their related intracellular signaling proteins. We focused on mGluR1 and mGluR5 because these receptors are G protein–coupled receptors that operate through heterotrimeric GTP-binding proteins and PLC activation, which regulates intracellular Ca^{2+} by phosphoinositide hydrolysis (Tanabe et al., 1992; Pin and Duvoisin, 1995). Activation of phosphoinositide-linked mGluRs initiates a cascade of events including the activation of PLCβ by G_q proteins, generation of inositol triphosphate and diacylglycerol, and subsequent mobilization of Ca^{2+} from nonmitochondrial intracellular stores (Pin and Duvoisin, 1995). Control dogs (n = 3) and ischemic dogs at 1 day (n = 2) and 7 days (n = 2) of recovery were anesthetized with pentobarbital, ventilated, and exsanguinated by intraaortic perfusion of ice-cold phosphate-buffered saline. The brains were quickly removed from the skull and placed on ice, and the hippocampus (septal) and anterior lobule of the cerebellum were isolated and frozen in isopentane. The samples were homogenized and subjected to differential centrifugation (Portera-Cailliau et al., 1996), and subcellular fractions were assayed for protein concentration using a Bio-Rad (Hercules, CA, U.S.A.) detection method. For immunoblotting, mitochondria-enriched membrane fractions or synaptic plasma membrane fractions (10, 12, or 15 μg of protein) were subjected to sodium dodecyl sulfate polyacrylamide gel electro-

phoresis (8, 10, or 15% gels) and transferred to nitrocellulose membrane by electroblotting (Martin et al., 1992, 1997a). Samples of control and ischemic dogs were always run in the same gel. To ensure that equivalent amounts of protein were loaded in each lane and that transfer was comparable, membranes were stained with Ponceau S before immunoblotting. Blots were then blocked with 2.5% nonfat dry milk with 0.1% Tween 20 in 50 mmol/L Tris-buffered saline (pH 7.4) and incubated overnight at 4°C with antibodies to mGluR1α, mGluR5, PLCβ₁, or Gα$_{q/11}$. Affinity-purified rabbit polyclonal antibodies to the C-terminal domains of mGluR1α and mGluR5 were used at a concentration of 0.5 μg IgG/mL (Martin et al., 1992; Blue et al., 1997). Affinity-purified antipeptide rabbit polyclonal antibodies to PLCβ₁ and Gα$_{q/11}$ were obtained from commercial sources (Santa Cruz Biotechnology, Santa Cruz, CA, U.S.A.) and were used at concentrations of 33 or 20 ng IgG/mL, respectively. In the same samples, the levels of proapoptotic protein Bax were measured, using commercial antibodies (Santa Cruz Biotechnology) at 150 ng IgG/mL, to evaluate whether changes in mGluR signaling proteins are associated with alterations in cell death protein levels. After the primary antibody incubation, membranes were washed and incubated with peroxidase-conjugated secondary goat anti-rabbit IgG (0.2 μg/mL) for 1 hour and developed with enhanced chemiluminescence (Amersham, Piscataway, NJ, U.S.A.). All blots were then reprobed with synaptophysin antibody (Boehringer-Mannheim) for a quantitative loading control.

Western blots were quantified densitometrically to evaluate brain regional changes in the levels of these proteins in postischemic animals relative to controls. Films were scanned using a Macintosh Adobe Photoshop program and an Agfa Arcus Plus scanner (Ridgefield Park, NJ, U.S.A.). Densitometric analysis was performed using Signal Analytics IP Lab Gel software (Scanalytics, Fairfax, VA, U.S.A.). Protein levels were expressed as relative optical density measurements, determined by comparing the density and area of the immunoreactive band in each lane scanned with control lanes in the same blot. The relative values for each animal were replicated in at least four immunoblotting experiments. Bax protein levels and signal transduction protein levels were expressed as percentages of control values. Mean percentages were compared among the recovery groups by a Wilcoxon signed rank test with the significance level set at $P < 0.05$.

Immunocytochemistry

From perfusion-fixed dogs (same as those used for hematoxylin and eosin staining and TUNEL), the right hemisphere was cut into 1-cm-thick coronal slabs, cryoprotected in 20% phosphate-buffered glycerol, and frozen in isopentane. Forebrain and cerebellar samples were cut at 40 μm on a sliding microtome, and sections were placed in antifreeze buffer for storage (−20°C) until immunocytochemical processing. A peroxidase antiperoxidase method (Martin et al., 1992; Fotuhi et

al., 1993) was used to detect mGluR1α, mGluR5, and PLCβ₁ immunoreactivities in hippocampus and cerebellar cortex of sham and ischemic dogs. The polyclonal antibodies to Bax were not used for immunocytochemical experiments because they recognize several proteins in addition to the proteins at 21 and 23 kDa. Affinity-purified goat anti-rabbit IgG F(ab)₂ fragments (Cappel, West Chester, PA, U.S.A.) were used as secondary antibodies. Immunoreactivity was visualized with diaminobenzidene as chromogen. At least four sections from each brain region from each dog in each experimental group were processed concurrently using the same batches of reagents to obviate tissue section variability in antigen localization. Immunocytochemical negative controls included omission of primary antibodies and competition of antibodies with synthetic peptides corresponding to the antigenic C-terminal domains of mGluR1α, mGluR5, and PLCβ₁.

RESULTS

Twenty dogs were subjected to 20 minutes of global incomplete cerebral ischemia. All dogs had similar severities of ischemia and were similar to those described previously (Sieber et al., 1995). Epidural temperature during ischemia was maintained at normothermic values. No ischemic dogs were eliminated from the study, and all dogs recovered for the designated survival time after ischemia.

CA1 pyramidal neuron and Purkinje cell degeneration overlaps with granule neuron death after global ischemia

The neuronal damage after transient global incomplete ischemia was progressive, as evidenced by the delayed reduction in neuronal density and the greater amount of ischemic cytopathology in neurons at 7 than at 1 day after ischemia (Table 1). At 1 day after ischemia, CA1 pyramidal neuron and cerebellar Purkinje cell densities were not significantly different from control values (Table 1). At 7 days after ischemia, 43% of CA1 pyramidal cells remained, while Purkinje cell densities were 78% of control (Table 1). The percentage of CA1 pyramidal neurons with ischemic cytopathology increased from 13% at 1 day of recovery to 52% at 7 days of recovery (Table 1). In cerebellum, the percentage of Purkinje cells with cytopathology was 24% at 1 day and 69% at 7 days after ischemia (Table 1). In hematoxylin and eosin sections of control animals, background neuronal injury (possibly due to the anesthesia, perfusion–

TABLE 1. *Neuropathology in dog hippocampus and cerebellum after global incomplete ischemia*

	CA1 neurons			Cerebellar Purkinje cells		
	Control	1 Day	7 Day	Control	1 Day	7 Day
% Neurons remaining	100 ± 2	97 ± 10	43 ± 10†	100 ± 8	82 ± 16	78 ± 16
% Neurons damaged	2 ± 1	13 ± 10*	52 ± 10†	3 ± 2	24 ± 11*	69 ± 6†

Values are mean ± SD. The percent neurons remaining is percent of baseline control. The percent neurons damaged is the percent of remaining neurons with ischemic cytopathology.
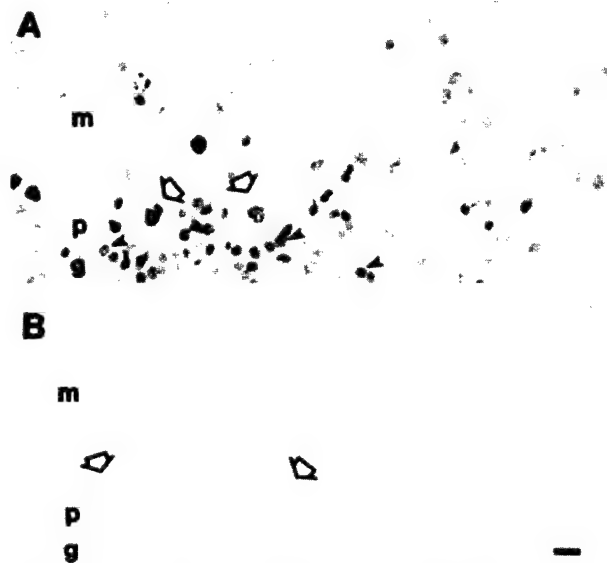* Significantly different from control ($P < 0.05$).
† Significantly different from control and 1 day ($P < 0.05$, Mann-Whitney test).

fixation, brain compression during removal from the skull, or histological processing) was ≤3% in CA1 and cerebellum (Table 1).
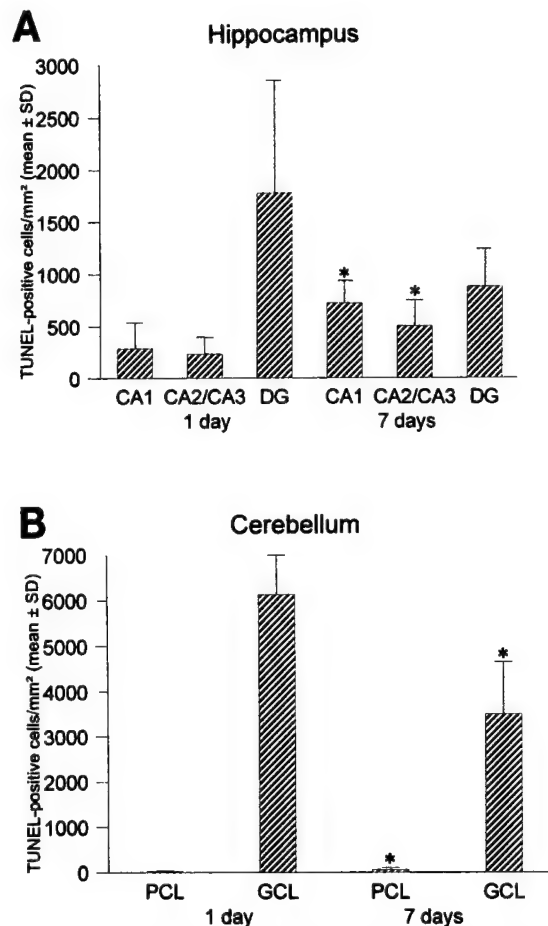
Neurons in hippocampus and cerebellar cortex were undergoing nuclear DNA fragmentation at 1 and 7 days after ischemia, as determined by TUNEL (Figs. 2 and 3). In hippocampus, subsets of neurons in the pyramidal cell layer of CA1 and CA2–superior CA3 (CA3a) were TUNEL-positive as well as subsets of granule neurons in the hippocampal dentate gyrus. In CA1, the number of TUNEL-positive cells/mm^2 was significantly greater ($P < 0.05$) at 7 than at 1 day, whereas more dentate gyrus granule neurons were TUNEL-positive at 1 than at 7 days (Fig. 3). In cerebellar cortex, the number of TUNEL-positive Purkinje cells at 7 days after ischemia was approximately twofold higher than at 1 day, whereas TUNEL-positive cells in the granule cell layer were nearly twofold higher at 1 than at 7 days (Fig. 3).

In pyramidal neurons of hippocampus and in Purkinje cells, the TUNEL-positive nuclei usually had reaction product that was random in distribution, with irregularly shaped aggregates, or had uniform and nonaggregated labeling, unlike the organized spherical clumping or crescentic capping of chromatin that was found in granule neurons (Figs. 2A and 5F–5H) and is characteristic of neuronal apoptosis (Portera-Cailliau et al., 1997a,b; Al-Abdulla et al., 1998; Martin et al., 1999).

In agarose gels, random (smearing) and internucleo-

FIG. 3. Quantification of terminal transferase-mediated nick end-labeling (TUNEL)-positive cells in hippocampus **(A)** and cerebellum **(B)** at 1 and 7 days after ischemia. Cresyl violet-counterstained TUNEL preparations were used to count TUNEL-positive cells in CA1, CA2–superior CA3 (CA3a), and dentate gyrus (DG) granule neuron layer of hippocampus and in the Purkinje cell layer (PCL) and granule cell layer (GCL) of cerebellar cortex. Values are means ± SD. Asterisks indicate that the values at 7 days were significantly different ($P < 0.05$, Mann–Whitney test) from corresponding values at 1 day.

somal fragmentation of DNA was detected in genomic DNA extracts of dog hippocampus and cerebellar cortex after ischemia (Fig. 4, lanes 2 and 4). These different patterns of DNA degradation coexisted, most prominently at 7 days after ischemia. The internucleosomal fragmentation was similar to the pattern detected during developmental PCD of neurons (Fig. 4, lane 1). No DNA fragmentation was detected in control dog hippocampus and cerebellar cortex (Fig. 4, lanes 3 and 5), and no fragmentation of DNA was observed at 6 hours after ischemia (data not shown).

CA1 pyramidal neuron and Purkinje cell death is necrosis, but granule neuron death is apoptosis after ischemia

With use of criteria for neuronal apoptosis established in previous experiments (Portera-Cailliau et al., 1997a,b;

FIG. 2. Nuclear DNA fragmentation in dog cerebellar cortex after global incomplete ischemia. m, molecular layer; p, Purkinje cell layer; g, granule cell layer. **(A):** At 7 days after ischemia, terminal transferase-mediated biotin-dUTP nick end-labeling (TUNEL)-positive cells are detected in the three layers of cerebellar cortex. Purkinje cells (arrows) and a subset of granule neurons (arrowheads) are TUNEL-positive. **(B):** Granule neurons and Purkinje cells (arrows) are not TUNEL-positive in sham control dog cerebellum. Bar = 14 μm.

FIG. 4. Analysis of DNA fragmentation patterns in dog hippo-campus and cerebellar cortex by agarose gel electrophoresis. Genomic DNA was isolated and fractionated from ischemic dog hippocampus (lane 2) and cerebellar cortex (lane 4) at 7 days of recovery and from control dog hippocampus (lane 3) and cerebellar cortex (lane 5). Programmed cell death in developing rat retina at postnatal day 19 served as a positive control for inter-nucleosomal fragmentation of DNA (lane 1). Brackets delineate internucleosomal fragments (lanes 1, 2, and 4). Smearing of DNA is also seen in ischemic dog hippocampus and cerebellar cortex (lanes 2 and 4). Base pair molecular mass markers (lane 6) are (top to bottom): 2,176, 1,766, 1,230, 1,033, 653, 517, and 453.

Al-Abdulla et al., 1998; Martin et al., 1998, 1999), the degeneration of CA1 pyramidal neurons and Purkinje cells after ischemia was not apoptosis (Fig. 5). The de-generation of these neurons was consistent with necrosis (Figs. 5A–5C). Whereas nuclear pyknosis and chromatin condensation into irregular clumps were observed in these dying neurons, this pattern was very dissimilar to that found in unequivocal neuronal apoptosis (Portera-Cailliau et al., 1997a,b; Al-Abdulla et al., 1998; Martin et al., 1998, 1999). These ultrastructural observations are consistent with the hematoxylin and eosin staining and TUNEL patterns found in CA1 pyramidal neurons and cerebellar Purkinje cells, indicating a nonapoptotic struc-ture, as shown previously (Martin et al., 1997a, 1998). In contrast, granule neuron degeneration in the dentate gy-rus and cerebellar cortex was apoptosis (Fig. 5D–H). For example, early structural changes were chromatin mar-gination and crescentic capping of chromatin at the nuclear envelope and dispersion of many ribosomes within the cytoplasm (Fig. 5F and G). These changes occurred in the presence of maintained mitochondrial morphology (Fig. 5G). Later in the progression of apop-tosis, granule neurons underwent condensation of chro-

matin into large, round clumps and convolution of the nuclear envelope and then budding (Fig. 5H).

To further evaluate the presence or absence of indica-tors for neuronal apoptosis after cerebral ischemia, im-munoblotting was used to evaluate the levels of Bax protein expression in hippocampus and cerebellum. A representative immunoblot of Bax expression in control and ischemic dogs is shown in Fig. 6. Bax levels at 1 and 7 days after ischemia did not differ significantly from control levels in homogenates of dorsal hippocampus, as quantified by comparing the density and area of the im-munoreactive band in each lane of ischemic dog homog-enate scanned with values of control dog lanes in the same blot. Bax protein levels (in relative optical density units, means ± SD) in hippocampus were 32.4 ± 6.2 (control), 27.9 ± 8.0 (1 day after ischemia), and 32.1 ± 10.5 (7 days after ischemia). In contrast, Bax protein expression was significantly ($P < 0.05$) increased to 128 ± 5% of control cerebellum values at 7 days after isch-emia but not at 1 day after ischemia.

Alterations in metabotropic glutamate receptor signaling pathways occur in hippocampus and cerebellum after ischemia

In homogenates of whole septal hippocampal forma-tion, mGluR1α protein levels (detected as an immuno-reactive band at 142 kDa) were unchanged, with values 108 and 114% of control at 1 and 7 days after ischemia, respectively (Table 2; Fig. 7); similarly, mGluR5 protein levels (detected as an immunoreactive band at 148 kDa) were unchanged, with values 105 and 112% of control at 1 and 7 days of recovery, respectively (Table 2; Fig. 7). The PLCβ$_1$ and Gα$_{q11}$ protein levels in hippocampus were also not changed significantly after ischemia. At 1 and 7 days after ischemia, PLCβ$_1$ protein values (de-tected as an immunoreactive 80-kDa band) were 95 and 122% of controls, respectively, and Gα$_{q11}$ protein values (detected as an immunoreactive 45-kDa band) were 98 and 81% of control values at 1 and 7 days after ischemia, respectively (Table 2; Fig. 7). The maintenance of mGluR1α, mGluR5, PLCβ$_1$, and Gα$_{q11}$ protein levels, notably at 7 days after ischemia, occurred despite neu-ronal degeneration and death in the dorsal hippocampus (Table 1; Figs. 2 and 3).

In homogenates of cerebellar cortex, mGluR1α and mGluR5 protein levels were significantly reduced after ischemia. mGluR1α levels were 75 and 68% of controls at 1 and 7 days after ischemia, respectively (Table 2; Fig. 8), whereas mGluR5 was reduced to 22% of control at 1 day and then returned to 55% of control levels by 7 days (Table 2; Fig. 8). In contrast, PLCβ$_1$ levels in cerebellar cortex were increased significantly to 173 and 213% of control at 1 and 7 days after ischemia, respectively, whereas Gα$_{q11}$ was reduced to 80% of control at 1 day
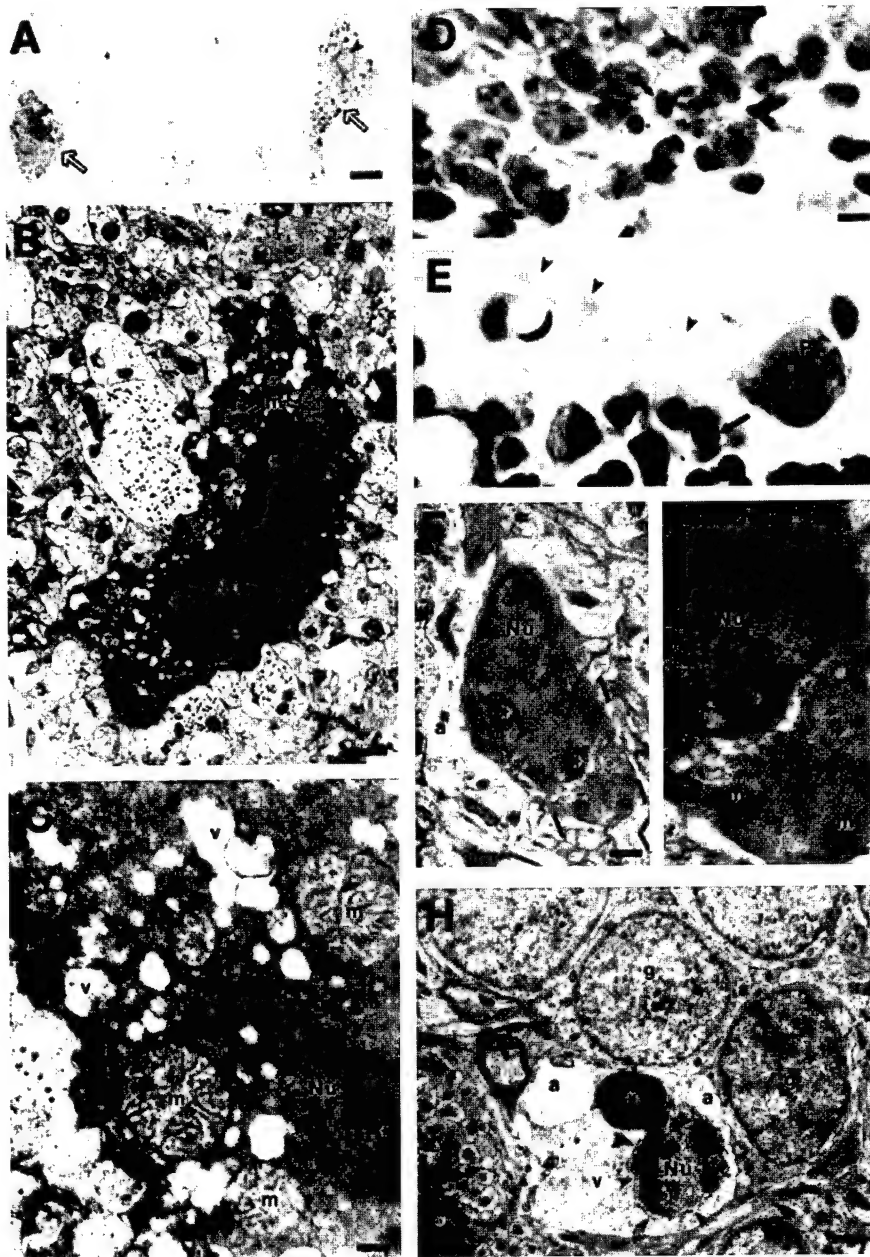
FIG. 5. Necrosis and apoptosis occur in distinct populations of neurons after ischemia. **(A)** Plastic section (1 μm thick) shows degenerating CA1 pyramidal neurons (arrows). The nucleus (arrowheads) in these neurons is dark and pyknotic, and the cytoplasm contains many small, clear vacuoles (corresponding to degenerating mitochondria and fragmented Golgi; see B) and dark granules (corresponding to lysosomes). These changes are consistent with cellular necrosis (Kerr et al., 1991; Wyllie et al., 1980; Portera-Cailliau et al., 1997b; Martin et al., 1998). Bar = 8 μm. **(B and C)** By electron microscopy, degeneration of CA1 neurons is morphologically necrotic. The cytoplasm of this representative neuron contains many swollen, degenerating mitochondria (m) and vacuoles (v). The pyknotic nucleus (Nu) contains many dispersed and irregularly shaped aggregates of chromatin throughout the nucleus (asterisks). Area in brackets is shown in C at higher magnification. Bars = 1.0 μm (B) and 0.2 μm (C). **(D)** Granule neuron degeneration in the hippocampal dentate gyrus after ischemia is apoptotic. Apoptotic granule neurons (arrows) are shrunken, and the nucleus displays chromatin clumping into dark, round aggregates. This neurodegeneration (arrows) occurs as isolated cells in a field of normal granule neurons. Bar = 5 μm. **(E)** Granule neuron degeneration in cerebellar cortex at 7 days after ischemia is also apoptotic. An isolated apoptotic cerebellar granule neuron (arrow) is shrunken, and the nucleus contains dark, round clumps of chromatin. Above this neuron is an injured Purkinje cell (P) showing ischemic degeneration of its dendrite (arrowheads). Bar = 6 μm. **(F)** The ultrastructure of granule neuron degeneration is consistent with apoptosis. At early morphologic stages of apoptosis, the cytoplasm and the nucleus (Nu) become dark and condensed, but the overall ultrastructural integrity of the neuron is not disrupted, in contrast to necrosis (cf. B and C). Apoptotic neurons are isolated from the surrounding neuropil by astrocytic processes (a). The chromatin aggregates (asterisks) as round clumps or crescents often at the periphery of the nucleus. Area in brackets is shown at higher magnification in G. Bar = 0.6 μm. **(G)** At higher magnification, the condensed chromatin (asterisk) within the nucleus (Nu) abuts the nuclear envelope (in contrast to the random aggregation of chromatin throughout the nucleus in necrosis; see B and C). Cisterns form in some areas at the cytoplasmic surface of the nuclear envelope (arrowheads). The mitochondria (m) remain intact (unlike the swelling and dissolution of the mitochondria in necrosis; see B and C) and are embedded in a cytoplasmic matrix that appears striated due to the organization of the cytoskeleton. These changes are typical of apoptosis in neurons (Portera-Cailliau et al., 1997a; Al-Abdulla et al., 1998; Martin et al., 1998). Bar = 0.3 μm. **(H)** At end-stage apoptosis, the nucleus (Nu) of granule neurons shows advanced chromatin condensation into round and crescentic aggregates (asterisks), some of which are extruded from the nucleus as the nuclear envelope ruptures (arrowheads). The residual cytoplasm, containing cytoskeletal and membranous debris and only few vacuoles (v), becomes infiltrated or enveloped by astrocytic processes (a). Nearby granule neurons (g) appear normal. Bar = 1.2 μm.

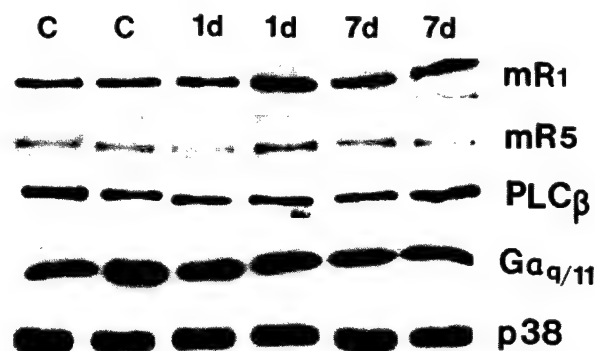C   C   1d   1d   7d   7d

Hippocampus

Cerebellum

Bax-α
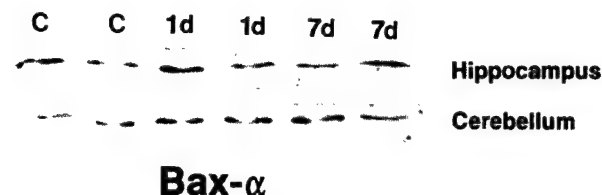
FIG. 6. Immunoblot analysis of Bax expression in mitochondria-enriched subcellular fractions of hippocampus (15 µg of protein/lane) and cerebellar cortex (12 µg of protein/lane) from sham control (c) and ischemic dogs at 1 day (1 d) and 7 days (7 d) of recovery. In hippocampus, Bax levels are unchanged at 1 and 7 days after ischemia. In cerebellar cortex, Bax levels are increased at 7 days afer ischemia.

Hippocampus

C   C   1d   1d   7d   7d

mR1
mR5
PLCβ
Gαq/11
p38

FIG. 7. Immunoblot analysis of metabotropic glutamate receptor (mGluR) 1α (mR1), mGluR5 (mR5), phospholipase Cβ (PLCβ), and Gαq/11 proteins in synaptic membrane fractions (10 µg of protein/lane) of hippocampus from sham control (c) and ischemic dogs at 1 day (1 d) and 7 days (7 d) of recovery. Blots were probed for synaptophysin (p38) as a loading control.

and then returned to control levels by 7 days (Table 2; Fig. 8).

The maintenance of some protein levels in regional homogenates, despite neuronal degeneration, suggested the possibility that changes occur in the cellular localization of mGluR1α, mGluR5, and PLCβ₁ after ischemia. We used immunocytochemistry to determine the localization of mGluR1α, mGluR5, and PLCβ₁ in hippocampus and cerebellum. In control dog hippocampus, mGluR1α is localized primarily within the stratum oriens of CA1 and in the dentate gyrus hilus, with only faint immunolabeling of granule cells (Fig. 9A). This pattern of mGluR1α localization in dog hippocampus is similar to the pattern shown in rat brain (Martin et al., 1992). In ischemic dogs, granule cell immunolabeling is augmented compared with controls (Fig. 9B), whereas the intensity of mGluR1α immunoreactivity in the neuropil of CA1 is diminished. In control dogs, mGluR5 is highly enriched in CA1 pyramidal cell bodies and in the neuropil of stratum oriens and stratum radiatum (corresponding to the dendritic fields of CA1 pyramidal neurons), whereas dentate gyrus granule neurons are less intensely immunoreactive than CA1. After ischemia, mGluR5 immunoreactivity in the CA1 pyramidal cell body and dendritic layers is reduced as compared with controls, but the dentate gyrus molecular layer, subiculum, and parahippocampal gyrus are more intensely immunoreactive compared with control (data not shown). In normal hippocampus, PLCβ₁ is highly enriched in cell bodies and proximal dendrites of pyramidal neurons and in the neuropil of CA1 (Fig. 9C) and is localized less intensely in the granule cells of the dentate gyrus (Fig. 9E). After ischemia, PLCβ₁ immunoreactivity is lost in the pyramidal cell body and dendritic (radiatum) layers of CA1 (Fig. 9D); in contrast, PLCβ₁ immunoreactivity is increased in the granule cell and molecular layers of the dentate gyrus (Fig. 9F) and in other locations corresponding to the distribution of the perforant path (not shown), suggesting an augmented presynaptic localization of PLCβ₁ after ischemia.

In control dog cerebellar cortex, mGluR1α is enriched in the neuropil of the molecular layer and in Purkinje cell bodies, but in the granule cell layer, occasional Golgi type II cells are immunopositive and granule cells are only weakly immunoreactive for mGluR1α (Fig. 9G). This pattern of mGluR1α localization in dog cerebellum

TABLE 2. *Quantitative immunoblot analysis of phosphoinositide-linked mGluR signal transduction proteins after global incomplete ischemia*

	Hippocampus			Cerebellar cortex		
	Control	1 Day	7 Days	Control	1 Day	7 Days
mGluR1α	164.4 ± 10.8	177.5 ± 0.4 (108%)	187.1 ± 5.3 (114%)	38.7 ± 11.6	29.2 ± 4.0* (75%)	26.1 ± 4.4* (68%)
mGluR5	148.6 ± 6.6	156.3 ± 10.0 (105%)	166.0 ± 16.9 (112%)	60.3 ± 21.2	13.3 ± 8.5* (22%)	32.9 ± 11.3* (55%)
PLCβ	78.4 ± 16.5	74.2 ± 8.2 (95%)	95.9 ± 26.0 (122%)	44.3 ± 5.0	76.9 ± 6.8* (173%)	94.3 ± 3.8* (213%)
Gαq/11	123.8 ± 20.4	121.4 ± 1.0 (98%)	99.9 ± 7.5 (81%)	110.3 ± 0.3	87.7 ± 12.6* (80%)	104.5 ± 21.9 (95%)

Values are mean ± SD of the relative optical density measurements of the immunoreactive bands at the appropriate molecular mass. Numbers in parentheses are percent of control value.

* Indicates significantly different from control ($P < 0.05$, Wilcoxon signed rank test).
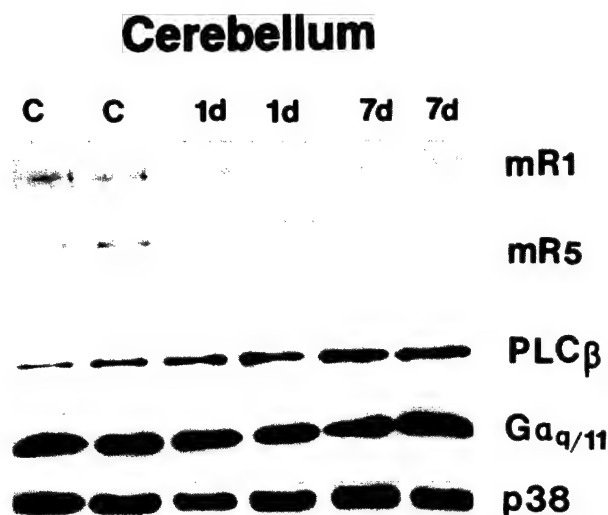
Cerebellum

FIG. 8. Immunoblot analysis of metabotropic glutamate receptor (mGluR) 1α (mR1), mGluR5 (mR5), phospholipase Cβ (PLCβ), and Gα_q/11 proteins in synaptic membrane fractions (10 μg of protein/lane) of cerebellar cortex from sham control (c) and ischemic dogs at 1 day (1 d) and 7 days (7 d) of recovery. Blots were probed for synaptophysin (p38) as a loading control.

is similar to the pattern shown in rat brain (Martin et al., 1992). After ischemia, mGluR1α immunoreactivity is reduced in the neuropil of the molecular layer but is increased in the granule cell layer (Fig. 9H). Like mGluR1α, mGluR5 staining in the cerebellum was less intense in the molecular layer after ischemia compared with control (data not shown). The PLCβ_1 level in control cerebellum is highly enriched in Purkinje cell bodies and dendrites extending throughout the molecular layer, which also contains diffuse neuropil immunoreactivity,
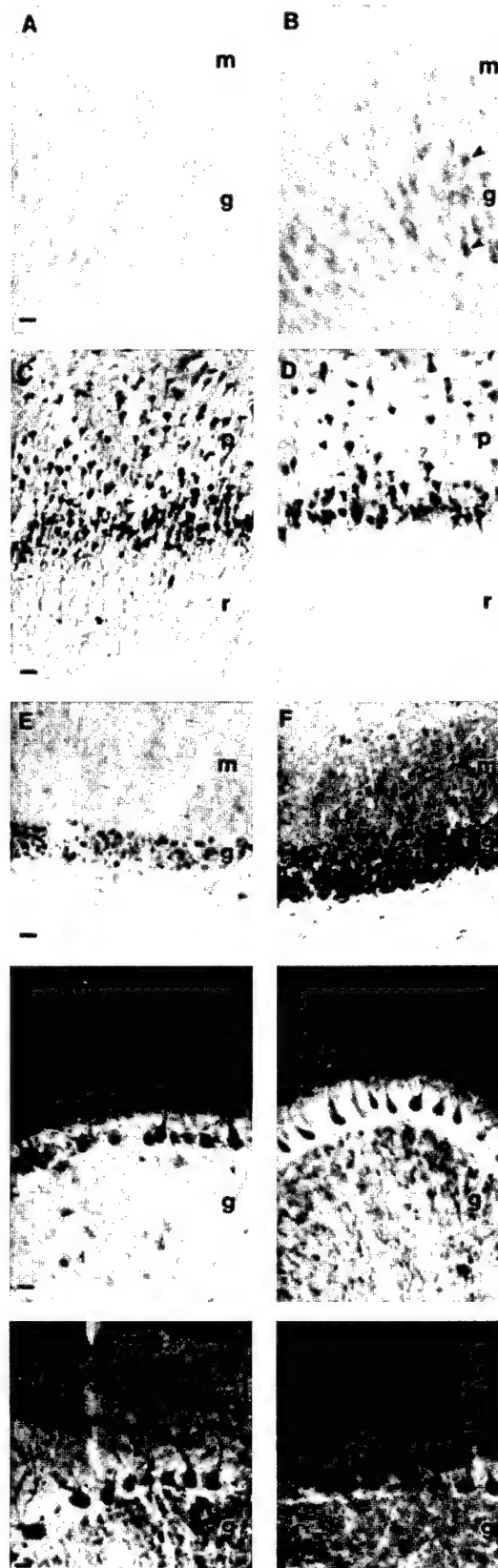
FIG. 9. Alterations occur in the regional and cellular localization of metabotropic glutamate receptor (mGluR) 1α and phospholipase Cβ (PLCβ) in hippocampus and cerebellar cortex at 7 days after global ischemia in dog. Photomicrographs on the left (**A, C, E, G,** and **I**) are from control dogs, and photomicrographs on the right (**B, D, F, H,** and **J**) are from ischemic dogs. The varying shades of darkness in these black-and-white photomicrographs reflect the intensity of immunoreactivity. In hippocampal dentate gyrus afer ischemia (**B**), granule cells (arrowheads) show increased mGluR1α immunoreactivity as compared with normal dogs (**A**). m, molecular layer; g, granule cell layer. Bar (**A**) = 7 μm. In CA1 afer ischemia (**D**), PLCβ immunoreactivity is reduced in the pyramidal cell body layer (p) and in the apical dendritic layer (stratum radiatum; r) as compared with controls (**C**). Bar (**C**) = 33 μm. In hippocampal dentate gyrus after ischemia (**F**), granule cells in the granule cell layer (g) and the neuropil of the molecular layer (m) have increased PLCβ immunoreactivity as compared with nonischemic dogs (**E**). Bar (**E**) = 16 μm. In the cerebellar cortex of postischemic dogs (**H**) compared with control dogs (**G**), mGluR1α immunoreactivity is diminished in the molecular layer (m), corresponding to a reduction in immunoreactive dendrites of Purkinje cells. In contrast, mGluR1α immunoreactivity in granule cells (g) is markedly increased after ischemia. Bar (**G**) = 18 μm. In the cerebellar cortex of postischemic dogs (**J**), immunoreactivity for PLCβ is enhanced in both the molecular layer (m) and the granule cell layer (g) as compared with nonischemic dogs (**I**). Bar (**I**) = 18 μm.

and the granule cell layer is not uniformly immunoreactive (Fig. 9I). After ischemia, PLCβ$_1$ immunoreactivity is increased in the neuropil of the molecular layer and in granule cells, whereas Purkinje cell labeling for PLCβ$_1$ is prominently decreased (Fig. 9J).

DISCUSSION

These experiments demonstrate that global ischemia results in two temporally overlapping, but distinct, forms of neuronal cell degeneration: necrosis of selectively vulnerable neurons (CA1 pyramidal neurons and cerebellar Purkinje cells) and apoptosis of granule neurons in dentate gyrus and cerebellum. Neuronal cell death in these regions is accompanied by differential changes in phosphoinositide-linked mGluR transduction mechanisms. Necrosis of CA1 neurons and Purkinje cells occurs in association with a loss of PLC-coupled mGluR signaling proteins, whereas apoptosis of granule neurons occurs in association with increases in proteins involved in PLC-coupled mGluR signaling.

Ischemic delayed degeneration of selectively vulnerable neurons is necrosis

The CA1 neurons undergo selective DND after ischemia in rodents (Ito et al., 1975; Kirino, 1982) and in dogs (Sato et al., 1990). The DND of cerebellar Purkinje cells is not studied commonly in rodent forebrain models of ischemia, but our study in dogs provided a novel opportunity to compare similarities among neuronal degeneration in hippocampus and cerebellum after ischemia. Our results show that ischemic delayed degeneration of CA1 pyramidal neurons and cerebellar Purkinje cells is similar structurally. The same conclusion has been made using a model of global complete ischemia in cats (Martin et al., 1998). Furthermore, our data demonstrate that the DND of selectively vulnerable neurons following global ischemia is cellular necrosis rather than apoptosis or a hybrid of apoptosis and necrosis. This degeneration of CA1 pyramidal neurons and Purkinje cells after ischemia is very distinct from neuronal apoptosis (Portera-Cailliau et al., 1997a; Al-Abdulla et al., 1998; Martin et al., 1998, 1999); it is also distinct from non-NMDA GluR-mediated excitotoxic neuronal apoptosis (Portera-Cailliau et al., 1997b; Martin et al., 1998), but it is very similar to NMDA receptor-mediated excitotoxic neuronal necrosis (Portera-Cailliau et al., 1997b; Martin et al., 1998; Ginsberg et al., 1999). Both the nucleus and the cytoplasm undergo ultrastructural perturbations consistent with cellular necrosis, with the main features being irregular clumping of chromatin, swelling and degeneration of organelles, extensive cytoplasmic vacuolation, destruction of plasma membrane integrity, and eventual dissolution of the cell. Moreover, dying CA1 neurons do not bud to form discrete, round nuclear fragments, as in apoptosis (cf. Fig. 4C and H) (Wyllie et al., 1980; Kerr

and Harmon, 1991; Martin et al., 1998). The nuclear pyknosis with condensation of chromatin into many small, irregularly shaped clumps in ischemic neurons contrasts with the formation of few, uniformly dense, and regularly shaped chromatin aggregates that occurs in neuronal apoptosis (Portera-Cailliau et al., 1997a; Al-Abdulla et al., 1998; Martin et al., 1998, 1999).

The cell plasma membrane and cytoplasmic organelles are damaged in necrotic neurons after ischemia. The immunocytochemically identified loss of mGluR–PLC signaling proteins in hippocampal pyramidal neurons in CA1 and Purkinje cells (as well as the loss of immunolabeling in their dendritic fields) is consistent with plasma membrane damage. The mitochondria swell and the inner mitochondrial membrane undergoes cristaeolysis. These mitochondrial abnormalities have been demonstrated in cellular necrosis (Laiho et al., 1971; Laiho and Trump, 1975) and can be produced when plasma membrane function and ATP synthesis are impaired (Laiho and Trump, 1975). Our observations are also consistent with previous findings showing that organelles that function in protein synthesis and posttranslational modification become structurally abnormal early in the course of ischemic neurodegeneration and are persistently abnormal during the process of neurodegeneration (Kirino et al., 1984; Martin et al., 1998). These structural changes are consistent with the finding that total protein synthesis is severely reduced by 6 hours after transient global forebrain ischemia and is reduced persistently in CA1 neurons, with the vast majority of pyramidal neurons never regaining their normal biosynthetic activity (Thilmann et al., 1986; Araki et al., 1990; Johansen and Diemer, 1990; Furuta et al., 1993). Cytoskeletal disintegration also occurs early after ischemia, particularly in dendrites, before the degeneration of neuronal cell bodies (Kitagawa et al., 1989; Yamamoto et al., 1990). This rapid disassembly and proteolysis of the cytoskeleton after ischemia (Kitagawa et al., 1989) contrast with the organized structure of the cytoskeleton and the cytoskeletal accumulation in neurons undergoing apoptosis (see Fig. 4G) (Al-Abdulla et al., 1998; Martin et al., 1998, 1999).

Nevertheless, previous studies have suggested that DND in hippocampus is apoptosis. The first observation suggesting this possibility was the finding that systemic treatment with protein synthesis inhibitors protected against CA1 neuron loss after global ischemia (Goto et al., 1990; Shigeno et al., 1990), although the hypothermic effects of protein synthesis inhibitors were not considered. However, other experiments have shown that protein and RNA synthesis inhibitors do not ameliorate postischemic DND in CA1 and that this neurodegeneration is not PCD (Deshpande et al., 1992). More recent studies have focused on DNA fragmentation. By *in situ* DNA end-labeling methods, many studies

have shown that selectively vulnerable populations of neurons undergo nuclear DNA fragmentation after global cerebral ischemia in the adult brain (Héron et al., 1993; MacManus et al., 1995; Nitatori et al., 1995). However, *in situ* end-labeling methods for DNA fail to discriminate among apoptotic and necrotic cell deaths (Grasl-Kraupp et al., 1995; Portera-Cailliau et al., 1997*b*; Martin et al., 1998) and can also detect DNA fragments during DNA synthesis (Lockshin and Zakeri, 1994); thus, these results *per se* cannot be interpreted as solely apoptosis. DNA integrity after global ischemia in adult brain has also been studied by gel electrophoresis. In DNA extracts of adult rat or gerbil brain, internucleosomal fragmentation has been found after transient global forebrain ischemia and has been interpreted as apoptosis occurring by PCD mechanisms (Okamoto et al., 1993; Héron et al., 1993; MacManus et al., 1995; Nitatori et al., 1995; Bhat et al., 1996). However, it is also uncertain whether internucleosomal DNA fragmentation is specific for apoptosis, because it occurs in ischemic liver necrosis (Fukuda et al., 1993), in NMDA receptor-mediated excitotoxic neuronal necrosis in adult brain (Portera-Cailliau et al., 1997*b*) and in culture (Gwag et al., 1997; Sohn et al., 1998), and in cells undergoing necrosis induced by calcium ionophores and heat shock (Collins et al., 1992). The analysis of DNA fragmentation patterns (and protein levels) in brain extracts is further confounded by tissue homogenization of heterogeneous cell systems, which precludes the evaluation of cell death on a cell-by-cell basis. Nonneuronal cells (e.g., astrocytes, oligodendrocytes, inflammatory cells, and vascular cells) also die following central nervous system injury, including ischemia–reperfusion and axotomy–target deprivation, and some of these nonneuronal cells die apoptotically (Martin et al., 1997*a*, 1998; Al-Abdulla et al., 1998). The interpretation of DNA fragmentation data is limited by the specificity and the caveats of the assay system, and, as concluded in previous studies (Kerr and Harmon, 1991; Collins et al., 1992; Portera-Cailliau et al., 1997*b*; Martin et al., 1998), cell structure is still the best indicator for classifying cell death *in vivo*. In our experiments, we found coexisting random and internucleosomal DNA fragmentation, and we attribute these different patterns to necrosis of pyramidal neurons and Purkinje cells and apoptosis of granule neurons within these regions. Our electron microscopic data support this conclusion.

This and previous ultrastructural studies illustrate that ischemic neurodegeneration in selectively vulnerable regions is not apoptosis (Kirino, 1982; Kirino and Sano, 1984; Kirino et al., 1984; Deshpande et al., 1992; Martin et al., 1998). These studies demonstrate that ischemic neurodegeneration has the typical features of cellular necrosis, consistent with the acute parenchymal cell death found in other organs after ischemia (Wyllie et al., 1980).

Yet, other studies with electron microscopic data have asserted that DND of CA1 pyramidal neurons after ischemia is apoptosis (Nitatori et al., 1995), although unambiguous ultrastructural evidence of apoptosis in these neurons in the adult brain has not been demonstrated. This discrepancy regarding whether DND fits the pattern of apoptosis is likely to be due to differences in criteria for identifying neuronal apoptosis and to the detail of the electron microscopic analysis. Alternatively, DND after ischemia may fall along a structural and mechanistic apoptosis–necrosis continuum (MacManus et al., 1995; Portera-Cailliau et al., 1997*a,b*; Martin et al., 1998). For example, GluR-mediated excitotoxic death of neurons occurs along an apoptosis–necrosis continuum, and the structure of excitotoxic neuronal degeneration is influenced by the subtype of GluR that is activated (Portera-Cailliau et al., 1997*a,b*). In the adult rat brain, the degeneration of neurons caused by NMDA receptor activation is structurally necrotic; however, the neuronal death produced by non-NMDA GluR activation is distinct from that caused by NMDA receptor stimulation. This non-NMDA receptor-mediated neuronal death in adult brain has some cytoplasmic and nuclear features reminiscent of neuronal apoptosis (Portera-Cailliau et al., 1997*b*). Thus, like non-NMDA GluR-mediated excitotoxicity, DND after ischemia could be a hybrid of apoptosis and necrosis, with the death of these neurons not strictly apoptosis or necrosis, according to a traditional binary classification of cell death, but occurring as intermediate or hybrid forms with coexisting characteristics that lie along a structural continuum with apoptosis and necrosis at the extremes. Because this continuum is influenced by the subtype of glutamate receptor that is activated, DND after ischemia may not be identical in every neuron, possibly because of the high diversity in the expression, localization, and function of GluR subtypes or the diversity in second messenger systems in the central nervous system. Surprisingly, however, we did not find ultrastructural evidence that ischemic DND resembles non-NMDA GluR-mediated excitotoxic neuronal death, but rather it is structurally very similar to NMDA receptor-mediated excitotoxic necrosis (Portera-Cailliau et al., 1997*a,b*; Martin et al., 1998).

Granule neurons undergo apoptosis after ischemia

The degeneration of granule neurons in dentate gyrus and cerebellum after global ischemia sharply contrasts with the degeneration of CA1 neurons and Purkinje cells. Granule neuron death after ischemia closely resembles apoptosis. Thus, granule neurons provide an internal standard for classic apoptosis with which CA1 pyramidal neuron and cerebellar Purkinje cell degeneration after ischemia can be compared to demonstrate that the death of these latter neurons is not apoptosis. As with apoptosis in nonneuronal tissues (Kerr and Harmon, 1991), in de-

veloping brain during naturally occurring PCD of neurons (Portera-Cailliau et al., 1997*a*), and in some neuronal groups after axotomy–target deprivation (Al-Abdulla et al., 1998; Martin et al., 1999), apoptosis of granule neurons was characterized morphologically by nuclear and cytoplasmic condensation. The most prominent alterations were condensation of chromatin into few, large, round clumps or crescentic caps, aggregation and lamination of the cytoskeleton, and cellular shrinkage. Membranous organelles, including mitochondria, remained intact until the late stages of apoptosis. Neurodegeneration after global ischemia involves entire neural systems, and neuronal connectivity as well as metabolic factors possibly dictate the pattern of selective vulnerability (Martin et al., 1997*b*). Granule neuron death may be a direct consequence of the ischemia, or it may be secondary to necrotic degeneration of hippocampal pyramidal neurons and cerebellar Purkinje cells and thus is a form of target deprivation-induced apoptosis (Martin et al., 1998, 1999; Al-Abdulla et al., 1998), because the targets of dentate granule neurons include hippocampal pyramidal neurons and the targets of cerebellar granule neurons are Purkinje cells. This possibility is supported by *in vitro* studies showing that, in response to serum deprivation, cerebellar granule neurons undergo transcription-dependent apoptosis (D'Mello et al., 1993; Watson et al., 1998) by activation of a pathway involving c-Jun phosphorylation (Watson et al., 1998). Similar mechanisms seem to be operative in a related *in vitro* paradigm (i.e., low potassium) of cerebellar granule neuron apoptosis (D'Mello et al., 1993; Watson et al., 1998), and, interestingly, activation of phosphoinositide-linked mGluRs blocks this neuronal apoptosis (Copani et al., 1995). Thus, augmented mGluR expression in cerebellar and hippocampal granule neurons after cerebral ischemia may signify a physiological attempt at neuroprotection rather than an event mediating the apoptosis.

Contribution of programmed cell death mechanisms in ischemic neurodegeneration

Gene products that regulate PCD of mammalian cells have been studied after ischemia. Bax mRNA is increased in both vulnerable and less vulnerable regions after ischemia (Chen et al., 1996). Changes in mRNA after cerebral ischemia are difficult to interpret in light of damage to organelles that function in protein synthesis and posttranslational processing, thereby potentially rendering the translation and formation of mature products inefficient. By immunoblotting, Bax protein in hippocampus is increased transiently at 6 hours after ischemia but then returns to control levels (Krajewski et al., 1995). We found no changes in Bax protein levels in hippocampus at 1 and 7 days after ischemia, but we observed an increase in Bax in cerebellum at 7 days after ischemia. A possible explanation for a lack of detection of changes in

Bax protein levels in hippocampus by immunoblotting is that apoptotic death of dentate gyrus granule neurons is less frequent than granule neuron death in cerebellum (see Fig. 3). Also, granule neurons compose a greater population of cells in cerebellum than in hippocampus (West et al., 1991; Korbo et al., 1993). However, a sustained postischemic increase in Bax protein levels has been shown in hippocampus but not cerebellum (Chen et al., 1996), although the contributions of different cells to this observation have not been identified. Important in this regard is the finding that mRNA and protein levels for the proapoptotic cysteine protease ICE interleukin-1 converting enzyme (caspase-1) are increased in hippocampus after global ischemia in gerbils, but this change is associated with inflammatory cells rather than selectively vulnerable CA1 pyramidal neurons (Bhat et al., 1996). In addition, after global ischemia in rat, caspase-3 mRNA levels are progressively elevated in CA1 at 24 to 72 hours, although most of the neurons are already lost by 72 hours, whereas caspase-3 mRNA is transiently elevated in dentate gyrus granule cells at 8 hours after ischemia (Chen et al., 1998). This latter pattern would be more consistent with a role for caspase-3 in the granule neuron apoptosis that we have identified. On the other hand, Bcl-2 overexpression in transgenic mice reduces hippocampal pyramidal neuron degeneration after global ischemia (Kitagawa et al., 1998), although this effect of Bcl-2 cannot yet be specifically ascribed to antiapoptotic activity, because this protein has additional functions in injured neurons (Chen et al., 1997). It is still uncertain, however, whether the absence of a classic apoptotic structure in selectively vulnerable neurons after ischemia is sufficient evidence to exclude the possibility that PCD may be operative, because all forms of PCD may not occur via apoptosis (Schwartz et al., 1993).

Metabotropic glutamate receptor signaling pathways after ischemia

The distinct forms of degeneration in different populations of hippocampal and cerebellar neurons after ischemia were accompanied by differential changes in proteins involved in phosphoinositide-coupled mGluR signal transduction. These changes were more easily identified by immunocytochemistry rather than by immunoblotting (except for PLCβ in cerebellum), perhaps because of overlapping and differential contributions of distinct populations of neurons that are not divisible in gel analyses of regional homogenates. Necrosis of CA1 neurons and Purkinje cell is associated with a loss of mGluRs and PLCβ. In contrast, apoptosis in granule cell populations in hippocampus and cerebellum is paralleled by increased expression of these proteins. Our results are consistent with the reported loss of mGluR1 and mGluR5 mRNA in CA1 after global ischemia (Iversen et al., 1994). This observation is not surprising when con-

sidering the postsynaptic, somatodendritic localization of these proteins (Martin et al., 1992; Blue et al., 1997) and the rapid damage to dendritic membranes and the cytoskeletal proteolysis that occur in these neurons after ischemia (Kitagawa et al., 1989; Yamamoto et al., 1990). These abnormalities further support our conclusion that hippocampal pyramidal neurons and Purkinje cells undergo necrosis after ischemia. In contrast, in granule neurons of dentate gyrus and cerebellum, immunoreactivity for mGluRs and PLCβ is enhanced. This finding is consistent with the concept that apoptosis results from the *de novo* expression or activation of a PCD program (Sen, 1992), but it is not clear whether changes in PLC-coupled mGluRs participate directly in the mechanisms for apoptosis in these neurons or whether these changes reflect the activation of compensatory survival signaling pathways (Copani et al., 1995).

The possible roles for PLC-coupled mGluRs in the mechanisms for necrotic degeneration of selectively vulnerable neurons after ischemia are uncertain. Activation of mGluRs is necessary for Purkinje cell survival *in vitro* (Mount et al., 1993) and protects neurons from oxidative stress (Sagara and Schubert, 1998). Thus, a loss of somatodendritic phosphoinositide-linked mGluRs in Purkinje cells and CA1 neurons may have a role in the necrosis of these neurons after ischemia. Alternatively, this loss is possibly a consequence of necrotic degeneration of these neurons. It is possible that augmented activity of PLC-coupled mGluR signal transduction proteins does not participate in the primary mechanisms for DND of CA1 pyramidal neurons and cerebellar Purkinje cells after ischemia. This conclusion is supported by the finding that neither pharmacological blockade of mGluRs nor ablation of the mGluR1 gene reduces ischemic and excitotoxic brain injury *in vivo* (Ferraguti et al., 1997). However, other observations suggest that endogenous activation of mGluR1 contributes to ischemic and excitotoxic neuronal degeneration (Bruno et al., 1999). Additional work is necessary to precisely identify the role of mGluR signaling in neurodegeneration after ischemia.

REFERENCES

Al-Abdulla NA, Portera-Cailliau C, Martin LJ (1998) Occipital cortex ablation in adult rat causes retrograde neuronal death in the lateral geniculate nucleus that resembles apoptosis. *Neuroscience* 86:191–209

Araki T, Kato H, Inoue T, Kogure K (1990) Regional impairment of protein synthesis following brief cerebral ischemia in the gerbil. *Acta Neuropathol* 79:501–505

Bhat RV, DiRocco R, Marcy VR, Flood DG, Zhu Y, Dobrzanski P, Siman R, Scott R, Contreras PC, Miller M (1996) Increased expression of IL-1β converting enzyme in hippocampus after ischemia: selective localization in microglia. *J Neurosci* 16:4146–4154

Blue ME, Martin LJ, Brennan EM, Johnston MV (1997) Ontogeny of non-NMDA glutamate receptors in rat barrel field cortex: I. Metabotropic receptors. *J Comp Neurol* 386:16–28

Bruno V, Battaglia G, Kingston A, O'Neill MJ, Catania MV, Di Grezia R, Nicoletti F (1999) Neuroprotective activity of the potent and selective mGluR1a metabotropic glutamate receptor antagonist, (+)-2-methyl-4-carboxyphenylglycine (LY367385): comparison with LY357366, a broader spectrum antagonist with equal affinity for mGluR1a and mGluR5 receptors. *Neuropharmacology* 38:199–207

Chen DF, Schneider GE, Martinou J-C, Tonegawa S (1997) Bcl-2 promotes regeneration of severed axons in mammalian CNS. *Nature* 385:434–439

Chen J, Zhu RL, Nakayama M, Kawaguchi K, Jin K, Stetler RA, Simon RP, Graham SH (1996) Expression of the apoptosis-effector gene, *bax*, is up-regulated in vulnerable hippocampal CA1 neurons following global ischemia. *J Neurochem* 67:64–71

Chen J, Nagayama T, Jin K, Stetler RA, Zhu RL, Graham SH, Simon RP (1998) Induction of caspase-3-like protease may mediate delayed neuronal death in the hippocampus after transient cerebral ischemia. *J Neurosci* 18:4914–4928

Collins RJ, Harmon BV, Gobé VC, Kerr JFR (1992) Internucleosomal DNA clevage should not be the sole criterion for identifying apoptosis. *Int J Radiat Biol* 61:451–453

Copani A, Bruno VMG, Barresi V, Battaglia G, Condorelli DF, Nicoletti F (1995) Activation of metabotropic glutamate receptors prevents neuronal apoptosis in culture. *J Neurochem* 64:101–108

Deshpande J, Bergstedt K, Linden T, Kalimo H, Wieloch T (1992) Ultrastructural changes in the hippocampal CA1 region following transient cerebral ischemia: evidence against programmed cell death. *Exp Brain Res* 88:91–105

Diemer NH, Valente E, Bruhn T, Berg M, Jírgensen MB, Johansen FF (1993) Glutamate receptor transmission and ischemic nerve cell damage: evidence for involvement of excitotoxic mechanisms. *Prog Brain Res* 96:105–123

D'Mello SR, Galli C, Ciotti T, Calissano P (1993) Induction of apoptosis in cerebellar granule neurons by low potassium: inhibition of death by insulin-like growth factor I and cAMP. *Proc Natl Acad Sci USA* 90:10989–10993

Ferraguti F, Pietra C, Valerio E, Corti C, Chiamulera C, Conquet F (1997) Evidence against a permissive role of the metabotropic glutamate receptor 1 in acute excitotoxicity. *Neuroscience* 79:1–5

Fotuhi M, Dawson TM, Sharp AH, Martin LJ, Graybiel AM, Snyder SH (1993) Phosphoinositide second messenger system is enriched in striosomes: immunohistochemical demonstration of inositol 1,4,5-trisphosphate receptors and phospholipase C β and γ in primate basal ganglia. *J Neurosci* 13:3300–3308

Fukuda K, Kojiro M, Chiu J-F (1993) Demonstration of extensive chromatin cleavage in transplanted Morris hepatoma 7777 tissue: apoptosis or necrosis? *Am J Pathol* 142:935–946

Furuta S, Ohta S, Hatakeyama, T, Nakamura, K, Sakaki S (1993) Recovery of protein synthesis in tolerance-induced hippocampal CA1 neurons after transient forebrain ischemia. *Acta Neuropathol* 86:329–336

Ginsberg SD, Portera-Cailliau C, Martin LJ (1999) Fimbria-fornix transection and excitotoxicity produce similar neurodegeneration in the septum. *Neuroscience* 88:1059–1071

Goto K, Ishige A, Sekiguchi K, Iizuka S, Sugimoto A, Yuzurihara M, Aburada M, Hosoya E, Kogure K (1990) Effects of cycloheximide on delayed neuronal death in rat hippocampus. *Brain Res* 534:299–302

Grasl-Kraupp B, Ruttkay-Nedecky B, Koudelka H, Bukowska K, Bursch W, Schulte-Hermann R (1995) *In situ* detection of fragmented DNA (TUNEL assay) fails to discriminate among apoptosis, necrosis, and autolytic cell death: a cautionary note. *FASEB J* 21:1465–1468

Gwag BJ, Koh JY, DeMaro JA, Ying HS, Jacquin M, Choi DW (1997)

Slowly triggered excitotoxicity occurs by necrosis in cortical cultures. *Neuroscience* 77:393–401

Héron A, Pollard H, Dessi F, Moreau J, Lasbennes F, Ben-Ari Y, Charriaut-Marlangue C (1993) Regional variability in DNA fragmentation after global ischemia evidenced by combined histological and gel electrophoresis observations in the rat brain. *J Neurochem* 61:1973–1976

Ishimaru MJ, Ikonomidou C, Tenkova TI, Der TC, Dikranian K, Sesma MA, Olney JW (1999) Distinguishing excitotoxic from apoptotic neurodegeneration in the developing rat brain. *J Comp Neurol* 408:461–476

Ito U, Spatz M, Walker JT, Klatzo I (1975) Experimental cerebral ischemia in Mongolian gerbils. I. Light microscopic observations. *Acta Neuropathol* 32:209–223

Iversen L, Mulvihill E, Haldeman B, Diemer NH, Kaiser F, Sheardown M, Kristensen P (1994) Changes in metabotropic glutamate receptor mRNA levels following global ischemia: increase of a putative presynaptic subtype (mGluR4) in highly vulnerable rat brain areas. *J Neurochem* 63:625–633

Johansen FF, Diemer NH (1990) Temporal profile of interneuron and pyramidal cell protein synthesis in rat hippocampus following cerebral ischemia. *Acta Neuropathol* 81:14–19

Kerr JFR, Harmon BV (1991) Definition and incidence of apoptosis: an historical perspective. In: *Apoptosis: the molecular basis of cell death* (Tomei LD, Cope FO, eds), Cold Spring Harbor: Cold Spring Harbor Laboratory Press, pp 5–29

Kirino T (1982) Delayed neuronal death in the gerbil hippocampus following ischemia. *Brain Res* 239:57–69

Kirino T, Sano K (1984) Fine structural nature of delayed neuronal death following ischemia in the gerbil hippocampus. *Acta Neuropathol* 62:209–218

Kirino T, Tamura A, Sano K (1984) Delayed neuronal death in rat hippocampus following transient forebrain ischemia. *Acta Neuropathol* 64:139–147

Kirino T, Robinson HPC, Miwa A, Tamura A, Kawai N (1992) Disturbance of membrane function preceding ischemic delayed neuronal death in the gerbil hippocampus. *J Cereb Blood Flow Metab* 12:408–417

Kitagawa K, Matsumoto M, Niinobe M, Mikoshiba K, Hata R, Ueda H, Handa N, Fukunaga R, Isaka Y, Kimura K, Kamada T (1989) Microtubule-associated protein 2 as a sensitive marker for cerebral ischemic damage. Immunohistochemical investigation of dendritic damage. *Neuroscience* 31:401–411

Kitagawa K, Matsumoto M, Tsujimoto Y, Ohtsuki T, Kuwabara K, Matsushita K, Yang G, Tanabe H, Martinou J-C, Hori M, Yanagihara T (1998) Amelioration of hippocampal neuronal damage after global ischemia by neuronal overexpression of Bcl-2 in transgenic mice. *Stroke* 29:2616–2621

Korbo L, Andersen BB, Ladefoged O, Míller A (1993) Total number of various cell types in rat cerebellar cortex estimated using an unbiased stereological method. *Brain Res* 609:262–268

Krajewski S, Mai JK, Krajewska M, Sikorska M, Mossakowski MJ, Reed JC (1995) Upregulation of bax protein levels in neurons following cerebral ischemia. *J Neurosci* 15:6364–6376

Laiho KU, Trump BJ (1975) Studies on the pathogenesis of cell injury. Effects of inhibitors of metabolism and membrane function on the mitochondria of Ehrlich ascites tumor cells. *Lab Invest* 32:163–182

Laiho KU, Shelburne JD, Trump BJ (1971) Observations on cell volume, ultrastructure, mitochondrial conformation and vital-dye uptake in Ehrlich ascites tumor cells. *Am J Pathol* 65:203–230

Lockshin RA, Zakeri A (1994) Programmed cell death: early changes in metamorphosing cells. *Biochem Cell Biol* 72:589–596

MacManus JP, Hill IE, Preston E, Rasquinha I, Walker T, Buchan AM (1995) Differences in DNA fragmentation following transient cerebral ischemia or decapitation ischemia in rats. *J Cereb Blood Flow Metab* 15:728–737

Martin LJ, Blackstone CD, Huganir RL, Price DL (1992) Cellular localization of a metabotropic glutamate receptor in rat brain. *Neuron* 9:259–270

Martin LJ, Brambrink AM, Lehmann C, Portera-Cailliau C, Koehler R, Rothstein J, Traystman RJ (1997a) Hypoxia-ischemia causes ab-

normalities in glutamate transporters and death of astroglia and neurons in newborn striatum. *Ann Neurol* 42:335–348

Martin LJ, Brambrink A, Koehler RC, Traystman RJ (1997b) Primary sensory and forebrain motor systems in the newborn brain are preferentially damaged by hypoxia-ischemia. *J Comp Neurol* 377: 262–285

Martin LJ, Al-Abdulla NA, Brambrink AM, Kirsch JR, Sieber FE, Portera-Cailliau C (1998) Neurodegeneration in excitotoxicity, global cerebral ischemia, and target deprivation: a perspective on the contributions of apoptosis and necrosis. *Brain Res Bull* 46:281–309

Martin LJ, Kaiser A, Price AC (1999) Motor neuron degeneration after sciatic nerve avulsion in adult rat evolves with oxidative stress and is apoptosis. *J Neurobiol* 40:185–201

Mount HTJ, Dreyfus CF, Black IB (1993) Purkinje cell survival is differentially regulated by metabotropic and ionotropic excitatory amino acid receptors. *J Neurosci* 13:3173–3179

Nakanishi S (1992) Molecular diversity of glutamate receptors and implications for brain function. *Science* 258:597–603

Nitatori T, Sato N, Waguri S, Karasawa Y, Araki H, Shibanai K, Kominami E, Uchiyama Y (1995) Delayed neuronal death in the CA1 pyramidal cell layer of the gerbil hippocampus following transient ischemia is apoptosis. *J Neurosci* 15:1001–1011

Okamoto M, Matsumoto M, Ohtsuki T, Taguchi A, Mikoshiba K, Yanagihara T, Kamada T (1993) Internucleosomal DNA cleavage involved in ischemia-induced neuronal death. *Biochem Biophys Res Commun* 196:1356–1362

Opitz T, Richter P, Carter AJ, Kozikowski AP, Shiozaki H, Reymann KG (1995) Metabotropic glutamate receptor subtypes differentially influence neuronal recovery from in vitro hypoxia/hypoglycemia in rat hippocampal slices. *Neuroscience* 68: 989–1001

Pin J-P, Duvoisin R (1995) The metabotropic glutamate receptors: structure and functions. *Neuropharmacology* 34:1–26

Portera-Cailliau C, Price DL, Martin LJ (1996) *N*-Methyl-D-aspartate receptor proteins NR2A and NR2B are differentially distributed in the developing rat central nervous system as revealed by subunit-specific antibodies. *J Neurochem* 66:692–700

Portera-Cailliau C, Price DL, Martin LJ (1997a) Excitotoxic neuronal death in the immature brain is an apoptosis-necrosis morphological continuum. *J Comp Neurol* 378:70–87

Portera-Cailliau C, Price DL, Martin LJ (1997b) Non-NMDA and NMDA receptor-mediated excitotoxic neuronal deaths in adult brain are morphologically distinct: further evidence for an apoptosis-necrosis continuum. *J Comp Neurol* 378:88–104

Sagara Y, Schubert D (1998) The activation of metabotropic glutamate receptors protects nerve cells from oxidative stress. *J Neurosci* 18:6662–6671

Sato M, Hashimoto H, Kosaka F (1990) Histological changes of neuronal damage in vegetative dogs induced by 18 minutes of complete global brain ischemia: two-phase damage of Purkinje cells and hippocampal CA1 pyramidal cells. *Acta Neuropathol* 80:527–534

Schwartz LM, Smith SW, Jones MEE, Osborne BA (1993) Do all programmed cell deaths occur via apoptosis? *Proc Natl Acad Sci USA* 90:980–984

Sen S (1992) Programmed cell death: concept, mechanism and control. *Biol Rev* 67:287–319

Sheardown MJ, Nielsen EØ, Hansen AJ, Jacobsen P, Honoré T (1990) 2,3-Dihydroxy-6-nitro-7-sulfamoyl-benzo(*F*)quinoxaline: a neuroprotectant for cerebral ischemia. *Science* 247:571–574

Shigeno T, Yamasaki Y, Kato G, Kusaka K, Mima T, Takakura K, Graham DI, Furukawa S (1990) Reduction of delayed neuronal death by inhibition of protein synthesis. *Neurosci Lett* 120:117–119

Sieber FE, Palmon SC, Traystman RJ, Martin LJ (1995) Global incomplete cerebral ischemia produces predominantly cortical neuronal injury. *Stroke* 26:2091–2096

Sohn S, Kim EY, Gwag BJ (1998) Glutamate neurotoxicity in mouse cortical neurons: atypical necrosis with DNA ladders and chromatin condensation. *Neurosci Lett* 240:147–150

Tanabe Y, Masu M, Ishii T, Shigemoto R, Nakanishi S (1992) A family of metabotropic glutamate receptors. *Neuron* 8:169–179

Thilmann R, Xie Y, Kleihues P, Kiessling M (1986) Persistent inhibi-

tion of protein synthesis precedes delayed neuronal death in post-ischemic gerbil hippocampus. *Acta Neuropathol* 71:88–93

Tominaga T, Kure S, Narisawa K, Yoshimoto T (1993) Endonuclease activation following focal ischemic injury in the rat brain. *Brain Res* 608:21–26

Watson A, Eilers A, Lallemand D, Kyriakis J, Rubin LL, Ham J (1998) Phosphorylation of c-jun is necessary for apoptosis induced by survival signal withdrawal in cerebellar granule neurons. *J Neurosci* 18:751–762

West MJ, Slomianka L, Gundersen HJG (1991) Unbiased stereological estimation of the total number of neurons in the subdivisions of the rat hippocampus using the optical fractionator. *Anat Rec* 231:482–497

Wyllie AH, Kerr JFR, Currie AR (1980) Cell death: the significance of apoptosis. *Int Rev Cytol* 68:251–306

Yamamoto K, Hayakawa T, Mogami H, Akai F, Yanagihara T (1990) Ultrastructural investigation of the CA1 region of the hippocampus after transient cerebral ischemia in gerbils. *Acta Neuropathol* 80:487–492

Yan G-M, Lin S-Z, Irwin RP, Paul SM (1995) Activation of G proteins bidirectionally affects apoptosis of cultured cerebellar granule neurons. *J Neurochem* 65:2425–2431

Lee J. Martin, Ph.D.
DAMD17-99-1-9553

Appendix

Mechanisms for neuronal degeneration in amyotrophic lateral sclerosis and in models of motor neuron death (Review)

LEE J. MARTIN[1,2], ANN C. PRICE[1], ADEEL KAISER[1], ARIF Y. SHAIKH[1] and ZHIPING LIU[1]

Departments of [1]Pathology, Division of Neuropathology, and [2]Neuroscience, Johns Hopkins, University School of Medicine, Baltimore, MD, USA

Abstract. Amyotrophic lateral sclerosis (ALS), also referred to as motor neurone disease, is a fatal neurological disease that is characterized clinically by progressive muscle weakness, muscle atrophy, and eventual paralysis. The neuropathology of ALS is primary degeneration of upper (motor cortical) and lower (brainstem and spinal) motor neurons. The amyotrophy refers to the neurogenic atrophy of affected muscle groups, and the lateral sclerosis refers to the hardening of the lateral white matter funiculus in spinal cord (corresponding to degeneration of the corticospinal tract) found at autopsy. Because the mechanisms for the motor neuron degeneration in ALS are not understood, this disease has no precisely known causes and no effective treatments. Very recent studies have identified that the degeneration of motor neurons in ALS is a form of apoptotic cell death that may occur by an abnormal programmed cell death (PCD) mechanism. In order to treat ALS effectively, we need to understand the mechanisms for motor neuron apoptosis more completely. Future studies need to further identify the signals for PCD activation in neurons as they relate to the pathogenesis of ALS and to clarify the molecular pathways leading to motor neuron apoptosis in animal and cell culture model systems. These studies should lead to a better understanding of motor neuron death and to the design of new therapeutic experiments critical for the future treatment of ALS.

Contents

1. Introduction

ALS is a human disease clinically characterized by progressive weakness, muscle atrophy, and eventual paralysis and death within 3-5 years of clinical onset (1). It is one of the most common neurodegenerative diseases with an adult onset, having an incidence of 1-2 per 100,000 individuals. This disease is neuropathologically characterized by progressive degeneration of upper and lower motor neurons in the brain and spinal cord. The mechanisms leading to degeneration of motor neurons in ALS are not understood. Two major forms of ALS exist: idiopathic (sporadic) and heritable (familial). The vast majority of ALS cases are sporadic with no known genetic component. The familial forms of ALS (FALS) are autosomal dominant and make up about 10-20% of all ALS cases. In a subset of familial ALS cases (about 5-10%), missense mutations have been identified (2) in the gene for superoxide dismutase 1 (SOD1, also known as Cu,Zn SOD).

A variety of hypothesis (Table I) have been proposed for the possible causes of neuronal death in ALS, including SOD1 mutations, abnormal uptake of excitatory amino acids leading to glutamate receptor-mediated excitotoxicity, deficiencies in neurotrophic factors, DNA damage, and autoimmunity. Recently, this laboratory (3) has provided strong evidence that motor neuron degeneration is due to an anomalous activation of programmed cell death (PCD). A better understanding of the pathogenesis of neuronal degeneration in this disease and in animal models that mirror this degeneration of motor neurons found in ALS is critical for the future development of effective therapies for patients with ALS.

2. ALS and mutant SOD1

Mutations have been identified in the SOD1 gene in a small subset of individuals with FALS (2,4). Thus, most current ideas regarding the mechanisms for motor neuron degeneration in

Correspondence to: Dr Lee J. Martin, Johns Hopkins University School of Medicine, Department of Pathology, 558 Ross Building, 720 Rutland Avenue, Baltimore, MD 21205-2196, USA

Table I. Some leading theories about motor neuron degeneration in ALS.

Mechanism	Comment
SOD1 mutation	Found in a subset of FALS cases. Resulting in a toxic gain-in-function or modified stability of SOD1
Excitotoxicity	Resulting from abnormal glutamate receptor activation and defects in glutamate transport
Neurotrophin withdrawal	Resulting from insufficient muscle cell- or glial cell-derived trophic support or defective neurotrophin receptor signaling
DNA damage/ repair defects	Resulting from oxidative stress or inefficient DNA-repair enzyme function. May involve both mitochondrial and nuclear DNA damage
Autoimmunity	Resulting from autoantibodies to motor neuron antigens
Aberrant programmed cell death	May be triggered by all of the above mechanisms

ALS center on the mutant forms of SOD1 found in FALS. Because SOD1 is widely expressed in cells throughout the body, and in CNS tissue the expression is very ubiquitous (5), the basis for the selective vulnerability of motor neurons in the presence of SOD1 mutations is not clear. Initial experiments suggested that mutations in SOD1 lead to motor neuron degeneration by decreasing its enzymatic activity, resulting in toxic effects of superoxide radicals inefficiently scavenged by mutant SOD1 (4). This hypothesis was supported by the finding that down-regulation of SOD1 causes apoptosis in neuronal cell cultures (6) and in slice cultures of spinal cord (7), and by the observation that microinjected normal wild-type SOD1 can delay apoptosis in cultured neurons deprived of trophic factors (8). However, it was observed that FALS-linked mutations in SOD1 do not generally impair enzymatic activity, but instead decrease protein stability (9). More recently, it has been proposed that mutant SOD1 acquires a neurotoxic gain in function. Mutations in SOD1 may convert this enzyme from a protein with antioxidant-antiapoptotic functions to a protein with apoptosis-promoting effects (10). In addition to the dismutation of superoxide, SOD1 also has peroxidase activity, and this peroxidase activity is enhanced in mutant SOD1 compared to normal SOD1 (11). This gain-of-function may lead to enhanced production of hydroxyl, superoxide, and peroxynitrite radicals (11,12). SOD1 catalyzes the nitration of

specific tyrosine residues in protein by peroxynitrite, which may contribute to the damaging gain-of-function resulting from SOD1 mutations (12). Neurofilaments are major structural proteins in motor neurons and, notably, neurofilament L is a target of tyrosine nitration by peroxynitrite (13). Other studies have revealed that Zn^{2+} affinity of mutant SOD1 is decreased and that neurofilament L binds Zn^{2+} with sufficient affinity to capture this cofactor from mutant and wild-type SOD1 (14). The loss of Zn^{2+} from wild-type SOD1 dramatically increases its efficiency for catalyzing peroxynitrite-mediated tyrosine nitration (14). Although neurofilament L is particularly susceptible to peroxynitrite-mediated nitration, tyrosine nitration of this protein is not elevated in spinal cords of sporadic ALS cases compared to controls (15). These altered properties of mutant SOD1 have not yet been causally-linked specifically to motor neuron damage in ALS. However, these observations are relevant to our recent findings that motor neuron degeneration in sporadic ALS and FALS is apoptosis (3) and that induced apoptosis of motor neurons in animal models is associated with peroxynitrite formation and hydroxyl radical damage to DNA (16).

Motor neuron degeneration occurs in mice with forced expression of mutant forms of the gene encoding for SOD1 (17,18). The motor neuron degeneration found in transgenic mice overexpressing the FALS mutant forms of SOD1 (17-19) is different structurally from the degeneration of motor neurons in sporadic and FALS (3). Rather than being a condensational form of death, these mouse motor neurons become swollen and severely vacuolated. Neither morphological nor biochemical evidence for apoptotic death of motor neurons has been shown in any of the SOD1 transgenic mouse models of ALS, and it is still uncertain whether motor neurons in these mouse models die or whether they remain in a severely vacuolated, atrophic state, similar to neurons in some models of axotomy and excitotoxicity (20,21). Although, the survival of FALS mice is prolonged when crossed with mice overexpressing Bcl-2 (22) or a dominant negative inhibitor of caspase-1 (23), the degeneration of motor neurons is not prevented (22), suggesting that neuronal degeneration in FALS mice is not apoptosis controlled by PCD mechanisms. The vacuolar and edematous degeneration of motor neurons in mice overexpressing mutant SOD1 (17-19) more closely resembles excitotoxic neuro-degeneration (24,25) or transsynaptic neuronal atrophy (but not death) induced by deafferentation (20,21). It is possible that the prominent neuropathological dissimilarity between motor neuron degeneration in existing transgenic mouse models and in ALS is related to differences in the level of mutant SOD1 expression and the rate of neuronal degeneration. We have found that rate of neuronal injury influences the cell death pathway, with neuronal necrosis evolving acutely and neuronal apoptosis progressing more slowly, despite similar mechanisms such as oxidative stress (26).

3. Excitotoxicity and neurodegeneration in ALS

The amino acid glutamate is the major excitatory neuro-transmitter in the CNS. Glutamate functions in synaptic neurotransmission by activating glutamate receptors (GluRs). Excessive activation of subtypes of GluRs is excitotoxic to neurons (25-28). GluR-mediated excitotoxicity has been

proposed to explain the patterns of selective neuronal cell death and clinical manifestations of ALS. This hypothesis is based on several different lines of evidence: an exogenous glutamate analogue may be responsible for the damage to upper motor neurons in lathyrism via actions at specific GluR subtypes (29); abnormalities in brain tissue excitatory amino acid metabolism may participate in the pathogenesis of Huntington's disease and olivopontocerebellar atrophy (two slowly progressive, chronic neurodegenerative disorders with selective neuronal vulnerability) (30,31); serum and cerebrospinal fluid concentrations of glutamate have been found to be increased in patients with sporadic ALS in some studies (32-34), although not in other studies (35,36); spinal cord and affected brain regions of patients with ALS have decreased synaptosomal glutamate uptake (37,38); the protein levels of glutamate transporter GLT1 are decreased in vulnerable regions in ALS (39); abnormal RNA processing of GLT1 transcripts may occur in some cases of ALS (40), although other groups have found these 'aberrant' forms of GLT1 transcripts in controls (41,42); and, lastly, the antiglutamate agent riluzole may slow the progression of ALS and improve survival of patients (43).

It still has not been determined satisfactorily if these changes in glutamate levels and glutamate uptake are primary or secondary to the disease process in ALS. For example, defects of glutamate transporter subtypes in ALS (37,38) could reflect a primary loss or inactivation of proteins or secondary effects of neurodegeneration. Neuronal cells have an important modulatory role in astroglial GLT1 expression because neurons liberate soluble factors that signal astroglial expression of GLT1 mRNA and protein (44) and, thus, neuronal loss or synaptic deafferentation may cause a downregulation of GLT1 expression (45,46). Therefore, the argument for glutamate excitotoxicity resulting from GLT1 loss or downregulation as a primary mechanism for neurodegeneration in ALS is, as yet, only speculation, but glutamate toxicity could contribute to the death of motor neurons even if alterations in GluRs or transporters are secondary changes.

The mechanisms through which activation of neuronal GluRs cause cell death involve alterations in cytosolic free Ca^{2+} homeostasis and activation of Ca^{2+}-sensitive proteases, protein kinases, endonucleases, lipases, and phospholipases (28,47). The acute effects of GluR excitotoxicity have been much better defined than the delayed effects on neurons, whereas the relationships between GluR-mediated excitotoxicity and neuronal death in slow, chronic neurodegeneration are only speculative. The delayed onset of neurodegeneration in patients with ALS could be related synergistically to progressive impairments in mitochondrial oxidative phosphorylation that accompany aging (48), to mutations in SOD1 and ensuing chronic, age-related intracellular damage by reactive free radicals (4), or to cumulative, age-related dysfunctional regulation of glutamate release, transport, and GluR activation (27,28,47,48). This possible synergism between abnormalities is exemplified by a study revealing that SOD1 mutations linked to FALS cause free radical damage to GLT1 and transporter inactivation (49).

However, like the patterns of SOD1 expression in CNS (5), neither differential subunit compositions of ion channel GluRs (AMPA and NMDA receptors) nor differential expressions of glutamate transporters appear to explain sufficiently the mechanisms that dictate the selective vulnerability of neurons in motor cortex and motor neurons in brainstem and spinal cord in ALS. This conclusion is based on many glutamate receptor/transporter expression and localization studies in animal and human CNS (50-57). The most convincing data indirectly implicating excitotoxicity as having a role in the pathogenesis of ALS is the selective loss of the glutamate transporter GLT1 in vulnerable regions in ALS (38,39). However, loss of synaptosomal glutamate uptake and loss of GLT1 protein also occur in Alzheimer's disease (58,59).

Experimental neuropathological studies have shown the possible consequences of glutamate uptake failure in the regulation of extracellular glutamate and neuronal survival in the CNS. For example, injection of the glutamate transporter inhibitor threo-3-hydroxy-DL-aspartate into rat striatum causes neurodegeneration (60). Mice genetically deficient in GLT1, although they develop normally without motor neuron degeneration, are more susceptible to edema formation than wild-type mice in a model of cold injury to the cerebral cortex (61). Nevertheless, the data in ALS is still indirect evidence for GluR-mediated excitotoxicity, and it is still uncertain whether glutamate transporter changes are related to the consequences of the disease or whether abnormalities in glutamate transporters and potential GluR excitotoxicity contribute mechanistically to the pathogenesis of ALS.

Most patients with ALS are maintained on mechanical ventilation, as a means of relieving symptoms of chronic hypoventilation and prolonging life, but patients die eventually from respiratory insufficiency (62). It has been argued that riluzole improves the survival of ALS patients by acting as a Na^+ channel blocker and increasing resistance to hypoxia (by reducing energy demand), not by anti-excitotoxic actions (63). Interestingly, there is *in vivo* evidence that GLT1 is preferentially more sensitive to cerebral hypoxia-ischemia than other glutamate transporters in animal models (45,64). It is also important to note that loss of glutamate transporter function and accumulation of extracellular glutamate does not necessarily lead to neurodegeneration (46,65-67). We also found that GluR-mediated excitotoxicity in adult CNS kills neurons by a mechanism that is different structurally from the pattern seen in ALS (3,21,24). Thus, it is possible that changes in astroglial glutamate transporters in individuals with ALS are possibly consequences of neurodegeneration, or, alternatively, these alterations are related to premortem agonal state.

4. ALS and neuronal cell death

Cellular degeneration can result in atrophy or death. Insults to neurons do not necessarily lead to cell death. In the CNS, neurons can survive an insult and exist chronically in an altered, atrophic state (20,21). In ALS, motor neurons die unequivocally and are eliminated (3). The process and molecular causes of motor neuron death in individuals with ALS are not fully understood.

Cell death can occur by different pathways. Depending on the type of cell and on the stimulus, cells die typically in either of two ways, generally described as apoptosis or necrosis (26,68,69). These two forms of cell death are thought to differ fundamentally in structure and mechanisms. Apoptosis is a

structurally organized PCD that is mediated by active, intrinsic mechanisms. However, PCD does not mean that the death is purely genetic and independent of epigenetic or environmental signals. For instance, PCD is often dependent on a variety trophic factors and cell-cell interactions. In contrast, cellular necrosis is though to be mechanistically and structurally a more rapid and random degeneration resulting from abrupt pathophysiological perturbations (e.g., osmotic, thermal, toxic, or traumatic) involving energy depletion, disruption of plasma membrane structural and functional integrity, rapid influx of Na^+, Ca^{2+} and water, and failure of cell volume homeostasis.

However, within the realm of neuronal cell death structure, 'shades of gray' can be observed (24,26,69,70). Our experiments using an animal model of excitotoxic degeneration of neurons led to the novel concept of an apoptosis-necrosis continuum for neuronal death *in vivo* (24,70). We concluded that excitotoxic death of neurons does not have to be strictly apoptosis or necrosis, according to a traditional binary classification of cell death structure, but it can also occur as intermediate or hybrid forms of cell death with coexisting characteristics that lie along a structural continuum with apoptosis and necrosis at the extremes. Features such as the subtypes of GluR that are activated influence where a dying neuron falls along this continuum. Therefore, excitotoxic neuronal death may not be identical in every neuron, possibly because of the high diversity in the expression, localization, and function of GluR subtypes and second messenger systems in the CNS (50-57). We also discovered that the structure of neuronal death is influenced by CNS maturity, because death of injured adult neurons only rarely occurs with apoptotic structural features that are identical to those seen during naturally occurring PCD in the developing nervous system (26,69). Thus, our concept of the apoptosis-necrosis structural continuum for neuronal cell death may be relevant ultimately for understanding neuronal death in neurodegenerative disorders.

5. Apoptosis contributes to the neuronal death in ALS

The ongoing identification of genetic and molecular regulatory mechanisms for PCD (Table II) has fueled the idea that abnormalities in the expression and functioning of cell death proteins may activate anomalous neuronal death in neuro-degenerative diseases (26,69,71-73). This possibility is supported by the finding that the genes for neuronal apoptosis inhibitory protein and survival motor neuron are either deleted partially or are mutant in some individuals with spinal muscular atrophy (a pediatric form of motor neuron disease) (72,74). However, it has been uncertain whether the neurodegeneration in ALS is apoptosis and is related causally to abnormalities in the molecular regulation of cell death and whether it is PCD.

We therefore evaluated critically the structure of degenerating motor neurons in postmortem cases of ALS and determined that it is a form of apoptosis (3). Interestingly, the nuclear morphology of degenerating motor neurons in individuals with ALS is not identical to classical neuronal apoptosis found in the developing CNS (26) or to excitotoxicity-induced neuronal apoptosis in the developing brain (26). Therefore, we have concluded that the death of

Table II. Molecular regulation of apoptosis.

Bcl-2 family		Caspase family	IAP family
Antiapoptotic proteins	Proapoptotic proteins		
Bcl-2[a]	Bax[a]	Apoptosis 'initiators': caspase-2, -8, -9, -10	NAIP
Bcl-x$_L$[b]	Bak[a]	Apoptosis 'executioners': caspase-3[a], -6, -7	IAP1
Boo	Bcl-x$_S$ Bad Bid Bik Mtd	Cytokine processors: caspase-1, -4, -5, -11, 12, -14	IAP2 XIAP

[a]Identifies proteins that have been shown to be abnormal in individuals with ALS (3). [b]Identifies proteins that have been shown to be unchanged in ALS (3).

neurons in ALS is a form of apoptosis that may differ slightly from classical apoptosis at the structural level (3). This interpretation is consistent with the concept that neuronal maturity, magnitude of target deprivation, and rate (i.e., progression or timing) of neuronal death may influence the structure of dying cells (26).

We also found that in selectively vulnerable CNS regions in individuals with ALS compared to age-matched controls, the proapoptotic proteins Bax and Bak are elevated in the mitochondrial-enriched membrane compartment but are reduced or unchanged in the cytosol (3). In contrast, the antiapoptotic protein Bcl-2 is decreased in the mitochondrial-enriched membrane compartment of vulnerable regions in ALS but is increased in the cytosol. Coimmunoprecipitation experiments demonstrated that Bax-Bax interactions are greater in the mitochondrial-enriched membrane compartment of ALS motor cortex compared to controls, whereas Bax-Bcl-2 interactions are decreased in the membrane compartment of ALS motor cortex compared to controls. We also found that caspase-3 is activated in ALS. Abnormalities were not found in somatosensory cortex of ALS cases. These measurements were made on discretely microdissected punches throughout the entire lumbar and cervical spinal cord as well as the motor and sensory cortical grey matter mantles. The spinal cord and motor cortical samples were as selective for motor neuron populations as possible without the aid of laser capture microscopy. Thus, we propose that a PCD mechanism, involving cytosol-to-membrane and membrane-to-cytosol redistributions of cell death proteins, participates in the pathogenesis of motor neuron degeneration ALS (3).

6. Molecular regulation of apoptosis

Apoptosis is an organized cell death. It is mediated by active, intrinsic PCD mechanisms. Three families of apoptosis-regulating genes have been identified in mammals (75-77). The molecular mechanisms for PCD (Table II) involve the activation of the caspase family of cysteine-containing, aspartate-specific proteases (14 members have been identified to date) and the interactions among cell death proteins in the Bcl-2 family (e.g., Bcl-2, Bcl-x_L, Bcl-x_S, Bax, Bak, Bid, and Bad), as well as modulation of cell death by the inhibitor of apoptosis protein (IAP) family.

Caspases exist as constitutively expressed, inactive proenzymes in healthy cells. Caspases are activated through regulated proteolysis (Table II). These proteins function in systematically dismantling and packaging the cell during apoptosis, with 'initiator' caspases activating 'executioner' caspases which subsequently cleave cellular substrates, thereby causing the molecular and structural changes of organized cell death. Active caspases can cleave nuclear proteins [e.g., polyADP-ribose polymerase (PARP), DNA-dependent protein kinases, heteronuclear ribonucleoproteins, or lamins], cytoskeletal proteins (e.g., actin and fodrin), and cytosolic proteins [e.g., other caspases and DNA fragmentation factor 45 (DFF-45)] (75,77). Other caspase family members function in inflammation by processing pro-inflammatory cytokines (Table II). Two different caspase cascades mediate PCD. One pathway is initiated by cytochrome c release from mitochondria, that promotes the activation of caspase-9 through Apaf-1 and then caspase-3 activation (78). Another pathway is initiated by the activation of cell-surface death receptors, including Fas and tumor necrosis factor receptor, leading to caspase-8 activation, that in turn cleaves and activates downstream caspases such as caspase-3, -6, and -7 (79,80).

Another group of apoptosis regulatory genes is the *bcl*-2 proto-oncogene family (Table II) (76). Of these genes, *bcl*-2, *bcl*-x_L, and *boo* are antiapoptotic, whereas *bax*, *bcl*-x_S, *bad*, *bak*, *bid*, *bik*, and *mtd* are proapoptotic. Membership into the family of Bcl-2-related proteins is defined by homology domains (BH1-BH4), which function in the interactions between members. Bcl-2 family members exist as monomers that form homo- or heterodimers and higher order multimers (76). For example, Bax can form homodimers or heterodimers with either Bcl-2 or Bcl-x_L (76). When Bax and Bak are present in excess, they can antagonize the antiapoptotic activity of Bcl-2. The formation of Bax homodimers is thought to promote apoptosis, whereas Bax heterodimerization with either Bcl-2 or Bcl-x_L appears to prevent apoptosis. Thus, the complex, steady-state array of protein-protein interactions among members of the Bcl-2 family functions in dictating whether a cell lives or dies. This complexity is further expanded because some proapoptotic proteins such as Mtd (called matador) can function independently of heterodimerization with survival-promoting Bcl-2 and Bcl-x_L (81).

Cell death is also regulated by the IAP (inhibitor of apoptosis protein) family (82). This family includes X-chromosome-linked IAP, IAP1, IAP2, and NAIP (neuronal apoptosis inhibitory protein). Survival motor neuron is another apoptosis inhibitory protein. The main identified mechanism by which IAPs suppress apoptosis is by the prevention of proteolytic processing of specific caspases (83). It appears that procaspase-9 is the major target of IAPs. However, IAPs do not prevent caspase-8-induced proteolytic activation of procaspase-3. IAPs can also block apoptosis by reciprocal interactions with the nuclear transcription factor NFκB (82). NAIP is abnormal in infants and children with spinal muscular atrophy (72-74). It is tempting to speculate about the possibility of IAP inactivation in ALS as a mechanism for motor neuron apoptosis, but this possibility remains to be examined. To date, the deletions in the genes for NAIP and survival motor neuron that have been identified in cases of spinal muscular atrophy have not been found in individuals with ALS (84).

In cell models of apoptosis based on *in vitro* experiments using human cell lines, activation of caspase-3 occurs when caspase-9 proenzyme (also known as Apaf-3) is bound by Apaf-1 in a process initiated by cytochrome c (identified as Apaf-2) and either ATP or dATP (78). Cytosolic ATP or dATP are required cofactors for cytochrome c-induced caspase activation. Apaf-1, a 130 kDa protein, serves as a docking protein for procaspase-9 (Apaf-3) and cytochrome c (78). Apaf-1 becomes activated when ATP is bound and hydrolyzed, with the hydrolysis of ATP and the binding of cytochrome c promoting Apaf-1 oligomerization (85). This oligomeric complex recruits and activates procaspase-9 which disassociates from the complex and becomes available to activate caspase-3. This stage is where IAPs can act to block apoptosis (83). Once activated, caspase-3 cleaves a protein with DNase activity (DFF-45), and this cleavage activates a pathway leading to the internucleosomal fragmentation of genomic DNA (86).

In response to several apoptosis-inducing agents, cytochrome c is released from mitochondria to the cytosol (87,88) through a mechanism that may involve the formation of membrane channels comprised of Bax and mitochondrial permeability transition pores (89). Bcl-2, or the closely related Bcl-x_L, blocks the release of cytochrome c from mitochondria and thus the activation of caspase-3 (78,90). The blockade of cytochrome c release from mitochondria by Bcl-2 and Bcl-x_L (90, 91) is possibly due to inhibition of Bax channel-forming activity in the outer mitochondrial membrane (89) or to the regulation of mitochondrial membrane potential and volume homeostasis (91). Bcl-x_L also has antiapoptotic functions by physically interacting with Apaf-1 and caspase-9 and inhibiting the Apaf-1-mediated maturation of caspase-9 (92). Boo can inhibit Bak- and Bik-induced apoptosis (but not Bax-induced cell death) possibly through heterodimerization and by interactions with Apaf-1 and caspase-9 (93).

Protein phosphorylation can regulate the functions of Bcl-2 family members. Following serine phosphorylation, Bcl-2 loses its antiapoptotic activity, possibly because it cannot maintain its antioxidant function (94). In addition to interacting with homologous proteins, Bcl-2 can associate with non-homologous proteins, including the protein kinase Raf-1 (95). Bcl-2 is thought to target Raf-1 to mitochondrial membranes, allowing this kinase to phosphorylate Bad at serine residues. Phosphorylated Bad translocates to the cytosol and interacts with soluble protein 14-3-3 and, when bound to protein 14-3-3, Bad is unable to interact with Bcl-2 and Bcl-x_L, thereby promoting survival (96). Non-phosphorylated Bad heterodimerizes with membrane-associated Bcl-2 and Bcl-x_L, thereby

displacing Bax from Bax-Bcl-2 and Bax-Bcl-x_L dimers and promoting cell death (97).

Cell death by apoptosis can also be signaled at the cell membrane by surface receptors of the tumor necrosis factor (TNF) receptor family. Fas (CD95/Apo-1) is a member of the TNF receptor family (79). Apoptosis through Fas is independent of new RNA or protein synthesis. The signal for apoptosis is initiated at the cell surface by aggregation of Fas, induced by the binding of the multivalent Fas ligand (FasL), a member of the TNF-cytokine family, expressed on activated T cells and natural killer cells. Clustering of Fas by FasL recruits Fas-associated death domain (FADD), a cytoplasmic adapter molecule that functions in the activation of the caspase 8-Bid pathway, thus forming the 'death-induced signaling complex' (DISC) (80). In this pathway, Bid (a proapoptotic family member that is a substrate for caspase-8) is cleaved in the cytosol, and then truncated Bid translocates to mitochondria, thereby functioning as a transducer of Fas apoptotic signals at the cell plasma membrane to the mitochondria (80). Bid translocation from the cytosol to mitochondrial membranes is associated with a conformational change in Bax (that is prevented by Bcl-2 and Bcl-x_L) and is accompanied by release of cytochrome c from mitochondria (98). At present it is not clear whether the Fas-caspase-Bid signaling pathway for apoptosis participates in the mechanisms for motor neuron apoptosis in ALS. Our laboratory is actively investigating this possibility.

Apoptosis can also be induced by the oncosuppressor protein p53 (99). This DNA binding protein functions in genome surveillance, DNA repair, and as a transcription factor. p53 commits to death cells that have sustained DNA damage from genotoxic agents and ROS (99). The mechanisms by which p53 induces apoptosis are not fully understood, although it is know that p53 is a direct transcriptional activator of the human *bax* gene (100) and a transcriptional repressor of the *bcl*-2 gene (101). This information is important because we have found increased Bax protein levels and decreased Bcl-2 protein in selectively vulnerable CNS regions in ALS (3). Thus, p53 may participate in the mechanisms for motor neuron death in ALS.

7. Autoimmunity and ALS

Another theory for the pathogenesis for ALS suggests that degeneration of upper and lower motor neurons is caused by an autoimmune response. Support for this theory is based on studies identifying antibodies to L-type voltage-gated Ca^{2+} channels in some patients with sporadic ALS, although the presence of these antibodies is not specific for ALS (102). These Ca^{2+} channel antibodies induce Ca^{2+}-dependent apoptosis in differentiated motor neurons in culture by a mechanism involving oxidative stress (103). Additional evidence supporting an immune mechanism for neuronal death in ALS is derived from experiments revealing greater numbers of cytotoxic T cells in ALS tissues compared to controls (104). Cytotoxic T cells induce their target cells to undergo PCD by perforin release and granzyme B activation or by Fas signaling (79). It is not yet clear whether Fas signaling contributes to the mechanisms for neuronal apoptosis in ALS. However, caution is warranted in this regard because these data may

signify an immune response in ALS tissues secondary to neurodegeneration, rather than a primary mechanism for motor neuron apoptosis.

Despite data suggesting an immunological contribution to the pathogenesis of ALS, to date, the disease process has not responded to immunosuppressive therapies. However, well recognized immunopathies, such as multiple sclerosis and diabetes, do not respond to known immunosuppression methods. Thus, the possible contributions of immunological abnormalities to the mechanisms for motor neuron death in ALS have yet to be fully explored.

8. PCD pathways and neuronal apoptosis

A control of PCD by cell death proteins has been demonstrated in the mammalian nervous system. The numbers of neurons may be increased (presumably resulting from deficient apoptosis) in some CNS regions in transgenic mice that overexpress the *bcl*-2 gene (105-107), in mice with *bax* gene-ablations (108), and in mice with caspase-3 (109), caspase-9 (110,111), and Apaf-1 (112) gene deletions. Caspase-3, caspase-9, and Apaf-1 deficiencies are embryonic lethal. In contrast, Bcl-2-deficient mice survive and show an interesting progressive degeneration of motor neurons after the PCD period during early postnatal development (113).

Support for the contribution of apoptosis in neurodegeneration is found in axotomy and trophic factor withdrawal experiments. Bcl-2 overexpression ameliorates the motor neuron death in newborn mice induced by facial nerve transection (114), sciatic nerve transection (105), or optic nerve transection (107). Caspases appear to participate in apoptosis of sensory and motor neurons. For example, inhibition of caspase-1 and caspase-2 blocks the apoptosis of dorsal root and sympathetic ganglion neurons when deprived of nerve growth factor (115,116); furthermore, in retina, inhibition of caspase activity protects axotomized ganglion cells from death after optic nerve transection in adult rat (117). Inhibition of caspase-1 also arrests the PCD of motor neurons *in vitro* resulting from trophic factor deprivation and *in vivo* during the period of naturally occurring cell death (118).

9. Oxidative stress induces neuronal apoptosis

Oxidative stress is a potent stimulus for apoptosis in a variety of *in vitro* systems, including cultured neurons (119-121). Reactive oxygen species (ROS), such as superoxide anion radical, hydrogen peroxide and hydroxyl radical, can directly damage macromolecules, including DNA, protein, and lipid membranes (122). The balance between endogenous ROS formation and antioxidant defense mechanisms is important for cellular survival. ROS are byproducts of oxidative metabolism. The mitochondrial electron-transfer chain is a primary generator of superoxide and peroxide (123), and damaged mitochondria produce greater amounts of superoxide ion (123). Point mutations in mitochondrial DNA caused by oxidative damage may lead to protein conformational changes and inefficient electron transfer to cytochrome c oxidase (124) and, hence, enhanced superoxide and peroxide formation. These observations are consistent with the idea that mitochondria participate in the effector stages of apoptosis (125)

through changes in apoptotic protein function and cytochrome c release.

10. DNA damage and DNA repair mechanisms in ALS

The accumulation of damaged DNA may be a primary abnormality in ALS (126). This damage may be either acquired or inherited. Elevated levels of oxidatively damaged DNA in the form of DNA adducts (e.g., 8-oxodeoxyguanosine) have been found in spinal cord tissue of ALS cases (127). In addition, increased concentrations of hydroxyl radical damaged DNA have been found in the motor cortex of sporadic ALS cases (128). It has been proposed that SOD1 linked FALS mutations cause an altered sensitivity to free radicals; however, lymphoblastoid cells from FALS patients with SOD1 gene mutations do not show impaired abilities to scavenge radiation-induced free radicals and to protect against DNA double-strand breaks (129).

DNA oxidation occurs at a significant rate *in vivo* and is counteracted by specific DNA repair mechanisms (130). Apurinic/apyrimidinc endonuclease (APE) is a critical enzyme in the DNA base-excision repair pathway, which is considered to be the predominant pathway for repair of oxidatively damaged DNA (131). Studies have suggested that DNA repair mechanisms are deficient in individuals with sporadic ALS (132,133), and, interestingly, the possible defects in APE may be cell or tissue type specific (134). Moreover, mutations in APE have been identified in sporadic ALS (135,136), further suggesting a possible role for defective DNA repair in the etiology of ALS.

11. Animal models of neuronal apoptosis in the adult CNS

It is important to study neuronal apoptosis in adult animal models because ALS is an adult onset neurodegenerative disease and CNS maturity has major influences on the structure of neuronal death (24,26,69). We found that the degeneration of motor neurons in individuals with ALS (3) has many similarities to the apoptosis of CNS neurons induced by axotomy and target deprivation in adult animals (16,137,138). This induced apoptosis is characterized morphologically by chromatolysis followed by a progressive sequence of neuro-filament accumulation, cytoplasmic and nuclear condensation, and cellular shrinkage. Degenerating motor neurons in ALS also undergo chromatolysis and then progressive cytoplasmic and nuclear condensation (3). Affected neurons show cyto-skeletal pathology in the form of neurofilament accumulation within the neuronal cell body and axon (139,140). Because motor neuron degeneration in sporadic and FALS is structurally different from the motor neuron degeneration found in trans-genic mice overexpressing the FALS mutant forms of SOD1 (3,17-19), animal models for *bona fide* neuronal apoptosis *in vivo* are critical for understanding the neurobiology of disease in ALS.

In two different animal models of axotomy-induced retro-grade neuronal apoptosis in the adult CNS, we have found that neuronal death occurs in association with the accumulation of functionally active mitochondria and oxidative stress (16,137, 138). Mitochondrial accumulation within the neuronal cell body and increased metabolic activity may cause excessive generation of ROS within the vicinity of the neuronal nucleus, depletion of mitochondrial and cytosolic antioxidant mechanisms, and subsequent oxidative damage to DNA (3,138). In both adult CNS models of neuronal apoptosis that are studied in our laboratory, the mitochondria become progressively damaged, as evidenced by the eventual loss of cytochrome c oxidase activity and by the swelling and cristeolysis that manifest concurrently with the incipient cyto-plasmic compaction of apoptosis, supporting the hypothesis that apoptosis-initiating factor(s) and cytochrome c are sequestered in the mitochondrial intermembrane space (78,90), which upon their release activate a PCD cascade (86-88). The finding that oxidative stress induces neuronal apoptosis *in vitro* (120,121,125) supports our idea that mitochondria may participate in the signaling of injured, chromatolytic motor neurons to enter apoptosis, possibly by releasing cytochrome c from mitochondria (87-88) or by generating excessive ROS and causing DNA damage-induced, p53 activation (99). We now have preliminary data suggesting that this retrograde apoptosis of motor neurons may be dependent on DNA damage-induced p53 activation (Martin LJ, *et al*, Soc Neurosci Abs. 25: 289, 1999). If normal trafficking of mitochondria into axonal and dendritic compartments is not re-established or effectively buffered, a sustained accumulation of active mitochondria in the vicinity of the nucleus may provide a source of DNA damaging ROS as well as Apaf-2. It has been suggested that hydroxyl radical production by microdialysis of hydroxyl radical generators can kill motor neurons in spinal cord (141). However, at present, it is uncertain if mitochondrial-derived ROS can trigger apoptosis of motor neurons *in vivo*.

Induced neuronal apoptosis in the adult CNS is associated with hydroxyl radical damage to DNA (16,138). Among the ROS, hydroxyl radicals are highly reactive and are thought to be genotoxic by interacting with DNA and producing DNA strand breaks and base modifications (122-124). Hydroxyl radicals are products of the transitional metal (e.g., iron) - catalyzed, Haber-Weiss- and Fenton-type reactions that use superoxide and hydrogen peroxide as substrates, respectively (123). Our recent experiments are important because they show the formation of hydroxyl radical-modified DNA during the progression of neuronal apoptosis *in vivo*.

In addition, our experiments indicate that peroxynitrite radicals are formed within motor neurons early after injury at preapoptotic stages of degeneration, based on the transient detection of intense nitrotyrosine immunoreactivity within subsets of ventral root axons and motor neuron cell bodies (16). The appearance of this intense nitrotyrosine immunoreactivity occurs prior to structural evidence for apoptosis in avulsed motor neurons. Nitric oxide synthase is induced in motor neurons after avulsion (142) and in primary cultures of embryonic motor neurons deprived of brain-derived neurotrophic factor (143). In this latter *in vitro* paradigm, motor neurons cultured in the absence of trophic factor exhibit nitrotyrosine immunoreactivity prior to the occurrence of apoptosis (143), similar to our findings *in vivo* (16). Inhibition of nitric oxide synthase reduces motor neuron loss after spinal root avulsion (144). Therefore, the accumulation of active mitochondria within neuronal cell bodies, combined

with nitric oxide induction (142), may lead to peroxynitrite formation and induction of motor neuron apoptosis *in vivo*.

Our observations in models of axotomy-induced neuronal apoptosis in the adult CNS may be important for the understanding of neuronal death in human, adult-onset neurodegenerative diseases such as ALS. Neurodegeneration in ALS has components of axotomy/target deprivation-like retrograde neuronal injury. In addition, evidence for oxidative damage has been found in postmortem brains from individuals with ALS, based on the detection of protein carbonyls, protein nitration, and DNA oxidation (126-128). Important unanswered questions regarding neuronal apoptosis in the adult CNS and in ALS center on the dependence of this process on specific molecules, including p53, Fas, Bax, and caspases. Trophic factor deprivation-induced apoptosis of motor neurons *in vitro* (108,118,143) and *in vivo* (108,118) is caspase- and Bax-dependent, as might be the case for motor neuron apoptosis in ALS (3).

12. Future hope for the understanding of ALS

Additional laboratory experiments are necessary to identify possible cellular and molecular causes for motor neuron apoptosis in individuals with ALS by analyzing, in postmortem CNS tissues, proteins that function in PCD pathways. In parallel, studies need to be conducted to identify the cellular and molecular similarities and differences among motor neuron degeneration in ALS and in animal models in which motor neurons degenerate. For example, mice genetically deficient in Fas/FasL, Bax, and p53, can be used to dissect the contribution of these molecules in controlling apoptosis in motor neurons *in vivo*. Once appropriate animal models for motor neuron apoptosis have been identified and characterized, new drugs or biological agents (caspase inhibitors, antioxidants, immunosuppressants, and neurotrophic factors) can be tested for safety and for their ability to abrogate motor neuron apoptosis. The demonstration that abnormal PCD mechanisms participate in the pathogenesis of motor neuron degeneration in ALS (3), and the clarification of the molecular pathways mediating motor neuron apoptosis, should lead to the identification of alternative treatments or cures for ALS. Our recent experiments with ALS CNS tissues (3) have important therapeutic implications for patients with ALS. Manipulations that cause an elevation and specific activation of Bcl-2 or IAPs and pharmacological treatment with caspase inhibitors may delay the onset or progression of motor neuron apoptosis in patients with ALS. In this regard though, elevations in antiapoptotic proteins may not be meaningful therapeutically unless the subcellular trafficking and targeting (i.e., to mitochondria) of proteins is efficient in motor neurons.

Acknowledgments

References

1. Kuncl RW, Crawford TO, Rothstein JD and Drachman DB: Motor neuron diseases. In: Diseases of the Nervous System. Clinical Neurobiology. Asbury AK, McKhann GM and McDonald WI (eds). WB Saunders, Philadelphia, pp1179-1208, 1992.
2. Rosen DR, Siddique T, Patterson D, Figiewicz DA, Sapp P, Hentati A, Donalsson D, Goto J, O'Regan JP, Deng H-X, Rahmani Z, Krizus A, McKenna-Yasek D, Cayabyab A, Gaston AM, Berger R, Tanzi RE, Halperin JJ, Harzfeldt B, van den Bergh R, Hung W-Y, Bird T, Deng G, Mulder DW, Smyth C, Laing NG, Soriano E, Pericak-Vance MA, Haines J, Rouleau GA, Gusella JS, Horvitz HR and Brown RH: Mutations in Cu/Zn superoxide dismutase gene are associated with familial amyotrophic lateral sclerosis. Nature 362: 59-62, 1993.
3. Martin LJ: Neuronal death in amyotrophic lateral sclerosis is apoptosis: possible contribution of a programmed cell death mechanism. J Neuropathol Exp Neurol 58: 459-471, 1999.
4. Deng H-X, Hentati A, Tainer JA, Iqbal Z, Cayabyab A, Hung W-Y, Getzoff ED, Hu P, Herzfeldt B, Roos RP, Warner C, Deng G, Soriano E, Smyth C, Parge HE, Ahmed A, Roses AD, Hallewell RA, Pericak-Vance MA and Siddique T: Amyotrophic lateral sclerosis and structural defects in Cu, Zn superoxide dismutase. Science 261: 1047-1051, 1993.
5. Furuta A, Price DL, Pardo CA, Troncoso JC, Xu Z, Taniguchi N and Martin LJ: Localization of superoxide dismutases in Alzheimer's disease and Down's syndrome neocortex and hippocampus. Am J Pathol 146: 357-367, 1995.
6. Troy CM and Shelanski ML: Down-regulation of copper/zinc superoxide dismutase causes apoptotic death in PC12 neuronal cells. Proc Natl Acad Sci USA 91: 6384-6387, 1994.
7. Rothstein JD, Bristol LA, Hosler B, Brown RH and Kuncl RW: Chronic inhibition of superoxide dismutase produces apoptotic death of spinal neurons. Proc Natl Acad Sci USA 91: 4155-4159, 1994.
8. Greenlund LJS, Deckwerth TL and Johnson EM: Superoxide dismutase delays neuronal apoptosis: a role for reactive oxygen species in programmed neuronal death. Neuron 14: 303-315, 1995.
9. Borchelt DR, Lee MK, Slunt HS, Guarnieri M, Xu ZS, Wong PC, Brown RH, Price DL, Sisodia SS and Cleveland DW: Superoxide dismutase 1 with mutations linked to familial amyotrophic lateral sclerosis possesses significant activity. Proc Natl Acad Sci USA 91: 8292-8296, 1994.
10. Rabizadeh S, Butler Gralla E, Borchelt DR, Gwinn R, Valentine JS, Sisodia S, Wong, P, Lee M, Hahn H and Bredesen DE: Mutations associated with amyotrophic lateral sclerosis convert superoxide dismutase from an antiapoptotic gene to a proapoptotic gene: studies in yeast and neural cells. Proc Natl Acad Sci USA 92: 3024-3028, 1995.
11. Wiedau-Pazos M, Goto JJ, Rabizadeh S, Gralla EB, Roe JA, Lee MK, Valentine JS and Bredensen DE: Altered reactivity of superoxide dismutase in familial amyotrophic lateral sclerosis. Science 271: 515-518, 1996.
12. Beckman JS, Carson M, Smith CD and Koppenol WH: ALS, SOD and peroxynitrite. Nature 364: 584, 1993.
13. Crow JP, Ye YZ, Strong M, Kirk M, Barnes S and Beckman JS: Superoxide dismutase catalyzes nitration of tyrosines by peroxynitrite in the rod and head domains of neurofilament-L. J Neurochem 69: 1945-1953, 1997.
14. Crow JP, Sampson JB, Zhuang Y, Thompson JA and Beckman JS: Decreased zinc affinity of amyotrophic lateral sclerosis-associated superoxide dismutase mutants leads to enhanced catalysis of tyrosine nitration by peroxynitrite. J Neurochem 69: 1936-1944, 1997.
15. Strong MJ, Sopper MM, Crow, JP, Strong WL and Beckman JS: Nitration of the low molecular weight neurofilament is equivalent in sporadic amyotrophic lateral sclerosis and control cervical spinal cord. Biochem Biophys Res Commun 248: 157-164, 1998.
16. Martin LJ, Kaiser A and Price AC: Motor neuron degeneration after sciatic nerve avulsion in adult rat evolves with oxidative stress and is apoptosis. J Neurobiol 40: 185-201, 1999.
17. Gurney ME, Pu H, Chiu AY, Dal Canto MC, Polchow CY, Alexander DD, Caliendo J, Hentati A, Kwon YW, Deng H-X, Chen W, Zhai P, Sufit RL and Siddique T: Motor neuron degeneration in mice that express a human Cu, Zn superoxide dismutase mutation. Science 264: 1772-1775, 1994.

18. Wong PC, Pardo CA, Borchelt DR, Lee MK, Copeland NG, Jenkins NA, Sisodia SS, Cleveland DW and Price DL: An adverse property of a familial ALS-linked SOD1 mutation causes motor neuron disease characterized by vacuolar degeneration of mitochondria. Neuron 14: 1105-1116, 1995.

19. Dal Canto MC and Gurney ME: Development of central nervous system pathology in a murine transgenic model of human amyotrophic lateral sclerosis. Am J Pathol 145: 1271-1280, 1994.

20. Ginsberg SD and Martin LJ: Ultrastructural analysis of the progression of neurodegeneration in the septum following fimbria-fornix transection. Neuroscience 86: 1259-1272, 1998.

21. Ginsberg SD, Portera-Cailliau C and Martin LJ: Fimbria-fornix transection and excitotoxicity produce similar neurodegeneration in septum. Neuroscience 88: 1059-1071, 1999.

22. Kostic V, Jackson-Lewis V, de Bilbao F, Dubois-Dauphin M and Przedborski S: Bcl-2: prolonging life in a transgenic mouse model of familial amyotrophic lateral sclerosis. Science 277: 559-562, 1997.

23. Friedlander RM, Brown RH, Gagliardini V, Wang J and Yuan J: Inhibition of ICE slows ALS in mice. Nature 388: 31, 1997.

24. Portera-Cailliau C, Price DL and Martin LJ: Non-NMDA and NMDA receptor-mediated excitotoxic neuronal deaths in adult brain are morphologically distinct: further evidence for an apoptosis-necrosis continuum. J Comp Neurol 378: 88-104, 1997.

25. Ikonomidou C, Qin YQ, Labruyere J and Olney JW: Motor neuron degeneration induced by excitotoxin agonists has features in common with those seen in the SOD-1 transgenic mouse model of amyotrophic lateral sclerosis. J Neuropathol Exp Neurol 55: 211-224, 1996.

26. Martin LJ, Al-Abdulla NA, Brambrink AM, Kirsch JR, Sieber FE and Portera-Cailliau C: Neurodegeneration in excitotoxicity, global cerebral ischemia, and target deprivation: a perspective on the contributions of apoptosis and necrosis. Brain Res Bull 46: 281-309, 1998.

27. Olney JW: Excitatory transmitter neurotoxicity. Neurobiol Aging 15: 259-260, 1994.

28. Choi DW: Excitotoxic cell death. J Neurobiol 23: 1261-1276, 1992.

29. Chase RA, Pearson S, Nunn PB and Lantos PL: Comparative toxicities of α- and β-N-oxalyl-L-α,β-diaminopropionic acid to rat spinal cord. Neurosci Lett 55: 89-94, 1985.

30. Beal MF, Matson WR, Swartz KJ, Gamache PH and Bird ED: Kynurenine pathway measurements in Huntington's disease striatum: evidence for reduced formation of kynurenic acid. J Neurochem 55: 1327-1339, 1990.

31. Plaitakis A: Glutamate dysfunction and selective motor neuron degeneration in amyotrophic lateral sclerosis: a hypothesis. Ann Neurol 28: 3-8, 1990.

32. Plaitakis A, Constantakakis E and Smith J: The neuroexcitotoxic amino acids glutamate and aspartate are altered in the spinal cord and brain in amyotrophic lateral sclerosis. Ann Neurol 24: 446-449, 1988.

33. Rothstein JD, Tsai G, Kuncl RW, Clawson L, Cornblath DR, Drachman DB, Pestronk A, Stauch B and Coyle JT: Abnormal excitatory amino acid metabolism in amyotrophic lateral sclerosis. Ann Neurol 28: 18-25, 1990.

34. Rothstein JD, Kuncl RW, Chaudhry V, Clawson L, Cornblath DR, Coyle JT and Drachman DB: Excitatory amino acids in amyotrophic lateral sclerosis: an update. Ann Neurol 30: 224-225, 1991.

35. Camu W, Billiard M and Baldy-Moulinier MB: Fasting plasma and CSF amino acid levels in amyotrophic lateral sclerosis: a subtype analysis. Acta Neurol Scand 88: 51-55, 1993.

36. Malessa S, Leigh PN, Bertel O, Sluga E and Hornykiewicz O: Amyotrophic lateral sclerosis: glutamate dehydrogenase and transmitter amino acids in the spinal cord. J Neurol Neurosurg Psychiatry 54: 984-988, 1991.

37. Rothstein JD, Martin LJ and Kuncl RW: Decreased glutamate transport by the brain and spinal cord in amyotrophic lateral sclerosis. N Engl J Med 326: 1464-1468, 1992.

38. Fray AE, Ince PG, Banner SJ, Milton ID, Usher PA, Cookson MR and Shaw PJ: The expression of the glial glutamate transporter protein EAAT2 in motor neuron disease: an immunohistochemical study. Eur J Neurosci 10: 2481-2489, 1998.

39. Rothstein JD, van Kammen M, Levey AI, Martin LJ and Kuncl RW: Selective loss of glial glutamate transporter GLT-1 in amyotrophic lateral sclerosis. Ann Neurol 38: 73-84, 1995.

40. Lin CL, Bristol LA, Dykes-Hoberg M, Crawford T, Clawson L and Rothstein JD: Aberrant RNA processing in a neurodegenerative disease: the cause for absent EAAT2, a glutamate transporter, in amyotrophic lateral sclerosis. Neuron 20: 589-602, 1998.

41. Meyer T, Münch C, Liebau S, Fromm A, Schwalenstöcker B, Völkel H and Ludolph AC: Splicing of the glutamate transporter EAAT2: a candidate gene of amyotrophic lateral sclerosis. J Neurol Neurosurg Psychiatry 65: 954, 1998.

42. Nagai M, Abe K, Okamoto K and Itoyama Y: Identification of alternative splicing forms of GLT1 mRNA in the spinal cord of amyotrophic lateral sclerosis. Neurosci Lett 244: 165-168, 1998.

43. Bensimon G, Lacomblez L, Meininger V and the ALS/Riluzole Study Group: A controlled trial of Riluzole in amyotropic lateral sclerosis. N Engl J Med 330: 585-591, 1994.

44. Gegelashvili G, Danbolt NC and Schousboe A: Neuronal soluble factors differentially regulate the expression of the GLT1 and GLAST glutamate transporters in cultured astroglia. J Neurochem 69: 2612-2615, 1997.

45. Martin LJ, Brambrink AM, Lehmann C, Portera-Cailliau C, Koehler R, Rothstein J and Traystman RJ: Hypoxia-ischemia causes abnormalities in glutamate transporters and death of astroglia and neurons in newborn striatum. Ann Neurol 42: 335-348, 1997.

46. Ginsberg SD, Rothstein JD, Price DL and Martin LJ: Fimbria-fornix transections selectively down-regulate subtypes of glutamate transporter and glutamate receptor proteins in septum and hippocampus. J Neurochem 67: 1208-1216, 1996.

47. Choi DW: Amyotrophic lateral sclerosis and glutamate: too much of a good thing? N Engl J Med 326: 1493-1495, 1992.

48. Beal MF: Does impairment in energy metabolism result in excitotoxic neuronal death in neurodegenerative illness? Ann Neurol 31: 119-130, 1992.

49. Trotti D, Rolfs A, Danbolt NC, Brown RH Jr and Hediger MA: SOD1 mutants linked to amyotrophic lateral sclerosis selectively inactivate a glial glutamate transporter. Nat Neurosci 2: 427-433, 1999.

50. Blackstone CD, Levey AI, Martin LJ, Price DL and Huganir RL: Immunological detection of glutamate receptor subtypes in human central nervous system. Ann Neurol 31: 680-683, 1992.

51. Martin LJ, Blackstone CD, Levey AI, Huganir RL and Price DL: AMPA glutamate receptor subunits are differentially distributed in rat brain. Neuroscience 53: 327-358, 1993.

52. Jakowec MW, Fox AJ, Martin LJ and Kalb RG: Quantitative and qualitative changes in AMPA receptor expression during spinal cord development. Neuroscience 67: 893-907, 1995.

53. Portera-Cailliau C, Price DL and Martin LJ: N-methyl-D-aspartate receptor proteins NR2A and NR2B are differentially distributed in the developing rat central nervous system as revealed by subunit-specific antibodies. J Neurochem 66: 692-700, 1996.

54. Brennan EM, Martin LJ, Johnston MV and Blue ME: The ontogeny of non-NMDA glutamate receptors in rat barrel field cortex. II. α-AMPA and kainate receptors. J Comp Neurol 386: 29-45, 1997.

55. Martin LJ, Furuta A and Blackstone CD: AMPA receptor protein in developing rat brain: GluR1 expression and localization change at regional, cellular, and subcellular levels with maturation. Neuroscience 83: 917-928, 1998.

56. Rothstein JD, Martin L, Levey AI, Dykes-Hoberg M, Jin L, Wu D, Nash N and Kuncl RW: Localization of neuronal and glial glutamate transporters. Neuron 13: 713-725, 1994.

57. Furuta A, Rothstein JD and Martin LJ: Glutamate transporter protein subtypes are expressed differentially during rat CNS development. J Neurosci 17: 8363-8375, 1997.

58. Masliah E, Alford M, DeTeresa R, Mallory M and Hansen L: Deficient glutamate transport is associated with neurodegeneration in Alzheimer's disease. Ann Neurol 40: 759-766, 1996.

59. Li S, Mallory M, Alford M, Tanaka S and Masliah E: Glutaamate transporter alterations in Alzheimer's disease are possibly associated with abnormal APP expression. J Neuropathol Exp Neurol 56: 901-911, 1997.

60. McBean GJ and Roberts PJ: Neurotoxicity of L-glutamate and DL-threo-3-hydroxyaspartate in the rat striatum. J Neurochem 44: 247-254, 1985.

61. Tanaka K, Watase K, Manabe T, Yamada K, Watanabe M, Takahashi K, Iwama H, Nishikawa T, Ichihara N, Kikuchi T, Okuyama S, Kawashima N, Hori S, Takimoto M and Wada K: Epilepsy and exacerbation of brain injury in mice lacking the glutamate transporter GLT-1. Science 276: 1699-1702, 1997.

62. Escarrabill J, Estopa R, Farrero E, Monasterio C and Manresa F: Long-term mechanical ventilation in amyotrophic lateral sclerosis. Respir Med 92: 438-441, 1998.

63. Obrenovitch TP: Amyotrophic lateral sclerosis, excitotoxicity and riluzole. Trends Pharmacol Sci 19: 9, 1998.
64. Seki Y, Feustel PJ, Keller RW Jr, Tranmer BI and Kimelberg HK: Inhibition of ischemia-induced glutamate release in rat striatum by dihydrokainate and an anion channel blocker. Stroke 30: 433-440, 1999.
65. Massieu L, Morales-Villagrán A and Tapia R: Accumulation of extracellular glutamate by inhibition of its uptake is not sufficient for inducing neuronal damage: an *in vivo* microdialysis study. J Neurochem 64: 2262-2272, 1995.
66. Levy LM, Lehre KP, Walaas SI, Storm-Mathisen J and Danbolt NC: Down-regulation of glial glutamate transporters after glutamatergic denervation in the rat brain. Eur J Neurosci 7: 2036-2041, 1995.
67. Ginsberg SD, Martin LJ and Rothstein JD: Regional deafferentation down-regulates subtypes of glutamate transporter proteins. J Neurochem 65: 2800-2803, 1995.
68. Kerr JFR, Wyllie AH and Currie AR: Apoptosis: a basic biological phenomenon with wide-ranging implications in tissue kinetics. Br J Cancer 26: 239-257, 1972.
69. Martin LJ, Portera-Cailliau C, Ginsberg SD and Al-Abdulla NA: Animal models and degenerative disorders of the human brain. Lab Anim 27: 18-25, 1998.
70. Portera-Cailliau C, Price DL and Martin LJ: Excitotoxic neuronal death in the immature brain is an apoptosis-necrosis morphological continuum. J Comp Neurol 378: 70-87, 1997.
71. Bredesen DE: Neural apoptosis. Ann Neurol 38: 839-851, 1995.
72. Roy N, Mahadevan MS, McLean M, Shutler G, Yaraghi Z, Farahani R, Baird S, Besner-Johnston A, Lefebvre C, Kang X, Salih M, Aubry H, Tamai K, Guan X, Ioannou P, Crawford TO, de Jong PJ, Surh L, Ikeda J-E, Korneluk RG and Mackenzie A: The gene for neuronal apoptosis inhibitory protein is partially deleted in individuals with spinal muscular atrophy. Cell 80: 167-178, 1995.
73. Liston P, Rpy N, Tamai K, Lefebvre C, Baird S, Cherton-Horvat G, Farahani R, McLean M, Ikeda J-E, MacKenzie A and Korneluk RG: Suppression of apoptosis in mammalian cells by NAIP and a related family of IAP genes. Nature 379: 349-353, 1996.
74. Lefebvre S, Burglen L, Reboullet S, Clermont O, Burlet P, Viollet L, Benichou B, Cruaud C, Millasseau P, Zeviani M, LePaslier D, Frezal J, Cohen D, Weissenbach J, Munnich A and Melki J: Identification and characterization of a spinal muscular atrophy-determining gene. Cell 80: 155-165, 1995.
75. Schwartz LM and Milligan CE: Cold thoughts of death: the role of ICE proteases in neuronal cell death. Trends Neurosci 19: 555-562, 1996.
76. Merry DE and Korsmeyer SJ: Bcl-2 gene family in the nervous system. Annu Rev Neurosci 20: 245-267, 1997.
77. Wolf BB and Green DR: Suicidal tendencies: apoptotic cell death by caspase family proteinases. J Biol Chem 274: 20049-20052, 1999.
78. Li P, Nijhawan D, Budihardjo I, Srinivasula SM, Ahmad M, Alnemri ES and Wang X: Cytochrome c and dATP-dependent formation of Apaf-1/caspase-9 complex initiates an apoptotic protease cascade. Cell 91: 479-489, 1997.
79. Cleveland JL and Ihle JN: Contenders in FasL/TNF death signaling. Cell 81: 479-482, 1995.
80. Li H, Zhu H, Xu C-J and Yuan J: Cleavage of Bid by caspase 8 mediates the mitochondrial damage in the Fas pathway of apoptosis. Cell 94: 491-501, 1998.
81. Inohara N, Ekhterae D, Garcia I, Carria R, Merino J, Merry A, Chen S and Núñez G: Mtd, a novel Bcl-2 family member activates apoptosis in the absence of heterodimerization with Bcl-2 and Bcl-X$_L$. J Biol Chem 273: 8705-8710, 1998.
82. LaCasse EC, Baird S, Korneluk RG and MacKenzie AE: The inhibitors of apoptosis (IAPs) and their emerging role in cancer. Oncogene 17: 3247-3259, 1998.
83. Deveraux QL, Roy N, Stennicke HR, van Arsdale T, Zhou Q, Srinivasula SM, Alnemri ES, Salvesen GS and Reed JC: IAPs block apoptotic events induced by caspase-8 and cytochrome c by direct inhibition of distinct caspases. EMBO J 17: 2215-2223, 1998.
84. Parboosing JS, Meininger V, Mckenna-Yasek D, Brown RN Jr and Rouleau GA: Deletions causing spinal muscular atrophy do not predispose to amyotrophic lateral sclerosis. Arch Neurol 56: 710-712, 1999.

85 .Zou H, Li Y, Liu X and Wang X: An Apaf-1-cytochrome *c* multimeric complex is a functional apoptosome that activates procaspase-9. J Biol Chem 274: 11549-11556, 1999.
86. Liu X, Zou H, Slaughter C and Wang X: DFF, a heterodimeric protein that functions downstream of caspase-3 to trigger DNA fragmentation during apoptosis. Cell 89: 175-184, 1997.
87. Kluck RM, Bossy-Wetzel E, Green DR and Newmeyer DD: The release of cytochrome c from mitochondria: a primary site for bcl-2 regulation of apoptosis. Science 275: 1132-1136, 1997.
88. Yang J, Liu X, Bhalla K, Kim CN, Ibrado AM, Cai J, Peng T-I, Jones DP and Wang X: Prevention of apoptosis by bcl-2: release of cytochrome c from mitochondria blocked. Science 275: 1129-1132, 1997.
89. Antonsson B, Conti F, Ciavatta A, Montessuit S, Lewis S, Martinou I, Bernasconi L, Bernard A, Mermod J-J, Mazzei G, Maundrell K, Gambale F, Sadoul R and Martinou J-C: Inhibition of bax channel-forming activity by bcl-2. Science 277: 370-372, 1997.
90. Liu X, Kim CN, Yang J, Jemmerson R and Wang X: Induction of apoptotic program in cell-free extracts: requirement for dATP and cytochrome c. Cell 86: 147-157, 1996.
91. Vander Heiden MG, Chandel NS, Williamson EK, Schumacker PT and Thompson CB: Bcl-x$_L$ regulates the membrane potential and volume homeostasis of mitochondria. Cell 91: 627-637, 1997.
92. Hu Y, Benedict MA, Wu D, Inohara N and Núñex: Bcl-x$_L$ interacts with Apaf-1 and inhibits Apaf-1-dependent caspase-9 activation. Proc Natl Acad Sci USA 95: 4386-4391, 1998.
93. Song Q, Kuang Y, Dixit VM and Vincenz C: Boo, a negative regulator of cell death, interacts with Apaf-1. EMBO J 18: 167-178, 1999.
94. Haldar S, Jena N and Croce CM: Inactivation of Bcl-2 by phosphorylation. Proc Natl Acad Sci USA 92: 4507-4511, 1995.
95. Wang H-G, Rapp UR and Reed JC: Bcl-2 targets the protein kinase raf-1 to mitochondria. Cell 87: 629-638, 1996.
96. Zha J, Harada H, Yang E, Jockel J and Korsmeyer SJ: Serine phosphorylation of death agonist Bad in response to survival factor results in binding to 14-3-3 not Bcl-x$_L$. Cell 87: 619-628, 1996.
97. Yang E, Zha J, Jockel J, Boise LH, Thompson CB and Korsmeyer SJ: Bad, a heterodimeric partner for Bcl-x$_L$ and Bcl-2, displaces Bax and promotes cell death. Cell 80: 285-291, 1995.
98. Desagher S, Osen-Sand A, Nichols A, Eskes R, Montessuit S, Lauper S, Maundrell K, Antonsson B and Martinou J-C: Bid-induced conformational change of bax is responsible for mito-chondrial cytochrome c release during apoptosis. J Cell Biol 144: 891-901, 1999.
99. Wyllie A: Clues in the p53 murder mystery. Nature 398: 237-238, 1997.
100. Miyashita T and Reed JC: Tumor suppressor p53 is a direct transcriptional activator of the human *bax* gene. Cell 80: 293-299, 1995.
101. Miyashita T, Krajewski S, Krajewska M, Wang HG, Lin HK, Liebermann DA, Hoffman B and Reed JC: Tumor suppressor p53 is a regulator of *bcl-2* and *bax* gene expression *in vitro* and *in vivo*. Oncogene 9: 1799-1805, 1994.
102. Appel SH, Smith RG, Alexianu MF, Engrlhardt JI and Stefani E: Autoimmunity as an etiological factor in sporadic amyotrophic lateral sclerosis. In: Advances in Neurology, Pathogenesis and Therapy of Amyotrophic Lateral Sclerosis. Serratrice GT and Munsat TL (eds). Lippincott-Raven, Philadelphia, pp47-57, 1995.
103. Smith RG, Siklos L, Alexianu ME, Engelhardt JI, Mosier DR, Colom L, Habib MA and Appel SH: Autoimmunity and ALS. Neurology 47 (Suppl.): S40-S45, 1996.
104. Kawamata T, Akiyama H, Yamada T and McGeer PL: Immuno-logic reactions in amyotrophic lateral sclerosis. Brain and spinal cord. Am J Pathol 140: 691-707, 1992.
105. Farlie PG, Dringen R, Rees SM, Kannourakis G and Bernard O: Bcl-2 transgene expression can protect neurons against developmental and induced cell death. Proc Natl Acad Sci USA 92: 4397-4401, 1995.
106. Martinou J-C, Dubois-Dauphin M, Staple JK, Rodriguez I, Frankowski H, Missotten, M, Albertini P, Talabot D, Catsicas S, Pietra C and Huarte J: Overexpression of bcl-2 in transgenic mice protects neurons from naturally occurring cell death and experimental ischemia. Neuron 13: 1017-1030, 1994.

107. Bonfanti L, Strettoi E, Chierzi S, Cenni MC, Liu X-H, Martinou J-C, Maffei L and Rabacchi SA: Protection of retinal ganglion cells from natural and axotomy-induced cell death in neonatal transgenic mice overexpressing bcl-2. J Neurosci 16: 4186-4194, 1996.

108. Deckwerth TL, Elliott JL, Knudson CM, Johnson EM, Snider WD and Korsmeyer SJ: Bax is required for neuronal death after trophic factor deprivation and during development. Neuron 17: 401-411, 1996.

109. Kuida K, Zheng TS, Na S, Kuan C-Y, Yang D, Karasuyama H, Rakic P and Flavell RA: Decreased apoptosis in the brain and premature lethality in CPP32-deficient mice. Nature 384: 368-372, 1996.

110. Kuida K, Haydar TF, Kuan C-Y, Gu Y, Taya C, Karasuyama H, Su MS-S, Rakic P and Flavell RA: Reduced apoptosis and cytochrome c-mediated caspase activation in mice lacking caspase-9. Cell 94: 325-337, 1998.

111. Hakem R, Hakem, A Duncan GS, Henderson JT, Woo M, Soengas MS, Elia A, de la Pompa JL, Kagi D, Khoo W, Potter J, Yoshida R, Kaufman SA, Lowe SW, Penninger JM and Mak TW: Differential requirement for caspase 9 in apoptotic pathways *in vivo*. Cell 94: 339-352, 1998.

112. Yoshio H, Kong Y-Y, Yoshida R, Elia AJ, Hakem A, Hakem R, Penninger JM and Mak TW: Apaf1 is required for mitochondrial pathways of apoptosis and brain development. Cell 94: 739-750, 1998.

113. Michaelidis TM, Sendtner M, Cooper JD, Airaksinen MS, Holtmann B, Meyer M and Thoenen H: Inactivation of bcl-2 results in progressive degeneration of motoneurons, sympathetic and sensory neurons during early postnatal development. Neuron 17: 75-89, 1996.

114. Dubois-Dauphin M, Frankowski H, Tsujimoto Y, Huarte J and Martinou J-C: Neonatal motoneurons overexpressing the bcl-2 protooncogene in transgenic mice are protected from axotomy-induced cell death. Proc Natl Acad Sci USA 91: 3309-3313, 1994.

115. Deshmukh M, Vasilakos J, Deckwerth TL, Lampe PA, Shivers BD and Johnson EM: Genetic and metabolic status of NGF-deprived sympathetic neurons saved by an inhibitor of ICE family proteases. J Cell Biol 135: 1341-1354, 1996.

116. Gagliardini V, Fernandez P, Lee RKK, Drexler HCA, Rotello RJ, Fishman MC and Yuan J: Prevention of vertebrate neuronal death by crmA gene. Science 263: 826-828, 1994.

117. Kermer P, Klöcker N, Labes M and Bähr M: Inhibition of CPP-32-like proteases rescues axotomized retinal ganglion cells from secondary cell death *in vivo*. J Neurosci 18: 4656-4662, 1998.

118. Milligan CE, Prevette D, Yaginuma H, Homma S, Cardwell C, Fritz LC, Tomaselli KJ, Oppenheim RW and Schwartz LM: Peptide inhibitors of the ICE protease family arrest programmed cell death of motoneurons *in vivo* and *in vitro*. Neuron 15: 385-393, 1995.

119. Hockenbery DM, Oltvai ZN, Yin X-M, Milliman CL and Korsmeyer SJ: Bcl-2 functions in an antioxidant pathway to prevent apoptosis. Cell 75: 241-251, 1993.

120. Ratan RR, Murphy TH and Baraban JM: Oxidative stress induces apoptosis in embryonic cortical cultures. J Neurochem 62: 376-379, 1994.

121. Bonfoco E, Krainc D, Ankarcrona M, Nicotera P and Lipton SA: Apoptosis and necrosis: two distinct events induced respectively by mild and intense insults with NMDA or nitric oxide/superoxide in cortical cell cultures. Proc Natl Acad Sci USA 92: 72162-72166, 1995.

122. Halliwell B and Gutteridge JMC: Oxygen free radicals and iron in relation to biology and medicine: some problems and concepts. Arch Biochem Biophys 246: 501-514, 1986.

123. Boveris A and Cadenas E: Cellular sources and steady-state levels of reactive oxygen species. In: Oxygen, Gene Expression, and Cellular Function. Biadasz Clerch L and Massaro DJ (eds). Marcel Dekker, New York, pp1-25, 1997.

124. Bandy B and Davison AJ: Mitochondrial mutations may increase oxidative stress: implications for carcinogenesis and aging? Free Radic Biol Med 8: 523-539, 1990.

125. Zamzami N, Susin SA, Marchetti P, Hirsch T, Gómez-Monterrey I, Castedo M and Kroemer G: Mitochondrial control of nuclear apoptosis. J Exp Med 183: 1533-1544, 1996.

126. Bradley WG and Krasin F: A new hypothesis of the etiology of amyotrophic lateral sclerosis. The DNA hypothesis. Arch Neurol 39: 677-680, 1982.

127. Fitzmaurice PS, Shaw IC, Kleiner HE, Miller RT, Monks TJ, Lau SS, Mitchell JD and Lynch PG: Evidence for DNA damage in amyotrophic lateral sclerosis. Muscle Nerve 19: 797-798, 1996.

128. Ferrante RJ, Browne SE, Shinobu LA, Bowling AC, Baik MJ, MacGarvey U, Kowall NW, Brown RH Jr and Beal MF: Evidence of increased oxidative damage in both sporadic and familial amyotrophic lateral sclerosis. J Neurochem 69: 2064-2074, 1997.

129. Mithal NP, Radunovic A, Figlewicz DA, McMillan TJ and Leigh PN: Cells from individuals with SOD-1 associated familial amyotrophic lateral sclerosis do not have an increased susceptibility to radiation-induced free radical production or DNA damage. J Neurol Sci 164: 89-92, 1999.

130. Lindahl T: Instability and decay of the primary structure of DNA. Nature 362: 709-715, 1993.

131. Demple B and Harrison L: Repair of oxidative damage to DNA: enzymology and biology. Annu Rev Biochem 63: 915-948, 1994.

132. Tandan R, Robison SH, Munzer JS and Bradley WG: Deficient DNA repair in amyotrophic lateral sclerosis cells. J Neurol Sci 79: 189-203, 1987.

133. Kisby GE, Miline J and Sweatt C: Evidence of reduced DNA repair in amyotrophic lateral sclerosis brain tissue. Neuroreport 8: 1337-1340, 1997.

134. Robison SH, Tandan R and Bradley WG: Repair of N-methyl-purines in DNA from lymphocytes of patients with amyotrophic lateral sclerosis. J Neurol Sci 115: 201-207, 1993.

135. Olkowski ZL: Mutant AP endonuclease in patients with amyotrophic lateral sclerosis. Neuroreport 9: 239-242, 1998.

136. Hayward C, Colville S, Swingler RJ and Brock DJH: Molecular genetic analysis of the APEX *nuclease* gene in amyotrophic lateral sclerosis. Neurology 52: 1899-1901, 1999.

137. Al-Abdulla NA, Portera-Cailliau C and Martin LJ: Occipital cortex ablation in adult rat causes retrograde neuronal death in the lateral geniculate nucleus that resembles apoptosis. Neuroscience 86: 191-209, 1998.

138. Al-Abdulla NA and Martin LJ: Apoptosis of retrogradely degenerating neurons occurs in association with the accumulation of perikaryal mitochondria and oxidative damage to the nucleus. Am J Pathol 153: 447-456, 1998.

139. Kato T, Hirano A and Kurland LT: Asymmetric involvement of the spinal cord involving both large and small anterior horn cells in a case of familial amyotrophic lateral sclerosis. Clin Neuropathol 6: 67-70, 1987.

140. Munoz DG, Greene C, Perl DP and Selkoe DJ: Accumulation of phosphorylated neurofilaments in anterior horn motor neurons of amyotrophic lateral sclerosis. J Neuropathol Exp Neurol 47: 9-18, 1988.

141. Liu D, Yang R, Yan X and McAdoo DJ: Hydroxyl radicals generated *in vivo* kill neurons in the rat spinal cord: electrophysiological, histological, and neurochemical results. J Neurochem 62: 37-44, 1994.

142. Wu W: Expression of nitric oxide synthase (NOS) in injured CNS neurons as shown by NADPH diaphorase histochemistry. Exp Neurol 120: 153-159, 1993.

143. Estévez AG, Spear N, Manuel SM, Radi R, Henderson CE, Barbeito L and Beckman JS: Nitric oxide and superoxide contribute to motor neuron apoptosis induced by trophic factor deprivation. J Neurosci 18: 923-931, 1998.

144. Wu W and Li L: Inhibition of nitric oxide synthase reduces motoneuron death due to spinal root avulsion. Neurosci Lett 153: 121-124, 1993.

Lee J. Martin, Ph.D.
DAMD17-99-1-9553

Appendix

Neuronal Death in Newborn Striatum after Hypoxia-Ischemia Is Necrosis and Evolves with Oxidative Stress

Lee J. Martin,[*,†,1] Ansgar M. Brambrink,[‡,2] Ann C. Price,[*]
Adeel Kaiser,[*] Dawn M. Agnew,[§] Rebecca N. Ichord,[¶]
and Richard J. Traystman[‡]

*Department of Pathology, Division of Neuropathology, †Department of Neuroscience,
‡Department of Anesthesiology and Critical Care Medicine, and ¶Department of Neurology,
Johns Hopkins University School of Medicine; and §School of Nursing,
University of Maryland, Baltimore, Maryland

The mechanisms for neurodegeneration after hypoxia-ischemia (HI) in newborns are not understood. We tested the hypothesis that striatal neuron death is necrosis and evolves with oxidative stress and selective organelle damage. Piglets (~1 week old) were used in a model of hypoxia-asphyxia and survived for 3, 6, 12, or 24 h. Neuronal death was progressive over 3–24 h recovery, with ~80% of putaminal neurons dead at 24 h. Striatal DNA was digested randomly at 6–12 h. Ultrastructurally, dying neurons were necrotic. Damage to the Golgi apparatus and rough endoplasmic reticulum occurred at 3–12 h, while most mitochondria appeared intact until 12 h. Mitochondria showed early suppression of activity, then a transient burst of activity at 6 h, followed by mitochondrial failure (determined by cytochrome c oxidase assay). Cytochrome c was depleted at 6 h after HI and thereafter. Damage to lysosomes occurred within 3–6 h. By 3 h recovery, glutathione levels were reduced, and peroxynitrite-mediated oxidative damage to membrane proteins, determined by immunoblots for nitrotyrosine, occurred at 3–12 h. The Golgi apparatus and cytoskeleton were early targets for extensive tyrosine nitration. Striatal neurons also sustained hydroxyl radical damage to DNA and RNA within 6 h after HI. We conclude that early glutathione depletion and oxidative stress between 3 and 6 h reperfusion promote damage to membrane and cytoskeletal proteins, DNA and RNA, as well as damage to most organelles, thereby causing neuronal necrosis in the striatum of newborns after HI.   © 2000 Academic Press

Key Words: apoptosis; cerebral palsy; cytochrome c; DNA damage; mitochondria; RNA oxidation

INTRODUCTION

Hypoxia-ischemia (HI) in newborns is a major cause of pediatric mortality and morbidity and causes brain damage resulting in life-long neurobehavioral handicaps. In human newborns (Volpe, 1995; Roland *et al.*, 1998; Maller *et al.*, 1998) and in some pediatric animal models (Martin *et al.*, 1997a,b), HI causes a character-

istic encephalopathy, with basal ganglia and somatosensory systems showing selective vulnerability. However, the mechanisms that cause this brain damage in HI neonates remain unclear. Glutamate receptor-mediated excitotoxic cell injury is a possible mechanism for this neuronal degeneration following HI in newborns (Olney, 1994; Martin *et al.*, 1998a). Using a newborn piglet model of cardiac arrest that causes reproducible damage to the basal ganglia (Martin *et al.*, 1997b,c), we found that the protein levels of specific subtypes of glutamate transporters (e.g., GLT1 and EAAC1) are reduced in striatum at 24 h recovery and thereafter (Martin *et al.*, 1997c) and that functional

---

[1] To whom correspondence and reprint requests should be addressed at Ross Bldg., Rm 558, 720 Rutland Ave, Baltimore, MD 21205. Fax: (410) 955-9777. E-mail: lmartin@welchlink.welch.jhu.edu.

[2] Present address: Department of Anesthesiology, Johannes Gutenberg-University, Mainz, Germany.

transport of glutamate is impaired in striatal synaptosomes by 6–12 h after HI (Natale *et al.,* 1999). The concept that excitotoxicity participates in the mechanisms for neuronal degeneration resulting from perinatal HI is supported by studies showing that the NMDA receptor antagonist MK-801 ameliorates brain damage in HI neonatal rats (McDonald *et al.,* 1987; Ford *et al.,* 1989). However, neither MK-801 (LeBlanc *et al.,* 1991) nor AMPA receptor antagonists (LeBlanc *et al.,* 1995; Martin *et al.,* 1997a; Brambrink *et al.,* 1999) afford neuroprotection in clinically relevant models of newborn HI. Although glutamate receptor excitotoxicity continues to be a potential mechanism for neurodegeneration in the perinatal period, the precise cellular and molecular pathways for neuronal death *in vivo* remain poorly understood.

Depending on the type of cell and on the stimulus, cells typically die in either of two ways generally described as apoptosis or necrosis (Kerr *et al.,* 1972; Martin *et al.,* 1998a). These two forms of cell death are thought to differ fundamentally at structural and mechanistic levels. Apoptosis is a structurally organized, programmed cell death that is mediated by active, intrinsic mechanisms. In contrast, cellular necrosis is though to be structurally a more rapid and random degeneration resulting from extrinsic insults to the cells, such as abrupt environmental perturbations (e.g., osmotic, thermal, toxic, or traumatic) and departures from physiological conditions, involving disruption of plasma membrane structural and functional integrity, rapid influx of Na^+, Ca^{2+}, and water, cell swelling, and subsequent dissolution of the cell (Choi, 1992). More recent experiments have revealed that the death of neurons can also be a hybrid of apoptosis and necrosis with overlapping characteristics (Portera-Cailliau *et al.,* 1997a,b). Some studies have suggested that neuronal death after HI in newborns is apoptosis (Beilharz *et al.,* 1995; Hill *et al.,* 1995; Cheng *et al.,* 1998). However, this conclusion is controversial (Martin *et al.,* 1998a). Neurodegeneration in the newborn striatum is advanced at 24 h after HI (Martin *et al.,* 1997c). Therefore, we tested the hypothesis that the progression of striatal neuron death after HI is rapid and necrotic structurally, but evolves orderly with successive subcellular abnormalities in different organelles, similar to excitotoxic neuronal necrosis (Portera-Cailliau *et al.,* 1997a,b). Because reactive oxygen species (ROS) are potent mediators of cell necrosis (McCord, 1985; Halliwell and Gutteridge, 1986), we also determined if striatal neuron death after HI emerges in association with acute oxidative stress and ROS-mediated damage to membrane proteins and nucleic acids.

MATERIALS AND METHODS

Piglet Model of HI

The animal protocol was approved by the Animal Care and Use Committee of the Johns Hopkins Medical Institutions and was described previously (Martin *et al.,* 1997a,b,c; Brambrink *et al.,* 1999). This piglet model was adopted because of its relevance to HI encephalopathy in human newborns and children (Johnston, 1998). One-week-old male or female piglets (~3 kg) were anesthetized with intraperitoneal (ip) sodium pentobarbital (65 mg/kg), intubated, and ventilated mechanically. Using sterile surgery, femoral arterial and venous catheters were placed into the thoracic aorta and inferior vena cava, respectively, and were tunneled subcutaneously exiting the skin for long-term access. Cephalothin (50 mg/kg) prophylaxis was administered intravenously. Oxygenation, ventilation, and acid-balance were all maintained at normal values. Rectal temperature was maintained at 38.5–39.5°C. Piglets received a maintenance infusion of intravenous lactated Ringer's solution (10 mg/kg/h), with additional analgesia and neuromuscular blockade provided by bolus intravenous fentanyl (10 μg/kg) and pancuronium (0.3 mg/kg), respectively. Baseline arterial blood gases, pH, hemoglobin, glucose, lactate, pulse rate, and blood pressure were measured (Brambrink *et al.,* 1999).

Piglets were then exposed to 30 min of hypoxia (SaO_2 30%), followed by 5 min of ventilation with room air (SaO_2 65%), and then 7 min of airway occlusion (SaO_2 5%), resulting in asphyxic cardiac arrest (Brambrink *et al.,* 1999). Piglets were resuscitated by ventilation with 100% O_2, manual chest compressions, intravenous epinephrine (0.1 mg/kg), and intravenous sodium bicarbonate (1 mEq/kg) until return of spontaneous circulation, usually within 2–3 min. Defibrillation (2 joules/kg) was performed for ventricular fibrillation, with intravenous lidocaine (1 mg/kg) if multiple defibrillations were required. Approximately 90% of piglets were successfully resuscitated. Piglets were allowed to awaken and were extubated when able to maintain spontaneous oxygenation and ventilation, usually within 8 h. Piglets drank formula milk, usually by 24 h recovery, or were tube fed if necessary. Animals (*n* = 23) were recovered for 3, 6, 12, or 24 h after the return of spontaneous circulation. Sham con-

trol animals ($n = 8$) were anesthetized and subjected to the surgical preparation but not the HI.

Preparation of Brain Samples

Piglet brains were harvested freshly for protein and DNA gel analyses and for biochemical assays, or were perfusion-fixed for *in situ* DNA fragmentation analysis, immunocytochemistry, enzyme histochemistry, and electron microscopy. Animals for fresh brain tissue ($n = 3$ or 4 per recovery time) were anesthetized deeply with sodium pentobarbital (65 mg/kg, ip) and exsanguinated with ice-cold phosphate-buffered saline (PBS). Brains were removed rapidly and placed on wet ice. The cerebrum was transected midsagittally, and the hemispheres were subdissected to obtain samples from the striatum (including putamen, caudate, internal capsule, nucleus accumbens). These samples were flash-frozen in cold isopentane and stored at $-70°C$ until used for extractions. From the left hemisphere of each of these animals, a thin brain slab containing the striatum was immersion fixed in 5% acrolein and processed for paraffin histology for quantification of neuronal damage in hematoxylin & eosin (H&E) stained sections.

Piglets for fixed brain tissue ($n = 2$ or 3 per recovery time) were anesthetized deeply with sodium pentobarbital (65 mg/kg, ip) and exsanguinated with ice-cold PBS, then perfused intraaortically for 20 min with ice-cold 4% paraformaldehyde plus 1% glutaraldehyde. Brains were removed and bisected midsagittally, and each hemisphere cut into 1-cm slabs. The left forebrain was used for paraffin histology and electron microscopy (EM). The right forebrain was cryoprotected in 20% glycerol-PBS for 24 h, frozen, and serial 40-μm sections through striatum were cut on a sliding microtome. Sections were stored in antifreeze buffer at $-20°C$ until they were used for DNA end-labeling, immunocytochemistry, and enzyme histochemistry.

Neuropathology, TUNEL, and Electron Microscopy

For quantification of neuronal degeneration after HI in all piglets ($n = 31$), coronal samples of striatum from the left hemisphere were paraffin-processed, and sections (10-μm-thick) were stained with H&E and the terminal transferase-mediated biotin-dUTP nick-end labeling (TUNEL) method for *in situ* detection of nuclear DNA fragmentation as described (Portera-Cailliau *et al.*, 1997a,b; Martin *et al.*, 1997c; Al-Abdulla *et al.*, 1998). The TUNEL method was used to identify dying cells after HI, although this technique is not specific for apoptosis (Grasl-Kraupp *et al.*, 1995; Martin *et al.*, 1998a, 2000). Comparable levels of the striatum from sham and HI piglets were used to determine the severity of striatal injury at 3, 6, 12, and 24 h recovery. In H&E sections, the density of principal striatal neurons and the percentage of remaining neurons with ischemic cytopathology were determined from six nonoverlapping, random 1000x microscopic fields in the putamen. The criteria for neuronal injury were cytoplasmic eosinophilia and vacuolation, perikaryal shrinkage, and nuclear pyknosis. H&E sections were also used for measurements of principal striatal neuron cell body volume and nuclear volume using ocular filar micrometry at 1000x. Neuronal cell body and nuclear volumes were calculated from $V = \pi/6(ab^2)$, where a = diameter of the major axis and b = the diameter of the minor axis (Martin *et al.*, 1986). In TUNEL preparations, the density of dying cells was determined by parcellating the putamen into six divisions and counting the number of TUNEL-positive nuclei in six microscopic fields at 1000x.

To determine whether the neuronal degeneration after HI has the structure of apoptosis, necrosis, or a hybrid form of death (Portera-Cailliau *et al.*, 1997a,b), samples (3 mm^3) of putamen from control and HI piglets (3, 6, 12, and 24 h) were osmicated, embedded in plastic, and evaluated by EM. Ischemic neurodegeneration was evaluated using ultrastructural criteria for cellular necrosis and apoptosis that we have described previously using *in vivo* models of neuronal degeneration (Portera-Cailliau *et al.*, 1997a,b; Al-Abdulla *et al.*, 1998; Martin *et al.*, 1998a, 1999, 2000).

DNA Isolation and Agarose Gel Electrophoresis

Because the TUNEL method identifies DNA fragmentation independent of mechanisms (Grasl-Kraupp *et al.*, 1995; Portera-Cailliau *et al.*, 1997a; Martin *et al.*, 1998a), we evaluated striatal neuropathology based on DNA fragmentation patterns in agarose gels. Genomic DNA was isolated from samples of sham control piglets ($n = 2$) and HI piglets at 3, 6, 12, and 24 h recovery (two animals/time). Striatal samples were homogenized in DNA extraction buffer containing 10 mM Tris (pH 7.4), 10 mM NaCl, 25 mM EDTA, 1% SDS, 1 mg/ml proteinase K, and incubated in the same buffer overnight at 37°C. DNA was extracted with an equal volume of salt saturated-phenol:chloroform:isoamyl alcohol (10:10:1) and the recovered aqueous phase was extracted with diethyl ether. DNA was precipitated with ethanol (2.5 vol). The DNA pellet was dissolved

in 0.1× SSC and incubated (37°C) with DNase-free RNase A (0.1 mg/ml) for 1 h and then overnight (37°C) with 0.1 mg/ml proteinase K. DNA was reextracted, precipitated, and dissolved in TE buffer. DNA samples were fractionated by agarose gel (1.2%) electrophoresis and were evaluated by ethidium bromide staining and by end labeling. For end labeling, DNA samples (~1.0 μg) were 3'-end labeled with digoxigenin-11-ddUTP using terminal transferase (Boehringer-Mannheim), precipitated, resuspended in TE buffer, fractionated, and transferred to nylon membrane followed by UV-crosslinking. Membranes were incubated in 2% nucleic acid blocking reagent (Boehringer-Mannheim) and then in blocking reagent containing 75 mU/ml antidigoxigenin Fab fragments conjugated to alkaline phosphatase (Boehringer-Mannheim). After washing, membranes were reacted with CSPD detection reagent (Boehringer-Mannheim) and exposed to Kodak X-OMAT film to visualize DNA.

Immunoblot Analyses

Striatal samples (0.4–0.6 g from each piglet) for immunoblot analysis were homogenized with a Brinkman Polytron in ice-cold homogenization buffer (20 mM Tris–HCl, pH 7.4, with 10% sucrose, 1 mM EDTA, 5 mM EGTA, 20 U/ml Trayslol, 20 μg/ml leupeptin, 20 μg/ml antipain, 20 μg/ml pepstatin, 20 μg/ml chymostatin, 0.1 mM phenylmethylsulfonyl fluoride, and 10 mM benzamidine). Crude homogenates were centrifuged at $1,000g_{av}$ for 10 min at 4°C. The supernatant (S1 fraction) was then centrifuged at $114,000g_{av}$ for 20 min. The resulting supernatant (S2 soluble fraction) was collected, and the pellet (P2 mitochondrial-enriched, membrane fraction) was washed in homogenization buffer (without sucrose) three times by resuspension, each followed by centrifugation at $114,000g_{av}$ for 20 min. The washed membrane fraction was resuspended fully in this buffer supplemented with 20% (wt/vol) glycerol. Protein concentrations in soluble and membrane fractions were measured by a Bio-Rad protein assay with bovine serum albumin as a standard. Samples were stored at −70°C.

Frozen striatal membrane and soluble fractions were thawed to 4°C, and samples (10 μg of total protein) were fractionated by sodium dodecyl sulfate–polyacrylamide gel electrophoresis (SDS–PAGE). Proteins were transferred electrophoretically to nitrocellulose filters. Gels were stained with Coomassie blue, and nitrocellulose membranes were briefly stained with Ponceau S to verify uniform protein transfer. Blots were washed with 50 mM Tris-buffered saline

(TBS) and subsequently blocked in 2.5% nonfat milk in 50 mM TBS/0.1% Tween 20. As a marker for peroxynitrite-mediated damage to protein tyrosines in membrane fractions, nitrotyrosine modification of proteins was detected with monoclonal and polyclonal antibodies (Upstate Biotechnology, Lake Placid, NY) used at a concentration of 1 μg IgG/ml. Peroxynitrite is a potent and relatively long lived ROS formed by a reaction between superoxide and nitric oxide (Beckman *et al.*, 1992). Subcellular fractions were also evaluated with organelle-specific antibodies to identify damage to these intracellular compartments over 24 h recovery. Blots of membrane proteins were probed with a monoclonal antibody (0.5 μg IgG/ml) to human cytochrome c oxidase subunit I (Molecular Probes, Eugene, OR) or a monoclonal antibody (3.4 μg IgG/ml) to rat Golgi 58K protein (Sigma, St. Louis, MO) as markers for mitochondria and the Golgi apparatus, respectively. Golgi 58K protein is a peripheral Golgi membrane protein that functions in microtubule binding (Bloom and Brashear, 1989). Blots of cytosolic proteins were probed with monoclonal antibody (100 ng IgG/ml) to pigeon cytochrome c (PharMingen, San Diego, CA) or with polyclonal antibodies (1 μg IgG/ml) to KDEL proteins (Affinity BioReagents, Golden, CO), as markers for mitochondrial membrane damage and degradation of cytochrome c and for endoplasmic reticulum (ER) membrane damage and release of ER lumenal proteins, respectively. The KDEL sequence at protein C-termini is an ER retention signal (Munro and Pelham, 1987). Primary antibodies to these proteins in soluble fractions were diluted in 2.5% nonfat milk or normal goat serum (NGS) prepared with 50 mM TBS/0.1% Tween 20. Blots were incubated with antibody overnight at 4°C. After the primary antibody incubation, the blots were washed and incubated (0.2 μg/ml) with goat anti-rabbit or goat anti-mouse IgG conjugated to horseradish peroxidase (Bio-Rad). Blots were again washed, and immunoreactive proteins were visualized within the linear range with an enhance chemiluminescence detection system (Amersham or Pierce) and exposed to radiographic film.

To identify proteins that are possible targets of nitrotyrosine modification, we used immunoprecipitation. Subcellular fractions (50 μg protein) were reacted overnight with monoclonal antibody to tubulin (Amersham). Immunocomplexes were captured with protein A-agarose bead slurry, washed, and subjected to SDS–PAGE for subsequent analysis by western blotting with polyclonal antibodies to nitrotyrosine. For negative control experiments, nitrotyrosine antibodies

were neutralized with nitrotyrosine-molecular weight standards (Upstate).

Protein levels were quantified densitometrically using a Macintosh Adobe Photoshop program, and analyzed using Signal Analytics IP Lab Gel software. Protein levels were expressed as percentage of control by comparing density of the protein band scanned to density of the same band in the control lane of the same blot. For a quantitative control for equal protein loading in each lane, blots of membrane proteins were reprobed (0.06 μg/ml) with a mouse monoclonal antibody to synaptophysin (Boehringer Mannheim), a membrane protein involved in synaptic vesicle fusion. The levels of synaptophysin (p38) in HI piglet striatum are not changed before 24 h recovery (Martin *et al.*, 1997b). The levels of nitrotyrosine-modified proteins, cytochrome c oxidase subunit I, and Golgi 58K protein were corrected for relative synaptophysin immunodensity. For a quantitative control for equal protein loading in each lane in blots of striatal soluble proteins, blots were reprobed (40–80 ng IgG/ml) with a mouse monoclonal antibody to tyrosine hydroxylase (Boehringer-Mannheim), the enzyme involved in dopamine synthesis in nigrostriatal terminals, or a mouse monoclonal antibody (1:2000) to synapse-associated protein-25 (SNAP-25, Sternberger Monoclonals). Nerve terminal degeneration in HI piglet striatum does not occur until after 24 h recovery (Martin *et al.*, 1997b,c). Thus, cytochrome c and KDEL protein levels in the cytosolic compartment were corrected for relative tyrosine hydroxylase or SNAP-25 immunodensity.

Cytochrome c Oxidase Assay

A colorimteric assay (Wharton and Tzagoloff, 1967) was used for biochemical measurements of cytochrome c oxidase (COX) activity in homogenates of control striatum ($n = 3$) and HI piglet ($n = 2$ or 3/time point) striatum at 3, 6, 12, and 24 h after reprefusion. Reduced cytochrome c (ferrocytochrome c) was prepared freshly for each experiment by mixing 1% cytochrome c (Sigma) with sodium hydrosulfite in potassium phosphate buffer. Samples (20 μg protein) of mitochondrial-enriched membrane fractions were reacted with ferrocytochrome c in potassium phosphate buffer (10 mM, pH 7.0) at room temperature. The decrease in absorbance was measured spectrophotometrically at 550 nm every 15 s. The activity of COX was defined in terms of the first-order velocity constant.

Acid Phosphatase Assay

HI and reperfusion are known to effect the stability and permeability of lysosomes (Frederiks and Marx, 1989). As an index of lysosomal membrane damage and destabilization of lysosomes (Frederiks and Marx, 1989; van Noorden, 1991), acid phosphatase activity was measured in cytosolic protein fractions of control striatum ($n = 3$) and HI piglet ($n = 2$ or 3/time point) striatum at 3, 6, 12, and 24 h recovery. In 2.5-ml plastic cuvettes, samples of soluble protein fractions (500 or 1000 μg total protein) were mixed at room temperature with 15 mM o-carboxyphenyl-phosphate in 150 mM sodium acetate buffer (pH 5.0) in a final reaction volume of 1.5 or 2.0 ml. The Δ_{Abs} was measured with a spectrophotometer (Pharmacia) over 2 min at 300 nm. Purified potato acid phosphatase (Boehringer-Mannheim) was used as a positive control (0.6–6 U/ml). Reactions were run in the absence or presence of the acid phosphate inhibitor sodium fluoride (Sigma). Acid phosphatase activity, based on results of triplicate experiments, was expressed as percentage of control.

Glutathione Assay

The levels of glutathione (GSH and GSSG) in soluble protein fractions of control piglet striatum ($n = 3$) and HI piglet striatum at 3, 6, 12, and 24 h reperfusion ($n = 2$ or 3/time point) were measured using a modification of the method of Tietze (Tietze, 1969). Disposable cuvettes were loaded with 650 μl of 100 mM potassium phosphate buffer (pH 7.5) containing 5 mM EGTA, 100 μg/ml 5,5'-dithiobis(2-nitrobenzoic acid), and 320 μg/ml NADPH. To this reaction mixture, 2 U/ml of GSH reductase and striatal soluble protein (500 μg) were added (with a final reaction volume of 1 ml), and the Δ_{Abs} was measured immediately with a spectrophotometer (Pharmacia) over 4 min at 412 nm. GSH levels, based on results of duplicate experiments, were expressed as percentage of control.

Immunocytochemical Analyses of Organelles and Oxidative Damage

Brain sections from perfusion-fixed control piglets ($n = 3$) and HI piglets at 3, 6, 12, and 24 h reperfusion ($n = 2$ or 3/time point) were removed from antifreeze buffer and washed in TBS. Free-floating sections were pretreated with H_2O_2/methanol (to eliminate endogenous peroxidase activity), rinsed, and then with sodium borohydride (for antigen retrieval), and blocked

in NGS. Sections were incubated for 48 h at 4°C with primary antibodies (see below). After primary antibody incubation, sections were incubated sequentially with affinity-purified F(ab)$_2$ fragments of goat anti-rabbit or anti-mouse IgG (Cappel) and then affinity-purified monoclonal goat anti-rabbit or goat anti-mouse antibody conjugated to horseradish peroxidase (Sternberger Monoclonals). Sites of antibody binding were visualized with H$_2$O$_2$ and diaminobenzidene as a chromogen.

Several different antibodies were used as immunocytochemical probes to identify the progression of subcellular abnormalities in striatal neurons after HI. As organelle probes, we used monoclonal antibody to Golgi 58K protein (15 μg IgG/ml) for the Golgi apparatus, monoclonal antibody (1 μg IgG/ml) to COX subunit I for mitochondria, polyclonal rabbit antibody (200 ng IgG/ml, Santa Cruz) to Rab5A for early endosomes (Simons and Zerial, 1993), and polyclonal rabbit antibody (10 μg IgG/ml, Affinity BioReagents) to KDEL sequence-containing proteins for the ER. To determine if striatal neurons undergo oxidative stress, peroxynitrite-mediated damage to proteins was identified using antibodies to nitrotyrosine (3 μg IgG/ml), and hydroxyl radical damage to DNA and RNA was detected with monoclonal antibody (30 μg IgG/ml) to 8-hydroxy-2'-deoxyguanosine (QED Bioscience, Inc and PharMingen, San Diego, CA). These antibodies react with hydroxyl radical modified DNA and RNA (Al-Abdulla and Martin, 1998; Martin et al., 1999). For competition controls, sections were reacted with antibody to 8-hydroxy-2'-deoxyguanosine (OHdG) that was incubated at 4°C for 24 h with 1000-fold concentrations of OHdG, 8-hydroxyguanosine (OHG) or guanosine (Cayman Chemical, Ann Arbor, MI). As additional controls, sections were digested with DNase (5–10 mg/ml) or RNase (11–50 mg/ml) prior to incubation with OHdG antibody.

Cytochrome c Oxidase Enzyme Histochemistry

To assay for mitochondrial function with spatial resolution, the COX histochemical method of Wong-Riley (1979) was used as described previously (Martin et al., 1997a,b). Forebrain sections from control piglets ($n = 3$) and HI piglets ($n = 2$ or 3/time point) were incubated concomitantly with freshly prepared enzymatic reaction medium consisting of 100 mM phosphate buffer (pH 7.4), 0.1% horse heart cytochrome c, 117 mM sucrose, and 1.4 mM diaminobenzidine tetrahydrochloride (Wong-Riley, 1979). The enzymatic specificity of this reaction in piglet brain has been

TABLE 1

Progression of Neuronal Degeneration in the Striatum after HI[a]

Group	Percentage neuronal damage	Neuronal density (cells/mm^2)
Control	0.4 ± 0.4	572.9 ± 22.3
3-h	15.7 ± 3.3[b,c]	515.5 ± 14.0
6-h	30.9 ± 4.7[b,c]	550.0 ± 14.1
12-h	47.2 ± 7.6[b,c]	535.0 ± 23.4
24-h	78.8 ± 3.9[b,c]	395.2 ± 19.8[b]

[a] Percentage of principal neurons with damage and neuronal density in the putamen of control and ischemic piglets at 3, 6, 12, and 24 h after HI. Measurements were made in H&E-stained sections. Percentage neuronal damage was estimated by identifying the fraction of neurons with ischemic cytopathology relative to the total number of neurons in microscopic fields of the striatum. All values are mean ± SEM.

[b] Significantly different ($P < 0.05$) from control.

[c] Significantly different ($P < 0.05$) from preceding recovery time.

shown (Martin et al., 1997b). After the reaction, sections were rinsed in phosphate buffer, mounted on glass slides, and coverslipped. Histochemical COX enzyme activity was quantified densitometrically using an image-processing system as described (Martin et al., 1997a,b).

Statistical Analysis of Data

All histological and biochemical measurements were made in duplicate or triplicate. Statistical analysis of measurements for percentage neuronal damage and neuronal and TUNEL-positive cell densities were performed using one-way analysis of variance. If there were significant differences among the group means as indicated by the F test, group means were further analyzed using Newman–Keuls test. Protein levels determined by immunoblotting were expressed as percentage of sham-control piglets. Mean percentages were compared among 3, 6, 12, and 24 h recovery groups by a Wilcoxon signed rank test. The level of significance was $P < 0.05$ in all tests.

RESULTS

Striatal Neuron Death after HI in Newborns Is Rapid and Progressive over 24 h

Prominent neuronal degeneration in the striatum of HI piglets occurred during 3 to 24 h recovery (Table 1; Fig. 1). Neurons were distinguished from glial and inflammatory cells by strict perikaryal and nuclear

A

B
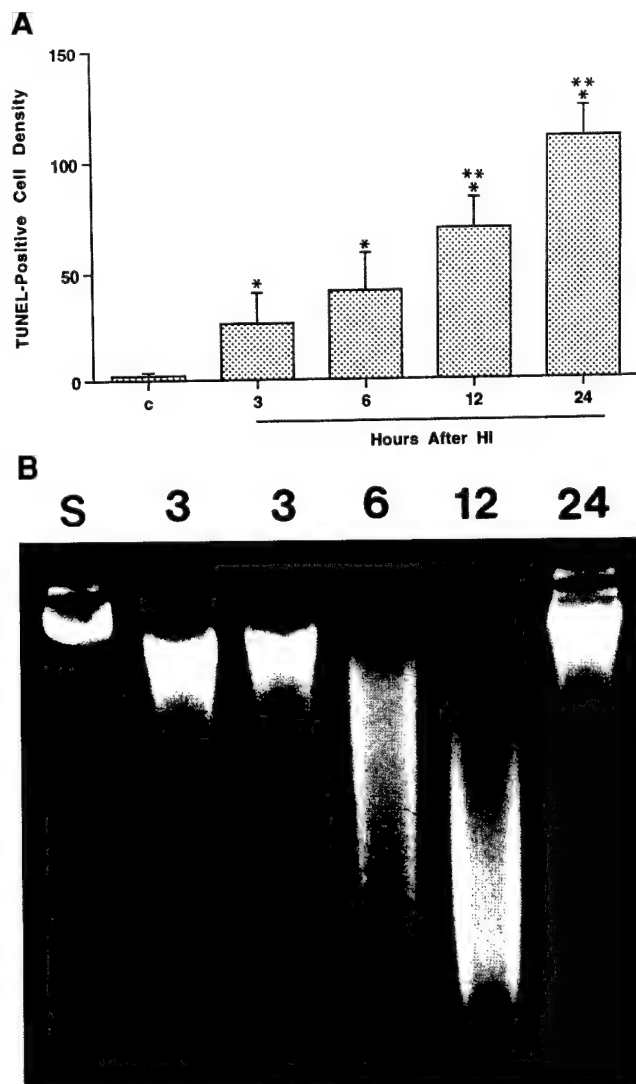
FIG. 1. DNA fragmentation begins by 3 h after HI and is progressive and consistent with cellular necrosis. (A) Striatal neuron death (in putamen) in control piglets (C) and piglets at 3, 6, 12, and 24 h after HI. TUNEL-positive cell densities (cells/mm^2) are mean + SEM. Asterisk indicates significant difference ($P < 0.05$) from control. Double asterisk indicates significant difference ($P < 0.05$) from control, 3 h and 6 h after HI. (B) Agarose gel fractionation of DNA isolated from the striatum of sham control piglets (S) and piglets at 3, 6, 12, and 24 h after HI. Maximal, random digestion of DNA occurs between 3 and 12 h recovery. At 24 h, most of the DNA digestion has advanced to small fragments that are not retained in agarose gels, but these DNA fragments are detectable by TUNEL in individual cells in striatal sections.

morphological criteria in H&E-stained sections (Martin *et al.*, 1997b,c). Neuronal injury was progressive, with percentage neuronal damage correlating significantly with time after HI (Table 1). In contrast, during early recovery, astroglia may be uninjured (Martin *et*

al., 1997c; Natale *et al.*, 1999). At 24 h after HI, neuronal density was reduced significantly, and ~79% of remaining principal neurons within the putamen were degenerating (Table 1), consistent with our previous findings at 24 h after HI (Martin *et al.*, 1997c).

The progression of striatal neuron injury revealed by H&E staining was paralleled by the occurrence of DNA fragmentation (Fig. 1). In TUNEL preparations counterstained with cresyl violet, nuclear DNA fragmentation in striatal neurons was progressive over 3–24 h after HI (Fig. 1A). During this time course, the majority of TUNEL-positivity was associated with neurons, because most glial cell death in striatum occurs after 24 h in this model, and the DNA condensation patterns in neurons and glia are distinct morphologically (Martin *et al.*, 1997c). By gel electrophoresis, the pattern of fragmentation in genomic DNA extracts of the striatum of HI piglets was consistent with cellular necrosis, with prominent random digestion of DNA occurring at 6 and 12 h after HI (Fig. 1B).

The Ultrastructure of Striatal Neuron Death after HI Is Necrosis

The structural progression of principal striatal neuron death in 1-week-old HI piglets was determined by EM (Figs. 2 and 3). The degeneration of these neurons was not apoptosis or a hybrid form of apoptosis and necrosis, based on previously established criteria for neuronal death (Portera-Cailliau *et al.*, 1997a,b; Al-Abdulla *et al.*, 1998; Al-Abdulla and Martin, 1998; Martin *et al.*, 1998a, 1999, 2000). Striatal neuron degeneration in newborn piglet brain during the first 24 h after HI is necrosis (Figs. 2 and 3). Both the cytoplasm and the nucleus undergo ultrastructural changes typical of cellular necrosis, with the main features being swelling of the cell body, swelling and degeneration of organelles, extensive cytoplasmic vacuolation, irregular clumping of chromatin and nuclear membrane disintegration, destruction of plasma membrane integrity, and eventual dissolution of the cell (Fig. 2). By 3 h reperfusion, the cell body of striatal neurons swells and many vacuoles are formed in the cytoplasm (Fig. 2B). Morphometric analysis showed that the volume of striatal neuron cell bodies (cytoplasm and nucleus) was 1265.7 ± 98.9 μm^3 (mean ± SEM) in control piglets, while, at 3 h after HI, striatal neuron cell body volume was 1716.4 ± 129.9 μm^3 (corresponding to a significant 36% increase in cell body volume). In contrast, the volume of striatal neuron nuclei was 527.6 ± 37.6 μm^3 (mean ± SEM) in control piglets, and, at 3 h after HI, striatal neuron nuclear volume was 388.2 ±
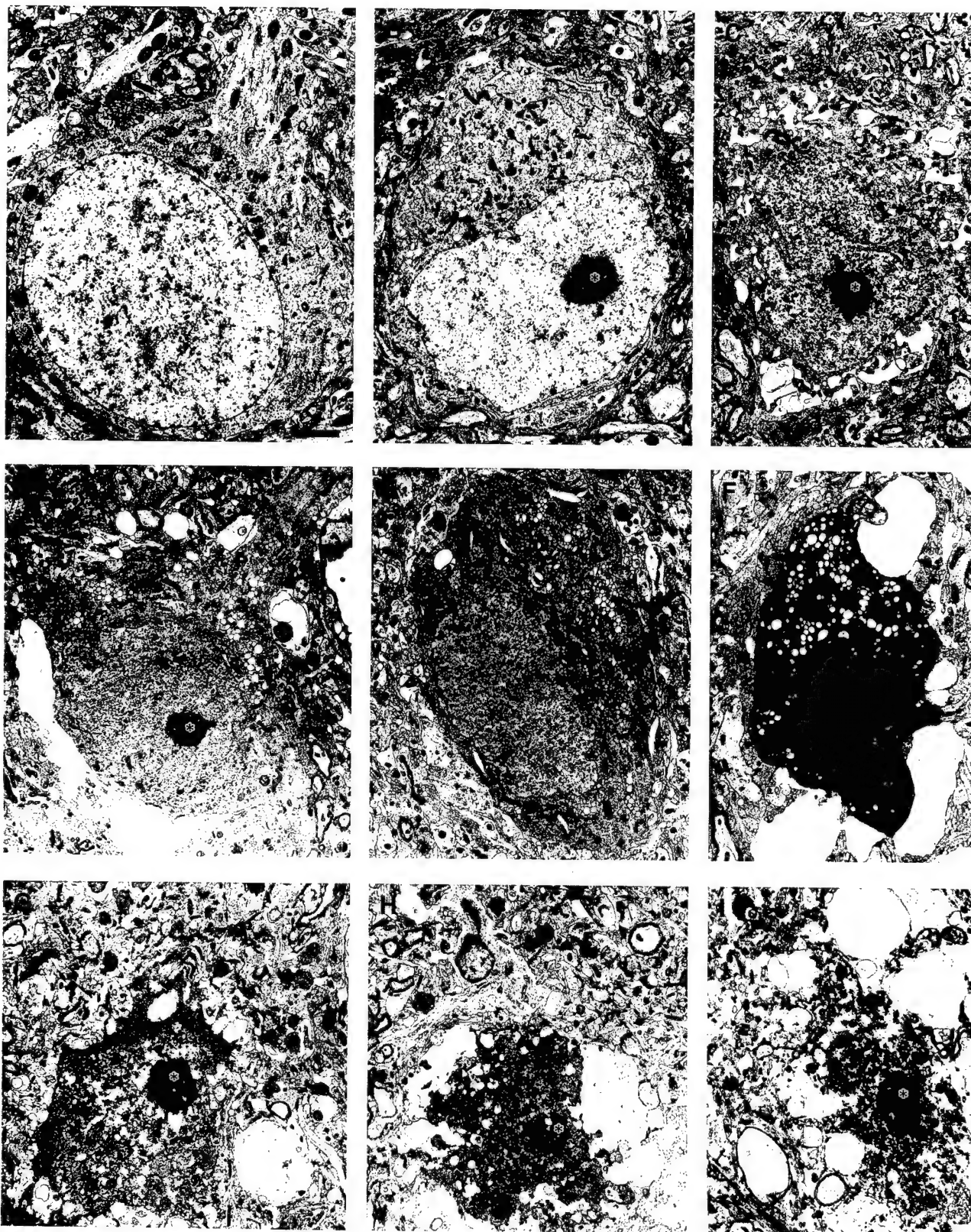
52.8 μm^3 (corresponding to a significant 26% decrease in nuclear volume). These measurements demonstrate that the cell body swelling is due the cytoplasmic swelling. Shrinkage of the nucleus coincides with incipient condensation of the nuclear matrix at 3 h after HI (Fig. 2B). The condensation of the nuclear matrix progresses during 6–12 h (Fig. 2), consistent with the progression and pattern of DNA fragmentation (Fig. 1). By 6 h, the rough ER dilates severely (Fig. 2C). Progressive cellular condensation commences by 12 h (Figs. 2D–2F). Between 6 and 12 h, the neurons become dark (osmophilic) and assume an angular shape, and the nucleus becomes pyknotic and forms irregularly shaped clumps of chromatin that are distributed throughout the nucleus with a darkened matrix. While nuclear pyknosis and chromatin condensation into irregular clumps is observed in these dying neurons, this pattern was very dissimilar to that found in neuronal apoptosis (Portera-Cailliau *et al.*, 1997a,b; Al-Abdulla *et al.*, 1998; Martin *et al.*, 1998a, 1999, 2000). During this process, the nucleolus remains obvious (Fig. 2, asterisks), this feature is distinct from the early disassembly of the nucleolus in apoptosis (Martin *et al.*, 1998a). Subsequently, the condensed cell body and nucleus disintegrate between 12 and 24 h, as cellular debris is dispersed into the extracellular compartment (Figs. 2F and 2G), consistent with the loss of neuronal density observed at 24 h (Table 1) and severe tissue inflammation thereafter (Martin *et al.*, 1997c).

Striatal neuron necrosis after HI evolves as a sequence of organelle abnormalities (Fig. 3), similar to the sequence found with NMDA receptor-mediated excitotoxic neuronal necrosis (Portera-Cailliau *et al.*, 1997a). By 3 h and progressing through 12 h after HI, neurons accumulate many, clear, round, membrane-bound vacuoles (Figs. 3B–3E) that may be derived from vesiculation of the Golgi apparatus (Donaldson *et al.*, 1990; Pavelka and Ellinger, 1993) or from increased formation of plasma membrane-derived endosomes (Simons and Zerial, 1993). By 6 h, the ER dilates severely, resulting in the formation of large cisterns, and the potential space between the apposing membranes of the nuclear envelope also dilates due to its continuity with the ER (Fig. 3C). ER swelling is associated with release of ER-bound ribosomes, and disaggregation of cytoplasmic polyribosomes to form monosomes. Between 6 and 12 h after HI, the ER collapses and becomes fragmented, and the nuclear membrane becomes discontinuous (Figs. 3C and 3D). ER collapse and fragmentation, ribosome release, and polysomal disaggregation coincide with the homogenization and darkening of the cytoplasmic matrix. During the first 12 h after HI, mitochondria appear to acculumate within the cell bodies of striatal neurons, and most mitochondria remain intact until about 6–12 h (Figs. 3B–3D), and then they swell and vacuolate and undergo cristaeolysis. At the time when most mitochondria show ultrastructural damage (i.e., at 12–24 h after HI), the plasma membrane ruptures and the condensed cytoplasm and fragmented nucleus are dispersed into the neuropil (Figs. 3F–3I).

Damage to the Golgi Apparatus and ER Occur Early after HI

We performed immunoblot and immunocytochemical experiments with specific organelle protein antibodies to identify the subcellular origin of the numerous vacuoles that accumulate in striatal neurons after HI and to identify possible molecular correlates of the structural abnormalities in organelles found by EM. To determine whether the Golgi apparatus or plasma

FIG. 2. EM analysis of striatal neuron degeneration in HI piglets. A normal principal striatal neuron from control piglet (A) is shown for comparison with neurons from piglets at 3, 6, 12, and 24 h after HI (B–I) arranged in a temporal sequence to show the predominant ultrastructural evolution of ischemic neuron necrosis. This neuronal death is not completely synchronized, because dying neurons can be found at different stages of degeneration at most times after HI; however, the neuronal profiles shown for each time represent the predominant stage of degeneration. Asterisks identify the nucleolus (when present in the plane of section). By 3 h after HI (B), the neuronal cell body swells (see text for measurements) and numerous, clear vacuoles are formed within the cytoplasm, increasing progressively over 9–12 h (C–E). At 6 h after HI (C), the arrays of rough ER are severely dilated (D, E) and then become fragmented, and the mitochondria become dark and condensed, as the cytoplasmic matrix becomes progressively dark and homogeneously granular. The overall contour of the cell changes from a round shape (A–C) to a fusiform or angular shape (D, E), as the neurons become shrunken 6–12 h after HI (F). Concurrently, during the first 12 h after HI, the nucleus shrinks (see text for measurements at 3 h) and the nuclear matrix progressively becomes uniformly dark (C–E) as numerous small, irregular clumps of chromatin are formed throughout the condensing nucleus (F). The nucleolus (asterisks) still remains prominent throughout this process (B–D), even until ultimate neuronal disintegration (G–I). Between 12 and 24 h, injured cells disintegrate as the dark, severely vacuolated cytoplasm, containing few discernible but very swollen mitochondria, undergoes dissolution, while the nucleus progressively forms more chromatin clumps and undergoes karyolysis (G–I). The cytoplasmic and nuclear debris is liberated into the surrounding neuropil (I). This neurodegeneration is structurally necrotic. Scale bar (A), 1.3 μm (same for B–I).
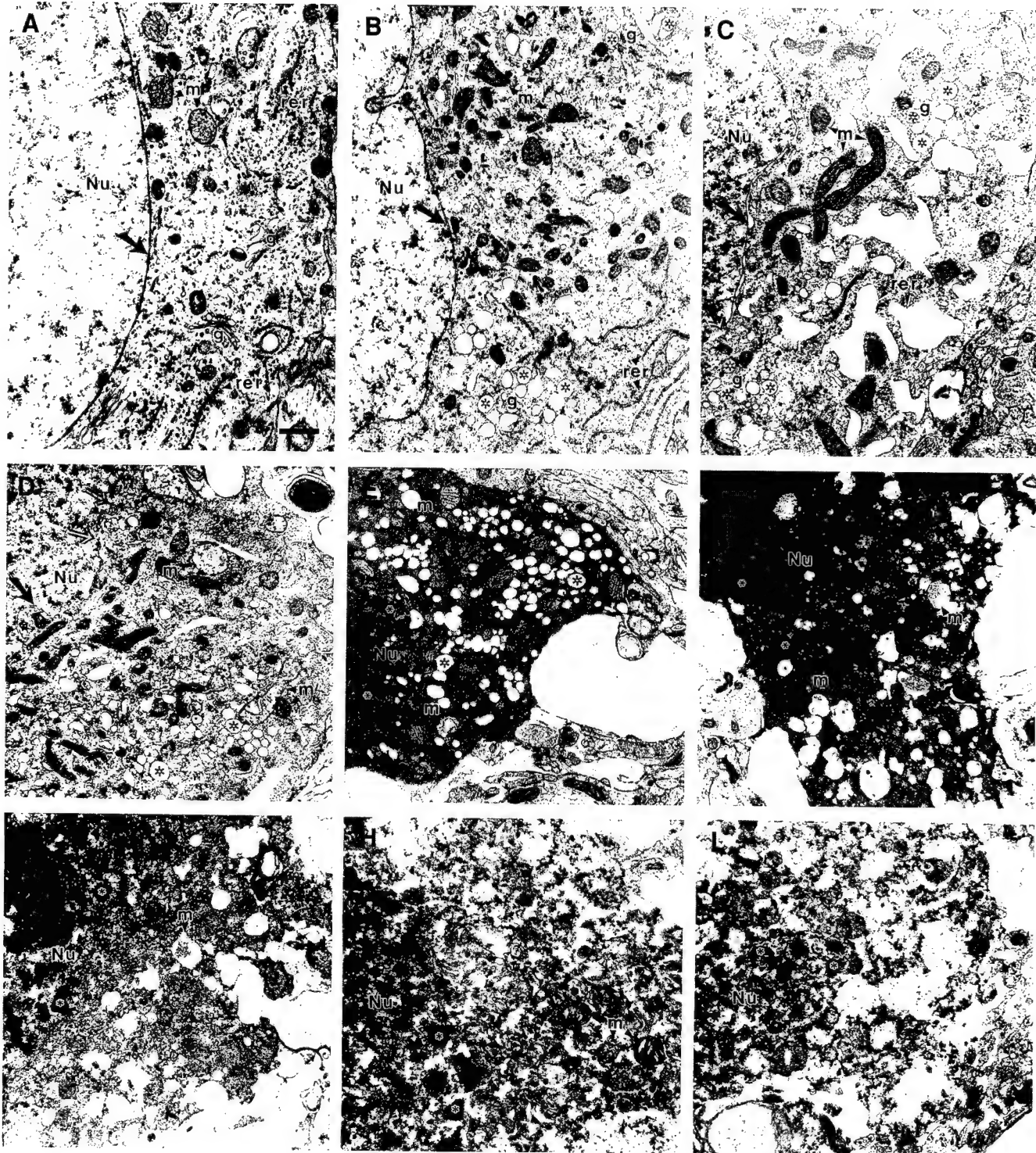
FIG. 3. Death of striatal neurons after HI progresses as a sequence of organelle abnormalities. (A) In control piglet, normal, principal, striatal neurons have abundant polyribosomes distributed throughout the cytoplasmic matrix, intact arrays of rough ER (rer) and Golgi stacks (g) and uniformly shaped mitochondria (m) with intact cristae. The nucleus (Nu) has a predominantly pale matrix and is surrounded by a continuous, bilaminar nuclear membrane (arrow). (B) By 3 h after HI, many clear vacuoles (asterisks) appear to be derived from swelling and vesiculation of the Golgi apparatus. The rough ER appears relatively normal, and the mitochondria are intact structurally but appear condensed. (C–E) By 6 h after HI, numerous vacuoles accumulate (asterisks) as the surrounding cytoplasmic matrix becomes progressively granular and dark. The rough ER becomes severely dilated, and ribosomes become unbound from the rough ER membrane. Polyribosomes disaggregate into
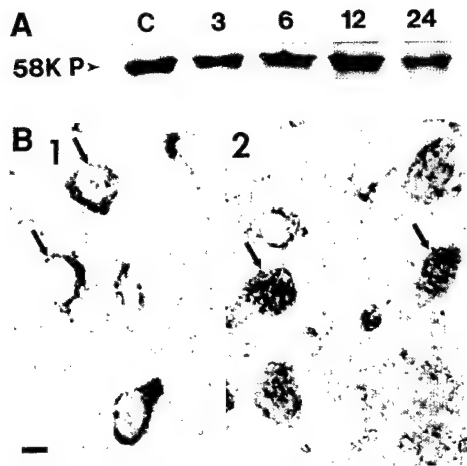
FIG. 4. The Golgi apparatus fragments early after HI. (A) Immunoblot analysis of the Golgi membrane protein (58K P) in subcellular membrane fractions of striatum from control (c) and HI piglets at 3, 6, 12, and 24 h postinsult. The levels of 58K protein are maintained until 24 h after HI. (B) Immunolocalization of Golgi 58K protein (black immunoperoxidase staining) shows the normal perinuclear location of the Golgi apparatus in control striatal neurons (1, arrows) and the prominent fragmentation of the Golgi apparatus and formation of vesicles in striatal neurons by 6 h after HI (2, arrows). Scale bar (B1, same for 2), 10 μm.

membrane endosomes are sources of the cytoplasmic vacuoles, antibodies to Golgi 58K protein and Rab5A were used. Golgi 58K protein levels in striatum remained unchanged ($P < 0.05$) until 24 h after HI (Fig. 4A), at which time levels were reduced significantly ($P < 0.05$) to ~50% of control, consistent with loss of striatal neurons (Table 1). However, despite maintained levels of protein at 3–12 h after HI, immunolocalization of Golgi 58K protein revealed that the Golgi apparatus in striatal neurons is dispersed and fragmented early after HI (Fig. 4B). In contrast, intracellular Rab5A immunoreactivity was lost in striatal neurons early after HI, while Rab5A immunoreactivity increased markedly in nonneuronal cells that ap-

peared to be microglia (Fig. 5). Therefore, the numerous vacuoles that accumulate within striatal neurons early after HI are likely to be derived from the Golgi apparatus rather than from the plasma membrane.

EM revealed that the ER undergoes massive swelling prior to its fragmentation (Figs. 2 and 3). We used antibodies to ER resident, KDEL sequence-containing proteins to track the progression of damage to the ER. In soluble protein fractions of control piglet striatum, protein disulfide isomerase (PDI), a lumenal ER-resident ~57 kDa protein (Munro and Pelham, 1987; Jiang et al., 1999), is undetectable or at very low levels (Fig. 6A). In contrast, as early as 3 h after HI, PDI levels in soluble protein fractions are detected at high levels compared to control piglet striatum (Fig. 6A). PDI levels remain high through 12 h after HI and then levels begin to dissipate by 24 h, consistent with the conclusion that active neuronal necrosis has tapered-off by 24 h. Immunolocalization of KDEL-proteins showed faint cytoplasmic labeling of striatal neurons in controls (Fig. 6B, 1); in contrast, the cytoplasm of striatal neurons was intensely immunoreactive at 6 and 12 h after HI (Fig. 6B, 2, 3). These results are consistent with the EM observations of ER dilatation and fragmentation at 6–12 h after HI, and they suggest that these structural changes are associated with ER membrane damage and release of ER resident proteins into the cytosol or increased accessibility of antibodies to KDEL proteins within ER fragments.

Striatal Mitochondria after HI Show Early Functional Suppression Followed by Transient Activation and Then Failure

EM showed that at 3 h after HI most mitochondria appear structurally intact, but at 6 h a subset of mitochondria swells and lyses while others appear to remain intact, and at 12 h most mitochondria are swollen and lytic (Figs. 2 and 3). Biochemical assay of COX in mitochondrial-enriched organelle fractions of piglet

monosomes, and these free ribosomes are dispersed in the cytoplasm causing the matrix to become granular. Most mitochondria appear condensed but a subset is very swollen and exhibits cristaeolysis. The nucleoplasmic matrix progressively becomes darker and the chromatin undergoes condensation into small clumps of various sizes (asterisks, D, E), while the nuclear membrane (solid black arrow) becomes less discernible and is breached in some locations (C and D, open arrows). (F) At 12 h after HI, the cytoplasmic matrix is homogeneously dark and most organelles are no longer discernible, except for swollen and degenerating mitochondria. Numerous vacuoles containing membranous debris are formed in the cytoplasm as more mitochondria degenerate and undergo cristaeolysis. The nuclear chromatin becomes prominently aggregated into clumps of various shapes and sizes, as the surrounding nucleoplasmic matrix becomes uniformly dark and the nuclear envelope looses integrity. (G, H) At 12–24 h after HI, the dark and condensed cytoplasm, containing degenerated mitochondria, undergoes fragmentation as the plasma membrane ruptures. The nucleus, containing chromatin clumps (asterisk), is no longer surrounded by an intact nuclear membrane and undergoes karyolysis. (I) At end-stage degeneration, cytoplasmic debris and nuclear debris with chromatin clumps (asterisk) are dispersed into the surrounding neuropil. Scale bar (A), 0.5 μm (same for B–I).
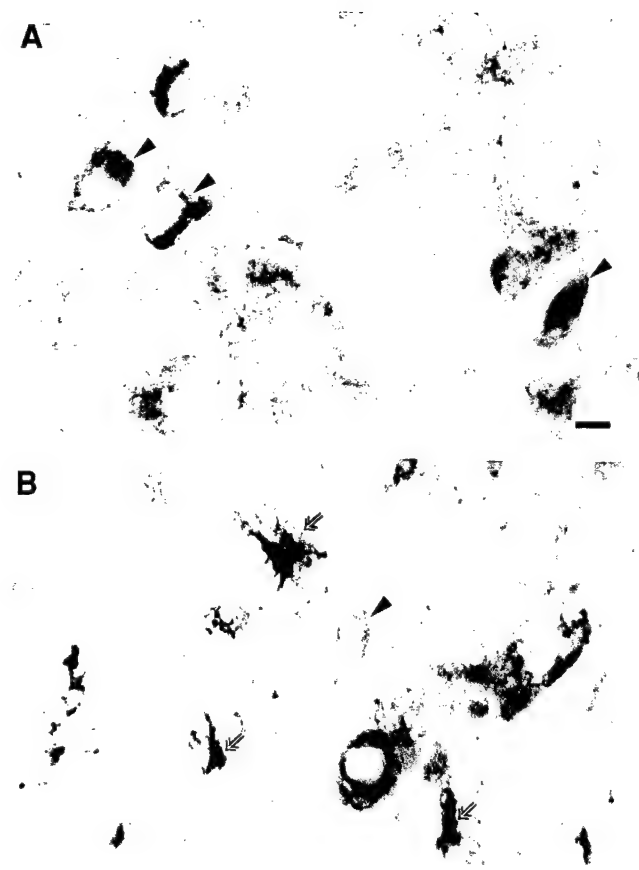
FIG. 5. Cell type-dependent changes in the endosomal compartment occur after HI as demonstrated by the immunolocalization of the plasma membrane early-endosome protein Rab5A. (A) In control striatal neurons (arrowheads), Rab5A-labeled endosomes fill the cytoplasm, and in some neurons (upper left arrowhead) Rab5A immunoreactivity is present as discrete particles on or near the cell surface. Nonneuronal cells and their processes in control striatum are only faintly immunoreactive for Rab5A. Scale bar, 8 μm (same for B). (B) At 6 h after HI, endosomal labeling of striatal neurons is markedly deficient (arrowhead), and cells that appear to be microglia are intensely immunoreactive for Rab5A (open arrows).

striatum revealed time-dependent functional changes. Activity was 37, 163, 72, and 81% of control at 3, 6, 12, and 24 h, respectively (Fig. 7A). COX subunit I levels were measured by immunoblotting in these same subcellular fractions. Piglet COX subunit I was detected as two major bands, corresponding to an ~40 kDa monomer and a multimeric high molecular mass aggregrate, consistent with the migration pattern of purified bovine COX (Fig. 7B). These forms of COX change differentially after HI. At 3 h, COX subunit I immunoreactivity (both monomeric and aggregated forms) was reduced markedly (Fig. 7B). The levels of the COX subunit I monomer returned to control

amounts at 6 h and then were decreased at 12 and 24 h (Fig. 7B). In contrast, levels of the aggregated form of COX subunit I were increased at 6–24 h after HI compared to control (Fig. 7B). To visualize mitochondria in piglet brain sections, COX subunit I antibodies were used for immunocytochemistry. Immunolocalization of COX subunit I in control striatum showed a finely particulate distribution within the neuropil (Fig. 7C, 1), consistent with a mitochondrial localization in cellular processes. After HI, the finely particulate COX subunit I immunoreactivity dissipated in the neuropil and many larger, swollen particles were formed (Fig. 7C, 2, 3). In addition, COX subunit I immunoreactivity
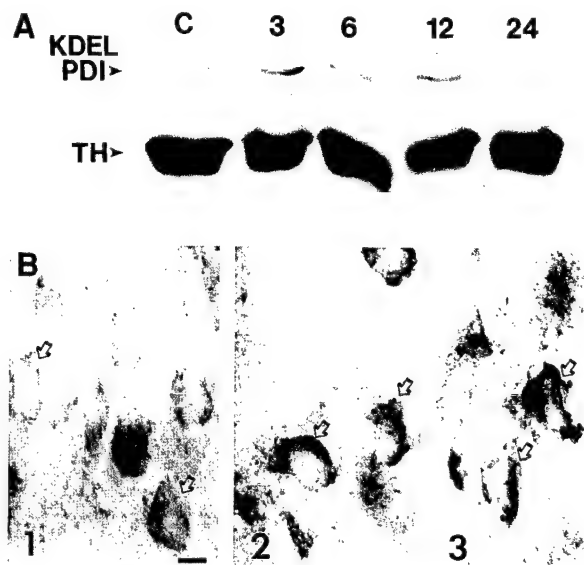
FIG. 6. The ER is damaged early after HI. (A) Immunoblot analysis of the KDEL sequence-containing ER lumenal protein, protein disulfide isomerase (PDI), in nondetergent solubilized cytosolic fractions of striatum from control (c) and HI piglets at 3, 6, 12, and 24 h postinsult. In control striatum, PDI levels are undetectable because it is retained with the lumenal compartment of the ER. At 3, 6, and 12 h after HI, PDI levels are markedly elevated in the soluble compartment compared to control, but by 24 h PDI levels are dissipating. Blots were reprobed with antibody to tyrosine hydroxylase (TH) as a protein loading control. (B) In control striatal neurons, immunolocalization of KDEL proteins (gray immunoperoxidase staining) shows diffuse cytoplasmic labeling consistent with specific ER localization (1, arrows). Scale bar (B1, same for 2 and 3), 10 μm. At 3 h after HI, the cytoplasmic immunoreactivity (black immunoperoxidase labeling) for KDEL proteins is increased in striatal neurons (2, arrows) with the most intense staining occurring peripherally in the cell body, consistent with the ER redistribution seen by EM (compare with Fig. 2B). At 12 h after HI, immunoreactivity for KDEL proteins is enriched highly in striatal neurons with shrunken and angular morphologies (arrows) at a time when the ER undergoes fragmentation as shown by EM (compare with Figs. 2 and 3).

accumulated transiently (notably at 6 h) in neuronal cell bodies, with some of this immunoreactivity appearing to delineate swollen mitochondria (Fig. 7C, 2, 3), consistent with the EM findings (compare Figs. 3D and 3E with Fig. 7C, 2, 3). To examine COX activity with greater spatial resolution in piglet brain sections, COX activity was assayed with a histochemical method, and reaction product was quantified by densitometry. These results generally paralleled the data obtained by biochemical assay and were most notable because histochemical activity for COX in putamen was increased at 6 h (Fig. 7D), consistent with the biochemical assay for COX (Fig. 7A).

Cytochrome c Is Depleted in Striatum after HI

The EM showed progressive structural damage to mitochondria, and the COX assays showed a temporal profile of mitochondrial suppression (at 3 h), activation (at 6 h), and then suppression (after 6 h) during striatal neuron necrosis. Therefore, we measured cytochrome c levels in piglet striatum as another marker for mitochondrial damage and metabolic impairment. Scant information is known about cytochrome c in pig brain. Under our assay conditions, we could detect amounts of cytochrome c as low as 500 pg (Fig. 8A). Procine brain cytochrome c migrated as a monomer of ~12 kDa and as dimers and multimers, similar to purified horse heart cytochrome c (Fig. 8A). Piglet brain cytochrome c was measured in the range of 5 ng, corresponding to ~0.05% of total soluble protein (Fig. 8A). Cytochrome c levels were normal at 3 h after HI, but by 6 h after HI and thereafter, cytochrome c was reduced to ~55% of control (Fig. 8B).

Lysosomal Membrane Integrity in Striatum Is Compromised by 6 h after HI

To understand some of the possible mechanisms for striatal neuron necrosis after HI, acid phosphatase activity was measured in soluble protein fractions (unexposed to detergent solubilization) of control and HI piglets (Table 2). This biochemical assay serves as an index of lysosomal membrane damage and destabilization and release of hydrolytic enzymes into the cytosol (Frederiks and Marx, 1989; van Noorden, 1991). In the presence of sodium fluoride (10 mM), acid phosphatase activity was inhibited ~95% (data not shown). Acid phosphatase activity was increased significantly above control levels at 6, 12, and 24 h after

HI (Table 2), demonstrating that damage to lysosomal membranes in striatum occurs between 3 and 6 h after HI.

Glutathione Levels in Striatum Are Depleted by 3 h after HI

A potent stimulus for cellular necrosis is oxidative stress (McCord, 1985). GSH functions in antioxidant mechanisms as a free radical scavenger, and the levels of GSH are often used as an index of oxygen radical production (Mizui *et al.*, 1992). Therefore, we measured GSH levels in piglet striatum after HI (Table 3). GSH in soluble protein fractions was significantly reduced to ~80% of control at 3 and 6 h after HI but returned to control levels by 12 h after HI (Table 3), demonstrating that oxidative stress occurs early (by 3 h) after HI newborn in piglets, but that this stress in the form of glutathione depletion is transient.

Peroxynitrite Damage to Striatal Membrane Proteins Occurs after HI

To determine if HI produces oxidative damage, striatal membrane fractions were immunoblotted for nitrotyrosine-modified proteins as a marker for peroxynitrite-mediated oxidative damage (Fig. 9A). An intensely reacting band of proteins at ~50 kDa showed nitration in control striatum. The nitrotyrosine-modification of this ~50-kDa protein was increased at 6 h after HI. Immunoprecipitation experiments demonstrated that this nitrotyrosine-modified, ~50-kDa protein is tubulin and that tubulin nitration is markedly increased by 6 h after HI (Fig. 9B) Another prominent band of nitrotyrosine immunoreactivity was detected at ~68–70 kDa (Fig. 9A), probably corresponding to nitration of the low molecular weight neurofilament (Strong *et al.*, 1998). This ~68- to 70-kDa protein band showed nitrotyrosine modification above control at 3, 6, 12, and 24 h after HI, with maximal nitration occurring at 6 h (Fig. 9A). To identify directly that neurons in the striatum sustain peroxynitrite-mediated oxidative damage after HI, brain sections from perfusion-fixed piglets were reacted with nitrotyrosine antibodies. In control piglet striatum, nitrotyrosine immunoreactivity was not detectable by immunocytochemistry (Fig. 9C, 1). Early after HI, striatal neurons showed intense nitrotyrosine immunoreactivity (Fig. 9C, 2, 3). In many putaminal neurons at 3 and 6 h after HI, nitrotyrosine immunoreactivity was lo-
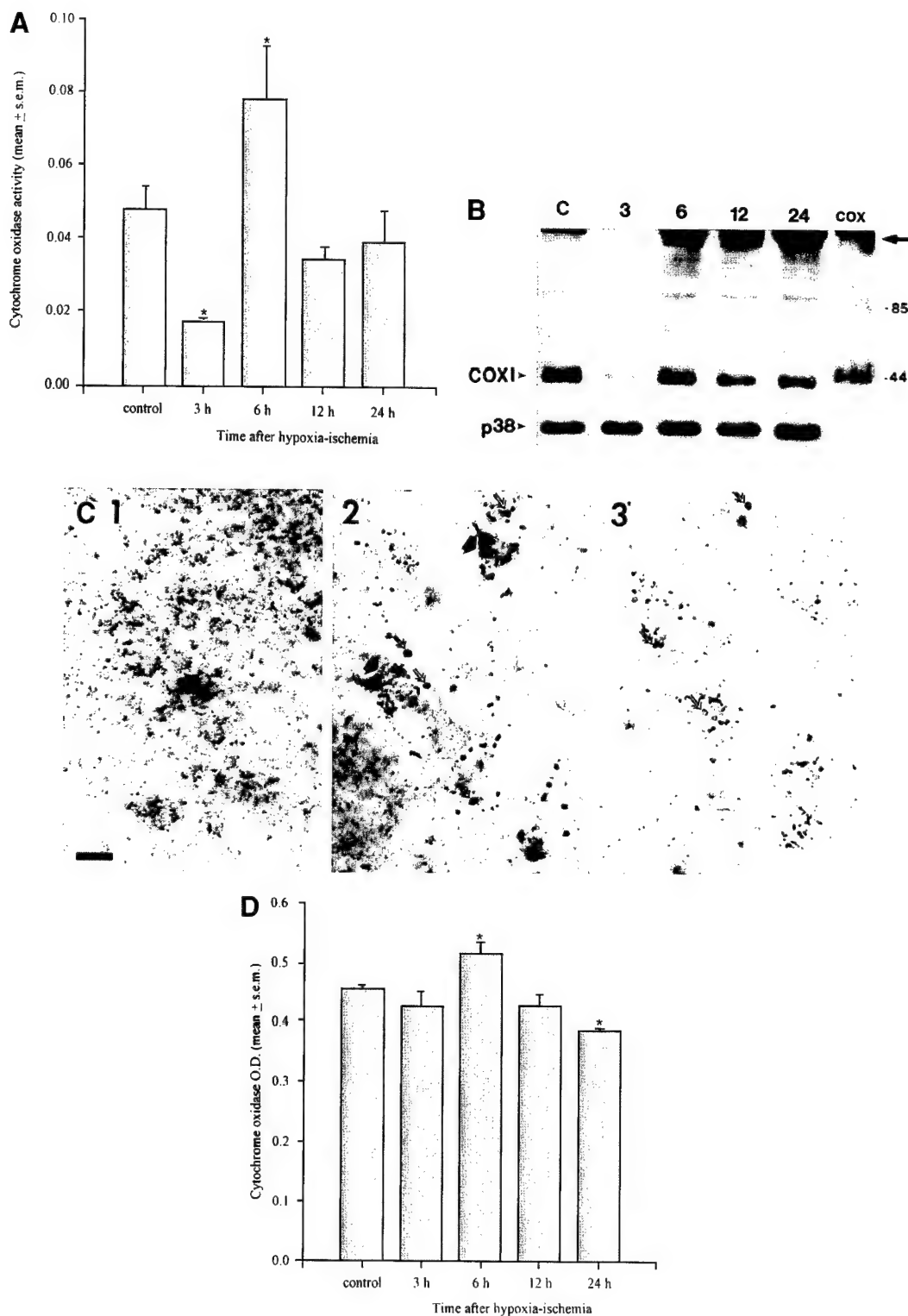
FIG. 7. Mitochondria undergo functional, molecular, and structural abnormalities in HI piglet striatum. (A) In mitochondrial-enriched subcellular fractions of control and HI piglet striatum (n = 2–3 per group), biochemical assay for COX activity shows a transient suppression of mitochondrial function at 3 h after HI, followed by a large burst of activity at 6 h recovery, and then reduced mitochondrial function thereafter. Asterisk indicates significant difference (P < 0.05) from control. (B) Immunoblot analysis of COX subunit I in mitochondrial-enriched fractions of striatum from control (c) and HI piglets at 3, 6, 12, and 24 h postinsult (n = 2–3 per group). Purified bovine COX (right

calized at a perinuclear location (Fig. 9C, 2), and at 12 h after HI this immunoreactivity was dispersed throughout the cytoplasm as small packets in subsets of neurons (Fig. 9C, 3). This localization of nitrotyrosine immunoreactivity was very reminiscent of the vesiculation and fragmentation of the Golgi apparatus observed by EM (Figs. 2 and 3) and light microscopy (Fig. 4B). To identify if Golgi apparatus-associated proteins are damaged by peroxynitrite radicals, we examined the possible colocalization of Golgi 58K protein and nitrotyrosine immunoreactivities by immunofluorescence. Striatal neurons in HI piglets showed precise colocalization of nitrotyrosine and Golgi 58K protein immunoreactivities (Fig. 10). These results demonstrate that peroxynitrite-mediated oxidative damage to membrane proteins occurs in the piglet striatum early after HI and that proteins associated with the Golgi apparatus are targets of peroxynitrite radicals.

Hydroxyl Radical Damage to DNA and RNA Occurs in Striatal Neurons after HI

To identify other possible forms of oxidative stress and other macromolecular targets of oxidative stress during the progression of neuronal necrosis after HI, we determined if nucleic acids are damaged by hydroxyl radicals using monoclonal antibodies that react with hydroxydeoxyguanosine (OHdG) and hydroxyguanosine (OHG) (Fig. 11). The characterization of these antibodies has been shown previously (Al-Abdulla and Martin, 1998; Martin *et al.*, 1999). These antibodies also weakly react with normal guanosine (Martin *et al.*, 1999), consistent with the faint cytoplasmic labeling suggestive of an RNA pattern in striatal neurons of control piglets (Fig. 11A). However, the pattern and intensity of immunoreactivity for OHG and OHdG was very different in piglet striatum after HI (Figs. 11B–11E). The intensity of immunoreactivity

in the cytoplasm of neurons and in the neuropil was much greater in striatum at 3 and 6 h after HI compared to controls. In addition, intense nuclear labeling occurred only in striatal neurons in HI piglets (Figs. 11C and 11D). Nonneuronal cells such as vascular endothelial cells also exhibited oxidative damage to DNA after HI (Fig. 11D). Digestion of RNA in brain sections with DNase-free RNase eliminated the cytoplasmic labeling of neurons and the neuropil labeling in HI piglet striatum, revealing the prominent nuclear immunoreactivity (Fig. 11D). Digestion of DNA with DNase diminished the nuclear labeling of striatal neurons in HI piglets (Fig. 11E). Preadsorption of OHdG antibodies with OHdG or OHG prior to the immunocytochemistry selectively competed the labeling in the different cellular compartments (data not shown), similar to experiments shown previously (Al-Abdulla and Martin, 1998; Martin *et al.*, 1999). These results demonstrate that both RNA and DNA undergo prominent hydroxyl radical damage early after HI.

DISCUSSION

We studied striatal neurodegeneration in a newborn animal model of HI that causes brain damage very similar to the pattern of injury found in human newborns that have experienced HI (Martin *et al.*, 1997a,b,c; Johnston, 1998). The clinical and neuropathological features of our piglet model are very different from those of the more commonly used newborn rat models (Martin *et al.*, 1997a; Brambrink *et al.*, 1999). Using this model, we tested the hypothesis that striatal neuron death is necrosis and evolves with oxidative stress and selective damage to organelles. The early neurodegeneration in newborn piglet striatum after HI is cellular necrosis and evolves rapidly through mechanisms associated with oxidative stress. A major strength of this study is that it consolidates in

lane) was used as a positive control. Molecular mass standards (in kDa) are indicated at right. Arrow identifies high molecular mass (> 200 kDa) multimeric complexes containing COX subunit I. Blots were reprobed with antibody to synaptophysin (p38) as a protein loading control. (C) Immunolocalization of mitochondria using antibody to COX subunit I. In control putamen (C1), mitochondria (grey immunoperoxidase staining) are localized as fine particles distributed diffusely throughout the neuropil without intense cytoplasmic labeling of striatal neuron cell bodies. Scale bar (C1, same for 2 and 3), 8 μm. At 6 h after HI, mitochondria accumulate within the cell bodies of striatal neurons (2, broad black arrowheads), as demonstrated by the cytoplasmic immunoreactivity (black immunoperoxidase labeling) for COX subunit I, while the neuropil immunoreactivity dissipates. Subsets of mitochondria within cellular processes in the neuropil (2, open arrows) and in neuronal cell bodies (2, broad black arrowheads) are dilated, consistent with the mitochondrial swelling seen by EM (compare with Fig. 3). At 12 h after HI, immunoreactivity for COX subunit I is reduced throughout the neuropil of putamen and many of the remaining mitochondria are swollen (3, open arrows), consistent with the disintegration of mitochondria found by EM. (D) Densitometric histochemical assay for COX enzyme activity in control and HI piglet putamen also revealed a transient elevation in mitochondrial function at 6 h recovery. Asterisks indicate significant difference ($P < 0.05$) from control followed by a loss of function at 24 h.

A

B
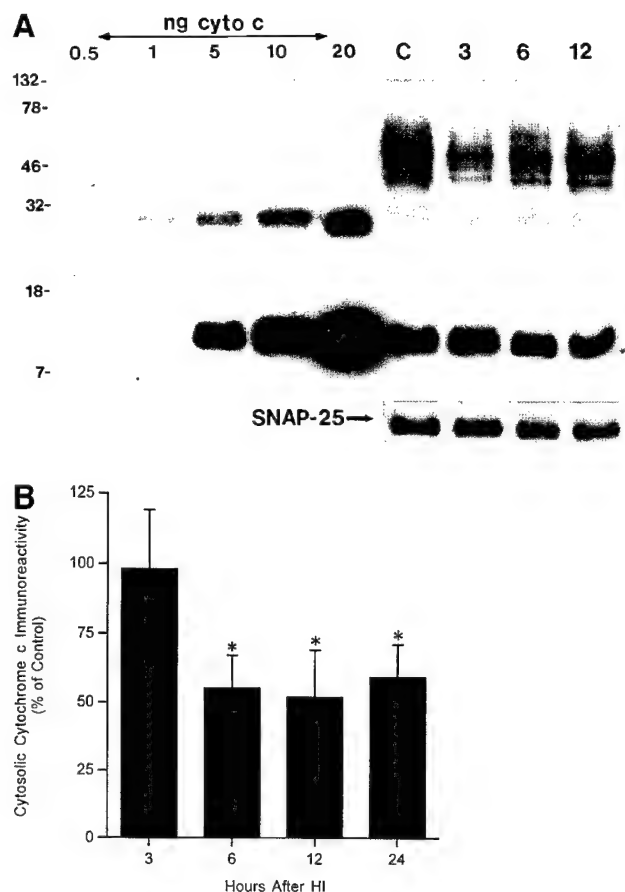
FIG. 8. Characterization of cytochrome c in pig brain and changes after HI: cytochrome c is depleted during striatal neuron necrosis. (A) Cytochrome c in piglet brain extracts was evaluated by immunoblotting and was compared to purified horse heart cytochrome c as a standard. Lanes were loaded with varying amounts of purified cytochrome c (0.5, 1, 5, 10, or 20 ng) or with 10 μg total soluble protein from striatal extracts of control (C) and HI (3, 6, or 12 h recovery) piglets. Molecular weight standards (in kDa) are shown at left. Purified cytochrome c monomer is detected at a molecular mass of ~12 kDa. The upper bands in the cytochrome c lanes are due to dimers or multimers of cytochrome c. Immunoreactive bands with similar mobilities are detected in piglet brain extracts. Blots were reprobed with synapse-associated protein-25 (SNAP-25) as a loading control for piglet extracts. (B) Densitometric analysis of cytochrome c protein levels in soluble fractions of striatum from piglets recovered for 3, 6, 12, or 24 h after HI. Cytochrome c immunodensity (2–3 piglets per group) was corrected for nerve terminal marker immunodensity in the same sample, then expressed as percentage control. Values are mean ± SEM. Asterisk indicates significant difference ($P < 0.05$) from control and 3 h after HI.

one set of experiments several observations previously reported as isolated fragments in less comprehensive papers. Furthermore, this study clarifies the controversial contributions of neuronal necrosis versus apoptosis to striatal degeneration after HI in newborns,

TABLE 2

Lysosomal Destabilization in Striatum after HI

Time after HI	Acid phosphatase activity (Percentage of control)[a]
3 h	119.7 ± 20.5
6 h	143.7 ± 16.1[b]
12 h	149.7 ± 15.9[b]
24 h	181.0 ± 5.2[b]

[a] See methods for assay. All values are mean ± SEM.
[b] Significantly different ($P < 0.05$) from control.

notably by demonstrating in piglets that neuronal apoptosis does not have a major contribution to this degeneration during the first 24 h after the hypoxic-asphyxic cardiac arrest. Apoptosis of neurons and neuroglia may, however, have a more prominent contribution to the neuropathology after HI in newborns as a form of delayed or secondary cell death that is related to target deprivation of interconnected brain regions (Martin *et al.*, 1997b, 1998a).

Neuronal Death in Striatum Begins Rapidly after HI and Is Necrosis

Striatal neuron degeneration begins before 3 h after HI and is progressive during the first 24 h after the insult. This degeneration is necrosis. Specific organelles are not targeted selectively. The nucleus, Golgi apparatus, ER, lysosomes, mitochondria, and cytoskeleton are all damaged. Proteins and nucleic acids (both RNA and DNA) are damaged by ROS. Protein constituents of the Golgi apparatus and/or Golgi complex-associated proteins (e.g., cytoskeletal proteins) are direct targets of peroxynitrite radicals. Thus, the damage is indiscriminate at the subcellular level and is consistent with acute oxidative stress. This
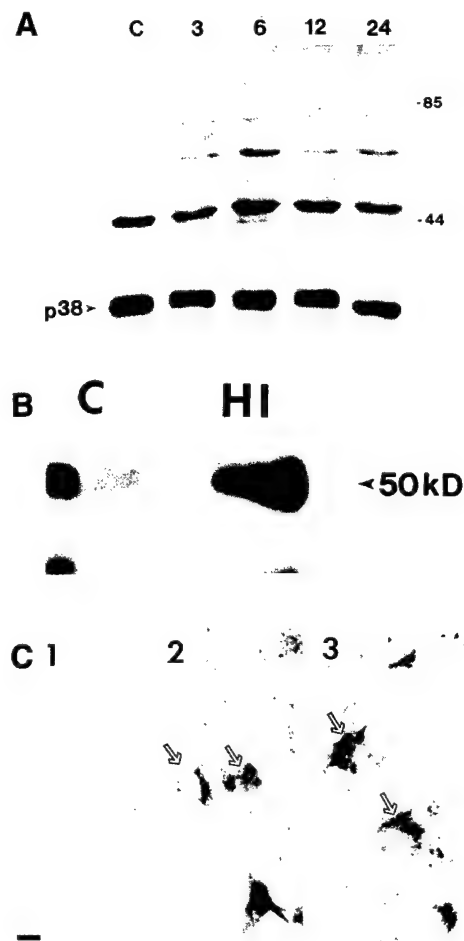
TABLE 3

Glutathione Levels in Striatum after HI

Time after HI	Glutathione level (percentage of control)[a]
3 h	81.3 ± 1.7[b]
6 h	80.7 ± 0.6[b]
12 h	91.0 ± 3.7
24 h	95.0 ± 2.5

[a] See methods for assay. All values are mean ± SEM.
[b] Significantly different ($P < 0.05$) from control.

FIG. 10. Double-label immunofluorescence for nitrotyrosine (A, green FITC labeling) and Golgi 58K protein (B, red Texas red labeling) demonstrates that nitrotyrosine immunoreactivity (A, arrowhead) occurs at fragments of the Golgi apparatus (B, arrowhead) in striatal neurons at 6 h after HI. Scale bar in A, 4 μm.

FIG. 9. Peroxynitrite-mediated oxidative damage to proteins occurs early after HI. (A) Immunoblot of nitrotyrosine-modified membrane proteins in striatum from control (c) and ischemic piglets at 3, 6, 12, and 24 h after HI. Molecular mass markers (in kDa) are indicated at right. Prominent increases in nitration after HI occur in proteins at ~50 and ~68 kDa. Blots were reprobed with antibody to synaptophysin (p38) as a protein loading control. (B) Immunoprecipitation demonstrated that tubulin (with a molecular mass of ~50 kDa) is a nitrated protein in control striatum (c). After HI, nitrotyrosine modification of tubulin is increased in striatum at 6 h (HI). Nitrotyrosine modification of a low molecular mass fragment of tubulin or a protein that interacts with tubulin (lower panels) is unchanged after HI. (C) Immunolocalization of nitrated proteins in striatal neurons after HI. In control striatum (C1), nitrotyrosine immunoreactivity is not detectable, but, at 6 (2) and 12 h (3) after HI, striatal neurons (open arrows) are intensely immunoreactive for nitrotyrosine. At 6 h after HI many neurons have a perinuclear localization of nitrotyrosine immunoreactivity, while at 12 h after HI, nitrotyrosine immunoreactivity is dispersed throughout the cytoplasm of striatal neurons. This pattern is reminiscent of the structural changes in the Golgi apparatus (see Figs. 2–4). Scale bar (C1, same for 2 and 3), 8 μm.

conclusion is further substantiated by the depletion of GSH by 3 h. This degeneration of striatal neurons after HI is very distinct structurally and biochemically from neuronal apoptosis (Martin *et al.*, 1998a). It is also distinct from non-NMDA glutamate receptor-mediated excitotoxic neuronal apoptosis, but it is very similar to NMDA receptor-mediated excitotoxic neuronal necrosis (Portera-Cailliau *et al.*, 1997a). Based on the onset of neuronal damage, the rate of progression of neuronal death, and on the widespread subcellular damage, we conclude that early neurodegeneration in striatum after HI in newborns is oxidative stress-induced cellular necrosis.

Our results demonstrating that neuronal death in the striatum of HI newborn piglets is necrosis differs from recent conclusions made by other groups using neonatal rats (Hill *et al.*, 1995; Beilharz *et al.*, 1995; Cheng *et al.*, 1998). This discrepancy regarding the occurrence of neuronal apoptosis after HI is partly due
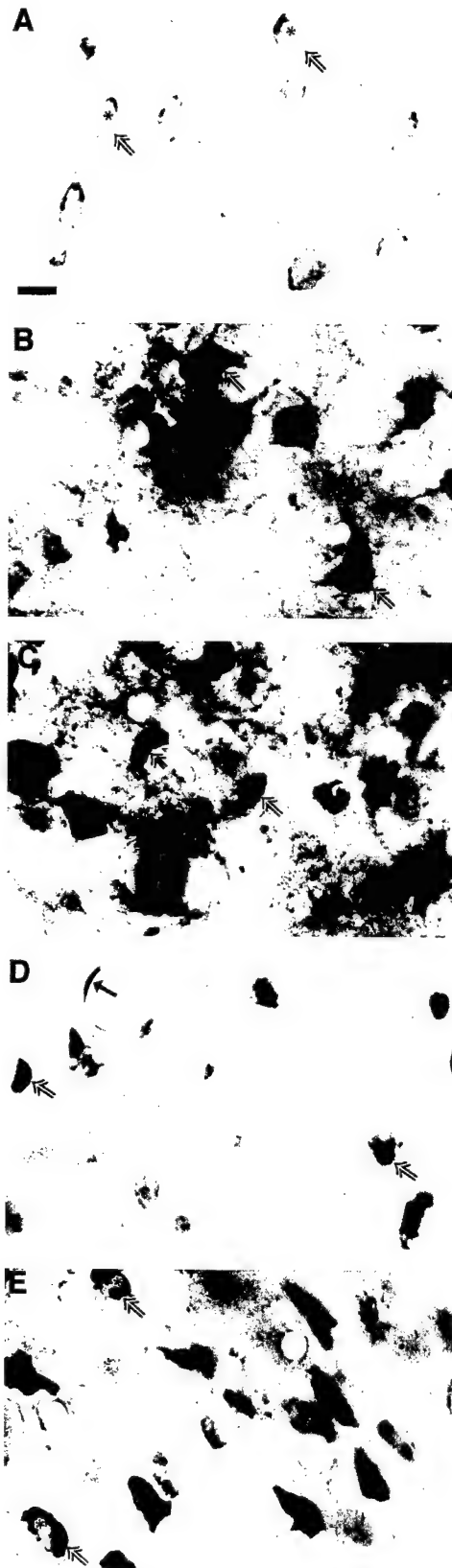
to differences in the criteria for apoptosis, differenes in the comprehensiveness of the EM analysis, and to differences in the animal species used for the experimental injury. It was reported that the ultrastructure of neuronal degeneration was apoptosis after HI in 1-week-old rat (Cheng *et al.*, 1998). However, this ultrastructure would be interpreted as necrosis by us and others (present study and Martin *et al.*, 1998a, 2000; Ishimaru *et al.*, 1999). The nuclear pyknosis with condensation of chromatin into many small, irregularly shaped clumps in ischemic neurons contrasts with the formation of few, uniformly dense and regularly shaped chromatin aggregates which occurs in neuronal apoptosis (Portera-Cailliau *et al.*, 1997a; Al-Abdulla *et al.*, 1998; Martin *et al.*, 1998a, 1999, 2000; Ishimara *et al.*, 1999). Alternatively, the data from neonatal rats may support our concept of the apoptosis-necrosis continuum for neuronal death (Portera-Cailliau *et al.*, 1997a,b; Martin *et al.*, 1998a) in that this neuronal degeneration may be a hybrid of necrosis and apoptosis. DNA fragmentation analyses (Hill *et al.*, 1995; Beilharz *et al.*, 1995; Cheng *et al.*, 1998) would support this interpretation, in view of a structure indicative of necrosis in the presence of internucleosomal laddering. Internucleosomal fragmentation of DNA was not found in HI piglets. Digestion of DNA in an internucleosomal pattern may not be specific for apoptosis, because it occurs in NMDA receptor-mediated excitotoxic neuronal necrosis in adult brain (Portera-Cailliau *et al.*, 1997a) and in neuronal culture (Gwag *et al.*, 1997), and in cells undergoing necrosis induced by calcium ionophores and heat shock (Collins *et al.*, 1992). Moreover, *in situ* end-labeling methods for DNA fail to discriminate among apoptotic and

FIG. 11. Prominent hydroxyl radical damage to RNA and DNA occurs in striatal neurons after HI. (A) In control striatal neurons (open arrows) faint labeling of the cytoplasm is detected with OHdG/OHG antibodies, corresponding to RNA labeling, while the nucleus (asterisks) and the neuropil is free of immunoreactivity. Scale bar, 25 μm (same for B–E). (B) By 6 h after HI, the cell bodies and processes of striatal neurons (open arrows) have intense cytoplasmic OHdG/OHG immunoreactivity. (C) By 12 h after HI, striatal neurons (open arrows) display intense OHdG/OHG immunoreactivity within the cytoplasm and the nucleus. (D) RNase digestion abolished the prominent cytoplasmic and neuropil labeling for OHG in striatal neurons after HI, revealing the intense nuclear labeling for OHdG (open arrows). Hydroxyl radical damage to DNA also occurs in vascular endothelial cells at 6 h after HI (solid black arrow). (E) In striatal neurons (open arrows) at 12 h after HI, DNase treatment diminished the labeling for OHdG within the nucleus (asterisk).

necrotic cell deaths (Grasl-Kraupp *et al.,* 1995; Portera-Cailliau *et al.,* 1997a; Martin *et al.,* 1998a) and can also detect DNA fragments during DNA synthesis (Lockshin and Zakeri, 1994). Additional observations demonstrating that a pan-caspase inhibitor is neuroprotective in neonatal rats after HI suggests a possible contribution of neuronal apoptosis (Cheng *et al.,* 1998) to this neuropathology; however, many caspase family members function in the proteolytic processing of proinflammatory cytokines, thus neuroprotective effects of pharmacological inhibition of all caspases may be mediated by mechanisms other than blocking apoptosis (e.g., anti-inflammation).

Furthermore, the rat pup model of neonatal HI and our newborn piglet model of HI are different from physiological, clinical, and neuropathological standpoints and are likely to exhibit different responses to injury. Rat pups and piglets (and other artiodactylous ungulates) near the day of birth are at very different stages of maturation with respect to glutamate receptors and glutamate transporters (Martin *et al.,* 1997c; Furuta *et al.,* 1997; Martin *et al.,* 1998b; Furuta and Martin, 1999; Northington *et al.,* 1998). In both pig and human, the peak of the brain growth spurt occurs near term, whereas that of rat occurs at about 7 days postnatally (Dobbing and Sands, 1979). Moreover, in pig, the percentage of adult brain weight at birth is much closer to human compared to that of rat (Dobbing and Sands, 1979). These fundamental neurobiological issues are very important when considering the relevance of experimental animals as models for brain injury in human newborns.

Striatal Neurons Undergo Widespread Organelle Damage after HI

Most organelles in vulnerable neurons are damaged after ischemia. Organelles that function in protein synthesis and posttranslational modification (i.e., the ER, polysomes, and Golgi apparatus) become structurally abnormal early after ischemia and are persistently abnormal during the process of neurodegeneration (Kirino *et al.,* 1984; Petito and Pulsinelli, 1984; Rafols *et al.,* 1995). Perturbations in the ER, ribosomes, and Golgi apparatus are consistent with the finding that total protein synthesis is severely reduced by 6 h after transient global forebrain ischemia and is reduced persistently in selectively vulnerable neurons (Thilmann *et al.,* 1986; Araki *et al.,* 1990). The ER damage and release of lumenal chaperone proteins found in HI piglets suggests that appropriate protein folding is also likely to be compromised. Our findings that the Golgi apparatus is structurally abnor-

mal and its protein constituents are possible targets of peroxynitrite radicals are consistent with other observations. Golgi membranes in neurons undergo lipid peroxidation after global ischemia (Rafols *et al.,* 1995). Furthermore, the finding that lysosomal membranes become destabilized in striatum after HI is consistent with results showing that lysosomal membrane stability is disrupted in liver after ischemia-reperfusion (Frederiks and Marx, 1989). Lysosomal instability and release of hydrolytic enzymes into the cytosol may propagate cellular necrosis by further damaging membranous organelles (Farber *et al.,* 1981).

Abnormalities in mitochondrial structure occur during cellular necrosis and can be produced when mitochondrial ATP synthesis fails and plasma membrane function is impaired (Laiho *et al.,* 1975). We found that mitochondrial function is suppressed at 3 h after HI, is sharply increased by 6 h reperfusion, and then mitochondrial enzymatic activity is lost. COX subunit I protein levels drop abruptly by 3 h after HI, followed by a return to baseline, and then a loss of protein is sustained. The loss of enzyme function and immunological delectability of protein at 3 h may reflect acute inactivation and epitope modification or proteolysis of mitochondrial proteins, possibly resulting from changes in intracellular pH and ionic strength, thermodynamic stability, or changes in the interactions of COX with endogenous modifiers such as ROS or other proteins (Bolli *et al.,* 1985; Wolff and Dean, 1986; Davies, 1987; Capaldi *et al.,* 1990). Mitochondrial proteins undergo oxidative inactivation by peroxynitrite. COX is a target of peroxynitrite-mediated inactivation (Bolaños *et al.,* 1995). In addition, H_2O_2 production can lead to formation of hydroxyl radicals and then lipid hydroperoxides that can damage mitochondrial membranes and inhibit mitochondrial functions (Ravindranath and Reed, 1990). The transient elevation of COX activity and reappearance of protein levels at 6 h suggests that the changes found at 3 h may be reversible. The enzyme complex may renature or undergo reversed modification or reversible inhibition, or rapid synthesis (COX subunit I is made intramitochondrially) (Capaldi, 1990; Bolli *et al.,* 1995). Moreover, we found that COX subunit I protein aggregates, forming large multimeric complexes after HI. This change in COX may signify increased covalent protein–protein interactions due to sulfhydryl oxidation and perturbations in redox state and is possibly related to the depletion of GSH levels early after HI. Loss of protein thiols by oxidation can lead to abnormalities in mitochondrial protein function and mitochondrial membrane permeability (Ravindranath and Reed, 1990).

Mitochondrial failure after HI is also suspected because cytochrome c is depleted. Cytochrome c has been identified as an apoptotic protease activating factor. Its regulated release from mitochondria and interactions with other proteins participate in the mechanisms for programmed cell death (Li *et al.*, 1997). However, cytochrome c translocation and cytoplasmic accumulation alone are insufficient for neuronal apoptosis (Deshmukh and Johnson, 1998). Cytochrome c accumulation in CNS tissue soluble fractions is presumed to be a marker for neuronal apoptosis after ischemia (Fujimura *et al.*, 1998). However, in the presence of widespread structural and biochemical abnormalities in striatum after HI, release of cytochrome c from mitochondria after ischemia is unlikely to be a physiologically regulated event, nor is it likely that downstream effector mechanisms for apoptosis are operative in striatal neurons after ischemia. Indeed, we found that cytochrome c is depleted in striatal cytosolic extracts after HI. This abnormality is consistent with mitochondrial failure, impaired oxidative phosphorylation, and neuronal necrosis. Importantly, the loss of cytochrome c may contribute to the oxidative stress by mobilizing iron from heme groups during its proteolysis. Overall, these changes point toward acute mitochondrial dysfunction contributing to the pathobiology of neuronal necrosis in the newborn striatum after HI.

Tubulin Is a Target of Oxidative Stress after HI in Newborn Brain

We found that tubulin is a target of extensive tyrosine nitration after HI. Tubulin is the major cytoskeletal protein in neurons that forms the microtubule network (Brady, 1991). Microtubules serve as tracks for the movement of mitochondria and lysosomes, and they are important in establishing and maintaining the shape, structural integrity, locations, and functions of the Golgi apparatus, ER, and mitochondria (Brady, 1991). Amino acid modification of tubulin by posttranslational nitrotyrosination causes microtubule dysfunction by a nitric oxide-dependent mechanism (Eiserich *et al.*, 1999), consistent with our finding that tubulin is a target of peroxynitrite. It is possible that nitrotyrosination of tubulin and microtubule dysfunction participate in the mechanisms for the organelle abnormalities that occur in striatal neurons after HI, including dispersion of the Golgi apparatus, dilation of the ER, accumulation and swelling of mitochondria, and destabilization of lysosomes. When cells are exposed to agents that perturb microtubule assembly,

the ER network redistributes, contracts, and then collapses towards the nucleus (Lee and Chen, 1988), and the Golgi apparatus fragments into small vesicles that are dispersed throughout the cytoplasm (Donaldson *et al.*, 1990; Pavelka and Ellinger, 1993). These changes are similar to those that we have found in striatal neurons after HI. Thus, oxidative damage to tubulin and microtubule dysfunction may provide a molecular mechanism for some of the subcellular abnormalities occurring in striatal neurons after HI.

Oxidative Stress Is a Mechanism for Striatal Neuron Necrosis in Newborns after HI

We found evidence for an early loss of antioxidant capacity and oxidative damage to proteins and nucleic acids. By 3 to 6 h after HI, GSH was depleted, peroxynitrite damaged membrane proteins (specifically Golgi-associated proteins), and nitration of tubulin increased. In addition, nucleic acids were damaged by hydroxyl radicals. Peroxynitrite oxidation of nucleosides may not be a major pathway (Uppu *et al.*, 1996). A more likely pathway for nucleoside oxidation by hydroxyl radical is from the transitional metal (iron)-catalyzed, Haber-Weiss- and Fenton-type reactions that use superoxide and H_2O_2 as substrates, respectively, thereby producing hydroxyl radicals (Boveris and Cadenas, 1997). Interestingly, redox-active heme and nonheme iron from cytochrome c breakdown may support hydroxyl radical formation in the cytosol and RNA oxidation.

The mitochondrial alterations that occur in dying striatal neurons after HI support our conclusion that oxidative stress participates in the mechanisms of neuronal necrosis. Mitochondria accumulated in the cell bodies of neurons by 6 h of reperfusion, and mitochondrial function was increased transiently at 6 h after reperfusion. Mitochondrial accumulation could be due to interruption of mitochondrial trafficking because of tubulin/microtubule perturbations or to dendritic attrition because dendrites are damaged early after ischemia (Kitagawa *et al.*, 1989; Yamamoto *et al.*, 1990). Alternatively, mitochondrial accumulation may be due to cell body shrinkage after the initial swelling stage during 3 h recovery. A possible consequence of this accumulation is that mitochondria are in closer proximity to each other and to the nucleus and other organelles within the perikaryon. The mitochondrial electron-transfer chain is a primary generator of superoxide and peroxide, and damaged mitochondria are believed to produce even more superoxide ion (Boveris and Cadenas, 1997). Excessive

generation of superoxide occurs in piglet brain during asphyxia-reventilation (Pourcyrous *et al.*, 1993). In addition, depletion of GSH has been shown to lead to mitochondrial swelling and lysis and then cellular necrosis (Meister, 1995), consistent with the abnormalities we observed by EM. We also found that depletion of GSH precedes mitochondrial swelling and lysis and loss of cytochrome c. Thus, mitochondrial accumulation and activation may be important mechanistically because peroxynitrite and hydroxyl radicals are highly reactive and short-lived (Boveris and Cadenas, 1997) and, therefore, need to be generated at sites near target organelles and macromolecules.

Conclusion

In a piglet model of HI brain damage in newborns, striatal neuron necrosis evolves rapidly. It is likely that widespread oxidative damage to organelles and macromolecules is a primary mechanism for striatal neurodegeneration. Based on the observations made here with this piglet model, neuroprotection strategies for the amelioration or prevention of the acute striatal damage in HI newborns should be implemented immediately after HI, before depletion of glutathione, oxidative stress, and subcellular injury. This information is important for the management of basal ganglia damage and neurological abnormalities in HI human newborns.

ACKNOWLEDGMENTS

REFERENCES

Al-Abdulla, N. A., Portera-Cailliau, C., & Martin, L. J. (1998) Occipital cortex ablation in adult rat causes retrograde neuronal death in the lateral geniculate nucleus that resembles apoptosis. *Neuroscience* **86**, 191–209.

Al-Abdulla, N. A., & Martin, L. J. (1998) Apoptosis of retrogradely degenerating neurons occurs in association with the accumulation of perikaryal mitochondria and oxidative damage to the nucleus. *Am. J. Pathol.* **153**, 447–456.

Araki, T., Kato, H., Inoue, T., & Kogure, K. (1990) Regional impairment of protein synthesis following brief cerebral ischemia in the gerbil. *Acta Neuropathol.* **79**, 501–505.

Beckman, J. S., Chen, J., Ischiropoulos, H., & Conger, K. A. (1992) Inhibition of nitric oxide synthesis and cerebral neuroprotection. In: *Pharmacology of Cerebral Ischemia* (J. Krieglstein and H. Ober-

pichler-Schwenk, Eds.), pp. 383–394. Wissenschaftliche Verlagsgesellschaft, Stuttgart.

Beilharz, E. J., Williams, C. E., Dragunow, M., Sirimanne, E. S., & Gluckman, P. D. (1995) Mechanisms of delayed cell death following hypoxic-ischemic injury in the immature rat: Evidence for apoptosis during selective neuronal loss. *Mol. Brain Res.* **29**, 1–14.

Bloom, G. S., & Brashear, T. A. (1989) A novel 58-kDa protein associates with the Golgi apparatus and microtubules. *J. Biol. Chem.* **264**, 16083–16092.

Bolaños, J. P., Heales, S. J. R., Land, J. M., & Clark, J. B. (1995) Effect of peroxynitrite on the mitochondrial respiratory chain: Differential susceptibility of neurones and astrocytes in primary culture. *J. Neurochem.* **64**, 1965–172.

Bolli, R., Nalecz, K. A., & Azzi, A. (1985) The interconversion between monomeric and dimeric bovine heart cytochrome c oxidase. *Biochime* **67**, 119–128.

Boveris, A., & Cadenas, E. (1997) Cellular sources and steady-state levels of reactive oxygen species. In: *Oxygen, Gene Expression, and Cellular Function* (L. Biadasz Clerch & D. J. Massaro, Eds.), pp. 1–25. Marcel Dekker, New York.

Brady, S. T. (1991) Molecular motors in the nervous system. *Neuron* **7**, 521–533.

Brambrink, A. M., Martin, L. J., Hanley, D. F., Becker, K. Y., Koehler, R. C., & Traystman, R. J. (1999) Effects of the AMPA receptor antagonist NBQX on the outcome of newborn pigs after asphyxic cardiac arrest. *J. Cereb. Blood Flow Metab.* **19**, 927–938.

Capaldi, R. A. (1990) Structure and function of cytochrome c oxidase. *Annu. Rev. Biochem.* **59**, 569–596.

Cheng, Y., Deshmukh, M., D-Costa, A., Demare, J. A., Gidday, J. M., Shah, A., Sun, Y., Jacquin, M. F., Johnson, Jr., E. M., & Holtzman, D. M. (1998) Caspase inhibitor affords neuroprotection with delayed administration in a rat model of neonatal hypoxic-ischemic brain injury. *J. Clin. Invest.* **101**, 1992–1999.

Choi, D. W. (1992) Excitotoxic cell death. *J. Neurobiol.* **23**, 1261–1276.

Collins, R. J., Harmon, B. V., Gobé, V. C., & Kerr, J. F. R. (1992) Internucleosomal DNA clevage should not be the sole criterion for identifying apoptosis. *Int. J. Radiat. Biol.* **61**, 451–453.

Corbett, E. F., Oikawa, K., Francois, P., Tessier, D. C., Kay, C., Bergeron, J. J. M., Thomas, D. Y., Krause, K.-H., & Michalak, M. (1999) Ca^{2+} regulation of interactions between endoplasmic reticulum chaperones. *J. Biol. Chem.* **274**, 6203–6211.

Davies, K. J. (1987) Protein damage and degradation by oxygen radicals. I. General aspects. *J. Biol. Chem.* **262**, 9895–9901.

Deshmukh, M., & Johnson, Jr., E. M. (1998) Evidence of a novel event during neuronal death: Development of competence-to-die in response to cytoplasmic cytochrome c. *Neuron* **21**, 695–705.

Dobbing, J., & Sands, J. (1979) Comparative aspects of the brain growth spurt. *Early Hum. Dev.* **3**, 79–83.

Donaldson, J. G., Lippincott-Schwartz, J., Bloom, G. S., Kreis, T. E., & Klausner, R. D. (1990) Dissociation of a 110-kD peripheral membrane protein from the Golgi apparatus is an early event in brefeldin A action. *J. Cell Biol.* **111**, 2295–2306.

Eiserich, J. P., Estévez, A. G., Bamberg, T. V., Ye, Y. Z., Chumley, P. H., Beckman, J. S., & Freeman, B. A. (1999) Microtubule dysfunction by posttranslational nitrotyrosination of α-tubulin: A nitric oxide-dependent mechanism of cellular injury. *Proc. Natl. Acad. Sci. USA* **96**, 635–6370.

Farber, J. L., Chien, K. R., & Mittnacht, Jr., S. (1981) The pathogenesis of irreversible cell injury in ischemia. *Am. J. Pathol.* **102**, 271–281.

Ford, L. M., Sanberg, P. R., Norman, A. B., & Fogelson, M. H. (1989) MK-801 prevents hippocampal neurodegeneration in neonatal hypoxic-ischemic rats. *Arch. Neurol.* **46**, 1090–1096.

Frederiks, W. M., & Marx, F. (1989). Changes in acid phosphatase activity in rat liver after ischemia. *Histochemistry* **93**, 161–166.

Fujimura, M., Morita-Fujimura, Y., Murkami, K., Kawase, M., & Chan, P. K. (1998) Cytosolic redistribution of cytochrome c after transient focal cerebral ischemia in rats. *J. Cereb. Blood Flow Metab.* **18**, 1239–1247.

Furuta, A., Rothstein, J. D., & Martin, L. J. (1997) Glutamate transporter protein subtypes are expressed differentially during rat CNS development. *J. Neurosci.* **17**, 8363–8375.

Furuta, A., & Martin, L. J. (1999) Laminar segregation of the cortical plate during corticogenesis is accompanied by changes in glutamate receptor expression. *J. Neurobiol.* **39**, 67–80.

Grasl-Kraupp, B., Ruttkay-Nedecky, B., Koudelka, H., Bukowska, K., Bursch, W., & Schulte-Hermann, R. (1995) In situ detection of fragmented DNA (TUNEL assay) fails to discriminate among apoptosis, necrosis, and autolytic cell death: A cautionary note. *FASEB J.* **21**, 1465–1468.

Gwag, B. J., Koh, J. Y., DeMaro, J. A., Ying, H. S., Jacquin, M., & Choi, D. W. (1997) Slowly triggered excitotoxicity occurs by necrosis in cortical cultures. *Neuroscience* **77**, 393–401.

Halliwell, B., & Gutteridge, J. M. C. (1986) Oxygen free radicals and iron in relation to biology and medicine: some problems and concepts. *Arch. Biochem. Biophys.* **246**, 501–514.

Hill, I. E., MacManus, J. P., Rasquinha, I., & Tuor, U. I. (1995) DNA fragmentation indicative of apoptosis following unilateral cerebral hypoxia-ischemia in the neonatal rat. *Brain Res.* **676**, 398–403.

Ishimaru, M. J., Ikonomidou, C., Tenkova, T. I., Der, T. C., Dikranian, K., Sesma, M. A., & Olney, J. W. (1990) Distinguishing excitotoxic from apoptotic neurodegeneration in the developing rat brain. *J. Comp. Neurol.* **408**, 461–476.

Jiang, X.-M., Fitzgerald, M., Grant, C. M., & Hogg, P. J. (1999) Redox control of exofacial protein thiols/disulfides by protein disulfide isomerase. *J. Biol. Chem.* **274**, 2416–2423.

Johnston, M. V. (1998) Selective vulnerability in the neonatal brain. *Ann. Neurol.* **44**, 155–156.

Kerr, J. F. R., Wyllie, A. H., & Currie, A. R. (1972) Apoptosis: A basic biological phenomenon with wide-ranging implications in tissue kinetics. *Br. J. Cancer* **26**, 239–257.

Kirino, T., Tamura, A., & Sano, K. (1984) Delayed neuronal death in rat hippocampus following transient forebrain ischemia. *Acta Neuropathol.* **64**, 139–147.

Kitagawa, K., Matsumoto, M., Niinobe, M., Mikoshiba, K., Hata, R., Ueda, H., Handa, N., Fukunaga, R., Isaka, Y., Kimura, K., & Kamada, T. (1989) Microtubule-associated protein 2 as a sensitive marker for cerebral ischemic damage. Immunohistochemical investigation of dendritic damage. *Neuroscience* **31**, 401–411.

Laiho, K. U., & Trump, B. J. (1975) Studies on the pathogenesis of cell injury. Effects of inhibitors of metabolism and membrane function on the mitochondria of Ehrlich ascites tumor cells. *Lab. Invest.* **32**, 163–182.

LeBlanc, M. H., Vig, V., Smith, B., Parker, C. C., Evans, O. B., & Smith, E. E. (1991) MK-801 does not protect against hypoxic-ischemic brain injury in piglets. *Stroke* **22**, 1270–1275.

LeBlanc, M. H., Li, X. Q., Huang, M., Patel, D. M., & Smith, E. E. (1995) AMPA antagonist LY293558 does not affect the severity of hypoxic-ischemic injury in newborn pigs. *Stroke* **26**, 1908–1915.

Lee, C., & Chen, L. B. (1988) Dynamic behavior of endoplasmic reticulum in living cells. *Cell* **54**, 37–46.

Li, P., Nijhawan, D., Budihardjo, I., Srinivasula, S. M., Ahmad, M., Alnemri, E. S., & Wang, X. (1997) Cytochrome c and dATP-dependent formation of Apaf-1/caspase-9 complex initiates an apoptotic protease cascade. *Cell* **91**, 479–489.

Lockshin, R. A., & Zakeri, A. (1994) Programmed cell death: Early changes in metamorphosing cells. *Biochem. Cell Biol.* **72**, 589–596.

Maller, A. I., Hankins, L. L., Yeakley, J. W., & Butler, I. J. (1998) Rolandic type cerebral palsy in children as a pattern of hypoxic-ischemic injury in the full-term neonate. *J. Child Neurol.* **13**, 313–321.

Martin, L. J., Doebler, J. A., & Anthony, A. (1986) Cytophotometric analysis of neuronal chromatin and RNA changes in oxotremorine-treated rats. *Proc. Soc. Exp. Biol. Med.* **181**, 41–48.

Martin, L. J., Brambrink, A., Koehler, R. C., & Traystman, R. J. (1997a) Neonatal asphyxic brain injury is neural system preferential and targets sensory-motor networks. In: *Fetal and Neonatal Brain Injury: Mechanisms, Management, and the Risks of Practice* (D. K. Stevenson and P. Sunshine, Eds.), pp. 374–399. Oxford Univ. Press, New York.

Martin, L. J., Brambrink, A., Koehler, R. C., & Traystman, R. J. (1997b) Primary sensory and forebrain motor systems in the newborn brain are preferentially damaged by hypoxia-ischemia. *J. Comp. Neurol.* **377**, 262–285.

Martin, L. J., Brambrink, A. M., Lehmann, C., Portera-Cailliau, C., Koehler, R., Rothstein, J., & Traystman, R. J. (1997c) Hypoxia-ischemia causes abnormalities in glutamate transporters and death of astroglia and neurons in newborn striatum. *Ann. Neurol.* **42**, 335–348.

Martin, L. J., Al-Abdulla, N. A., Brambrink, A. M., Kirsch, J. R., Sieber, F. E., & Portera-Cailliau, C. (1998a) Neurodegeneration in excitotoxicity, global cerebral ischemia, and target deprivation: A perspective on the contributions of apoptosis and necrosis. *Brain Res. Bull.* **46**, 281–309.

Martin, L. J., Furuta, A., & Blackstone, C. D. (1998b) AMPA receptor protein in developing rat brain: Glutamate receptor-1 expression and localization change at regional, cellular, and subcellular levels with maturation. *Neuroscience* **83**, 917–928.

Martin, L. J., Kaiser, A., & Price, A. C. (1999) Motor neuron degeneration after sciatic nerve avulsion in adult rat evolves with oxidative stress and is apoptosis. *J. Neurobiol.* **40**, 185–201.

Martin, L. J., Sieber, F. E., & Traystman, R. J. (2000) Apoptosis and necrosis occur in separate neuronal populations in hippocampus and cerebellum after ischemia and are associated with differential alterations in metabotropic glutamate receptor signaling pathways. *J. Cereb. Blood Flow Metab.* **20**, 153–167.

McCord, J. M. (1985) Oxygen-derived free radicals in postischemic tissue injury. *N. Engl. J. Med.* **312**, 159–163.

Meister, A. (1995) Mitochondrial changes associated with glutathione deficiency. *Biochimica et Biophysica Acta* **1271**, 35–42.

McDonald, J. W., Silverstein, F. S., & Johnston, M. V. (1987) MK-801 protects the neonatal brain from hypoxic-ischemic damage. *Eur. J. Phramacol.* **140**, 359–361.

Mizui, T., Kinouchi, H., & Chan, P. H. (1992) Depletion of brain glutathione by buthionine sulfoximine enhances cerebral ischemic injury in rats. *Am. J. Physiol.* **262**, H313–H317.

Munro, S., & Pelham, H. R. (1987) A C-terminal signal prevents secretion of lumenal ER proteins. *Cell* **48**, 899–907.

Natale, J. E., Brambrink, A. M., Traystman, R. J., & Martin, L. J. (1999) Hypoxia-ischemia in newborn piglets produces early defects in striatal high-affinity glutamate uptake. *Pediatric Res.* **45**, 345A.

Northington, F. J., Traystman, R. J., Koehler, R. C., Rothstein, J. R., & Martin, L. J. (1998) Regional and cellular expression of glial (GLT1) and neuronal EAAC1 glutamate transporter proteins in ovine fetal brain. *Neuroscience* **85**, 1183–1194.

Olney, J. W. (1994) Excitatory transmitter neurotoxicity. *Neurobiol. Aging* **15**, 259–260.

Pavelka, M., & Ellinger, A. (1993) Early and late transformations occurring at organelles of the Golgi area under the influence of brefeldin A: An ultrastructural and lectin cytochemical study. *J. Histochem. Cytochem.* **41**, 1031–1042.

Petito, C. K., & Pulsinelli, W. A. (1984) Sequential development of reversible and irreversible neuronal damage following cerebral ischemia. *J. Neuropathol. Exp. Neurol.* **43**, 141–153.

Portera-Cailliau, C., Price, D. L., & Martin, L. J. (1997a) Non-NMDA and NMDA receptor-mediated excitotoxic neuronal deaths in adult brain are morphologically distinct: Further evidence for an apoptosis-necrosis continuum. *J. Comp. Neurol.* **378**, 88–104.

Portera-Cailliau, C., Price, D. L., & Martin, L. J. (1997b) Excitotoxic neuronal death in the immature brain is an apoptosis-necrosis morphological continuum. *J. Comp. Neurol.* **378**, 70–87.

Pourcyrous, M., Leffler, C. W., Bada, H. S., Korones, S. B., & Busija, D. W. (1993) Brain superoxide anion generation in asphyxiated piglets and the effect of indomethacin at therapeutic dose. *Pediatric Res.* **34**, 366–36.

Rafols, J. A., Daya, A. M., O'Neil, B. J., Krause, G. S., Neumar, R. W., & White, B. C. (1995) Global brain ischemia and reperfusion: Golgi apparatus ultrastructure in neurons selectively vulnerable to death. *Acta Neuropathol.* **90**, 17–30.

Ravindranath, V., & Reed, D. J. (1990) Glutathione depletion and formation of glutathione-protein mixed disulfide following exposure of brain mitochondria to oxidative stress. *Biochem. Biophys. Res Comm.* **169**, 1-75–1079.

Roland, E. H., Poskitt, K., Rodriguez, E., Lupton, B. A., & Hill, A. (1998) Perinatal hypoxic-ischemic thalamic injury: Clinical features and neuroimaging. *Ann. Neurol.* **44**, 161–166.

Simons, K., & Zerial, M. (1993) Rab proteins and road maps for intracellular transport. *Neuron* **11**, 789–799.

Strong, M. J., Sopper, M. M., Crow, J. P., Strong, W. L., & Beckman, J. S. (1998) Nitration of the low molecular weight neurofilament is equivalent in sporadic amyotrophic lateral sclerosis and control cervical spinal cord. *Biochem. Biophys. Res. Commun.* **248**, 157–164.

Thilmann, R., Xie, Y., Kleihues, P., & Kiessling, M. (1986) Persistent inhibition of protein synthesis precedes delayed neuronal death in postischemic gerbil hippocampus. *Acta Neuropathol.* **71**, 88–93.

Tietze, F. (1969) Enzymic method for quantitative determination of nanogram amounts of total and oxidized glutathione: Applications to mammalian blood and other tissues. *Anal. Biochem.* **27**, 502–522.

Uppu, R. M., Cueto, R., Squadrito, G. L., Salgo, M. G., & Pryor, W. A. (1996) Competitive reactions of peroxynitrite with 2'-deoxyguanosine and 7,8-dihydro-8-oxo-2'-deoxyguanosine (8-oxodG): Relevance to the formation of 8-oxodG in DNA exposed to peroxynitrite. *Free Rad. Biol. Med.* **21**, 407–411.

Van Noorden, C. J. F. (1991) Assessment of lysosomal function by quantitative histochemical and cytochemical methods. *Histochem. J.* **23**, 429–435.

Volpe, J. J. (1995) *Neurology of the Newborn.* Saunders, Philadelphia.

Wang, C. C. (1998) Protein disulfide isomerase assists protein folding as both an isomerase and a chaperone. *Ann. N.Y. Acad. Sci.* **864**, 9–13.

Wharton, D. C., & Tzagoloff, A. (1967) Cytochrome oxidase from beef heart mitochondria. *Methods Enzymol.* **10**, 245–250.

Wolff, S. P., & Dean, R. T. (1986) Fragmentation of proteins by free radicals and its effect on their susceptibility to enzymic hydrolysis. *Biochem. J.* **234**, 399–403.

Wong-Riley, M. T. T. (1979) Changes in the visual system of monocularly sutured or enucleated cats demonstrable with cytochrome oxidase histochemistry. *Brain Res.* **171**, 11–28.

Yamamoto, K., Hayakawa, T., Mogami, H., Akai, F., & Yanagihara, T. (1990) Ultrastructural investigation of the CA1 region of the hippocampus after transient cerebral ischemia in gerbils. *Acta Neuropathol.* **80**, 487–492.

Injury-Induced Apoptosis of Neurons in Adult Brain is Mediated by p53-Dependent and p53-Independent Pathways and Requires Bax

Lee J. Martin[1,2], Adeel Kaiser[1], Jonathan W. Yu[1], JoAnne E. Natale[3], and Nael A. Al-Abdulla[1,4]

Departments of [1]Pathology, Division of Neuropathology, [2]Neuroscience, and [3]Anesthesiology/Critical Care Medicine, and [4]Wilmer Eye Institute, Johns Hopkins University School of Medicine, Baltimore, Maryland, U.S.A.

Abbreviated title: Mechanisms of neuronal apoptosis in brain

Number of: text pages (30), figures (7), tables (0)
Number of words: abstract (214), introduction (486), discussion (1478)

Correspondence and reprint requests to:
Lee J. Martin, Ph.D.
Johns Hopkins University School of Medicine
Department of Pathology, 558 Ross Building
720 Rutland Avenue
Baltimore, Maryland 21205-2196
Telephone: 410-502-5170
Fax: 410-955-9777
Email: lmartin@jhmi.edu

ABSTRACT

The mechanisms for injury-induced neuronal apoptosis within the CNS are not understood. We used a rodent model of cortical injury to induce retrograde neuronal apoptosis in thalamus. In this animal model, unilateral ablation of the occipital cortex in rat and mouse results in unequivocal neuronal apoptosis in the dorsal lateral geniculate nucleus (LGN) by 7 days postlesion. We tested the hypothesis that p53 and Bax regulate this retrograde neuronal apoptosis. We found using immunocytochemistry that p53 accumulates in nuclei of neurons destined to undergo apoptosis. By immunoblotting, p53 levels increase (~150% of control) in the LGN by 5 days after occipital cortex ablation. In nuclear-enriched fractions, p53 is activated (~3-fold) in the ipsilateral LGN at 5 days postlesion, as shown by DNA binding assay. The levels of procaspase-3 increase at 4 days postlesion, and caspase-3 is activated prominently at 5 days postlesion. To identify if neuronal apoptosis in the adult brain is dependent on p53 and Bax, cortical ablations were done on null mice. In $p53^{-/-}$ mice, the severity of neuronal apoptosis is significantly attenuated (~34%), and in $bax^{-/-}$ mice neuronal apoptosis in the dorsal LGN is blocked completely. We conclude that neuronal apoptosis in the adult thalamus after cortical injury is mediated by both p53-dependent and p53-independent cell death pathways and requires Bax.

Key words: Alzheimer's disease, amyotrophic lateral sclerosis, DNA damage, programmed cell death, head trauma, thalamus

Apoptosis is an organized form of cell death that is mediated by active, intrinsic mechanisms (Arends et al., 1990; Kerr and Harmon, 1991). Apoptosis in the nervous system is important for a variety of reasons. Apoptotic death of neurons and non-neuronal cells occurs normally in the developing nervous system (Glücksmann, 1951; Oppenheim, 1991), and defects in apoptosis can cause cerebral malformations (Kuida et al., 1996; Hakem et al., 1998). Apoptosis might also participate in the pathogenesis of abnormal neuronal death in chronic and acute neurodegenerative disorders. For example, the genes for neuronal apoptosis inhibitory protein and survival motor neuron protein are either deleted partially or are mutant in some children with pediatric forms of motor neuron disease such as spinal muscular atrophy (Roy et al., 1995; Lefebvre et al., 1995). The neuronal and glial degeneration in age-related neurological disorders such as Alzheimer's disease and amyotrophic lateral sclerosis also may be forms of apoptosis (Anderson et al., 1996; Kitamura et al., 1999; Martin et al., 2000a). In acute neurodegenerative disorders, apoptosis of neurons and nonneuronal cells may contribute to the neuropathology in animal models of cerebral ischemia (MacManus et al., 1997; Martin et al., 1998; Martin et al., 2000b) and spinal cord trauma (Liu et al., 1997). Therefore, understanding the molecular regulation of apoptosis is relevant to not only nervous system development but also neurodegeneration in pathological conditions.

Apoptosis can be induced by the oncosuppressor protein p53 (Vogelstein and Kinzler, 1992; Levine, 1997). This DNA binding protein functions in genome surveillance, DNA repair, and as a transcription factor. p53 commits to death cells that have sustained DNA damage from reactive oxygen species (ROS) and other genotoxic agents. The mechanisms by which p53 induces apoptosis are largely unknown. p53 is a direct transcriptional activator of the *bax* gene (Miyashita and Reed,

1995) and a transcriptional repressor of the *Bcl-2* gene (Miyashita et al., 1994); thus, apoptosis is thought to be executed by molecular cascades involving expression or activation of p53, Bax, and caspases (Polyak et al., 1997).

The understanding of the mechanisms for apoptosis in nervous system cells is less advanced compared to cells of non-nervous tissue origin. Seminal studies have shown recently that Bax is critical for apoptosis of neurons in cell culture (Deckwerth et al., 1996; Miller et al., 1997; Putcha et al., 1999) and is required for neuronal apoptosis during development (Deckwerth et al., 1996). However, the mechanisms for injury-induced neuronal apoptosis within the CNS are much less understood as compared to cell culture and developmental paradigms. We have developed and characterized recently an injury model of unequivocal neuronal apoptosis within the rodent brain. In this model, occipital cortex ablation reliably causes neuronal apoptosis in the dorsal lateral geniculate nucleus (dLGN) of thalamus (Al-Abdulla et al., 1998; Al-Abdulla and Martin, 1998). We used this model to test the hypothesis that injury-induced apoptosis of neurons in the adult brain is controlled by p53, Bax, and caspases.

MATERIALS AND METHODS

Animals

Adult male rats and mice were used for these experiments. Sprague-Dawley rats (Charles River, Wilmington, MA) weighed ~150-200 g. Mice (Jackson Labs) were genetically deficient in the *bax* gene (bax $^{-/-}$, n = 16) or the *p53* gene (p53 $^{-/-}$, n = 10) and were 6-8 weeks of age when used. C57/B6 mice (n = 20) served as controls for bax-null mice, and 129/SV mice (n = 10) served as

controls for p53-null mice. The animals were housed in a colony room with a 12 h:12 h-light/dark cycle and *ad libitum* access to food and water. The Animal Care and Use Committee of the Johns Hopkins University School of Medicine approved the animal protocol.

Model of neuronal apoptosis *in vivo*

A unilateral occipital cortex ablation served as the model for producing axotomy and target deprivation of neurons and subsequent apoptosis selectively in the dLGN (Al-Abdulla et al., 1998; Al-Abdulla and Martin, 1998). Rats and mice were anesthetized with a mixture of enflurane:oxygen:nitrous oxide (1:33:66) and placed in a stereotaxic apparatus. After a midline scalp incision, a craniotomy was made and the dura was incised using a sharp 22-gauge needle. The cortex underlying the craniotomy was then aspirated using a blunt-tipped 22-gauge needle connected to a vacuum line, without damaging the surrounding venous sinuses and the underlying hippocampus (Fig. 1, top). Postlesion survival times after occipital cortex ablation were 1, 2, 3, 4, 5, 6, 7, and 14 days.

Retrograde labeling of corticopetal projection neurons in mouse dLGN

The retrograde tracer Fluorogold (FG, Fluorochrome, Inc., Englewood, CO) was injected into mouse visual cortex to identify corticopetal projection neurons in the dLGN. An occipital craniotomy was performed, and 100 nl of 5% FG in deionized-distilled H_2O was injected slowly into the cortex over 10 minutes using a 25-gauge 0.5 ml blunt-tip syringe (Hamilton, Reno, NV). Three days later, mice (n = 5) were anesthetized and underwent an occipital cortex ablation as

described above. FG-injected mice with occipital cortex ablations recovered for 4 days before being perfused for light microscopic analysis. Identification of corticopetal projection neurons was done by direct fluorescence and by immunodetection of FG using a polyclonal antibody (diluted 1:10,000; Chemicon, Inc., Temecula, CA) as described (Al-Abdulla et al., 1998; Martin et al., 1999).

Neuron counting

At 7 and 14 days after occipital cortex ablation, Bax-deficient mice, p53-deficient mice, and respective control mice were anesthetized with an overdose of chloral hydrate and perfused intra-cardially with ice-cold phosphate buffer-saline (PBS, 100 mM, pH 7.4), delivered by a perfusion pump, followed by 4% paraformaldehyde in ice-cold PBS. After perfusion-fixation, brains were allowed to remain *in situ* for 1 hour before they were removed from the skull. After the brains were removed, they were cryoprotected in 20% glycerol-PBS, uniformly blocked, and frozen under pulverized dry ice. Transverse, symmetrical sections (40 μm) through the thalamus were cut using a sliding microtome. Sections (every 5th) from each mouse brain were mounted on glass slides and stained with cresyl violet for neuronal counting.

The counting of neurons in the ipsilateral and contralateral dLGN was done at 1000x magnification as described (Al-Abdulla et al., 1998). Three brain sections from each mouse were used to count neurons without apoptotic structural changes (using strict morphological criteria, see Fig. 1 top, a). These criteria included a round, open, pale nucleus (not condensed and darkly stained), granular Nissl staining of the cytoplasm, and a diameter of ~20-25 μm. With these criteria,

astrocytes, oligodendrocytes, and microglia were excluded from the counts. The total number of neurons was counted in three, non-overlapping fields in the dLGN of ipsilateral and contralateral thalamus. Neuronal counts were used to determine group means and variances and comparisons among groups were performed using a one-way analysis of variance and a Student's *t*-test.

Localization of p53 in dLGN after occipital cortex ablation

We evaluated whether p53 is induced in dLGN neurons after cortical damage. Rats at 1, 3, 4, 5, 6, and 7 days postlesion (n= 4 to 6 per time point) and mice at 5, 6, and 7 days postlesion (n= 4-10 per time point) were used for the immunocytochemical detection of p53. These animals were anesthetized and perfusion-fixed, and the brains were prepared as described above. p53 was detected in rat and mouse brain sections using a standard immunoperoxidase method with diaminobenzidine as chromogen and cresyl violet counterstaining. Two different commercial antibodies were used: BMG-1B1, 1 µg IgG/ml (Boehringer-Mannheim) and Pab240, 1 µg IgG/ml (Santa Cruz). The specificities of these antibodies were demonstrated by immunoblotting (see below). These antibodies are highly specific for detecting a major protein band at ~53 kD that has the same mobility as purified p53. Furthermore, the immunoreactivity detected with this antibody is exclusively nuclear and is found only in subsets of cells. Negative controls were sections from p53-null mice and other sections with primary or secondary antibody omitted.

Immunoblotting for p53 and caspase-3

Rats were used to measure p53 and caspase-3 protein levels during the progression of

neuronal apoptosis. Samples of LGN were collected for immunoblotting at 1, 4, 5, and 6 days after

occipital cortex ablation (n = 9-17 rats per time point). Animals were deeply anesthetized with

chloral hydrate, decapitated, and the brain was removed quickly and placed on ice. Under a

stereomicroscope, the cerebral cortex was reflected to visualize the dorsal thalamus. The LGN is

readily discernible by surface landmarks. Using iridectomy scissors, the LGN from ipsilateral

(target deprived) and contralateral (control) thalamus was microdissected from each rat and frozen

quickly on dry ice. LGN samples from target-deprived and control sides were pooled for each time

point. We verified the accuracy of the LGN microdissection by removing LGN samples and then

immersion-fixing the brainstems in 4% paraformaldehyde. Afterwards the brainstems were

cryoprotected, cut, and rostral brainstem sections were stained with cresyl violet and viewed

microscopically (data not shown).

LGN samples were homogenized in cold 20 mM Tris HCl (pH 7.4) containing 10% (wt/vol)

sucrose, 20 U/ml aprotinin (Trasylol), 20 μg/ml leupeptin, 20 μg/ml antipain, 20 μg/ml pepstatin A,

20 μg/ml chymostatin, 0.1 mM phenylmethylsulfonyl fluoride, 10 mM benzamidine, 1 mM

EDTA, and 5 mM EGTA. Crude homogenates were centrifuged at 1,000 g_{av} for 10 minutes (4C),

and the resulting pellet consisting of the nuclear-enriched fraction was resuspended in

homogenization buffer (without sucrose) supplemented with 20% (wt/vol) glycerol. The supernatant

was then centrifuged at 54,000 g_{av} for 20 minutes (4C) to yield soluble and membrane-fractions.

This subcellular fractionation protocol has been verified (Martin, 2000). Protein concentrations in

nuclear and soluble fractions were measured by a Bio-Rad protein assay with bovine serum albumin

as a standard.

Immunoreactivities for p53 and caspase-3 (proenzyme and active forms) were measured in the LGN after occipital cortex ablation. Nuclear-enriched and soluble cell fractions from ipsilateral and contralateral LGN samples were subjected to 15% sodium dodecyl sulfate polyacrylamide gel electrophoresis (SDS-PAGE) and transferred to nitrocellulose membrane by electroelution as described (Martin, 1999). The positive control for p53 was purified *E. coli*-expressed human p53 (Oncogene Research Products). The positive control for active caspase was purified active caspase-3 (BioVision Research Products). The reliability of sample loading and electroblotting in each experiment was evaluated by staining nitrocellulose membranes with Ponceau S before immunoblotting. Blots were blocked with 2.5% nonfat dry milk with 0.1% Tween 20 in 50 mM Tris-buffered saline (pH 7.4), then incubated overnight at 4C with antibody. Two different p53 antibodies were purchased commercially and were a sheep anti-human recombinant p53 (BMG-1B1, Boehringer Mannheim) and a mouse monoclonal antibody to p53-β glactosidase fusion protein containing the p53 domain corresponding to amino acids 156-214 (Pab240, Santa Cruz). The nuclear-enrichment of the LGN subcellular fractions was verified by the presence of NeuN (Martin, 2000; data not shown), as detected with a mouse monoclonal antibody (Chemicon). Caspase-3 was detected with a rabbit polyclonal antibody that binds both the proenzyme and the active subunits (Santa Cruz). The antibodies were used at the following concentrations to visualize immunoreactive proteins within the linear range: 2-3 μg IgG/ml (BMG-1B1), 1-2 μg IgG/ml (Pab240), 0.2-0.4 μg IgG/ml (NeuN), and 0.4 μg IgG/ml (caspase-3). After the primary antibody incubation, blots were washed and incubated with horseradish peroxidase-conjugated secondary antibody (0.2 μg/ml), developed with enhanced chemiluminescence (Pierce), and exposed to x-ray film. The blots were

then reprobed with a monoclonal antibody to synaptophysin (Boehringer Mannheim) or synapse-associated protein-25 (SNAP-25) as controls for protein loading.

To quantify p53, caspase-3, and synaptic protein immunoreactivities, films were scanned and densitometry was performed as described (Martin, 1999). Protein levels were expressed as relative optical density measurements, determined by comparing the density and area of the immunoreactive bands from ipsilateral LGN samples to corresponding bands in contralateral control lanes in the same blot. The immunodensities for p53 and caspase-3 were normalized to synaptic proteins. The values for each time point were replicated in triplicate or quadruplicate experiments. The group means and variances were evaluated by one-way analysis of variance, and subsequent statistical evaluations for significance were made using a two sample Student's t-test.

p53-DNA binding assay

We evaluated whether p53 in LGN samples had competent DNA binding activity. A p53-consensus, double stranded oligonucleotide (Santa Cruz, sc2579) was 3'-end labeled with digoxigenin-11-ddUTP using terminal transferase (Boehringer Mannheim), precipitated, and resuspended in TE buffer. DNA-p53 binding reactions were carried out at room temperature for 40 minutes with 1 ng DNA probe and 20 μg nuclear extract protein (from ipsilateral and contralateral LGN samples) in 10 mM Tris buffer (pH 7.5), 50 mM NaCl, 5 mM $MgCl_2$, 1 mM dithiothreitol, 1 mM EDTA, 5% glycerol, and 2 μg herring sperm DNA. For supershift assays, nuclear fractions were incubated (1 h at room temperature) with p53 antibody (10 μg/ml) prior to the reaction with oligonucleotide. The samples were resolved by electrophoresis through a nondenaturing 4%

polyacrylamide gel (pre-run for 30 mins at 33 V) and transferred overnight to nylon membrane

followed by UV-crosslinking. Membranes were incubated in 2% nucleic acid blocking reagent

(Boehringer Mannheim) and then in blocking reagent containing 75 mU/ml antidigoxigenin Fab

fragments conjugated to alkaline phosphatase (Boehringer Mannheim). After washing, membranes

were reacted with CSPD detection reagent (Boehringer Mannheim) and exposed to Kodak X-

OMAT film to visualize DNA.

RESULTS

Occipital cortex ablation in adult mouse causes neuronal apoptosis in the dLGN

The development and characterization of this model of neuronal apoptosis in rat have been

shown (Al-Abdulla et al., 1998; Al-Abdulla and Martin, 1998; Martin et al., 1998). We have

adapted this model of occipital cortex ablation to the mouse brain (Fig. 1 top). The results in

wildtype C57/B6 and 129/SV mice are similar to the data obtained in rat; therefore, they are

described only briefly. The visual cortex was ablated in mouse, as verified by injecting occipital

neocortex with FG and retrogradely labeling the projection neurons in the dLGN (Fig. 1 bottom).

The lesion in mouse brain is consistent. The inter-animal variability is minimal in the extent of the

cortical aspiration in the anterior-posterior and medial-lateral axes and in the depth of the lesion. It

extends throughout the entire thickness of the cortex at the lesion site, but the underlying

hippocampus is spared (Fig. 1 top). This model of occipital cortex ablation in adult wildtype

C57/B6 and 129/SV mice causes significant apoptotic death of dLGN neurons (~90% loss of

neurons, see below) over a period of 7 days (Fig. 1, top a-d). During this period the majority of

dLGN neurons pass consecutively through chromatolysis (Fig. 1 top, b), condensation of chromatin

into several round mini-masses (Fig. 1 top, c), and then apoptosis (Fig. 1 top, d). This structural

progression of neuronal apoptosis *in vivo* has been described previously (Martin et al., 1999). Tract-

tracing with FG shows that these apoptotic neurons are geniculocortical projection neurons (Fig. 1

bottom, inset).

p53 accumulates in dLGN neurons after occipital cortex lesions

In normal rat and mouse brain, the level of immunocytochemically detectable p53 is low.

Immunoreactivity is observed mostly in the nuclei of some glial cells in the brain parenchyma and

in ependymal cells lining the ventricular system. p53 immunoreactivity is rarely observed in

neurons in control brain (Fig. 2A, E). After occipital cortex ablation, p53 immunoreactivity

accumulates in the nucleus of neurons in the ipsilateral dLGN of rat (Fig. 2B) and mouse (Fig. 2F).

At 1 day and 2 days postlesion, the localization of p53 in the ipsilateral dLGN does not differ from

the contralateral dLGN. In ipsilateral dLGN neurons, p53 immunoreactivity is elevated at 3 days

through 6 days postlesion and is most prominent at 5 days. This accumulation of p53 in neurons is

much more conspicuous in the mouse brain compared to the rat brain (Fig. 2B,F). At 6 days

postlesion, astroglia show an induction of p53 in both ipsilateral and contralateral dLGN (Fig.

2C,D).

p53 levels increase in the LGN after occipital cortex ablation

p53 levels in rat LGN after occipital cortex ablation were measured by immunoblotting. p53

in rat brain tissue is resolved at ~53 kD as two closely migrating immunoreactive bands (Fig. 3) by

SDS-PAGE (15% gels), consistent with phosphorylated and dephosphorylated forms of p53

(Levine, 1997). These immunoreactive bands migrate as a major single band in 10% gels (data not

shown). The migration of these immunoreactive proteins from rat LGN coincides with the migration

and detection of purified human-p53 by SDS-PAGE (Fig. 3). At 5 days postlesion, p53 levels are

increased significantly (p < 0.05) in the ipsilateral LGN (150% ± 13% of control, mean ± sem). At 6

days postlesion, p53 levels are not different (92% ± 3% of control, mean ± sem) from the

contralateral LGN. Experiments with the two different antibodies to p53 showed similar results.

p53-DNA binding is elevated transiently in the LGN after occipital cortex ablation

Gel-shift analysis of p53-DNA binding proteins in nuclear extracts of target-deprived and

control LGN samples revealed a broad band corresponding to the p53 oligomer-DNA complex (Fig.

4). The specificity of p53-DNA binding was demonstrated by the disappearance of signal when

labeled probe was omitted, when an excess of unlabeled oligonucleotide was included, and when

nuclear protein fractions were omitted. Furthermore, this band was shifted to a higher molecular

mass by p53 antibody (data not shown). p53-DNA binding was increased markedly (291.0% ±

15.6% of control, mean ± SD) at 5 days in ipsilateral LGN compared to contralateral LGN,

corresponding to a 3-fold increase in DNA binding of p53. In contrast, at 6 days when neuronal

apoptosis is structurally advanced, the binding activity of p53 in ipsilateral LGN was decreased

(68.5% ± 1.0% of control, mean ± SD) compared to contralateral LGN (Fig. 4).

Caspase-3 is activated in the LGN after occipital cortex ablation

Activation of caspase-3 is a major downstream event in most forms of PCD (Kuida et al., 1996). The levels of procaspase-3 and active caspase-3 subunits were measured by immunoblotting soluble protein fractions of discrete LGN microdissections from rats at 1, 4, 5, and 6 days after the cortical lesion (Fig. 5). Procaspase-3 was detected as a prominent band of immunoreactivity at ~32 kD, and the active subunits were detected at ~17-20 kD (Fig. 5A). At 1 day postlesion, the levels of procaspase-3 and active caspase-3 are unchanged; however, at 4 days, the levels of procaspase-3 and activated caspase are both significantly elevated (Fig. 5B). A prominent peak in caspase-3 activation occurs at 5 days as procaspase-3 levels return to control levels. At 6 days postlesion, caspase-3 activation is attenuated significantly compared to 5 days, although levels of active caspase-3 remain higher than in the control LGN (Fig. 5B).

Loss of the p53 tumor suppressor function protects neurons from retrograde neuronal apoptosis

Mice with targeted deletions of the p53 gene (p53$^{-/-}$) were used to test the hypothesis that neuronal apoptosis in adult brain is p53-dependent (Fig. 6). At 7 days after occipital cortex ablation, the number of neurons in the ipsilateral dLGN of wildtype 129/SV mice was 13.4% ± 2.9% (mean ± sem) of contralateral dLGN; in contrast, the number of neurons in the ipsilateral dLGN of p53-deficient mice was 47.0% ± 11.0% (mean ± sem) of contralateral dLGN. Thus, loss of p53 function protects neurons from neuronal apoptosis in the adult brain.

Bax is required for thalamic neuron apoptosis after cortical injury

We used mice with targeted deletions of the bax gene (bax$^{-/-}$) to test the hypothesis that

neuronal apoptosis in the adult brain is Bax-dependent (Fig. 7). At 7 days after occipital cortex

ablation, the number of neurons in the ipsilateral dLGN of wildtype C57/B6 mice was 9.0% ± 1.0%

(mean ± sem) of contralateral dLGN; in contrast, the number of neurons in the ipsilateral dLGN of

Bax-deficient mice was 88.0% ± 10.0% (mean ± sem) of contralateral dLGN. To determine

whether this effect is sustained, mice were survived for twice as many days. At 14 days after

occipital cortex ablation, the number of neurons in the ipsilateral dLGN of wildtype C57/B6 mice

was 9.3% ± 2.0% (mean ± sem) of contralateral dLGN, whereas the number of neurons in the

ipsilateral dLGN of Bax-deficient mice was 95.0% ± 9.0% (mean ± sem) of contralateral dLGN.

Thus, deletion of Bax results in sustained protection against neuronal apoptosis in brain.

DISCUSSION

These experiments demonstrate that neuronal apoptosis within the adult brain is modulated

by p53 and requires Bax. Ablation of the occipital cortex in rat and mouse causes retrograde

neurodegeneration in the dLGN. This neuronal degeneration in rat is apoptosis (Al-Abdulla et al.,

1998; Al-Abdulla and Martin, 1998). Similar neurodegeneration occurs in mouse as shown here.

We now extend our understanding of the mechanisms of cortical damage-induced, retrograde

neuronal apoptosis in brain by showing that it occurs in association with the induction and

activation of p53 as well as induction and activation of caspase-3. Interestingly, however, this

neuronal apoptosis may occur by both p53-dependent and p53-independent mechanisms, while, in marked contrast, Bax is necessary for retrograde neuronal apoptosis in the adult brain.

p53 is altered during the progression of neuronal apoptosis in the LGN, leading to the suspicion that p53 participates in mechanisms of this neuronal apoptosis. We found that p53 accumulates in neuronal nuclei prior to apoptosis, p53 protein levels transiently increase, and p53 is activated (DNA-binding activity) in nuclear extracts of LGN. We have identified previously three stages of neuronal apoptosis *in vivo*. After axotomy and target deprivation, neurons pass consecutively through chromatolysis, somatodendritic shrinkage, and apoptosis (Al-Abdulla et al., 1998; Al-Abdulla and Martin, 1998; Martin et al., 1999). We have hypothesized that some yet to be identified key events associated with DNA damage occur during chromatolysis that commit neurons to apoptosis (Al-Abdulla et al., 1998; Al-Abdulla and Martin, 1998; Martin et al., 1999). This fate contrasts with other models of axonal injury that induce chromatolysis followed by recovery, rescue, and regeneration of neurons (Martin et al., 1998). In our cortical ablation model, the nuclear accumulation and activation of p53 occurs during the chromatolytic stage of retrograde neuronal apoptosis at 3 to 5 days postlesion and was thus considered to be possibly a key signal for the transition of chromatolytic LGN neurons into apoptosis.

Increased levels of p53 result primarily from increased stability of the protein (Levine, 1997). In unstressed cells, the level of p53 protein is low. The half-life of p53 is short (~5-20 min) due to rapid degradation. p53 protein levels can be increased when the half-life of the protein is extended due to diminished degradation. Inhibition of the 26 S proteosome increases p53 levels (Maki et al., 1996). Alternatively, p53 levels can be increased because the rate of initiation of p53

mRNA translation is enhanced (Levine, 1997). p53 exists in a latent, inactive form that requires modification to become active. DNA damage can activate p53 (Levine, 1997). Increases in p53 levels are proportional to the extent of DNA damage, with several different types of DNA lesions being potent signals for p53 activation, including double- and single-strand breaks and adduct formation (Levine, 1997). An induction and activation of p53 in the LGN is consistent with our earlier results showing that DNA damage occurs in LGN neurons during apoptosis (Al-Abdulla and Martin, 1998).

p53 functions as a DNA transcription factor (Vogelstein and Kinzler, 1992; Levine, 1997; Miyashita et al., 1994; Miyashita and Reed, 1995). The carboxyl terminus of p53 is important for controlling p53-DNA binding functions in response to single strands of DNA (Jayaraman and Prives, 1995). Therefore, to determine whether there was a corresponding increase in transcription factor activity of p53, DNA binding experiments were performed. At 5 days after cortical damage, p53-DNA binding activity is increased markedly in the ipsilateral LGN, indicating that the p53 is functional. By binding to promoters, p53 activates the transcription of many genes. *Bax* (Miyashita and Reed, 1995) and redox-related genes (Polyak et al., 1997) are transcriptional targets of p53. These targets are relevant to LGN neuron degeneration because this neuronal death is apoptosis and these neurons sustain oxidative damage to DNA (Al-Abdulla and Martin, 1998).

We found that loss of p53 function by targeted mutations in the p53 gene attenuated significantly the magnitude of neuronal apoptosis; thus, p53 modulates the apoptotic process in neurons. However, p53 deficiency does not completely rescue LGN neurons from apoptosis, as does Bax deficiency. It is therefore evident from the partial rescue that this form of neuronal apoptosis

can occur independent of p53. A similar attenuation of neuronal apoptosis occurs in p53-deficient mice after adrenalectomy (Sakhi et al., 1998). Because LGN neuron apoptosis can occur in the absence of p53, changes in p53 during the chromatolytic stage of retrograde neuronal apoptosis cannot be solely the key signal for the transition of chromatolytic LGN neurons into apoptosis. Neurons can undergo p53-dependent and p53-independent apoptosis that appears to be dictated by the initiating stimulus that triggers DNA damage (Wood and Youle, 1995). Based on our observations it seems likely that both p53-dependent and p53-independent pathways for apoptosis are operative in the death mechanisms of LGN neurons. Further studies must therefore be conducted to identify the upstream signals that trigger this cortical damage-induced neuronal apoptosis in thalamus.

Because deletion of the p53 gene protects only partially against neuronal apoptosis within the brain, the significance of the induction and activation of p53 during the progression of LGN neuron apoptosis becomes ambiguous. It is noteworthy however that two genes (p73 and p63) have been identified that have significant sequence homology to p53 (Mills et al., 1999). These p53 homologues may participate in the mechanisms for neuronal apoptosis in the absence of p53. p73 can activate p53-responsive promoters and can induce apoptosis when overexpressed in p53-deficient tumor cells (Fang et al., 1999). p63 isoforms contain transactivation domains that can transactivate p53 reporter genes and induce apoptosis (White and Prives, 1999). Deletion of p73 appears to have greater effects in the nervous system as compared to p53 (Yang et al., 2000). Therefore, in the absence of p53, the possible contributions of p73 and p63 in neuronal apoptosis need to be explored.

We found that LGN neuron apoptosis requires Bax. This conclusion is based on the finding the LGN neurons in Bax-deficient mice do not undergo apoptosis after occipital cortex ablation. By extending the postlesion survival time, we found that the rescue of neurons was sustained. This finding demonstrates, for the first time, that retrograde neuronal apoptosis within the adult brain is Bax-dependent, programmed cell death.

Bax is a member of the *bcl-2* protooncogene family (Merry and Korsmeyer, 1997). Bax is thought to function by forming channels in mitochondrial membranes (Antonsson et al., 1997). When active, these channels may allow the release of cytochrome c from mitochondria to the cytosol. In cell culture models of apoptosis, activation of caspase-3 occurs when caspase-9 proenzyme is bound by apoptotic protease-activating factor-1 (Apaf-1) in a process initiated by cytochrome c and either ATP or dATP, which are required cofactors for cytochrome c-induced caspase activation (Liu et al., 1996; Li et al., 1997). Apaf-1, a 130 kD protein, serves as a docking protein for procaspase-9 and cytochrome c (Li et al., 1997). Apaf-1 becomes activated with the binding and hydrolysis of ATP and the binding of cytochrome c, promoting Apaf-1 oligomerization (Zou et al., 1999). This oligomeric complex recruits and activates procaspase-9 that disassociates from the complex and becomes available to activate caspase-3. In the LGN, we found a large increase in procaspase-3 levels at 4 days postlesion and then a prominent activation of caspase-3 at 5 days postlesion. The activation of caspase-3 coincides with our previous demonstration that mitochondria accumulate in a perinuclear location at 3 to 5 days postlesion (Al-Abdulla and Martin, 1998). The changes in caspase-3 that we found in our model of neuronal apoptosis with the adult brain are consistent with studies showing that activation of caspase-3 participates in the mechanisms

of retinal ganglion cell death after optic nerve transection (Kermer et al., 1998; Kermer et al., 1999).

Once activated, caspase-3 cleaves a protein with DNase activity (DFF-45), and this cleavage

activates a pathway leading to the fragmentation of genomic DNA. We have identified dLGN

neurons undergoing nuclear DNA fragmentation at 6 and 7 days postlesion (Al-Abdulla et al., 1998;

Al-Abdulla and Martin, 1998).

Our findings on the requirement of Bax for injury-induced neuronal apoptosis in the adult

brain are consistent with work in other neuronal death systems. Bax is important for developmental

programmed cell death of neurons (Deckwerth et al., 1996). In cell culture, Bax deficiency blocks

apoptosis of cerebellar granule neurons induced by low potassium (Miller et al., 1997). In addition,

nerve growth factor (NGF) withdrawal induces neonatal sympathetic neurons to undergo apoptosis

that is Bax-dependent (Deckwerth et al., 1996) and involves a subcellular redistribution of Bax

(Putcha et al., 1999). As with adult LGN neurons, neonatal facial motor neurons from Bax-deficient

mice survive after axotomy (Deckwerth et al., 1996). Furthermore, the cerebellar granule neuron

apoptosis in *Lurcher* mice is thought to be induced by target deprivation and is Bax-dependent but

p53-independent (Doughty et al., 2000). Thus the mechanisms of injury-induced neuronal death in

the adult thalamus after cortical injury is consistent with neuronal apoptosis after trophic factor

deprivation.

REFERENCES

Al-Abdulla NA, Portera-Cailliau C, Martin LJ (1998) Occipital cortex ablation in adult rat causes retrograde neuronal death in the lateral geniculate nucleus that resembles apoptosis. Neuroscience 86:191-209.

Al-Abdulla NA, Martin LJ (1998) Apoptosis of retrogradely degenerating neurons occurs in association with the accumulation of perikaryal mitochondria and oxidative damage to the nucleus. Am J Pathol 153:447-456.

Anderson AJ, Su JH, Cotman CW (1996) DNA damage and apoptosis in Alzheimer's disease: Colocalization with c-jun immunoreactivity, relationship to brain area, and effect of postmortem delay. J Neurosci 16:1710-1719.

Antonsson B, Conti F, Ciavatta A, Montessuit S, Lewis S, Martinou I, Bernasconi L, Bernard A, Mermod J-J, Mazzei G, Maundrell K, Gambale F, Sadoul R and Martinou J-C (1997) Inhibition of bax channel-forming activity by bcl-2. Science 277:370-372.

Arends MJ, Morris RG, Wyllie AH (1990) Apoptosis. The role of endonuclease. Am J Pathol 136:593-608.

Cregan SP, MacLaurin JG, Craig CG, Robertson GS, Nicholson DW, Park DS, Slack RS (1999) Bax-dependent caspase-3 activation is a key determinant in p53-induced apoptosis in neurons. J Neurosci 19: 7860-7869.

Deckwerth TL, Elliott JL, Knudson CM, Johnson EM Jr, Snider WD, Korsmeyer SJ (1996) Bax is required for neuronal death after trophic factor deprivation and during development. Neuron

17:401-411.

Doughty ML, De Jager PL, Korsmeyer SJ, Heintz N (2000) Neurodegeneration in *Lurcher* mice occurs via multiple cell death pathways. J Neurosci 20:3687-3694.

Fang L, Lee SW, Aaronson SA (1999) Comparative analysis of p73 and p53 regulation and effector functions. J Cell Biol 147:823-830.

Glücksmann A (1951) Cell deaths in normal vertebrate ontogeny. Biol Rev 26:59-86.

Hakem R, Hakem, A Duncan GS, Henderson JT, Woo M, Soengas MS, Elia A, de la Pompa JL, Kagi D, Khoo W, Potter J, Yoshida R, Kaufman SA, Lowe SW, Penninger JM, Mak TW (1998) Differential requirement for caspase 9 in apoptotic pathways in vivo. Cell 94:339-352.

Jayaraman L, Prives C (1995) Activation of p53 sequence-specific DNA binding by short single strands of DNA requires the p53 C-terminus. Cell 81:1021-1029.

Kermer P, Klöcker N, Labes M, Bähr M (1998) Inhibition of CPP-32-like proteases rescues axotomized retinal ganglion cells from secondary cell death *in vivo*. J Neurosci 18:4656-4662.

Kermer P, Klöcker N, Labes M, Thomsen S, Srinivasan A, Bähr M (1999) Activation of caspase-3 in axotomized rat ganglion cell in vivo. FEBS Lett 453:361-364.

Kerr JFR, Harmon BV (1991) Definition and incidence of apoptosis: An historical perspective. In: Apoptosis: The molecular basis of cell death (Tomei LD, Cope FO, eds), pp 5-29. Cold Spring Harbor, NY: Cold Spring Harbor Laboratory Press.

Kitamura Y, Taniguchi T, Shimohama S (1999) Apoptotic cell death in neurons and glial cells: implications for Alzheimer's disease. Jpn J Pharmacol 79:1-5.

Kuida K, Zheng TS, Na S, Kuan C-Y, Yang D, Karasuyama H, Rakic P, Flavell RA (1996)

Decreased apoptosis in the brain and premature lethality in CPP32-deficient mice. Nature 384:368-372.

Lefebvre S, Burglen L, Reboullet S, Clermont O, Burlet P, Viollet L, Benichou B, Cruaud C, Millasseau P, Zeviani M, LePaslier D, Frezal J, Cohen D, Weissenbach J, Munnich A, Melki J (1995) Identification and characterization of a spinal muscular atrophy-determining gene. Cell 80:155-165.

Levine AJ (1997) p53, the cellular gatekeeper for growth and division. Cell 88:323-331.

Li P, Nijhawan D, Budihardjo I, Srinivasula SM, Ahmad M, Alnemri ES, Wang X (1997) Cytochrome c and dATP-dependent formation of Apaf-1/caspase-9 complex initiates an apoptotic protease cascade. Cell 91:479-489.

Liu X, Kim CN, Yang J, Jemmerson R, Wang X (1996) Induction of apoptotic program in cell-free extracts: requirement for dATP and cytochrome c. Cell 86:147-157.

Liu XZ, Xu XM, Hu R, Du C, Zhang SX, McDonald JW, Dong HX, Wu YJ, Fan GS, Jacquin MF, Hsu CH, Choi DW (1997) Neuronal and glial apoptosis after traumatic spinal cord injury. J Neurosci 17:5395-5406.

MacManus JP, Rasquinha I, Tuor U, Preston E (1997) Detection of higher-order 50- and 10-kbp DNA fragments before apoptotic internucleosomal cleavage after transient cerebral ischemia. J Cereb Blood Flow Metab 17:376-387.

Maki CG, Huibregtse JM, Howley PM (1996) *In vivo* ubiquitination and proteasome-mediated degradation of p53. Cancer Res 56:2649-2654.

Martin LJ (1999) Neuronal death in amyotrophic lateral sclerosis is apoptosis: possible contribution

of a programmed cell death mechanism. J Neuropathol Exp Neurol 58:459-471.

Martin LJ, Kaiser A, Price AC (1999) Motor neuron degeneration after sciatic nerve avulsion in adult rat evolves with oxidative stress and is apoptosis. J Neurobiol 40:185-201.

Martin LJ, Price AC, Kaiser A, Shaikh AY, Liu Z (2000a) Mechanisms for neuronal degeneration in amyotrophic lateral sclerosis and in models of motor neuron death. Int J Mol Med 5:3-13.

Martin LJ, Sieber FE, Traystman RJ (2000b) Apoptosis and necrosis occur in separate neuronal populations in hippocampus and cerebellum after ischemia and are associated with differential alterations in metabotropic glutamate signaling pathways. J Cereb Blood Flow Metab 20:153-167.

Martin LJ (2000) p53 is abnormally elevated and active in the CNS of patients with amyotrophic lateral sclerosis. Neurobiol Disease, in press.

Merry DE, Korsmeyer SJ (1997) Bcl-2 gene family in the nervous system. Ann Rev Neurosci 20: 245-267.

Mills AA, Zheng B, Wang XJ, Vogel H, Roop DR, Bradley A (1999) p63 is a p53 homologue required fo limb and epidermal morphogenesis. Nature 398:708-713.

Miller TM, Moulder KL, Knudson CM, Creedon DJ, Deshmukh M, Korsmeyer SJ, Johnson EM Jr (1997) Bax deletion further orders the cell death pathway in cerebellar granule cells and suggests a caspase-independent pathway to cell death. J Cell Biol 139:205-217.

Miyashita T, Krajewski S, Krajewska M, Wang HG, Lin HK, Liebermann DA, Hoffman B, Reed JC (1994) Tumor suppressor p53 is a regulator of *bcl-2* and *bax* gene expression in vitro and in vivo. Oncogene 9:1799-1805.

Miyashita T, Reed JC (1995) Tumor suppressor p53 is a direct transcriptional activator of the human *bax* gene. Cell 80:293-299.

Oppenheim RW (1991) Cell death during development of the nervous system. Ann Rev Neurosci 14:453-501.

Polyak K, Xia Y, Zweier JL, Kinzler KW, Vogelstein B (1997) A model for p53-induced apoptosis. Nature 389:300-305.

Putcha GV, Deshmukh M, Johnson EM Jr (1999) Bax translocation is a critical event in neuronal apoptosis: regulation by neuroprotectants, Bcl-2, and caspases. J Neurosci 19:7476-7485.

Roy N, Mahadevan MS, McLean M, Shutler G, Yaraghi Z, Farahani R, Baird S, Besner-Johnston A, Lefebvre C, Kang X, Salih M, Aubry H, Tamai K, Guan X, Ioannou P, Crawford TO, de Jong PJ, Surh L, Ikeda J-E, Korneluk RG, Mackenzie A (1995) The gene for neuronal apoptosis inhibitory protein is partially deleted in individuals with spinal muscular atrophy. Cell 80:167-178.

Sakhi S, Gilmore W, Tran ND, Schreiber SS (1996) p53-deficient mice are protected against adrenalectomy-induced apoptosis. NeuroReport 8:233-235.

Vogelstein B, Kinzler KW (1992) p53 function and dysfunction. Cell 70:523-536.

White E, Prives C (1999) DNA damage enables p73. Nature 399:734-737.

Wood KA, Youle RJ (1995) The role of free radicals and p53 in neuron apoptosis *in vivo*. J Neurosci 15:5851-5857.

Yang A, Walker N, Bronson R, Kaghad M, Oosterwegel M, Bonnin J, Vagner C, Bonnet H, Dikkes P, Sharpe A, McKeon F, Caput D (2000) p73-deficient mice have neurological, pheromonal and

inflammatory defects but lack spontaneous tumors. Nature 404:99-103.

Zou H, Li Y, Liu X, Wang X (1999) An Apaf-1-cytochrome *c* multimeric complex is a functional

apoptosome that activates procaspase-9. J Biol Chem 274:11549-11556.

FIGURE LEGENDS

Figure 1. Occipital cortex ablation causes apoptosis of geniculocortical projection neurons in mouse

brain.

Top image: Nissl-stained section through a lesioned mouse brain demonstrating the medial-lateral

extent of the cortical ablation (asterisk). The depth of the lesion consistently reaches the corpus

callosum, but the underlying hippocampus remains intact. The LGN ipsilateral to the lesion is

identified (arrow). Scale bar = 1.5 mm. **a-d.** From the ipsilateral dLGN, neurons are shown at the

different stages during the progression of neuronal apoptosis (Al-Abdulla et al., 1998; Martin et al.,

1999). A normal dLGN neuron (a); a neuron in the chromatolytic stage (b); a neuron in early

apoptosis showing early chromatin condensation into mini-masses (c); and a neuron at endstage

apoptosis with a least two, discrete, large round nuclear masses (d). Scale bar = 50 μm. **Bottom**

image: Corticopetal projection neurons undergo apoptosis in the dLGN following cortical ablation

in mouse. After FG injection into the mouse occipital cortex, the dLGN is strongly labeled (yellow

cells), showing that these cells are geniculocortical projection neurons. Scale bar = 200 μm.

Prelabeling of neurons with FG prior to ablation identifies these apoptotic neurons as

geniculocortical projection neurons (inset). By fluorescence microscopy, cytoplasmic FG labeling

(yellow granules) is detected within a degenerating neuron and simultaneous staining with Hoechst

33258 (light-blue) reveals the chromatin clumps consistent with apoptosis.

Figure 2. p53 immunoreactivity accumulates in neuronal nuclei in the dLGN after occipital cortex

lesions. In rat brain at 5 days postlesion, neurons in the contralateral dLGN are not immunoreactive

for p53 (A), but in the ipsilateral dLGN, p53 immunoreactivity has accumulated in the nucleus of neurons (B, arrowheads). In rat brain at 6 days postlesion, subsets of small cells with an astroglial morphology (including an ellipsoidal pale nucleus and radiating processes) in the contralateral dLGN now have nuclear p53 immunoreactivity (C, dotted arrows). Reactive astroglia (D, dotted arrow) in the ipsilateral dLGN expresss p53, but endstage apoptotic neurons (small, double arrows) are not immunoreactive. In mouse brain at 5 days postlesion, neurons in the contralateral dLGN are not immunoreactive for p53 (E), but in the ipsilateral dLGN, p53 immunoreactivity has accumulated in the nucleus of many neurons (F, arrowheads). Scale bar (in A) = 10 μm (same for B-F).

Figure 3. p53 increases transiently in rat LGN after occipital cortex ablation.
Immunoblot analysis of p53 levels in the nuclear fractions of microdissected ipsilateral and contralateral LGN samples at 5 and 6 days postlesion. Purified, bacterially-expressed human p53 was used as a positive control (far right lane). p53 is increased in the ipsilateral LGN at 5 days (5di) compared to the contralateral LGN (5dc). At 6 days postlesion, the ipsilateral LGN (6di) is not significantly different from control (6dc). In the contralateral LGN at 6 days (6dc), the levels of p53 are significantly greater than in the contralateral LGN at 5 days (5dc). See test for quantitative measurements using densitometry. Synaptophysin (p38) was used as a loading control.

Figure 4. p53 is activated transiently in rat LGN after occipital cortex ablation.
Electrophoretic mobility shift assay for p53-DNA binding function in nuclear fractions of microdissected ipsilateral and contralateral LGN samples at 5 and 6 days postlesion. Nuclear

extracts were incubated with digoxigenin-labeled p53 consensus oligonucleotide and p53-DNA

binding was detected with antibodies to digoxigenin. p53-DNA binding activity is greatly increased

(~3-fold) in the ipsilateral LGN at 5 days postlesion (fp, free probe). See Results for measurements.

Figure 5. Caspase-3 is increased and activated transiently in rat LGN after occipital cortex ablation.

A. Immunoblot analysis of procaspase-3 and activated caspase-3 in the soluble fractions of

microdissected ipsilateral (Ipsi) and contralateral (Contra) LGN samples at 1, 4, 5, and 6 days

postlesion. Synaptophysin (p38) was used as a loading control. **B.** Densitometric quantification of

procaspase 3 and activated caspase-3 levels. Values are mean ± standard deviation. The level of pro-

caspase is increased significantly ($p < 0.05$) at 4 days poslesion. The levels of activated caspase-3

are increased significantly ($p < 0.05$) at 4, 5 and 6 days postlesion, with peak activation occurring at

5 days postlesion.

Figure 6. Loss of p53 protects neurons from apoptosis after cortical damage. Occipital cortex

lesions were done on p53$^{+/+}$ (wildtype, n= 10) and p53$^{-/-}$ mice (n=10) that were survived for 7

days. Neurons were counted in the ipsilateral and contralateral (control) dLGN. Values are mean ±

standard deviation. p53 deficiency caused significant (asterisk, $p < 0.05$) protection against

apoptosis of LGN neurons.

Figure 7. Neuronal apoptosis in thalamus after cortical damage requires Bax. Occipital cortex

lesions were done on bax$^{+/+}$ (wildtype, n= 20) and bax$^{-/-}$ mice (n=16) that were survived for 7 and

14 days. Neurons were counted in the ipsilateral and contralateral (control) dLGN. Values are mean

± standard deviation. Bax deficiency completely blocked the apoptosis of dLGN neurons, and this

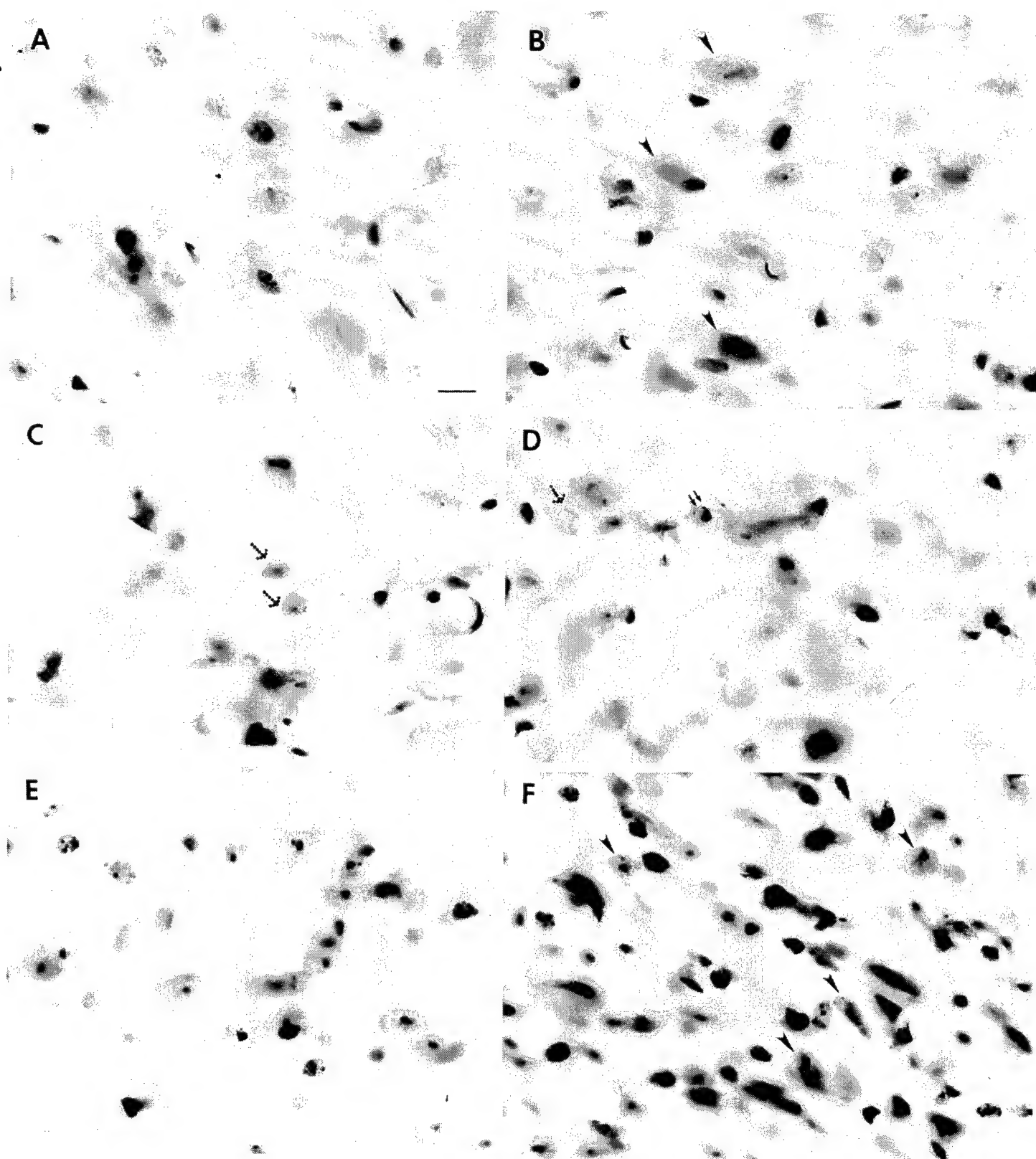effect was sustained (asterisk, $p < 0.05$).

FIGURE 1 TOP
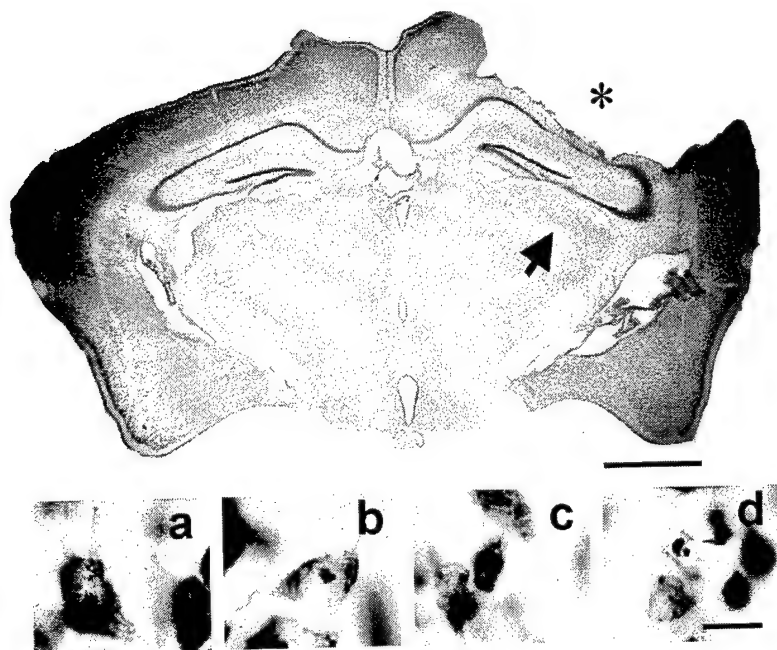
FIGURE 1 BOTTOM
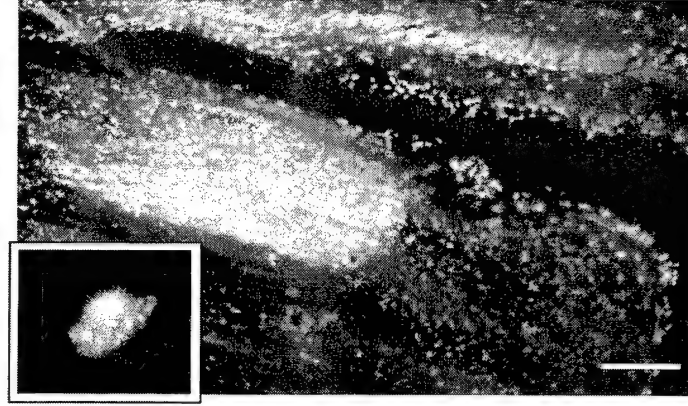
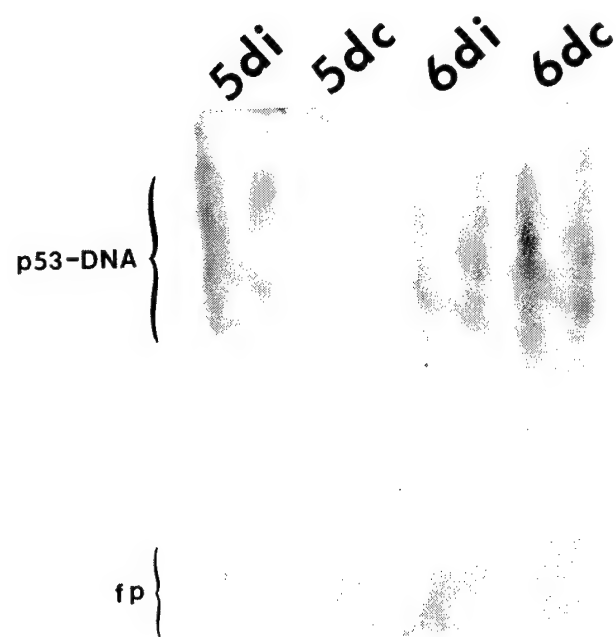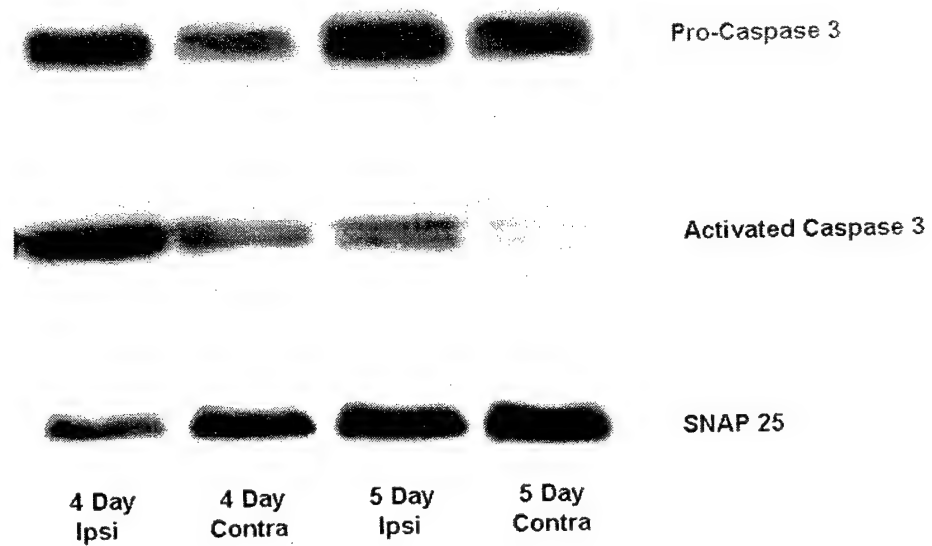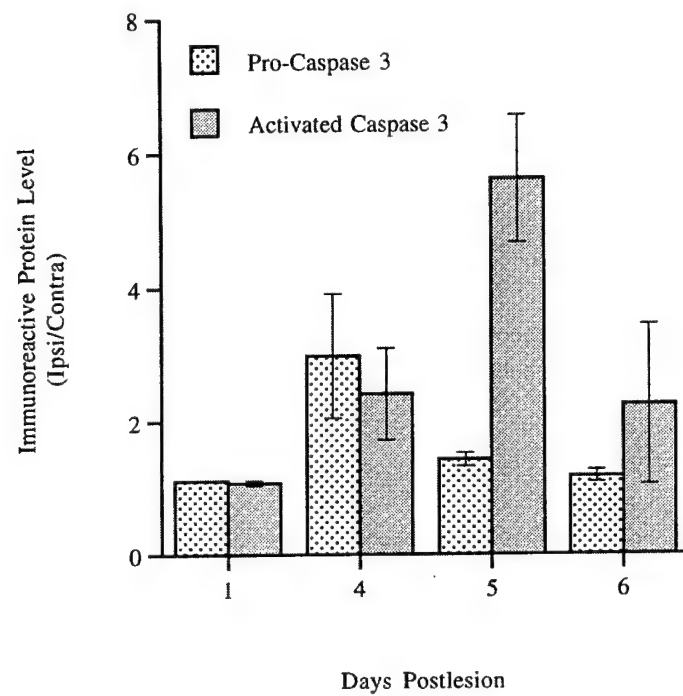FIGURE 2

FIGURE 3

FIGURE 4

FIGURE 5A

Pro-Caspase 3

Activated Caspase 3

SNAP 25

4 Day
Ipsi

4 Day
Contra

5 Day
Ipsi

5 Day
Contra

FIGURE 5B

Days Postlesion
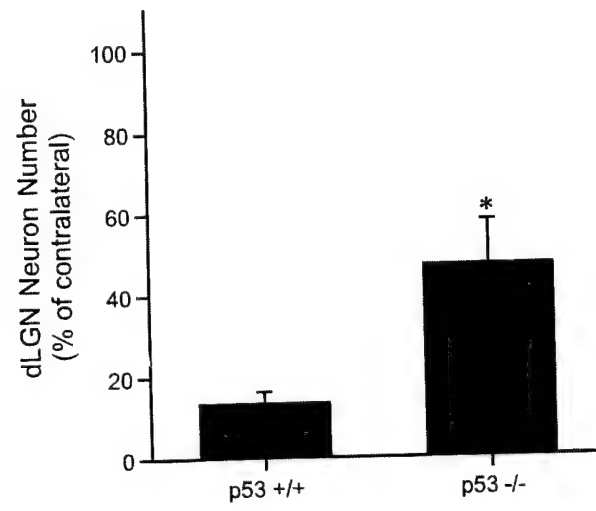
FIGURE 6

FIGURE 7
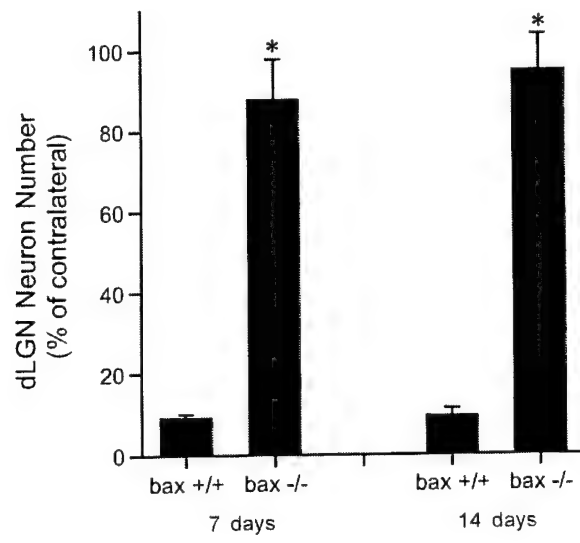
May 8, 2000

DNA Single-Strand Breaks Occur Rapidly in Motor Neurons After *in vitro* Oxidative Stress and *in vivo* Axotomy as Demonstrated by the Comet Assay

Zhiping Liu[1] and Lee J. Martin[1,2]

Departments of [1]Pathology, Division of Neuropathology, and [2]Neuroscience, Johns Hopkins

University School of Medicine, Baltimore, Maryland, U.S.A.

Abbreviated title: DNA damage in adult motor neurons

Number of : text pages (47), figures (10), tables (0)
Number of words: abstract (250), introduction (498), discussion (1595)

Correspondence and reprint requests to:
Lee J. Martin, Ph.D.
Johns Hopkins University School of Medicine
Department of Pathology, 558 Ross Building
720 Rutland Avenue
Baltimore, Maryland 21205-2196
Telephone: 410-502-5170
Fax: 410-955-9777
Email: lmartin@jhmi.edu

ABSTRACT

DNA-single strand breaks (SSB) are a major form of early DNA damage induced by oxidative stress. Reactive oxygen species (ROS) can directly damage DNA and are involved in the pathogenesis of motor neuron apoptosis in animal models and in patients with amyotrophic lateral sclerosis. We tested the hypothesis that DNA-SSB occur in adult motor neurons subjected to oxidative stress *in vitro* and to axotomy *in vivo*. We used single-cell gel electrophoresis (comet assay) which detects mainly DNA-SSB under alkaline elution conditions. We developed and characterized a motor neuron-enriched cell suspension from adult rat spinal cord ventral horn. This cell suspension is ~84% neurons (by NeuN immunophenotyping), 86% of these neurons being motor neurons (by CAT immunoreactivity), and 72% of these motor neurons are α-motor neurons (by retrograde tracing). Adult motor neuron viability in suspension was ~61% after 12 h incubation. Exposure of these cells to nitric oxide (NO) donor sodium nitroprusside (SNP), H_2O_2, or SNP plus H_2O_2 induced rapid DNA damage that was dose- and time-related, as represented by comet formation and cell loss. H_2O_2 at a nontoxic concentration potentiated the neurotoxicity of NO donor. Different forms of ROS caused distinct DNA damage fingerprints, indicating different target domains of DNA and different severities of DNA damage. In an *in vivo* model of motor neuron apoptosis (sciatic nerve avulsion), DNA-SSB accumulate very slowly in injured motor neurons prior to apoptosis and the comet fingerprint is similar to NO toxicity. Thus, adult motor neurons are vulnerable to genomic DNA instability after injury.

Key words: amyotrophic lateral sclerosis, apoptosis, DNA damage, nitric oxide, programmed cell death, single-cell gel electrophoresis, spinal cord injury

Motor neuron degeneration is the cause of amyotrophic lateral sclerosis (ALS) (Martin et al., 2000). This degeneration may be a form of aberrantly-occurring apoptosis (Martin, 1999). Experimental injury to peripheral nerves in animal models also causes apoptosis of spinal motor neurons (Martin et al., 1999a). The signal transduction pathways and the molecular mechanisms mediating motor neuron apoptosis are not understood. Oxidative stress has been implicated in the pathogenesis of both ALS (Bradley and Krasin, 1982) and motor neuron apoptosis after experimental lesioning (Martin et al., 1999a). Oxidative damage to DNA is found in individuals with ALS (Bradley and Krasin, 1982; Fitzmaurice et al., 1996; Ferrante et al. 1997), but it is not known if DNA damage occurs specifically within motor neurons in these patients. Oxidative damage to DNA has been shown directly in motor neurons after axotomy (Martin et al., 1999a). Reactive oxygen species (ROS) by themselves or in combination with other species of free radicals, such as nitrite or nitric oxide (NO), can directly damage genomic DNA (Szabó and Ohshima, 1997). Cells that have sustained DNA damage from ROS and other genotoxic agents undergo apoptosis by engaging molecular cascades involving expression or activation of p53, Bax, and caspases (Polyak et al., 1997). Several different types of DNA lesions are potent signals for p53 activation, including double- and single-strand breaks, adduct formation, as well as insertion/deletion mismatches (Levine, 1997). The earliest and major type of DNA damage among these forms of DNA lesions is DNA-single strand breaks (SSB). It is possible that motor neurons in the adult brain and spinal cord are particularly sensitive to ROS and that cumulative DNA damage in the form of DNA-SSB is a signal for motor neurons to undergo apoptosis. We therefore tested two related hypotheses. Oxidative stress produces DNA-SSB in adult motor neurons *in vitro*, and early DNA damage occurs in adult motor neurons that undergo apoptosis *in vivo*.

Suitable motor neuron model systems and DNA damage assays need to be identified to study the possible role of DNA-SSB in the mechanisms for motor neuron apoptosis. To evaluate oxidative stress-mediated DNA damage in adult motor neurons, we developed and characterized a short-term, motor neuron-enriched cell suspension system prepared from spinal cord ventral horn enlargements of adult rat. These cell suspensions were treated with hydrogen peroxide (H_2O_2) and a nitric oxide (NO) donor *in vitro* to identify if these oxidants cause DNA-SSB in adult motor neurons. To assay for DNA damage at early stages (i.e., DNA-SSB) directly in motor neurons, we used the single-cell gel electrophoresis method, also known as the 'comet' assay. The comet assay is an established method for identifying strand breaks in DNA (Singh et al., 1988; Kindzelskii and Petty, 1999; Morris et al., 1999). The comet assay detects DNA-SSB in individual cells, based on the principles of alkaline elution. We applied this assay to the sciatic nerve avulsion model in adult rat (Martin et al., 1999a), to determine the kinetics of DNA-SSB *in vivo* prior to motor neuron apoptosis.

MATERIALS AND METHODS

Animals and tissues.

Male Sprague-Dawley rats (Charles River, Wilmington, MA), weighing ~150-200 g, were used for these experiments. The animals were housed in a colony room with a 12 h:12 h-light/dark cycle and *ad libitum* access to food and water. The animal protocol was approved by the Animal Care and Use Committee of the Johns Hopkins University School of Medicine. Naive rats without experimental manipulations and rats with experimental manipulations were used in these experiments. The manipulations used were retrograde tracing of motor neurons and sciatic nerve

avulsions.

Spinal cord tissues for motor neuron cell suspension preparations were harvested from animals that were anesthetized deeply with a mixture of enflurane/oxygen/nitrous oxide (1:33:66) and then decapitated. The cervical and lumbar enlargements from rats without experimental lesions were removed. The entire lumbar enlargements (divided into ipsilateral and contralateral sides) were used from rats exposed to tracers and from rats with sciatic nerve avulsions. After removing the pia, lumbar/cervical enlargements were dissected under a surgical microscope segment by segment, and then the segments were microdissected into gray matter columns of ventral horn without appreciable contamination of dorsal horn and surrounding white matter funiculi.

For retrograde labeling of motor neurons, rats were anesthetized deeply with enflurane/oxygen/nitrous oxide (1:33:66), and, under sterile conditions, the sciatic nerve was exposed within the middle of the upper hindlimb. The nerve was transected by cutting, and either 50 µl of 2% nuclear yellow (NY) or 2.5% DAPI was applied to the proximal nerve stump for 1 h using tracer-saturated Gelfoam placed in a sterile Eppendorf tube. The animal incision was closed with the bottom of Eppendorf tube containing NY or DAPI remaining applied to the proximal stump of the sciatic nerve. Two animals were used for each tracer. The animals were allowed to survive for 48 h before they were killed.

The unilateral sciatic nerve avulsion model was used as an *in vivo* model for apoptosis of spinal motor neurons (Martin et al., 1999a). Rats were anesthetized deeply with enflurane/oxygen/nitrous oxide (1:33:66). A midline incision was made in the lateral aspect of the left pelvis and upper hindlimb. The sciatic nerve was located by blunt retraction of the biceps femoris and gluteus muscles and was tracked proximally to an extravertebral location deep within

the pelvis. A steady, moderate traction was applied to the sciatic nerve with forceps until the nerve

separated from the spinal cord, resulting in a mixed motor-sensory root avulsion. Muscle retraction

was released and the overlying skin was sutured. Postlesion survival times following sciatic nerve

avulsion were 5, 7, 10, 14, and 28 days (n = 2-4 rats per time point). Sham control rats (n = 3) were

subjected to the anesthesia, muscle retraction, and sciatic nerve visualization, but the nerve was not

avulsed.

Preparation, sorting, characterization, and counting of spinal motor neuron-enriched cell suspensions.

Preparation of cell suspensions from spinal cord ventral horns. After quick isolation, gray matter

tissue columns from spinal cord ventral horns of lumbar/cervical enlargements were collected and

rinsed in a cell culture dish on ice containing dissection medium (1x Ca^{2+} and Mg^{2+} free Hanks'

balanced salt solution, GibcoBRL, Grand Island, NY, supplemented with glucose and sucrose).

After cutting into smaller pieces, ventral horn samples were digested (20 min) with 0.25% trypsin-

EDTA (Gibco) in a tissue culture incubator (5% CO_2 and 95% air, at 37°C). This mixture was

titurated gently with a transfer pipet. The cell suspension was transferred to a 5 ml-centrifugation

tube on ice, and the remaining small pieces of ventral horn gray matter were further digested in

trypsin-EDTA (16 min). The total cell suspension was then centrifuged at different speeds for cell

sorting.

Sorting of cell suspensions. To isolate a spinal motor neuron-enriched fraction, cell suspensions

were centrifuged (Beckman GPR model centrifuge) at 200 rpm for 5 min (4°C). The supernatant

was collected and then centrifuged at 400 rpm, 800 rpm and then 2,500 rpm. After each spin (for 5

min), the pellet was resuspended in 100 μl phosphate-buffered saline (PBS, pH 7.4), fixed with 1 ml

of 4% paraformaldehyde (4°C for 1 h) and then characterized using immunocytochemistry or cresyl

violet staining.

Characterization of sorted cell suspensions. Cell suspensions from the ventral horns of cervical and

lumbar enlargements after sorting by differential centrifugation were characterized by

immunofluorescence. After fixation the cells were repelleted, and each pellet was resuspended with

250 μl PBS. An aliquot of cell suspension (50 μl) was applied to a gelatin-coated slide and a

coverslip (24 mm x 30 mm) was overlaid gently to form a monolayer of cells. The slides were then

air-dried. The following antibodies were used: a mouse monoclonal anti-neuronal nucleus (NeuN,

diluted 1:20), a neuron-specific marker (Chemicon International Inc., Temecula, CA); a mouse

monoclonal anti-choline acetyltransferase (CAT, diluted 1:5), a motor neuron marker (Roche

Molecular Biochemicals, Indianapolis, IN); a rabbit polyclonal anti-glial fibrillary acidic protein

(GFAP, diluted 1:20), an astroglial marker (DAKO, Denmark); and a monoclonal mouse anti-

CD11b/c IgG2a (OX-42, diluted 1:20), a microglial/macrophage marker (Harlan Sera-Lab,

England).

Air-dried slides were rinsed (1 h) in PBS to separate the slides from the coverslips. The cells

did not attach to the coverslips because they were not coated with adhesive; instead, the cells were

attached to the gelatin-coated slides. The slides were permeabilized (30 min) in 1% Triton X-100

and then treated (30 min) with 1% of bovine serum albumin (BSA). The diluted primary antibodies

were applied to the slides, and the slides were incubated (24 h at room temperature) in a humidified

box. After primary antibody incubation, the slides were rinsed in PBS. Alexa conjugated anti-mouse IgG (diluted 1:100, Molecular Probes, Eugene, OR) was used to visualize NeuN, CAT and OX-42, and Cascade blue conjugated anti-rabbit IgG (diluted 1:100, from Molecular Probes) was used to visualize GFAP. The slides were incubated (4 h at room temperature) in a humidified, dark box. The slides were washed and coverslipped with propidium iodide/antifade (Ventana, Tucson, Arizona). The slides were observed and photographed under a Zeiss fluorescence microscope. The preparation of cell suspensions from rats used for retrograde tracing of motor neurons was identical to that described above. The slides were coverslipped with or without propidium iodide/antifade and were observed under the same fluorescence microscope but with UV emission.

Counting of different cell types in cell suspensions. To identify the cell fraction that was enriched in motor neurons, the specific types of cells were identified by cell-specific markers and were counted. To estimate the total number of neurons, the number of NeuN positive cells were compared to the total number of cells identified by propidium iodide staining and by NeuN staining. The percentages of CAT positive cells relative to NeuN positive cells were calculated to determine the proportion of spinal motor neurons in the cell suspensions. The fraction of DAPI or NY positive cells relative to the total number of NeuN positive cells was also calculated to determine the proportion of spinal motor neurons issuing sciatic nerve axons. The numbers of labeled cells from 6 different microscopic fields (400x) were averaged from each case and then a total mean was derived from the preparations from three different cases.

The viability of the cell suspensions was measured by the trypan blue assay and counting cells in a hemocytometer with phase contrast microscopy. Viability, as determined by exclusion of

trypan blue, was evaluated immediately after the cells were isolated and after incubation for 6, 12, and 24 h.

Exposure of motor neuron-enriched cell suspensions to H_2O_2 and/or NO donor.

To determine whether oxidative stress causes DNA-SSB in adult motor neurons, motor neuron-enriched cell suspensions were exposed to H_2O_2 and the NO donor, sodium nitroprusside (SNP), or a combination of H_2O_2 and SNP. Motor neuron cell suspensions (the 400 rpm preparation) were prepared from naive rats. For the comet assay, motor neuron cell suspensions were exposed to different doses of H_2O_2 in a medium containing 90% Neurobasal-A (Gibco), 5% horse serum, 5% fetal bovine serum (both sera were heat inactivated) and 1x glutamine (Gibco). The cells were exposed to H_2O_2 in a tissue culture incubator (containing 5% CO_2 and 95% air, 37°C) for the different times. For controls, cells were not exposed to H_2O_2 but were incubated for the same times in medium. After exposure, the treatment groups were collected into 5 ml centrifuge tubes and repelleted at 4°C for 5 min. Each pellet was resuspended and subjected to the comet assay.

Motor neuron cell suspensions (400 rpm preparation) were prepared from naive rats and were exposed to SNP (Sigma, St. Louis, MO) for different durations ranging from 15 min to 4 h. Exposure concentrations of 10 μM, 100 μM, 300 μM, and 800 μM were used. Motor neuron cell suspensions were also exposed to H_2O_2/SNP simultaneously for the same durations as exposure to SNP only. The exposure was done in a medium containing 90% Neurobasal-A (Gibco), 5% horse serum, 5% fetal bovine serum (both sera were heat inactivated) and 1x glutamine (Gibco) in a tissue culture incubator (containing 5% CO_2 and 95% air, 37°C) for the different times. For controls, samples of the same cell suspensions were incubated in medium for the same time in the absence of

SNP.

Comet assay.

To detect DNA-SSB on an individual cell basis, motor neuron cell suspensions that were exposed to H_2O_2, SNP, and H_2O_2/SNP were analyzed by the comet assay. In addition, to identify DNA-SSB in motor neurons undergoing apoptosis *in vivo*, the comet assay was used on motor neuron cell suspensions prepared from rats with sciatic nerve avulsions. The 400 rpm cell preparations from ipsilateral or contralateral sides of ventral horns of lumbar enlargements of animals with unilateral sciatic nerve avulsions were subjected directly to comet assay immediately after they were sorted and repelleted. All the procedures for comet assay were done under low light to avoid DNA damage by strong light.

Preparation of cell microgels on slides. The cell microgels were prepared as layers. The first layer of gel was made by applying 200 μl of regular melting point agarose (0.7%) on individual superfrosted glass microscope slides (3" x 1", thickness 1mm) and a coverslip was laid gently on the agarose. After gel solidification at 4°C, the coverslip was removed, and 50 μl of a mixture of cell suspension (containing ~ 4.4 x 10^4 motor neurons) and low-melting point agarose was applied to the first gel layer. The low-melting point agarose was prepared in 0.1 M PBS and kept at 37°C , and the cell suspension-agarose mixture was maintained at 37°C. The slides were then coverslipped and placed at 4°C for solidification of the cell suspension-agarose mixture. After the second layer solidified, the coverslips were removed and 100 μl of low-melting point agarose was added on top of the cell layer. The gels were recoverslipped, and the slides were placed on ice for gel

solidification.

Lysis of cells, DNA unwinding, gel electrophoresis, and DNA staining. Coverslips were removed

from the cell microgels and the slides were covered with 1.5 ml of lysis buffer (pH 10) containing

2.5 M NaCl, 100 mM EDTA, 1% sodium lauryl sarcosine, 10 mM Tris, and Triton X-100 (final

concentration 1%, freshly added immediately before use). Microgels of oxidant- and vehicle-treated

cells were lysed for 30 min at room temperature. Microgels of cells prepared from avulsion rats

were lysed for 1 h at room temperature. After draining, microgels were treated with DNA-

unwinding solution (300 mM NaOH, 1 mM EDTA, pH 12) for 30 min. After DNA-unwinding, the

microgels were placed in a horizontal gel electrophoresis chamber filled with DNA-unwinding

solution and subjected to electrophoresis (300 mA) for 20 min (oxidant/control treated cell

preparations) or 30 min (lesioned/unlesioned sciatic nerve avulsion samples). After neutralizing

microgels with 0.4 M Tris-HCl (pH 7.5) for 20 min, they were stained (30 min) with 20 μg/ml

ethidium bromide. Subsequently, the gels were washed and coverslipped. The analysis and

photography were performed using a Zeiss fluorescence microscope.

Counting comets and intact cells in cell microgels. The number of cells with comets were counted

in microgels prepared from motor neurons exposed to oxidants *in vitro* and from motor neurons

isolated from *in vivo* avulsion experiments. For cell preparations exposed to H_2O_2, SNP, and

H_2O_2/SNP, cells incubated for the same time in medium without oxidant were used as controls.

Three to five separate experiments from different animals were done for each type of *in vitro*

oxidant exposure experiment. For the unilateral sciatic nerve avulsion experiments, comet assays

were performed on 2-4 rats for each recovery time (5, 7, 10, 14, and 28 days). The contralateral

(unlesioned) side of the spinal cord from rats with sciatic nerve avulsions was used as the control for

each time point. The number of comets and large intact cell nuclei regarded as motor neurons

stained by ethidium bromide were counted in 6 microscopic views at 200x from microgels of H_2O_2

or/and SNP exposed cells and from sciatic nerve avulsion animals. The percentage of comets

relative to the total number of cells (total number of comets and total number of intact cell nuclei)

were determined and group means were calculated. The data were analyzed using a Student's *t* test.

DNA fragmentation analysis of motor neuron-enriched cell suspensions exposed to oxidative stress.

Immediately after sorting the ventral horn cell preparations, the 400 rpm cell suspension

from both cervical and lumbar enlargements (n = 13 rats) were divided into wells. These motor

neuron-enriched cell suspensions were treated at room temperature with either 10 mM H_2O_2, 10 μM

SNP or vehicle in medium for 60 min and 90 min. The cells were then collected and repelleted.

Samples with the same treatments were pooled, and genomic DNA was extracted. Three separate

experiments were performed.

Agarose gel electrophoresis for DNA fragmentation. To identify the pattern of DNA fragmentation

after oxidative stress, DNA was extracted from motor neuron-enriched cell suspensions exposed to

H_2O_2 and/or NO donor and their vehicle/time controls. Immediately after the exposure, the cells

were pelleted, washed in PBS, repelleted and then lysed with 1% SDS in lysis buffer. The samples

were treated with Proteinase K overnight and then genomic DNA was extracted with

phenol:chloroform:isoamyl alcohol. After digesting RNA with DNase-free RNase followed by

repurification, DNA (10 µg) from each sample was end-labeled with digoxigenin as described

(Portera-Cailliau et al., 1997; Martin, 1999). DNA was fractionated in a 1.5% agarose gel,

transferred to nylon membrane, UV-crosslinked, incubated with a digoxigenin antibody conjugated

to alkaline phosphatase, and detected with Lumi Phos 530 (Boehringer Mainnheim) followed by

exposure to Kodak X-Omat AR film (Eastman Kodak, Rochester, NY).

Structural analysis of motor neuron-enriched cell suspensions.

We evaluated the structure of adult motor neuron cell suspensions and the structural changes

in these cells exposed to H_2O_2 and NO donor. After sorting, control and treated motor neurons

(prepared from 3 rats for each condition) were fixed with 1% glutaraldehyde and 2%

paraformaldehyde, and processed for plastic embedding. Motor neuron cell pellets were cut at 1 µm

and stained with toluidine blue for high-resolution light microscopy and were also thin-sectioned for

electron microscopy.

RESULTS

A motor neuron-enriched cell suspension can be isolated from adult spinal cord

To study the kinetics of DNA damage induced by oxidative stress in adult motor neurons *in*

vitro and DNA damage in adult motor neurons undergoing apoptosis *in vivo*, model systems for

isolating adult motor neurons and for detecting early DNA damage in individual motor neurons

needed to be developed. When ventral horn samples are exposed to mild digestion and then

fractionated by differential low speed centrifugation, a cell suspension comprised mostly of motor

neurons was isolated. Most of the spinal motor neurons are found in the 400 rpm pellet and most of the cells in this fraction are motor neurons (Fig. 1).

After resuspending the 400 rpm pellet, the cell suspension was even, without visible tissue pieces. Microscopically, most cells were uniformly round and large (volumes of ~98-653 μm^3) or middle-sized (volumes of ~32-63 μm^3). These cells were identified as neurons by NeuN staining (Fig. 1A,B) and were identified as motor neurons by CAT immunofluorescence (Fig. 1E, F) and retrograde labeling with NY and DAPI (Fig. 1G). Motor neuron nuclei showed strong labeling for NeuN. The NeuN reactivity was very strong in nuclei and blocked the staining with propidium iodide. Only very small cells without NeuN reactivity (glial cells) could be counterstained with propidium iodide (Fig. 1C,D). CAT staining was localized in cell perikarya and thus the nuclei were counterstained with propidium iodide (Fig. 1E,F). A few large cells were entirely or partially surrounded by astroglial processes as revealed by GFAP staining (Fig. 1H). A small population of glial cells was scattered throughout the motor neuron-enriched cell suspension, with only occasional OX-42-positive microglial cells being identified.

Cell counting confirmed that ~84% cells in this suspension of the 400 rpm pellet from cervical and lumbar ventral horns were neurons (Fig. 1A). Of these neurons, ~86% were spinal motor neurons by CAT positivity (Fig. 1E). Retrograde tracing revealed that ~72% of cells in the 400 rpm cell suspensions from lumbar enlargements were DAPI labeled (Fig. 1G), thus identifying these cells as α-motor neurons with axons in the sciatic nerve. We estimated that the total number of medium and large cells, which are most likely motor neurons, in the 400 rpm cell suspension from spinal cord enlargements was $4.0 \times 10^6 \pm 0.22 \times 10^6$.

The cell suspension compositions of the fractions yielded by the other centrifugation speeds

were distinctly different from that found at 400 rpm. Mostly small-sized cells and fewer middle-sized cells were found in the cell suspensions made from the 800 rpm pellet. Individual glial cells and small cell clusters formed by 3-5 glial cells were observed. Cell sizes ranged from 10 μm^3 to 51 μm^3. The smaller cells were found to be mostly glia. The larger cells in the 800 rpm fractions were similar in size to the smaller cells in the 400 rpm fraction. These cells of ~50 μm^3 were mostly smaller neurons. Only rarely were large, CAT-positive or DAPI-labeled cells observed in the cell suspensions from the 800 rpm fraction. In the cell suspensions from the 2500 rpm pellets, the largest cell bodies were ~11 μm^3 (which is similar in size to the smallest cells in the 800 rpm fraction). Tiny cell bodies and cellular processes were observed within the 2500 rpm cell suspensions. The composition of the 200 rpm fraction (it was too loose to be a pellet) was heterogeneous and contained partially digested white matter with aggregates of glial cells. This fraction contained many microvessel fragments composed of endothelial cells (cell body diameters ~2.5 μm x 15 μm) and attached perivascular cells. Most of these cells had small cell bodies (volumes ~36.8-50.1 μm^3) and appeared to be astroglia as revealed by cresyl violet and propidium iodide staining (for nuclei). Isolated cells that appeared to be neurons were rarely found in the 200 rpm fraction, indicating that the mild tissue digestion was effective and that neurons were liberated from the tissue but did not pellet after very low speed centrifugation.

To evaluate the viability of the motor neuron cell suspensions, we used the trypan blue assay (Fig. 2). Immediately after the preparation of the cell suspension, isolated motor neurons excluded trypan blue. At 6 h and 12 h incubation 74% and 61% of motor neurons remained viable, respectively. At 24 h incubation, 37% of the motor neurons still remained viable.

Oxidative stress rapidly causes DNA-SSB in motor neurons

To identify DNA-SSB in motor neurons after oxidative stress, the comet assay was used (Fig. 3). The alkaline conditions for cell lysis, DNA unwinding, and gel electrophoresis dictate the specificity of this assay for DNA-SSB (Singh et al., 1988; Kohn, 1991). Control and experimental motor neuron-enriched cell suspensions were cast into microgels, and then were lysed, followed by DNA unwinding treatment and gel electrophoresis. In gels stained with ethidium bromide, cells with intact genomic DNA have an evenly stained, smooth round nucleus without a tail (Fig. 3Ba). In contrast, cells with DNA-SSB have a tail and a stained nucleus, with both the tail and the head comprising the comet (Fig. 3Ba,b). Comets were classified as new comets or matured comets. New comets had a very large, round and brightly stained head and a very short tail formed by DNA granules very close to the head (Fig. 7b). Matured comets had longer tails and smaller heads (Fig. 3Ca-d,f). The new comets are cells with incipient, very early DNA damage, presumably consisting of very large DNA fragments. The matured comets have progressive DNA damage in these cells, although the DNA damage in these cells is still at an early stage, because the alkaline condition is favorable for the unwinding and electrophoresis of only DNA-SSB. Generally, the sizes of comet heads are larger than intact cell nuclei, indicating that the packaging of genomic DNA was loose because of DNA-SSB and unwinding.

In control groups (i.e., motor neuron enriched cell suspensions incubated in medium only), the majority of large cells was intact, although a background number of comets was observed (Fig. 3A,B). The number of background comets was significantly higher ($p < 0.05$) at 30 min, 60 min, and 90 min compared to 15 mins (Fig. 3A), although from 15 min to 90 min in medium, this value remained at ~10% or fewer (Fig. 3A). Control samples were also evaluated at 4 h, 6 h, 8 h and 12 h

of incubation. Even at 12 h, most of the cells embedded in the microgels were intact. The overall

cell density in the microgels did not change appreciably over 12 h incubation (Figs. 4B, 5B).

Meanwhile, the comet patterns changed slowly with increased time in medium, indicating that DNA

damage was progressing very slowly (Fig. 3B). In controls at 15 min, with the background percent

of comets ~4.4% (Fig. 3A), most of the comets were new comets or early mature comets (Fig.

3Ba,b). At 0.5 h, 1 h, 1.5 h, and 2 h and even longer incubation times (4 h, 6 h, 8 h and 12 h), the

comet heads were still large and brightly stained and the tails consisted of scattered, granular DNA

fragments (Fig. 3Bc,d,e).

With 15 min exposure to 10 mM H_2O_2, the number of comets in motor neuron cell

suspensions increased significantly ($p < 0.05$) to 19%, compared to control (Fig. 3A). These comets

had a large, round and densely stained head with a tail shorter than 310 µm (but much longer than

the tail of comets in 15 min controls, see Fig. 3Bb). The tails were formed by fine DNA granules

and were distinctly different from the control comet tails formed by large DNA granules (Fig. 3Bc).

This pattern reveals that by 15 mins exposure to H_2O_2 the extent of DNA damage in motor neurons

is already greater than control comets, as indicated by the longer tails representing smaller DNA

fragments.

With 30 min of exposure to 10 mM H_2O_2, the number of comets increased compared to

control and 15 min H_2O_2 exposure (Fig. 3A). About 26% of the motor neurons had DNA damage.

Two comet patterns predominated. Some comets had a small head and a long (about 620 µm), thin

tail (Fig. 3Ca), and other comets had a head with an intensely stained core and a halo as well as a

tail longer than 310 µm (Fig. 3Cb). The tails were still visibly granular with finer granules than

those motor neurons treated 15 min with H_2O_2.

The DNA damage in motor neurons treated with H_2O_2 progressed with longer exposure. With 60 min exposure to 10 mM H_2O_2, the percentage of motor neurons with comets was 31% (Fig. 3A). The comet heads were small and irregular or were loosely-stained 'ghost' heads (Fig. 3Cc,d), and the tails were generally very long (> 620 µm) compared to 30 min exposure. These tails had a finely particulate DNA pattern. Motor neuron comets with discontinuous tails comprised of two separate parts (with a total length longer than 1 mm) could be seen frequently, though both parts still had very fine DNA granules. With 90 min exposure to 10 mM H_2O_2, the percentage of comets decreased significantly compared to control and 60 min H_2O_2 exposure (Fig. 3A), although the number of comets in the control group at 90 min incubation was similar to controls at 30 mins (Fig. 3A). Comets observed with 90 min exposure to 10 mM H_2O_2 had loosely packed and reticulated DNA in the head and a faint, short tail (Fig. 3Ce), indicating that the DNA damage was more severe than only DNA-SSB.

Exposure of motor neuron cell suspensions to 150 mM H_2O_2 generated many comets at 30 min, essentially all motor neurons had comets at 45 min, and most cells were fragmented at 60 and 90 min. The comets formed by exposure to very high concentrations of H_2O_2 were characterized by an irregularly-shaped head with a broad tail consisting of very fine granules (Fig. 3Cf). This pattern reflects rapid, severe DNA damage in motor neurons, with the smaller irregular head generated by appreciable DNA elution from the nucleus to form the broad, long tail composed of fine DNA fragments that are small and quickly eluted from nuclei. Motor neurons displayed DNA damage earlier (after 30 mins) than smaller neurons and glial cell (after 45 mins and longer exposure to 150 mM H_2O_2, indicating that motor neurons are more vulnerable than smaller neurons and glial cells to oxidative stress.

Exposure of motor neuron cell suspensions to low concentrations of H_2O_2 gave surprising

results (Fig. 4A). After exposure cells to 1 mM H_2O_2, the percentage of comets decreased

significantly to a very low level at 15 min, 30 min, 1 h, 2 h, 4 h, 6 h, 8 h (data are not shown for 4 h,

6 h, 8 h) compared to control (Fig. 4A). The few comets observed had a specific pattern. These

comets had a large, round head and a wide tail with a neck (Fig. 6a,b). The tail was composed of

very fine granules.

NO induces DNA damage in motor neurons and synergies with H_2O_2 in killing motor neurons

NO has been implicated in the toxicity of motor neurons in individuals with ALS (Beckman

et al., 1993) and in experimental models *in vitro* (Estévez et al., 1998) and *in vivo* (Wu and Li,

1993; Martin et al., 1999a). Using our cell suspension preparation and the comet assay, we tested

the hypothesis that NO causes DNA damage in motor neurons. The NO donor SNP induced dose-

and time-related DNA damage in motor neurons. Exposure to different concentrations of SNP for

different durations induced DNA-SSB.

Exposure to 10 μm SNP caused a time-dependent increase in the percent comets from 15

min to 60 mins (Fig. 4A). Some of the early appearing comets most likely disappeared between two

successive times according to the comet pattern analysis (Fig. 4C). At 15 mins, most of the comets

had large heads, being either packed densely or displaying a very bright granular coma around the

head (Fig. 4Ca,b). The tails, when present, blended with the coma and were granular, short, and

broad. At 30 mins, the cores of most of the comet heads were smaller and the tails were longer than

those at 15 min (Fig. 4Cc,d). The number of comets in the 30 min SNP exposed cells was

significantly greater than that at 15 min, thus new comets were formed. After 1 h exposure, the

number of comets further increased (Fig. 4A) and their tails were long (Fig. 4Ce,f). At 2 h after

exposure, the percentage of comets decreased compared to 1 h but was still greater than control

(Fig. 4A). Interestingly, most of these comets had a dense core head with a coma, and a broad, short,

granular tail, indicating they were new comets, instead of matured comets from 60 min (Fig. 4Cg,h).

The absence of significant change in motor neuron number from 15 min to 2 h exposure to 10 μM

(Fig. 4B), indicates that many of these cells remained in the cell suspension after they transiently

displayed their comet.

Motor neurons treated with 100 μM SNP showed an abrupt increase in the percentage of

comets at 15 min, but the number of comets did not change over 2 h (Fig. 5A). The comet patterns

were similar to those observed with 10 μM SNP exposure. With brief exposure (15 min), many of

the comets were new comets (Fig. 5Ca,b). With longer exposure times, mature comets prevailed

(Fig. 5Cc,d). The heads of these long-tailed comets had a very specific appearance (Fig. 5Cd),

notably they possessed DNA-poor compartments in the core. No significant change occurred in

motor neuron number between 15 min to 2 h exposure compared to time-matched controls (Fig.

5B), further indicating that comet formation is transient and reflects early DNA damage in the form

of DNA-SSB. With 2 h of exposure to 100 μm SNP comets had large heads and diffuse comas and

short granular tails (Fig. 5Ce), indicating DNA damage is at an earlier stage. Some nuclei were

large, swollen, and vacuolated (Fig. 5Ce). These two patterns may reflect different stages of DNA

damage.

After exposure to 300 μM or 800 μM SNP, the number of comets decreased compared to

lower concentrations of SNP, and the decrease in cell density with longer incubation was more

obvious than with lower dose exposures (data not shown). With these higher concentrations of SNP,

an entirely different type of comet pattern emerged. The DNA staining of the heads was faint and loosely granulated or clumped, and the heads manifested a range of sizes from either large to very small (Fig. 5Cf, g, h). The tails were usually broad and very granular, particularly for the comets with the smaller heads (Fig. 5Cf, g, h).

Combined exposure to SNP and H_2O_2 was potently neurotoxic to motor neurons. Because H_2O_2 at a concentration of 10 mM caused prominent DNA damage (Fig. 3A,C), while, in contrast, 1 mM H_2O_2 seemed to protect against spontaneous, background DNA damage in motor neurons (Figs. 4A, 5A) we used 1 mM H_2O_2 in combination with SNP. Exposure to 10 µM SNP and 1 mM H_2O_2 induced a sudden and prominent loss of cells by 15 min (Fig. 4B). This loss of motor neurons was found consistently through 2 h. Many nuclear fragments of motor neurons were found throughout the microgels (Fig. 6c,d,e,f); therefore, it is likely that the magnitude of cell loss is underestimated. Some motor neurons had characteristic new comets, while the DNA in other nuclei was condensed and marginated at the periphery with the center of the nucleus low in DNA (Fig. 6d). The heads of other comets were very small with tightly packed DNA, while their tails were comparatively large and smear-like with a spindle shape and a narrow neck between the head and the tail (Fig. 6e,g,h). These comets were considered to be from contaminating glial cells.

In the 100 µM SNP and 1 mM H_2O_2 exposed groups, the loss of cells was rapid (Fig. 5B), and cellular fragmentation was more obvious (Fig. 6f); furthermore, the number of comets was greater than the number in each corresponding time in the 10 µM SNP and 1 mM H_2O_2 groups (Figs. 4A, 5A). Most of these comets had a glial cell pattern, although at 15 min, irregularly shaped large heads typical of motor neuron comets were observed.

Different oxidants produce distinct patterns of DNA damage in motor neurons

The DNA staining and comet patterns revealed that different forms of oxidative stress generally have different DNA damage fingerprints, with each chemical insult having its own major comet pattern. Furthermore, exposure of cells to different doses or different durations gave different patterns as well, though there was some overlap. The nuclei of healthy motor neurons were similar in size and DNA staining regardless of lysis, unwinding, and electrophoresis of DNA. However, some intact, round nuclei were much larger than the majority of healthy nuclei and were stained very brightly (Fig. 7a). This type of nucleus could be found in control groups at every time point and in groups treated with 1 mM H_2O_2 (early times, such as 15 min, 30 min, 1 h and 2 h), 10 mM H_2O_2 and 10 μM SNP (15 min and 30 min), and in motor neurons at 5 days after avulsion (see below for details). This nuclear pattern might reflect the presence of few DNA-SSB, because the DNA was unwound thoroughly by alkaline conditions and the chromatin packaging was very loose. The comet assay is sensitive enough for detecting one break per 2 X 10^{10} Daltons of DNA (Singh et al., 1988). The lack of a tail is probably because the single-strand DNA was too long (large) to be eluted from the motor neuron nucleus. A similar phenomenon occurred in glial cell nuclei after exposure to 100 μM SNP plus 1 mM H_2O_2 (Fig. 7l). Some intact glial cell nuclei (Fig. 7l), much smaller that neuronal nuclei (Fig. 7a), were stained more brightly and were larger that other smaller nuclei.

New comets had different types of patterns. The most frequent pattern was a large, round, densely staining head with a short, granular tail consisting of large granules close to the head (Fig. 7b). This pattern was observed in most of the control groups (even at 12 h) and in motor neurons treated for short durations (15 min) with 10 mM H_2O_2 or 10, 100, 300, or 800 μM SNP. Another

pattern consisted of a head with a densely staining round core surrounded by a dense DNA halo (Fig. 7c) or large granules (Fig. 7e). The former type was found with H_2O_2 and was occasionally found in control groups. The latter type of new comet was characteristic of the SNP treated motor neurons and may represent incipient DNA damage at few sites with the formation of large DNA single strands surrounding the head and forming a short comet tail.

Matured comets had longer or very long tails compared to new comets. Early matured comets had a large, densely stained head and a tail shorter than 620 µm formed by scattered large granules (Fig. 7d). This type of comet occurred in some untreated motor neurons incubated from 1 to 12 h, and probably represents background dying cells after dissection from spinal cord and trypsin digestion. The SNP treated cells had a characteristic type of matured comet appearing with a large head and very bright halo, and a longer tail ($\sim$310 µm) consisting of very scattered large granules (Fig. 7f). This comet was found most frequently with 10 µM SNP at 30 min or 1 h. This pattern indicates that DNA damage progressed from the new comets, and the configuration of the genomic DNA changed, allowing the large single strands to elute from the nuclei more quickly.

The morphology of matured comets was more diverse than with the new comets. We observed matured comets with medium-sized heads and densely staining, intermediate tail lengths (>310 µm). Some motor neuron comets had a head with a bright granular halo and a broad granular tail as broad as the heads' coma (Fig. 7g). This type of matured comet was also typical for SNP exposure, but the DNA damage was more advanced compared to the new comets observed with SNP. This matured comet was associated frequently with motor neurons exposed to 10 µM SNP for 30 min, 1 h and 2 h, as well as 100 µM SNP for 30 min and occasionally with motor neurons exposed to 100 µM SNP plus 1 mM H_2O_2. Because the tail was very broad and there are many

granules, the extent of DNA damage and the configuration of the genomic DNA are very amenable for the comet assay, as DNA-SSB are much more prevalent in these motor neurons compared to motor neurons with new comets. Another type of comet typical for SNP exposure is a very progressed form (Fig. 7h). The head consists of only scattered large granules, and the tail is also composed of large granules and is long (~620 μm or longer).

With motor neurons treated with 10 mM H_2O_2, characteristic comet patterns emerged. At 30 min, motor neuron comets had a densely staining core in the head and a circular profile of DNA around the core (Fig. 7i). These heads were much smaller than the new comet heads with this halo pattern. The tails consisted of fine granules, indicating that the DNA-SSB are numerous and the lengths of the DNA single strands in the tail are shorter than those in the comets typically found with SNP. In motor neurons treated with 10 mM H_2O_2 for longer times (1 h), comets had a small densely stained head and thin, long tails (620 μm or longer) consisting of fine granules (Fig. 7j). Apparently, the DNA damage progressed further, and the single strands of DNA fragments are more numerous and shorter.

In motor neurons exposed to 1 mM H_2O_2, there was a specific neuronal comet pattern, in the presence of decreased comet numbers. The head was large and round, typical of neuronal comets. The tail of these comets had a narrow neck, and the broad part of the tail was short and consisted of very fine granules (Fig. 7m). The large part of the tail may consist of short DNA single strands because they appeared as fine dots rather than large granules. The DNA damage may have accumulated very rapidly and then the damaged ceased in keeping with the shape of the broad tail with a narrow neck.

In cell suspensions exposed to SNP and H_2O_2, DNA damage occurred in both motor neurons

and glial cells. The neuronal comets had an irregular head, either blebbed (Fig. 7k) or fragmented

(data is not shown). Glial cell comets had very small heads, and the tails were very long with a neck

(Fig. 7p). Most of the comets associated with cells exposed to SNP plus H_2O_2 were stained

incompletely and faintly with ethidium bromide. This comet pattern is similar to a pattern found

under neutralized elution conditions (data not shown) and thus may reflect some double-stranded

DNA breaks.

**DNA-SSB accumulate in motor neurons *in vivo* early after injury and the pattern is similar to
DNA damage induced by NO donor exposure *in vitro***

We applied the comet assay to an *in vivo* model of motor neuron degeneration. At 5 days

after sciatic nerve avulsion, many (26%) lumbar motor neurons from the lesion side had comets

(Fig. 8A), but very few motor neurons (1.8%) from the unleisoned side had comets. The heads of

these motor neuron comets were large, round and bright, and the tails were very short and consisted

of scattered large granules close to the heads (Fig. 8Ba,b). Many intact cells were stained with

ethidium bromide in preparations from both ipsilateral and contralateral sides of lumbar

enlargements, but these cells were not as brightly stained and as large as the comet heads, revealing

that in the latter cells the DNA packaging was loose. The pattern of these comets was similar to

motor neuron comets caused by 10 mM H_2O_2 exposure for 15 min (Fig. 7b).

At 7 days after sciatic nerve avulsion, the number of motor neuron comets in the lesioned

side of spinal cord was increased significantly (35%, $p < 0.05$) compared to 5 days (Fig. 8A). These

comets had large heads (although not as intensely stained as those at 5 days) and short granular tails

that were longer than those at 5 days (Fig. 8Bc,d). These comets appeared as intermediates between

control comets (Fig. 7b or 7d) and comets from SNP treated motor neurons (Fig. 7e or 7f), but they were most similar to SNP new comets (Fig. 7e). No comets were found with motor neurons from the unlesioned side at 7 days postlesion. Thus, both the number of motor neurons with DNA damage and the extent of DNA-SSB in these neurons increase between 5-7 days after sciatic nerve avulsion.

Subsets of lumbar motor neurons (23%) on the lesioned side had comets at 10 days after sciatic nerve avulsion (Fig. 8A). Many of these comets had heads with a coma and a short granular tail (Fig. 8Be). Other comets had a small head or no head and a much longer tail (as long as 1240 μm, Fig. 8Bg,h). The tails were still comprised of large granules, though they were finer than those at 5 and 7 days. These comet patterns (Fig. 8Be,g) are similar to the comets in motor neurons induced by SNP (Fig. 7f, h). The heads of some comets had a nucleus that was fragmented or blebbing (Fig. 8Bf), indicating the advanced progression of DNA damage in motor neurons at 10 days after sciatic nerve avulsion. We therefore examined the 800 rpm cell suspension to identify motor neurons with comets, because these cells may be lighter after advanced DNA damage and are not precipitated at 400 rpm. Some comets were found in the 800 rpm cell suspensions (Fig. 8Bh). No comets were observed in the 400 rpm and 800 rpm cell suspensions from ventral horns of the unlesioned spinal cord at 10 days postlesion. At 14 days, 20 days, and 28 days after sciatic nerve avulsion, no comets were observed in motor neurons from either ipsilateral or contralateral lumbar ventral horns.

DNA damage caused by H_2O_2 and NO donor is different.

To identify relationships between DNA damage detected by the comet assay and DNA

fragmentation, motor neuron cell suspensions were exposed to 10 mM H_2O_2 or 10 μM SNP, and genomic DNA was extracted for gel electrophoresis. A hybrid of internucleosomal fragmentation and random fragmentation of DNA was observed in motor neurons exposed to H_2O_2 for 60 min and 90 min (Fig. 9). The DNA fragmentation coincides with the comet assay for the cells exposed to H_2O_2 for 60 min which detected about 31% comets (Fig. 3A). For 90 min exposure, the number of comets decreased (Fig. 3A), while DNA gel electrophoresis showed a ladder-smear hybrid (data not shown). In contrast, no prominent DNA fragmentation as either smear or ladder patterns was detected with 10 μM SNP, although the band of genomic DNA was slightly smaller than control (Fig. 9), consistent with the interpretation that the SNP comet pattern with large DNA granules corresponds to high molecular weight fragments caused by relatively few DNA-SSB. No obvious fragmentation was found in control samples incubated for the same time (Fig. 9). By the comet assay, a low level of spontaneous comets was found, but these were not reflected in DNA gels, thus confirming that the comet assay is a sensitive method for detecting early DNA damage in individual cells.

Degeneration of adult motor neurons after oxidative stress in vitro mirrors the comet assay.

We evaluated by light and electron microscopy the structure of adult motor neurons exposed H_2O_2 and NO donor (Fig. 10). The structure of control motor neuron cell bodies after 15 min and 90 min incubation in culture medium is preserved (Fig. 10a,b,k). These cells are large and round with a large nucleus containing dispersed chromatin throughout nucleoplasmic matrix. The cell membrane and the nuclear membrane are intact. Most mitochondria are intact. A few large vacuoles are present in the cytoplasm in some motor neurons. These vacuoles appear to be derived from distended Golgi

cisterns or from swollen mitochondria. These observations show motor neurons appear healthy after isolation and even after brief incubation under culture conditions.

Exposure to SNP and SNP plus H_2O_2 caused structural abnormalities in motor neurons that were dose- and time-related. After 15 min exposure to 10 μM SNP, motor neurons exhibited early chromatin condensation that was more prominent at 1 h exposure (Fig. 10b,c,l). SNP also induced massive swelling and degeneration of motor neuron mitochondria (Fig. 10l). The nuclear condensation and chromatin clumping was much more prominent after exposure to 100 μM SNP (Fig. 10e,f). After exposure to the combination of SNP plus H_2O_2, both cytoplasmic and nuclear condensation was obvious at 15 min, and, by 1 h, the nuclear condensation was very pronounced (Fig. 10g-j,m).

DISCUSSION

We studied DNA damage in motor neurons and have made several new findings. Oxidative stress to adult motor neurons by H_2O_2 and NO donor exposure *in vitro* causes rapid DNA-SSB. These ROS induce distinct DNA damage profiles; thus, comet patterns can serve as a fingerprint for different ROS-mediated insults to motor neurons. DNA-SSB also occur early in motor neurons *in vivo* prior to apoptosis induced by avulsion. The early DNA damage fingerprint in motor neurons destined to undergo apoptosis (Martin et al., 1999a) is similar to the fingerprint left by NO toxicity *in vitro*.

Adult motor neurons can be studied *in vitro*

We developed a new model system to study effects of ROS on DNA stability in motor

neurons. Motor neurons from adult spinal cord cannot be used to establish cell cultures; therefore, we developed a short-term, motor neuron-enriched cell suspension prepared from spinal cord ventral horn enlargements of adult rat. After trypsin digestion, adult motor neurons were fractionated by centrifugation, yielding a motor neuron-enriched cell suspension. The motor neuron enrichment of this cell system was characterized by immunophenotyping (e.g., CAT and NeuN), retrograde tracing, and electron microscopy. The majority of these motor neurons remain viable over short-term incubation (up to 12 h after isolation), and ~40% of these cells are still viable at 24 h incubation. This motor neuron system is very different from cultured embryonic motor neurons (Estévez et al., 1998). However, the purpose of our study was to evaluate whether ROS and axonal injury cause DNA instability in adult motor neurons, because of the relevance to ALS. Neurodegeneration can vary depending on neuronal maturity (Portera-Cailliau et al., 1997). We were interested specifically in determining how quickly ROS cause DNA-SSB in mature motor neurons and if DNA-SSB occur early during the *in vivo* progression of motor neuron apoptosis in the adult spinal cord.

ROS cause DNA-SSB in motor neurons

To assay for DNA damage at early stages, we used the single-cell gel electrophoresis method (comet assay). This assay is an established method for identifying strand breaks in DNA and, based on the principles of alkaline elution (Kohn, 1991), is the most sensitive method for detecting DNA-SSB in individual cells (Ostling and Johanson, 1984; Singh et al., 1988; Kindzelskii and Petty, 1999; Morris et al., 1999). We demonstrate the usefulness of this technique for identifying the occurrence and progression of early DNA damage in individual motor neurons that

are injured by ROS *in vitro* and axotomy *in vivo*.

H_2O_2 has dose- and time-related effects on adult motor neurons. H_2O_2 (10 mM) induces prominent DNA-SSB, evidenced by the increase in comet percentage and the comet patterns. Previous studies have shown that H_2O_2 induces DNA damage in leukocytes (Singh et al., 1988; Kindzelskii and Petty, 1999) and HeLa cells (Szmigiero and Studzian, 1988). The predominant form of DNA damage produced by H_2O_2 is SSB, with the ratio of double-strand to single-strand DNA breaks estimated to be 1 to 2000. Based on the comet patterns obtained at 15, 30 and 60 min of exposure to 10 mM H_2O_2, a progressive accumulation of DNA-SSB occurs in motor neurons. The heads become smaller and the tails become longer; thus, there is a shift to the mature comet pattern. At 90 min exposure, motor neurons with DNA-SSB have passed the comet moment, thus DNA-SSB are less frequently detected. Alternatively, motor neurons with DNA damage may disappear from the preparation because they are smaller and lighter or broken and thus are not captured by repelleting. These explanations may account for the decreased comet number and cell density after 90 min exposure.

A lower concentration of H_2O_2 caused an unexpected result. Motor neurons treated with 1 mM H_2O_2 had lower DNA damage. The explanation for this finding is uncertain. DNA repair mechanisms may be stimulated in motor neurons exposed to 1 mM H_2O_2, so that fewer comets are observed compared to controls. DNA repair kinetics are very rapid, with significant repair of DNA-SSB in leukocytes occurring within 2 minutes after irradiation (Mendiola-Cruz and Morales-Ramíres, 1999). DNA-SSB are repaired by DNA repair enzymes, some of which are enriched in motor neurons (Duguid et al., 1995). Thus, DNA-SSB induced by 1 mM H_2O_2 as well as those occurring spontaneously may be repaired. Perhaps only when levels of non-repaired or misrepaired

DNA damage are above a threshold level, motor neurons display comets. Alternatively, this concentration of H_2O_2 may be insufficient for inducing DNA damage in healthy motor neurons in suspension for a short time (possibly related to antioxidant enzymes in the medium), but it may enhance DNA damage in already dying or injured motor neurons that then disappear from the 400 rpm preparation when repelleting after exposure. However, 1 mM H_2O_2 exposure for up to 2 h was not sufficient enough to cause a loss of cells compared to time-matched controls. Therefore, the activation of DNA repair pathways in motor neurons is a possibility that warrants further examination.

NO may participate in the pathogenesis of motor neuron degeneration in ALS (Beckman et al., 1993) and in experimental models (Wu and Li, 1993; Estévez et al., 1998; Martin et al., 1999a). We tested the hypothesis that motor neurons exposed to NO donor accumulate DNA damage. Our results show that SNP is a potent inducer of DNA-SSB in motor neurons. Experiments with plasmid DNA have shown that NO and superoxide in combination or peroxynitrite alone induce DNA damage (Salgo et al., 1995; Inoue and Kawanishi, 1995). NO *per se* does not cause breakage to plasmid DNA. However, peroxynitrite causes prominent single-stranded DNA breaks at concentrations as low as 1 μM, with much higher concentrations (> 1 mM) needed for double-strand DNA breaks (Szabó and Ohshima, 1997). NO competes effectively with superoxide dismutase for superoxide to form peroxynitrite (Beckman et al., 1993). After injury, motor neurons become metabolically activated (Martin et al., 1999a); thus, endogenous superoxide production could be augmented in motor neurons because of injury related to dissection and digestion. These previous observations along with our recent results suggest that peroxynitrite may potently induce DNA-SSB in adult motor neurons.

Motor neurons exposed to NO donor develop DNA damage that is different from damage caused by H_2O_2. With SNP, DNA granules are prominent within the heads and tails of new comets and early mature comets and are very scattered in the heads of advanced comets. These ethidium bromide-positive large granules are likely to be very large single-strand fragments of DNA. With H_2O_2, DNA damage occurs first at peripheral chromatin domains and then the inner nuclear core chromatin, as reflected by comets with discrete halos and comets with very small heads and tails comprised of fine granules. The lengths of DNA fragments caused by H_2O_2 exposure are probably very different from the DNA damage caused by NO. This conclusion is supported by DNA fragmentation analysis. H_2O_2 induced a prominent smear-ladder hybrid of DNA fragments in motor neurons. This pattern is consistent with the comet assay finding showing tails consisting of very fine DNA granules. These tails are apparently internucleosomal and random fragments of DNA. Thus, H_2O_2 causes many smaller DNA fragments because of numerous SSB. In contrast, genomic DNA was mostly intact in motor neurons exposed to SNP for 60 mins. Therefore, the large DNA granules typical of the SNP comet patterns are likely to be very large fragments of DNA produced by fewer SSB. Thus, different oxidants may cause distinct DNA damage fingerprints, and different chromatin domains (Ferreira et al., 1997) in motor neurons may have differential vulnerabilities to ROS.

When motor neurons are exposed to NO donor in the presence of H_2O_2 (at a concentration that is apparently subthreshold for DNA damage, or possibly even protective), the combination is potently cytotoxic. Exposure of motor neurons to both SNP (10 μm or 100 μM) and 1mM H_2O_2 induces DNA damage and cell loss that are much more severe than that caused by either SNP (10 μM, 100 μM, 300 μM or 800 μM) or 1 mM H_2O_2 alone. The explanation for this toxic synergy is speculative. Peroxynitrite, formed by donated NO and endogenous superoxide, may cause

membrane damage resulting in the mobilization of transitional metals that bind DNA and locally catalyze the formation of highly toxic hydroxyl radicals or hydroxyl-like intermediates from H_2O_2.

DNA-SSB accumulate in motor neurons after axotomy with a fingerprint similar to NO toxicity

We applied the comet assay to an *in vivo* model of motor neuron apoptosis in adult spinal cord. Sciatic nerve avulsion in adult rat causes apoptosis of lumbar motor neurons over 7 to 14 days (Martin et al., 1999a). These motor neurons exhibit oxidative stress in the form of hydroxyl radical damage to DNA and peroxynitrite damage. At seven days after the lesion, subsets of motor neurons are undergoing DNA fragmentation as detected by *in situ* end labeling. Here, we found early DNA-SSB in motor neurons at 5 days after the lesion. The comet assay revealed a slow progression of DNA damage in motor neurons during 5-10 days postlesion. As comet tails become longer, the granules become finer, while the comet head shape becomes irregular. The comets of motor neurons after avulsion and the comets of motor neurons exposed to SNP *in vitro* are similar. This finding supports the idea that NO toxicity participates in the mechanisms for motor neuron apoptosis in the adult spinal cord (Martin et al., 1999a). Accumulation of DNA-SSB could be a primary signal for motor neuron apoptosis, possibly through p53-mediated pathways (Jayaraman and Prives, 1995). p53 is induced in adult motor neurons prior to apoptosis (Martin et al., 1999b), apparently coinciding with early DNA damage.

REFERENCES

Beckman JS, Carson M, Smith CD, Koppenol WH (1993) ALS, SOD and peroxynitrite. Nature 364:548.

Bradley WG, Krasin F (1982) A new hypothesis of the etiology of amyotrophic lateral sclerosis. The DNA hypothesis. Arch Neurol 39:677-680.

Duguid JR, Eble JN, Wilson TM, Kelly MR (1995) Differential and subcellular expression of the human multifunctional apurinic/apyrimidinic endonuclease (APE/ref-1) DNA repair enzyme. Cancer Res 55:6097-6102.

Estévez AG, Spear N, Manuel SM, Radi R, Henderson CE, Barbeito L, Beckman JS (1998) Nitric oxide and superoxide contribute to motor neuron apoptosis induced by trophic factor deprivation. J Neurosci 18:923-931.

Ferrante RJ, Browne SE, Shinobu LA, Bowling AC, Baik MJ, MacGarvey U, Kowall NW, Brown RH Jr, Beal MF (1997) Evidence of increased oxidative damage in both sporadic and familial amyotrophic lateral sclerosis. J Neurochem 69:2064-2074.

Ferreira J, Paolella G, Ramos C, Lamond AI (1997) Spatial organization of large-scale chromatin domains in the nucleus: a magnified view of single chromosome territories. J Cell Biol 139:197-1610.

Fitzmaurice PS, Shaw IC, Kleiner HE, Miller RT, Monks TJ, Lau SS, Mitchell JD, Lynch PG (1996) Evidence for DNA damage in amyotrophic lateral sclerosis. Muscle Nerve 19:797-798.

Inoue S, Kawanishi S (1995) Oxidative DNA damage induced by simultaneous generation of nitric oxide and superoxide. FEBS Lett 371:86-88.

Jayaraman L, Prives C (1995) Activation of p53 sequence-specific DNA binding by short single

strands of DNA requires the p53 C-terminus. Cell 81:1021-1029.

Kindzelski AL, Petty HR (1999) Ultrasensitive detection of hydrogen peroxide-mediated DNA damage after alkaline single cell gel electrophoresis using occultation microscopy and TUNEL labeling. Mutation Res 426:11-22.

Kohn KW (1991) Principles and practice of DNA filter elution. Pharmac Ther 49:55-77.

Levine AJ (1997) p53, the cellular gatekeeper for growth and division. Cell 88:323-331.

Martin LJ, Kaiser A, Price AC (1999a) Motor neuron degeneration after sciatic nerve avulsion in adult rat evolves with oxidative stress and is apoptosis. J Neurobiol 40:185-201.

Martin LJ, Kaiser A, Price AC (1999b) Oxidative stress and p53 induction may participate in the mechanisms for motor neuron apoptosis in adult spinal cord. Soc Neurosci Abstr 25:289.

Martin LJ (1999) Neuronal death in amyotrophic lateral sclerosis is apoptosis: possible contribution of a programmed cell death mechanism. J Neuropathol Exp Neurol 58:459-471.

Martin LJ, Price AC, Kaiser A, Shaikh AY, Liu Z (2000) Mechanisms for neuronal degeneration in amyotrophic lateral sclerosis and in models of motor neuron death. Int J Mol Med 5:3-13.

Mendiola-Cruz MT, Morales-Ramírez P (1999) Repair kinetics of gamma-ray induced DNA damage determined by single cell gel electrophoresis assay in murine leukocytes in vivo. Mutation Res 433:45-52

Morris EJ, Drexiler JC, Cheng K-Y, Wilson PM, Gin RM, Geller HM (1999) Optimization of single-cell gel electrophoresis (SCGE) for quantitative analysis of neuronal DNA damage. BioTechniques 26:282-289.

Ostling O, Johanson KJ (1984) Microelectrophoretic study of radiation-induced DNA damage in individual mammalian cells. Biochem Biophys Res Comm 123:291-298.

Polyak K, Xia Y, Zweier JL, Kinzler KW, Vogelstein B (1997) A model for p53-induced

apoptosis. Nature 389:300-305.

Portera-Cailliau C, Price DL, Martin LJ (1997) Non-NMDA and NMDA receptor-mediated

excitotoxic neuronal deaths in adult brain are morphologically distinct: further evidence for an

apoptosis-necrosis continuum. J Comp Neurol 378:87-104.

Salgo MG, Stone K, Squadrito GL, Battista JR, Pryor WA (1995) Peoxynitrite causes DNA nicks

in plasmid pBR322. Biochem Biophys Res Comm 210:1025-1030.

Singh NP, McCoy MT, Tice RR, Schneider EL (1988) A simple technique for quantitation of

low levels of DNA damage in individual cells. Exp Cell Res 175:184-191.

Szabó C, Ohshima H (1997) DNA damage induced by peroxynitrite: subsequent biological

effects. Nitric Oxide: Biology and Chemistry 1:373-385.

Szmigiero L, Studzian K (1988) H_2O_2 as a DNA fragmenting agent in the alkaline elution

interstrand crosslinking and DNA-protein crosslinking assays. Anal Biochem 168:88-93.

Wu W, Li L (1993) Inhibition of nitric oxide synthase reduces motoneuron death due to spinal

root avulsion. Neurosci Lett 153:121-124.

FIGURE LEGENDS

Figure 1: Characterization of the cell suspension of adult motor neurons. Scale bars: A (same for C), 100 µm; B (same for D), 25 µm; E (same for F), 18 µm; G, 10 µm; H, 12 µm. **A.** The majority of cells (~84% of the total number of cells) in the 400 rpm preparation exhibit NeuN immunofluorescence (green), demonstrating that these cells are neurons (box delineates area shown in B). **B.** NeuN immunofluorescence (green) is intense in the nuclei of these neurons, while the cytoplasm was labeled weakly or not labeled. **C.** Propidium iodide (PI, red) counterstaining of cell suspensions immunolabeled for NeuN (identical field is shown in A) reveals that NeuN positive cells exclude PI. Smaller nonneuronal glial cells are labeled with PI but not for NeuN. **D.** PI staining identifies the glial cell nuclei in samples stained for NeuN (same field is shown in B). **E and F.** Most of the neurons (~86% of total NeuN positive cells and 72% of total cells in the 400 rpm cell suspension) show choline acetyltransferase (CAT) immunofluorescence (E). CAT immunoreactivity is localized in the perikarya of motor neurons and thus these cells have PI nuclear staining (E, arrows, and F, red). **G.** Prelabeling lumbar motor neurons with retrograde tracer DAPI (blue) shows that most of the α-motor neurons with sciatic nerve axons sort into the 400 rpm cell suspension, and they comprise ~62% of the total cells. **H.** Only a few GFAP-positive astroglial cells and scattered GFAP processes (blue staining) are observed in the 400 rpm cell suspension. Some astroglial processes are attached to large neurons (red).

Figure 2: Viability of adult motor neurons in cell suspension over 24 h incubation in supplemented Neurobasal A, as evaluated by trypan blue staining. The number of viable cells and the total number of cells (viable cells plus trypan blue-stained cells) were counted in a hemocytometer under phase

contrast microscopy. Double asterisk denotes significant difference (p < 0.01) and single asterisk

denotes significant difference (p < 0.05) compared to the earlier time point.

Figure 3: H_2O_2 causes DNA-SSB in motor neurons. **A.** Histogram of the percentage of comets in

both control and 10 mM H_2O_2 treated motor neurons. Values are mean ± sem. Among the control

groups, the background number of comets was significantly greater (+, p < 0.05) at 30 min, 60 min,

and 90 min compared to 15 min. Exposure to 10 mM H_2O_2 increased significantly (**, p < 0.01) the

percentage of comets in motor neurons at 15 min, 30 min, and 60 min compared to the respective

time-control groups. With 60 min exposure to 10 mM H_2O_2, the number of comets was significantly

increased (o, p < 0.05) compared to 15 min exposure. With 90 min of exposure, the number of

comets decreased significantly compared to 90 min control (*, p < 0.05) and compared to 60 min

H_2O_2 (oo, p < 0.05).

B. Representative motor neuron comets in control groups. Scale bars: a, 190 µm; b (same for c, d,

e), 48 µm. **a.** Panoramic view of the cell distribution and a single comet in a microgel from a 400

rpm cell suspension incubated for 15 min under control conditions. The cell nuclei and the comet

are stained with ethidium bromide. Many large intact nuclei without comets are seen. **b.** Single

motor neuron comet at higher magnification. The comet consists of a head and a short tail. **c.** A

motor neuron comet in a 1 h control group with scattered large granules of DNA fragments in the

comet tail. **d.** At 2 h in the control groups, the comet head is still large and the tail is still short and

is comprised of fine DNA granules. **e.** An intact nucleus and a comet from a control group at 4 h.

The comet head is still large and the tail is still short and granular.

C. Representative motor neuron comets after exposure to 10 mM H_2O_2. Scale bars: a (same for c),

190 μm; e (same for b, d), 48 μm; f, 110 μm. **a.** After 30 min exposure to H_2O_2, the comet heads are

smaller and the tails longer than control comets, but the heads are more regular and the tails shorter

than those comets seen after 1 h exposure (compare with Cc and Cd). A large intact nucleus is

shown for comparison with the comets. **b.** Comets observed after 30 min exposure to H_2O_2. A dense

DNA core is surrounded by a less dense and reticular halo or coma of DNA. **c and d.** After 60 min

exposure to H_2O_2, the comet heads are more irregular and the tails are very long (> 620 μm or even

longer than 1 mm) and discontinuous. **e .** After 90 min exposure to 10 mM H_2O_2, DNA damage is

very severe and nuclei have large, irregular reticular heads, indicating the unwinding and uncoiling

of genomic DNA. The tail of this comet is short and stained faintly, indicating few DNA-SSB

remaining. **f.** After 45 min exposure to 150 mM H_2O_2 the comets have irregular small heads, and

much DNA is eluted from the nucleus forming long tails with broad ends.

Figure 4. Comet assay on motor neuron cell suspensions exposed to 10 μm SNP, 1 mM H_2O_2, or 10

μm SNP plus 1 mM H_2O_2. **A.** Histogram of comet assay results. Values are mean ± sem.

Compared to the untreated control groups, the percentage of comets decreased significantly (**, $p <$

0.01) after exposure to 1 mM H_2O_2 for 30 min, 60 min and 90 min. In contrast, 10 μm SNP induced

a marked increase (**, $p < 0.01$) in the number of comets at 15 min, 30 min, and 60 min exposure as

compared to the control groups. This increase in comets was significantly (++, $p < 0.01$) time-

related (e.g., 15 min vs 30 min, 30 min vs 1 h, and 15 min vs 1 h or 2 h). At 2 h, the percent comets

.in 10 μm SNP exposed motor neurons decreased significantly ($p < 0.01$) as compared to 1 h. After

exposure of motor neurons to 10 μm SNP plus 1 mM H_2O_2 the percent comets was decreased

significantly (*, $p < 0.05$ or **, $p < 0.01$) at 30 min, 1 h, and 2 h compared to the corresponding

control groups. Among the 10 μm SNP plus 1 mM H_2O_2 exposure times, the percent comets

increased significantly (+, $p < 0.05$) between 1 h and 2 h. The percent comets in the motor neurons

exposed to 10 μm SNP was significantly higher (oo, $p < 0.01$) than the percent comets found with 1

mM H_2O_2, or 10 μm SNP plus 1 mM H_2O_2 at 30 min, 1 h, and 2 h. There was no significance

difference among corresponding groups exposed to 1 mM H_2O_2 or 10 μm SNP plus 1 mM H_2O_2.

B. Histogram of the number of cells in the comet assay microgels. Value are mean ± sem. Cell

number was not significantly different among the untreated control groups over 2 h. Decreases in

cell number were found at 1 h ($p < 0.05$) and 2 h ($p < 0.01$) after 1 mM H_2O_2 compared to 15 min

after H_2O_2 and at 1 h and 2 h after 10 μm SNP compared to 15 min after SNP; however, no

decreases were found relative to time-matched controls. The most prominent decrease in cell

number was observed in motor neurons exposed to 10 μm SNP plus 1 mM H_2O_2 as compared to the

corresponding control groups and to treatments with either 1 mM H_2O_2 or 10 μm SNP alone.

C. Comets profiles after exposure to 10 μm SNP. Scale bars: a (same for c, e, and g), 275 μm; h

(same for b, d, and f), 70 μm. **a.** Comets in the cell suspensions exposed to 10 μm SNP for 15 min

have bright, large heads and very short, broad tails formed by large granules of DNA. **b.** A typical

comet (from C,a) observed with 10 μm SNP for 15 min. A nucleus with intact DNA is nearby.

c. The comets in the motor neurons exposed to 10 μm SNP for 30 min are more numerous than at

15 min, and their tails are longer. **d.** Typical comets (from C,c) observed with 10 μm SNP for 30

min. **e.** After 1 h exposure to 10 μm SNP the tails of comets are longer than the earlier time points.

f. The tail of a comet (from C,e) is much longer, but still granular. **g.** The comets of cells exposed to

10 μm SNP for 2 h have a similar pattern as some of the comets in samples exposed to 10 μm SNP

for 1h, but the nuclei appeared swollen in many cells compared to the 1h exposed samples. **h.**

Comet (from g) after exposure to 10 μm SNP for 2 h showing a short tail that merges with the

coma of the head.

Figure 5. Comet assay for motor neuron cell suspensions exposed to 100 μm SNP, 1 mM H_2O_2, and

100 μm SNP plus 1 mM H_2O_2. **A.** Histogram of the number of comets in microgels. Values are

mean ± sem. The percentages of comets in all the groups exposed to 100 μm SNP are significantly

higher than in the corresponding control groups, demonstrating that SNP at this dose induces DNA

damage in many cells. The level of significance was greater in the 15 min, 30 min and 1 h groups

(**, $p < 0.01$) compared to the 2 h group (*, $p < 0.05$). Exposure time-effects were not apparent with

100 μm SNP, reflecting that comet formation was transient rather than persistent, thus they

appeared and disappeared. Comet percentages in cells exposed to 100 μm SNP plus 1 mM H_2O_2

were increased significantly at 30 min ($p < 0.01$) and 1 h ($p < 0.05$), compared to untreated controls,

with comet numbers peaking at 30 min. The increase of comets may involve DNA damage in glial

cells, based on the comet patterns and the obvious fragmentation of most motor neurons (see Figure

6). With 100 μm SNP plus 1 mM H_2O_2, the percentages of comets at most times (30 min, 1 h and 2

h) were significantly higher (ΔΔ, $p < 0.01$) compared to the number of comets in cells exposed to 1

mM H_2O_2, but cells exposed to 100 μm SNP plus 1 mM H_2O_2 for 15 min (o, $p < 0.05$) and 2 h (oo, p

< 0.01) have significantly lower percentages of comets compared to the 100 μm SNP groups. At 2 h

of exposure to 100 μm SNP plus 1 mM H_2O_2 , the percentage of comets was significantly (#, p <

0.05) lower compared to 1 h exposure to the same treatment.

B. Histogram of cell number in the comet assay microgels. Values are mean ± sem. With 1 h

exposure to 100 μm SNP alone, cell number was lower relative to 15 min; however compared to

time-matched control cells, cell number was unchanged after exposure to 100 μm SNP alone.

Control and 1 mM H_2O_2 exposure groups are the same as those shown in Figure 4B. A prominent

loss of cells occurred at all times after exposure to 100 μm SNP plus 1 mM H_2O_2 (**, p < 0.01, for

15 min and 30 min; *, p < 0.05 for 1 h and 2 h) as compared to their control groups. Comparison

among groups exposed to 100 μm SNP plus 1 mM H_2O_2 and groups exposed to 100 μm SNP

showed that cell number is significantly (oo, p < 0.01) lower in the former groups at 15 min and 30

min. Comparison between groups exposed to 100 μm SNP plus 1 mM H_2O_2 and groups exposed to

1 mM H_2O_2 showed that cell number is significantly lower (Δ, p < 0.05; ΔΔ, p < 0.01) in former

groups at 15 min, 30 min and 2 h.

C. Comets profiles in cells treated with 100 μm and 300 μm SNP. Scale bars: a, 215 μm; d (same

for b, c, e), 52 μm; f (same for g, h), 60 μm. **a.** Panoramic view of cells and comets after 30 min

exposure to 100 μm SNP. **b.** Two comets (from C,a) with large heads, conspicuous comas, and

short granular tails. **c.** A comet after exposure to 100 μm SNP for 1 h displays a larger head and

longer granular tail than those shown for 30 min exposure. An intact nucleus is seen at the left of the

comet. **d.** Mature comet from cells exposed to 100 μm SNP for 1h with a head containing a DNA-

poor core and a very long tail. **e.** With 2 h of exposure to 100 μm SNP comets can be found with

large heads and diffuse comas and short granular tails, indicating DNA damage is at an earlier stage.

However, some nuclear profiles are large, swollen, and vacuolated. These two patterns may reflect

different stages of DNA damage. **f-h.** With 4 h exposure to 300 μm SNP, comet patterns were very

distinct. The heads of the comets were different in their DNA quantities. The comet (in f) has a

granular head and the comet (in g) has a smaller head than that in f, while the comet in h had almost

no head. The tails of these comets are composed of large granules typical of the SNP pattern.

Figure 6. Comets in the samples exposed to 1 mM H_2O_2 or 1 mM H_2O_2 with different doses of SNP (10 μm, 100 μm or 300 μm). Scale bars: a (same for e, g, h), 142 μm; c (same for b), 280 μm; d (same for f), 68 μm. **a.** Most nuclei in the cells exposed to 1 mM H_2O_2 for 15 min are large and intact without DNA damage. The comets typically found after exposure to 1 mM H_2O_2 have a large head and short tail with a narrow neck. **b.** After exposure to 1 mM H_2O_2 for 6 h the comet patterns are similar to the pattern found at 15 min. **c.** After exposure of cells to 100 μm SNP and 1 mM H_2O_2 for 15 min, cell density is low (see Fig. 5B). Large cells (i.e., motor neurons) are particularly sensitive to oxidants. Some large neuronal comets have irregular heads. Other comets appeared to originate from contaminating glial cells (see Fig. 1H). **d.** Two neuronal comets (shown at higher magnification from 6c) with one comet having a large round head with a prominent coma and a short, faint tail, and the other comet having an irregular head. **e.** Exposure of cells to 100 μm SNP and 1 mM H_2O_2 for 15 min also produced DNA damage in contaminating glial cells (see Fig. 1H). The heads of these comets are very small and the tails are very long with a narrow neck. The small heads (i.e., nucleus) and the narrow neck of the tail indicate that they are glial cell comets. **f.** After cells were exposed to 100 μm SNP and 1 mM H_2O_2 for 15 min, normal cell nuclei are observed rarely, but swollen nuclei and nuclear fragments containing DNA are observed frequently. **g.** Glial cell comets, based on the pattern and size, are found after exposure to 10 μm SNP plus 1 mM H_2O_2 for 30 min. **h.** A glial cell comet (after exposure to 300 μm SNP plus 1 mM H_2O_2 for 4 h) with a head that is fragmenting, indicating a late stage of nuclear damage and severe DNA damage.

Figure 7. Comet patterning as visualized by single-cell gel electrophoresis and ethidium bromide staining. Scale bars: a (same for b-i, k-m), 42 μm; p (same for j, n, o), 150 μm.

a. A large intact neuronal nucleus. The DNA is stained brightly, but no comet is present. **b.** A typical new comet with a large head and a very short tail, consisting of a few large granules. This type of comet appeared as background comets in control cells, cells exposed to 10 µM SNP for short time (15 min), and in lumbar motor neurons at 5 days after sciatic nerve avulsion. **c.** A comet with a head surrounded by a halo and a very short tail. **d.** A comet with a longer tail consisting of scattered large granules. This comet type is observed in control samples incubated for >2 h, indicating slowly progressed DNA damage. **e.** Comets with a large intensely-staining head surrounded by a very bright coma. These comets were observed often in neurons exposed to 10 µM SNP and in lumbar motor neurons at 10 days after sciatic nerve avulsion. **f.** Comets with a bright head and coma and a longer tail formed by very scattered large granules. This is the typical pattern of comet in the samples exposed to NO donor. **g.** Comets with a dissipating head and broad tail composed of more densely distributed granules. This is a matured comet pattern (from the comets shown in e or f) observed in cells exposed to lower concentrations of NO donor (10 µM SNP). **h.** Typical comet pattern with cells exposed to higher doses of SNP (300 µM, 800 µM) or to 100 µM SNP for a longer time period (4 h). The heads are small and granular and the tails consist of very large granules. **i.** A comet with a distinct head consisting of a halo surrounding a core (from cells exposed to 10 mM H_2O_2 for 30 min). **j.** A comet with a small head and very long thin tail found in cells exposed to 10 mM H_2O_2 for 30 or 60 min. **k.** Comets with irregular heads and faintly staining tails were observed in cells exposed to 100 µM (or 10 µM) SNP plus 1 mM H_2O_2 for 15 min, 30 min or 1h. **l.** A bright intact nucleus and a very small nucleus observed in cells exposed to 100 µM SNP with 1 mM H_2O_2 for 1h. The bright nucleus is much larger and stained more intensely than the smaller nucleus; both are glial cell nuclei (because even the larger nucleus is much smaller than the

nucleus shown in 7a). **m.** Comets from cells exposed to 1 mM H_2O_2 for 15 min show a typical

pattern. This pattern is a large head and a short broad tail with a short neck. **n.** The comets from

cells exposed to 150 mM H_2O_2 for 45 min show a distinct pattern. The tail is broad and long, and

the head is still large, indicating the DNA damage is very severe and the unwinding of DNA is

thorough, allowing for intense ethidium bromide staining. **o.** Two comets in cells exposed to 150

mM H_2O_2 for 45 min. These cells were prepared as a total cell suspension from ventral horn

enlargements without sorting. One comet is a large neuronal comet, and the other is a probable glial

cell comet. **p.** A glial cell comet in a field of swollen cells or cellular fragments from cells exposed

to 100 μM SNP and 1 mM H_2O_2 for 1h. The head is very small and the tail is very long with a

narrow neck and is stained faintly.

Figure 8. DNA-SSB occur in motor neurons after unilateral sciatic nerve avulsion.

A. Percent comets in lumbar motor neuron cell suspensions (400 rpm preparations) from the

lesioned side of spinal cord. The percentage of comets (to total number of large cells embedded)

increased significantly ($p < 0.05$) at 5 days (5D) and 7 days (7D) postlesion (with significantly more

comets at 7 days compared to 5 days), and then decreased at 10 days (10D) postlesion.

B. Motor neuron comets after unilateral sciatic nerve avulsion. Scale bars: a, h (same for c), 132

μm; g (same for b, d-f), 60 μm. **a.** At 5 days postlesion, the comet heads are large and round and

the tails are very short. **b.** A typical 5 day comet (from Ba) with a short tail. **c.** At 7 days postlesion,

the comet heads are large and the tails are longer than at 5 days, indicating the accumulation of

DNA-SSB. **d.** A typical 7 day comet (from Bc) with a tail that is formed by scattered, large DNA

granules. These comets are very similar to those produced by SNP but not H_2O_2. **e-g.** At 10 days

the similarities between the comets produced by axotomy and those produced by SNP become much more prominent. The comets (shown in e) have heads with a granular coma and granular tails similar to the comets found in cells exposed to 10 μM or 100 μM SNP. Some comets have an irregular head and a granular tail (shown in f). Other comets (shown in g) have longer tails formed by scattered large granules. **h.** At 10 days after the lesion, motor neurons comets can be found in the 800 rpm cell suspensions. These comets have long tails, indicating accumulation of many DNA-SSB.

Figure 9. Gel electrophoresis analysis of DNA damage in motor neuron cell suspensions. Motor neuron cell suspensions were treated as time-controls or were exposed to 10 μM SNP or 10 mM H_2O_2 for 60 min. Genomic DNA was extracted, end-labeled with digoxigenin, fractionated (1.5% gel), transferred to nylon membrane after which DNA was visualized with antibodies to digoxigenin. Genomic DNA was intact in control motor neurons. In motor neurons treated with NO donor, the genomic DNA band was slightly lower in size compared to control. In motor neurons exposed to H_2O_2, genomic DNA was fragmented as a coexisting smear-ladder pattern. Molecular weight (MW) standards (in base pairs) are: from top to bottom- 2176, 1766, 1230, 1033, 653, 517, 453, 394, 298, 234, and 220.

Figure 10. Structure of adult motor neurons in suspension as revealed by high-resolution light microscopy and electron microscopy. a-j, 1 μm-think plastic sections; scale bar (shown in a): a, 4.36 μm; b, 4.84 μm ; c,d,f, 3.6 μm ; e, 3.38 μm; g, 4.32 μm; h, 3.75 μm; i, 4.88 μm; j, 2.86 μm. k-m; electron micrograph scale bars: k, 2.52 μm; l, 3.27 μm; m, 4.68 μm.

a, b. Motor neurons incubated for 15 min (a) and 90 min (b) in medium under control conditions. The cells are round with a nucleus containing dispersed chromatin surrounded by mostly intact cytoplasm, although some vacuoles are present. **c, d.** Motor neurons incubated for 15 min (c) and 60 min (d) in 10 μM SNP. At 15 min, the nucleus appears relatively normal; however, at 1h the nucleus shows clumping of chromatin. Many more mitochondria are swollen compared to control. **e, f.** Motor neurons incubated for 15 min (e) and 60 min (f) in 100 μM SNP. At 15 min, the motor neurons are similar to those seen at 1 h with exposure to 10 μM SNP, and at 1 h the nucleus shows prominent chromatin clumping. **g, h.** Motor neurons incubated for 15 min (g) and 60 min (h) in 10 μM SNP plus 1 mM H_2O_2. Motor neurons undergo both cytoplasmic and nuclear condensation at 15 min and at 1 h the nucleus is condensed and the cytoplasm then becomes paler. **i, j.** Motor neurons incubated for 15 min (i) and 60 min (j) in 100 μM SNP plus 1 mM H_2O_2. The cytoplasmic damage is more severe compared to 10 μM SNP plus 1 mM H_2O_2, particularly at 1 h it is fragmented. **k.** The ultrastructure of time-control (90 min) motor neurons is normal. Most of the mitochondria are intact and not swollen and the cytoplasmic matrix is enriched in ribosomes and rough endoplasmic reticulum. The nucleus has dispersed chromatin. **l.** After exposure to 10 μM SNP for 1 h the cytoplasm is dark, severely vacuolated (corresponding to massively swollen mitochondria) and the nucleus is condensing. **m.** After exposure to 10 μM SNP plus 1 mM H_2O_2 for 15 min, mitochondria are swollen and the chromatin is condensing at the periphery of the nucleus.
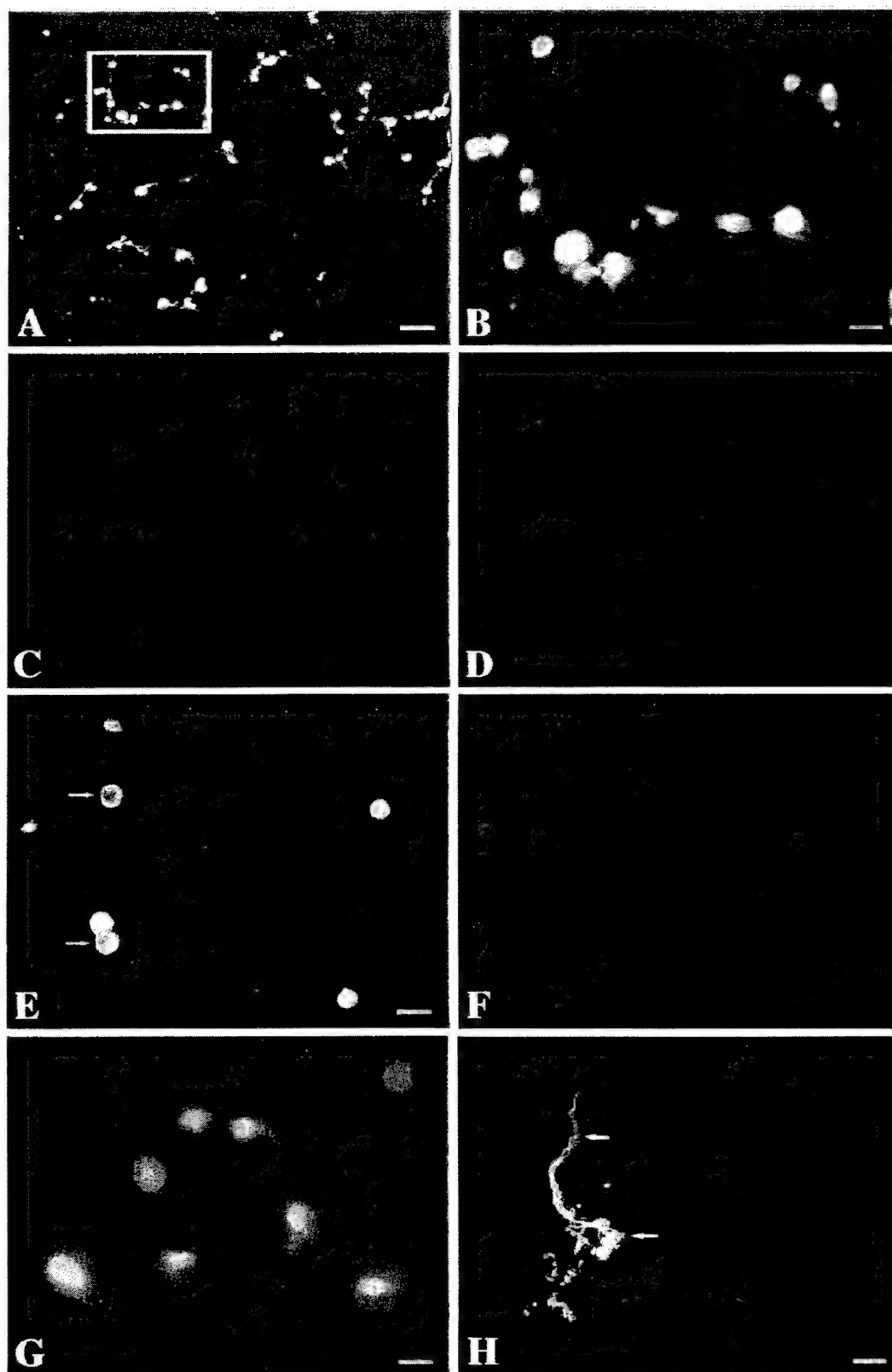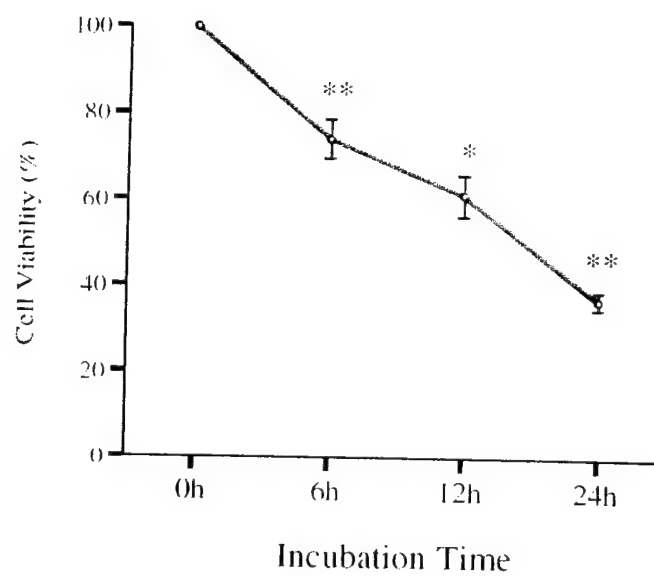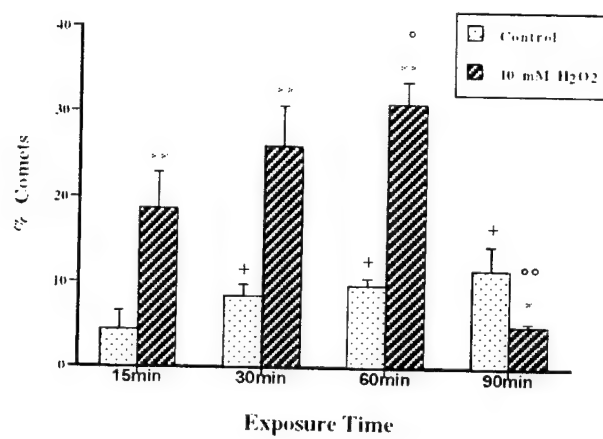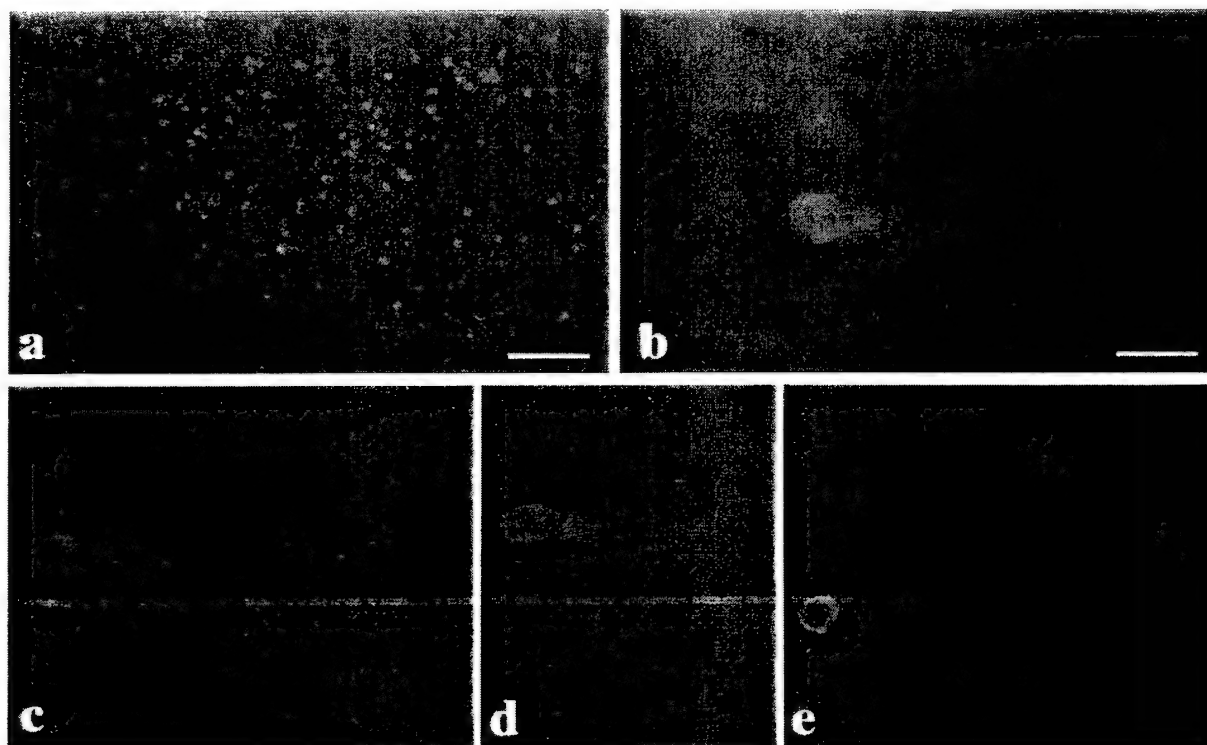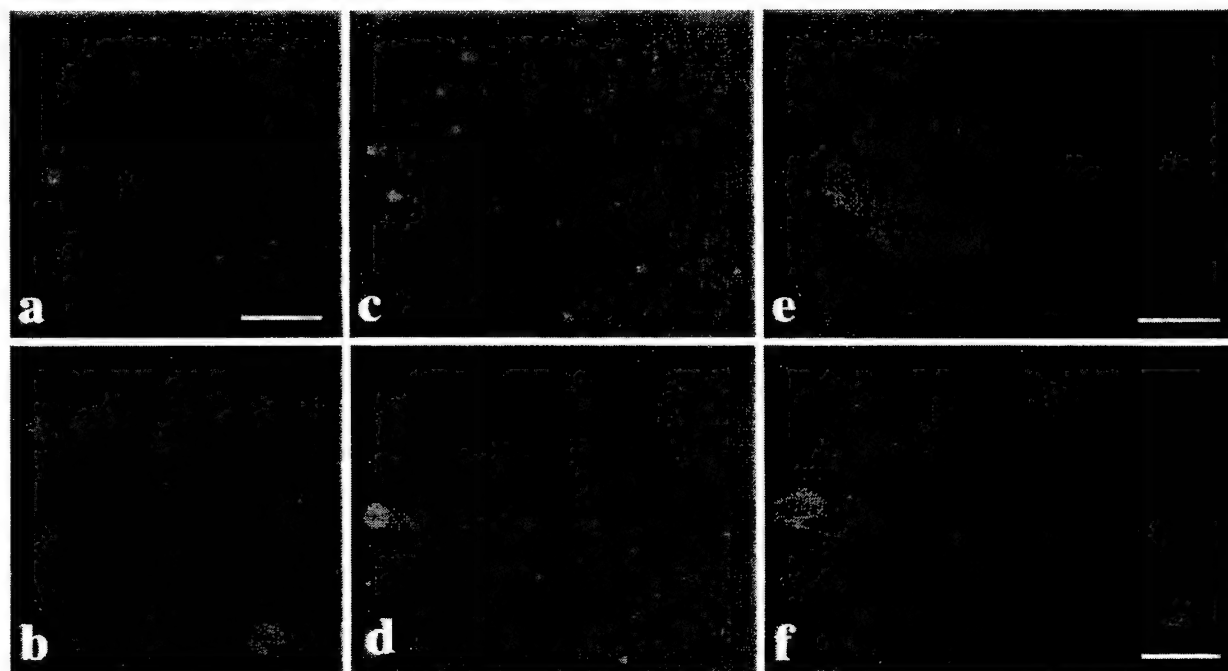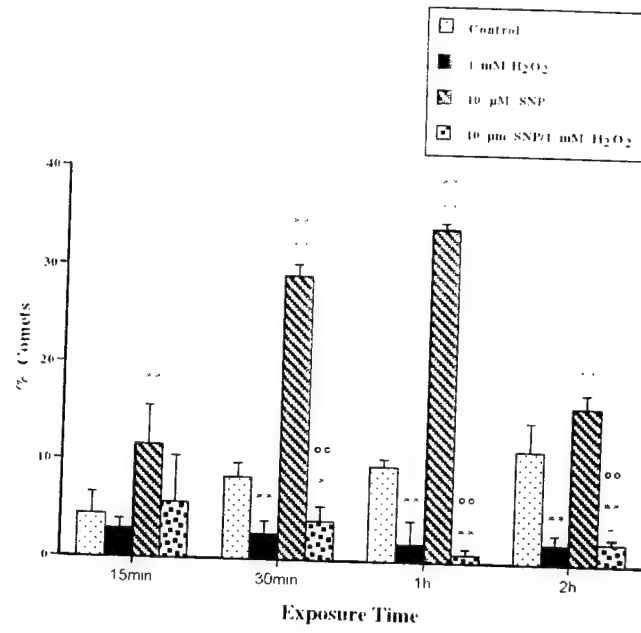
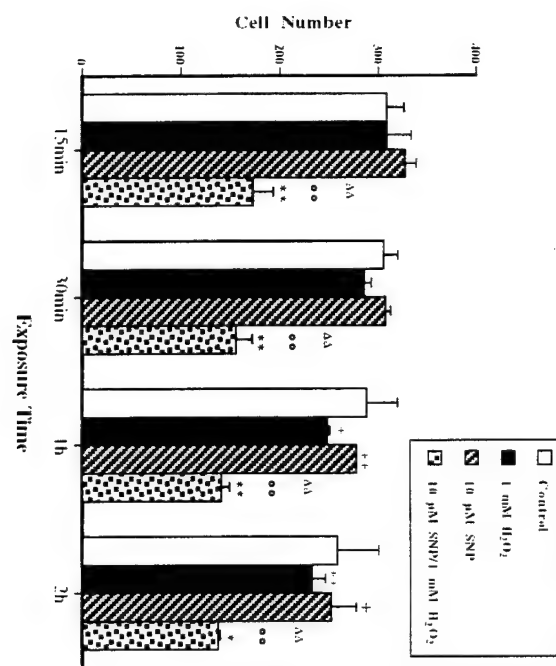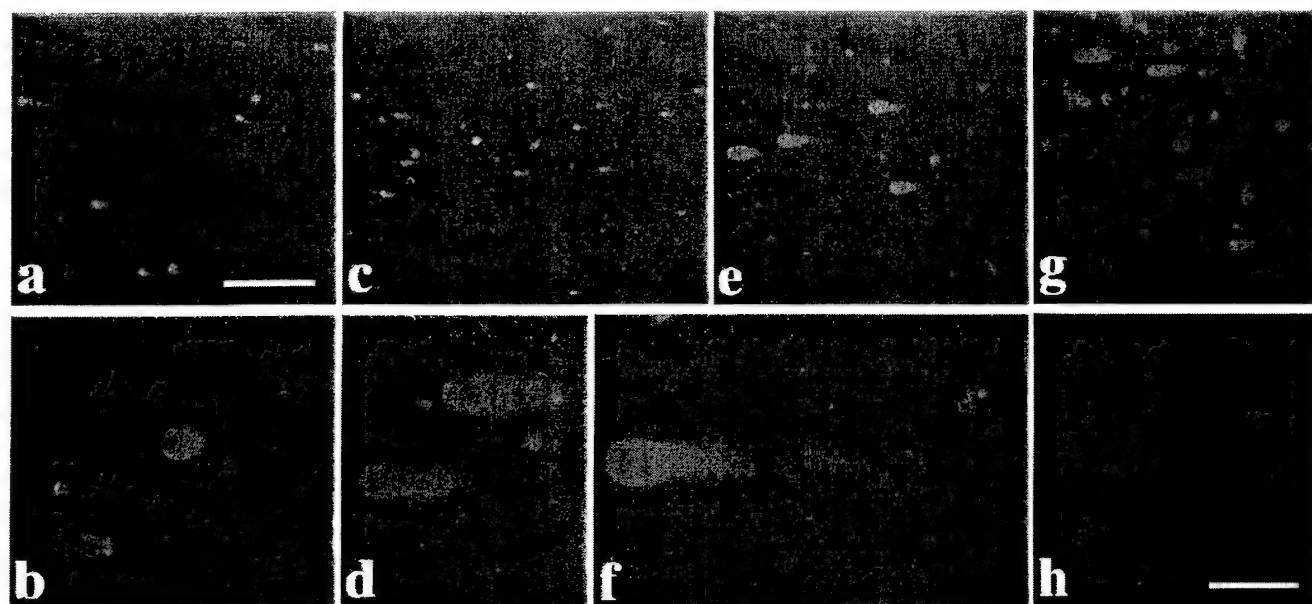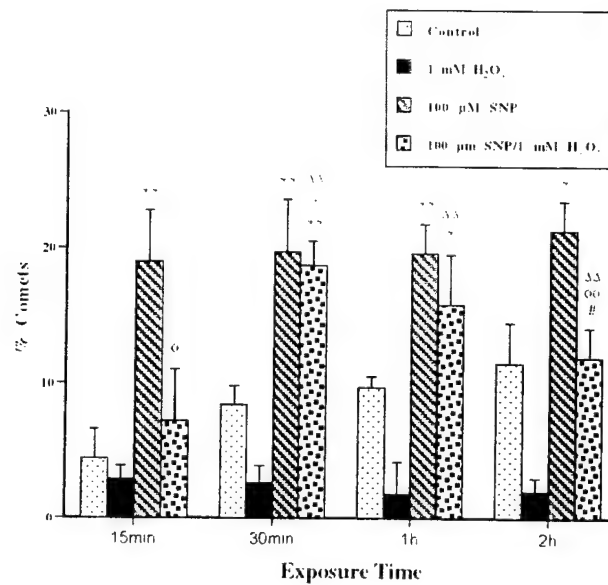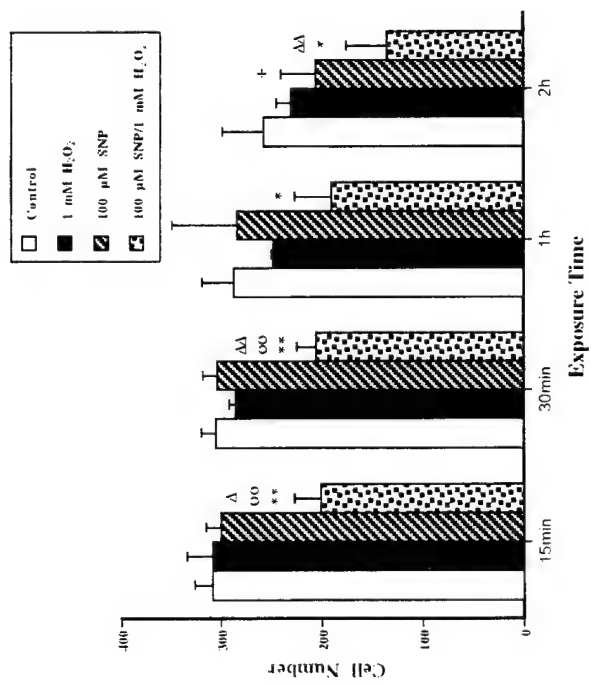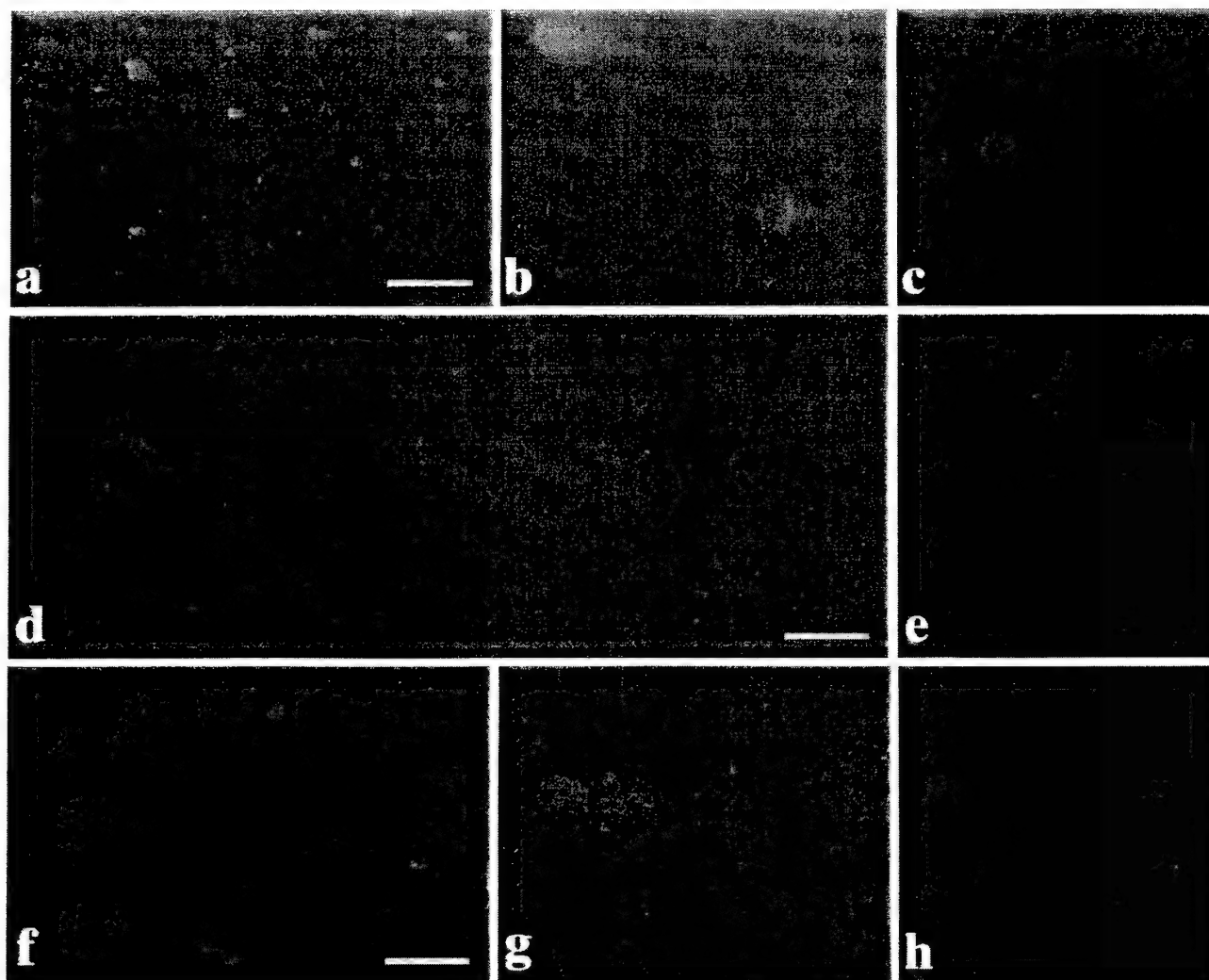FIGURE 1

FIGURE 2

FIGURE 3A

B

C

FIGURE 3B, C

FIGURE 4A

FIGURE 4B

FIGURE 4C

FIGURE 5A

FIGURE 5B

FIGURE 5C

FIGURE 6

FIGURE 7

% Comet

Days Post Lesion

5D 7D 10D
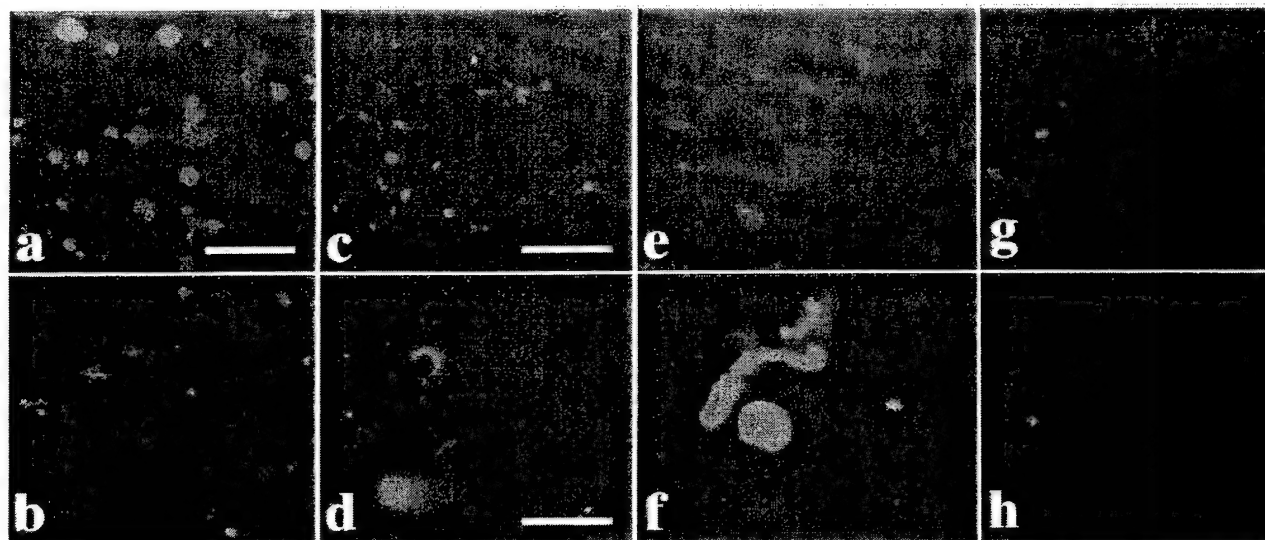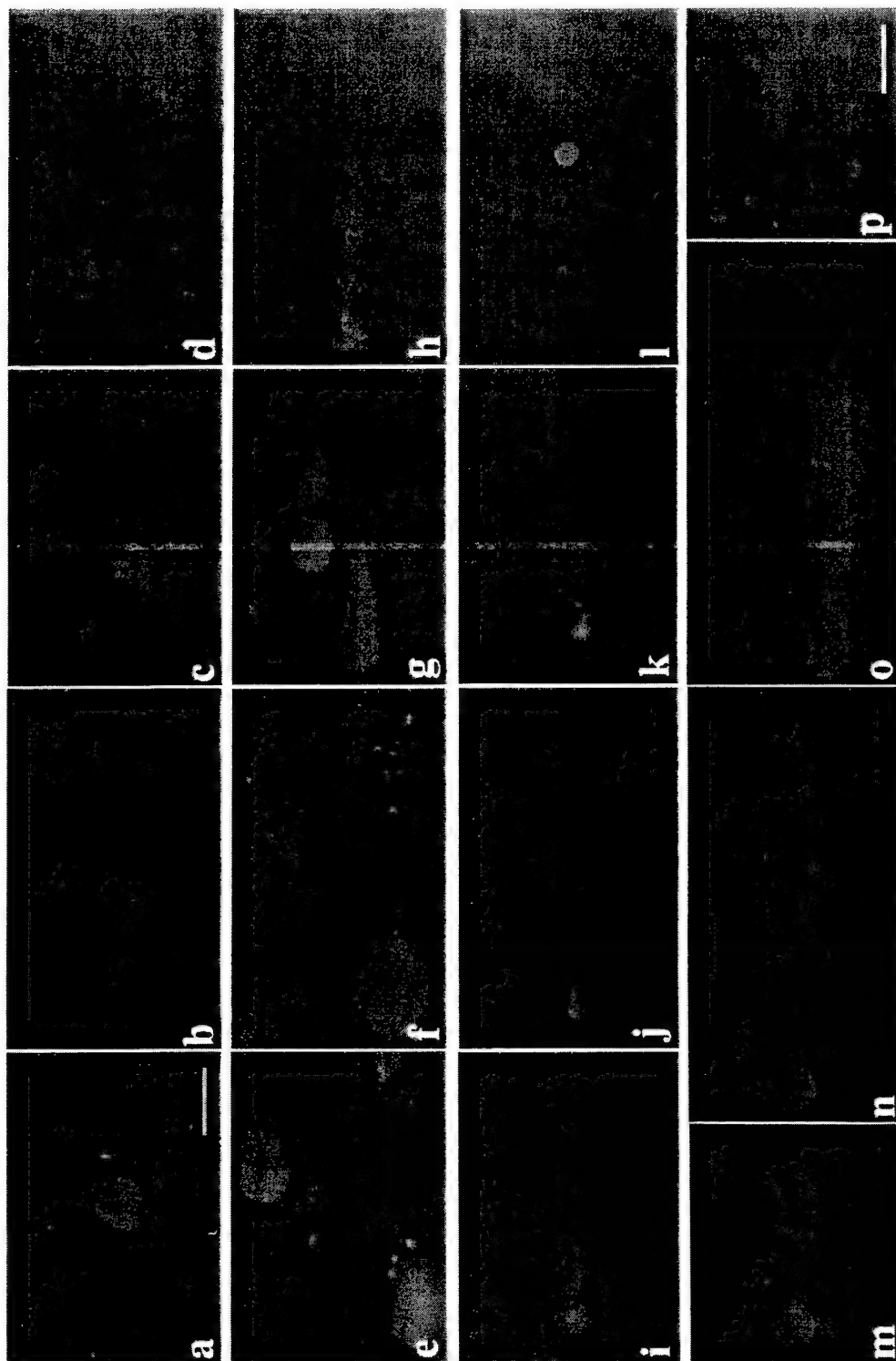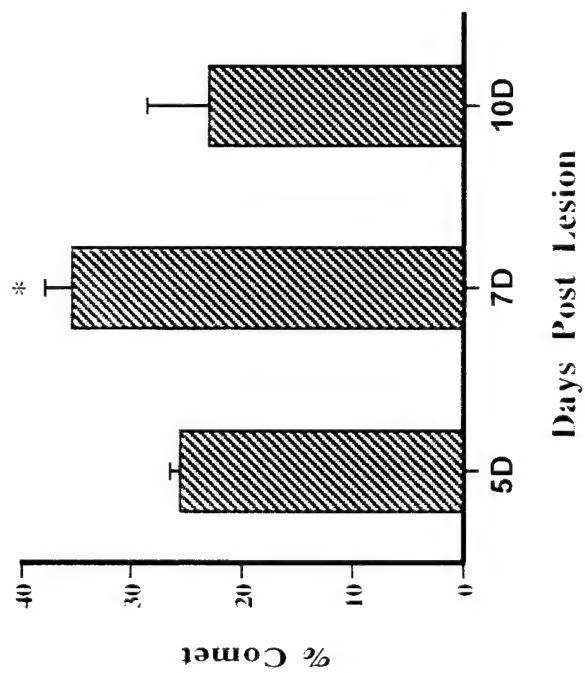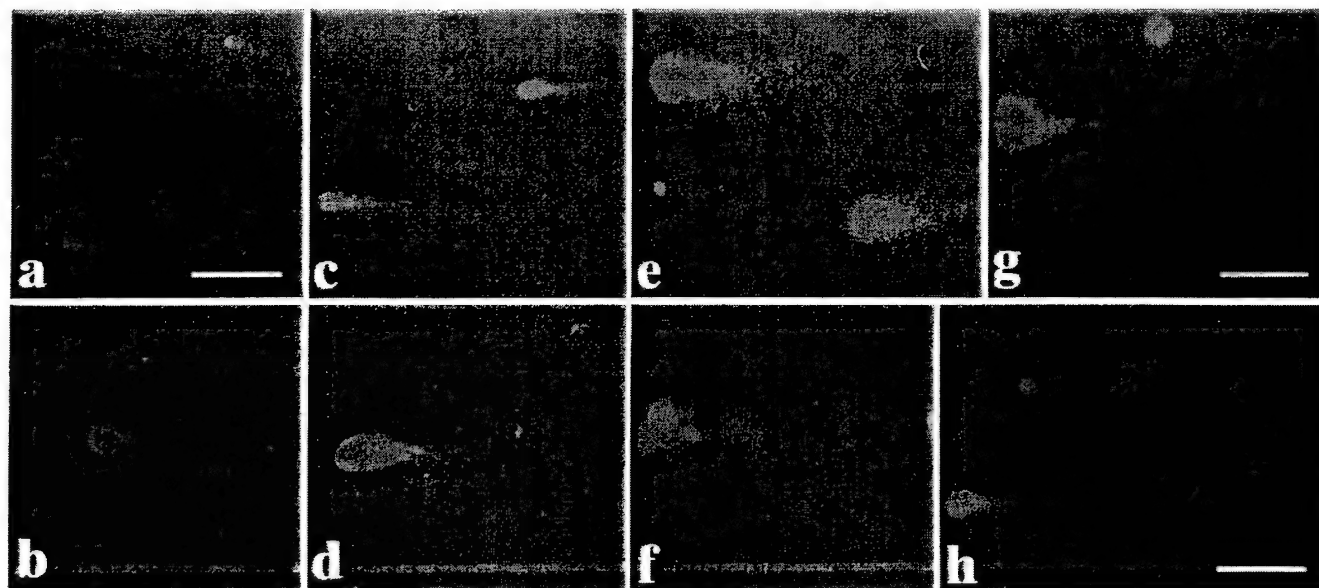
FIGURE 8A

FIGURE 8B

FIGURE 9

Control SNP H₂O₂ MW
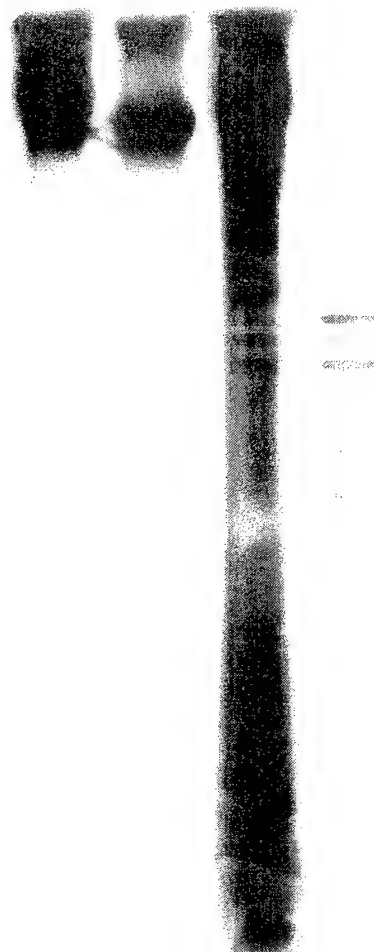
FIGURE 10
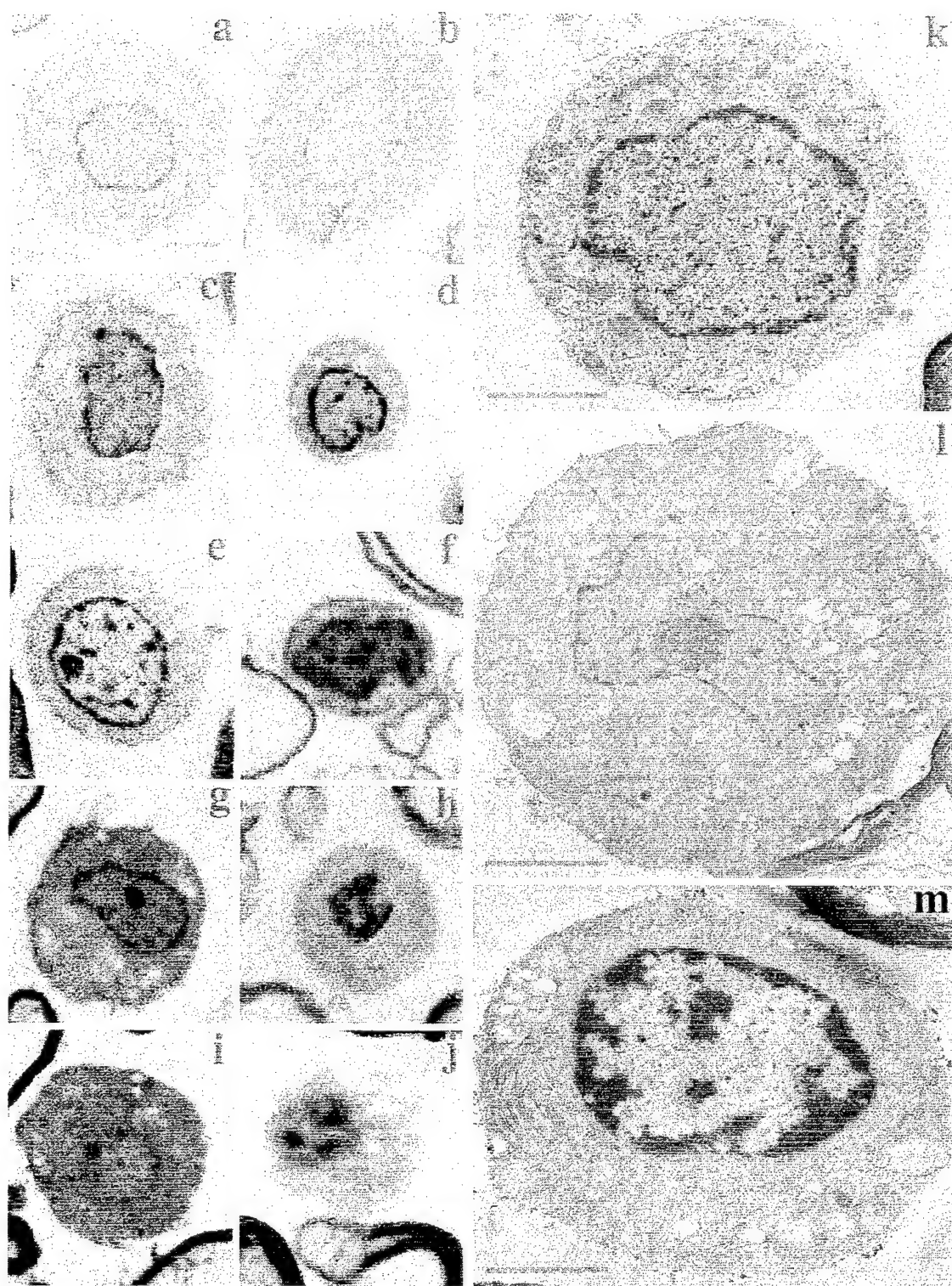
EARLY NEURODEGENERATION AFTER HYPOXIA-ISCHEMIA IN NEONATAL RAT IS

NECROSIS WHILE DELAYED NEURONAL DEATH IS APOPTOSIS

Frances J. Northington, M. D. [1], Donna M. Ferriero, M. D.[2], Ernest M. Graham, M.D.[3], Richard

J. Traystman, Ph.D. [4], and Lee J. Martin, Ph.D. [5].

Eudowood Neonatal Pulmonary Division, Departments of Pediatrics [1], Gynecology/Obstetrics [3],

Anesthesiology/Critical Care Medicine [4] and Pathology [5]. The Johns Hopkins Medical

Institutions, Baltimore, MD 21287. Dept. of Neurology [2], University of California-San

Francisco, San Francisco, CA 94143

Running head title: Neuronal injury after neonatal hypoxia-ischemia

Corresponding Author:
Frances J. Northington, M.D.
Eudowood Neonatal Pulmonary Division
Department of Pediatrics
CMSC 210
Johns Hopkins Hospital
600 N. Wolfe Street
Baltimore, MD 21287
410-955-5259
410-955-0298 fax
fnorthin @ welchlink.welch.jhu.edu

Abstract

We used silver staining to demonstrate neuronal cell body, axonal, and terminal degeneration in brains from p7 rat pups recovered for 0,1.5,3,6,24,48,72 h, and 6 days following hypoxia-ischemia. We found that initial injury is evident in ipsilateral forebrain by 3h following hypoxia-ischemia, while injury in ventral basal thalamus develops at 24h. A secondary phase of injury occurs at 48h in ipsilateral cortex, but not until 6 days in basal ganglia. Initial injury in striatum and cortex is necrosis, but in thalamus the neurodegeneration is primarily apoptosis. Degeneration also occurs in bilateral white matter tracts, and in synaptic terminal fields associated with apoptosis in regions remote from the primary injury. These results show that hypoxia-ischemia in the developing brain causes both early and delayed neurodegeneration in CNS systems in which the morphology of neuronal death is determined by time, region and patterns of neuronal connectivity.

Introduction

While acute perinatal brain injury does not account for the majority of cerebral palsy (Nelson and Grether, 1999), the neurologic handicaps caused by perinatal anoxia due to asphyxia and lack of cerebral blood flow are severe (Lorenz et al., 1998). The mechanisms for brain injury after hypoxia/ischemia are thought to include energy failure, free radical damage, cytokine and excitatory amino acid release and caspase-dependant cell death (Barks and Silverstein, 1992; Cheng et al., 1998; Hagan et al., 1996; Liu et al., 1996; Martin et al., 1997; McDonald et al., 1988). Yet, the mechanisms that underlie the overall pattern and timing of neuronal injury after neonatal hypoxia-ischemia remain unclear. Understanding the role of neuronal connections in the evolution of hypoxic-ischemic injury in the immature brain is necessary to fully explain the modes of neurodegeneration and the subsequent cognitive, motor, sensory and attentional disabilities that occur after perinatal brain injury (Lorenz et al., 1998).

Necrosis is a likely cause of acute neuronal cell death in the ipsilateral cortex and basal ganglia after neonatal hypoxic-ischemic injury (Rice, 1981; Towfighi et al., 1995) but the structure of cell death in remote regions has not been investigated. Demonstration that caspase inhibitors provide neuroprotection in this model (Cheng et al., 1998), suggests that cell death can occur by both necrosis and apoptosis or by cytokine-mediated inflammatory reaction. Neuronal cell death following trophic factor withdrawal, as occurs after interruption of neuronal connectivity by axotomy and during brain development, also has characteristics of apoptosis (Eves et al., 1996; Li et al., 1998).

During the perinatal period, neuronal connections are forming between brain regions (Bolz et al., 1990; Shatz, 1996). Developing neurons are highly dependent on trophic support. Interruption of neuronal connectivity and resultant target deprivation causes cell death in the

immature brain more rapidly and frequently than in the mature brain (Miller and Kuhn, 1997). Loss of connectivity from deafferentation is also a mechanism of injury in the developing brain (Kotak and Sanes, 1997; Miller and Kuhn, 1997). The potential for neuronal connectivity to dictate the selective distribution of brain injury in the neonate has been suspected (Martin et al., 1997). However, the role of neuronal connectivity in mediating the timing, pattern, and extent of delayed injury in newborns remains unknown.

Thus, brain damage after hypoxia-ischemia in newborns could result from mechanisms directly related to the hypoxic-ischemic insult per se, (e.g. energy failure and acute cell necrosis) and from secondary mechanisms triggered by the resultant early-occurring neurodegeneration. In this study, we tested the hypothesis that selective regional vulnerability and mode of neuronal cell death after hypoxia-ischemia are dictated by the distribution of neuronal connections in the immature brain.

Methods

Hypoxia-ischemia in p7 rats: The Rice-Vannucci **(Rice, 1981)** neonatal adaptation of the Levine procedure **(Levine, 1960)** was used to cause hypoxic ischemic brain injury in seven day old (p7) rats. In brief, rat pups were anesthetized with 2.5% halothane, 15% nitrous oxide, in O_2. The right common carotid artery was permanently ligated (in sham controls the ligature was passed around the artery and removed). After the wound was sutured, the pups recovered from anesthesia and returned to the dam. 2 hours later, pups were placed in an airtight container in a 37^0 C water bath through which humidified 8% O_2, balance nitrogen flowed for 150 min. After hypoxia, pups were returned to the dam until sacrifice.

Brains were retrieved at 0, 1.5, 3, 6, 24, 48, 72 hours, and 6 days (n=6 for each time point) following the end of hypoxia. The multiple early time points were chosen because our data, as well as that of others, showed a faster progression of injury after hypoxia-ischemia in neonates as compared to adults (Martin et al., 1997; Towfighi et al., 1995). These time points would allow detection of small, but possibly important, differences in time of onset of injury within regions undergoing primary acute neurodegeneration. The later time points allow identification of the extent of injury in axonal pathways and in remote regions. Control groups consisted of a) sham operated littermates b) littermates with carotid ligation not exposed to hypoxia, and c) littermates exposed to hypoxia alone. Sham controls were sacrificed on postnatal day 7, 8, 9, 10, and 14 (n= 4 at each age) to control for occurrence of naturally occurring cell death in the developing brain. Hypoxia only controls, sacrificed at 24 and 72 h and 6 days after hypoxia, were used to demonstrate that injury in remote regions is not due to systemic hypoxemia (n= 6 at each time point). Ligation only controls, sacrificed at 24 and 72 h and 6 days after surgery, were used to validate our use of the model (n= 6 at each time point).

All animal studies received prior approval from the Animal Care and Use Committee of Johns Hopkins University School of Medicine and were performed in accordance with the NIH "Guide for the Care and Use of Laboratory Animals", U.S. Department of Health and Human Services 85-23, 1985.

Retrograde Tracing: To reveal the afferent and efferent connections with the ipsilateral cortex, anesthetized p4 pups (n=6) were secured in a miniature stereotaxic apparatus (Stoelting, Wood Dale, IL), the scalp incised, the skull overlying the parasaggital parietal/occipital cortex removed and 10nl of the flouresent retrograde tracer, Flurogold (Flurochrome Inc., Englewood, CO),

injected into the superficial cortex. The scalp was sutured and the pups returned to the dam until

p7. To demonstrate the presence cell death within regions with connections to the ipsilateral

cortex, rat pups (n=6) injected with flurogold on p4 were exposed to hypoxia-ischemia as

described above and perfused 48 hours after hypoxia for combined flurogold

immunocytochemistry and cresyl violet staining.

Tissue preparation: Animals were killed with an overdose of pentobarbital, 65mg/kg IP, and

exsanguinated with cold 0.1 M PBS (pH7.4) via intra-cardiac perfusion. Brains were perfusion

fixed with 4% paraformaldehyde in PBS for 30m at 4ml/min. The brains were removed, post-

fixed in 4% paraformaldehyde overnight, cryoprotected in 30% sucrose and frozen in isopentane

(-30^0). 60μ coronal sections were cut on a sliding microtome for cresyl violet,

immunocytochemistry, and silver staining.

Immunocytochemistry: In preparation for detection of retrograde labeling, sections were washed

in 0.05M TBS (pH=7.4, 3 x 10m), endogenous peroxidase activity blocked with cold

methanol/H_2O_2, permeabilized with 0.04% triton (TX) (30 m), and blocked with 4% normal goat

serum (NGS)/0.01% TX (60m). Tissues were incubated with anti-flurogold antibody

(Chemicon, Temecula, CA) 1:5000) in 2%NGS/0.01%TX overnight at 4^0C. Sections were

washed (TBS, 3X10m), incubated with GARB (Fab_2) (ICN-Cappel, West Chester, PA, 1:75,

60m), washed, and incubated with rabbit peroxidase anti-peroxidase (Sternberger Monoclonals,

Baltimore, MD) (1:200, 60m). Immunoreactivity was detected using diaminobenzidine as the

chromagen.

Apoptotic Profiles: Both silver and cresyl violet staining allowed examination of nuclear

morphology in degenerating cells with ready identification of necrotic and apoptotic cells in

most cases. Counts of cells within the thalamus meeting the light microscopic morphologic

criteria for apoptosis (Martin et al., 1998) were counted in three, 400x fields with the aid of a

grid on cresyl violet stained sections. Only cells with a few clearly defined large, regular

chromatin clumps were counted as apoptotic. Counts in the three fields were averaged to give a

single value for each animal.

Silver-Staining: Silver staining allows identification of aggregated neurofilament proteins in

degenerating neuronal elements within specific neuroanatomical regions. It has been validated

and is a highly reproducible technique for identification of neuronal injury (Du et al., 1998). For

silver staining, coronal sections were washed repeatedly in PBS for 48 hours to remove sucrose.

Tissue was reimmersed in 4% paraformaldehyde/0.1M PBS x 96 hours. FD Neuro Silver Kit (FD

Neurotechnologies Inc., Baltimore, MD) was used for silver staining. Silver-stained tissue was

mounted, cover-slipped without dehydration in ETOH, and protected from light.

Optical Densitometry: Optical Densitometry (OD) was used for quantitative analysis of time

course of neurodegeneration after hypoxia-ischemia within the cortex, striatum, and thalamus.

Previous time courses, in this model have utilized cresyl violet and H&E histochemistry. OD of

silver stained sections, allowed the contribution of axonal, terminal and cell body damage to the

overall progression of injury after hypoxia-ischemia to be determined in contrast to the previous

methods which primarily evaluated injury to the cell body.

Silver stained sections from 3 coronal levels were analyzed. The levels were 1) anterior

striatum, 2) mid striatum at the level of the anterior commissure, and 3) the level of hippocampal dentate gyrus, including ventral basal thalamic nuclei. Parasagittal cortex and striatum were analyzed in all 3, and 2 of the 3 coronal levels respectively. Within the thalamus, the ventral basal complex including lateral geniculate nucleus, which has major projections to cortex was analyzed. Time of onset of initial neurodegeneration and additional progression of injury were compared between ipsilateral cortex, striatum, and thalamus.

Sections were digitized using an image analysis system and LA Inquiry Software (Loats Assoc., Westminster, MD). OD measurements were obtained from outlined areas of interest in parasagittal cortex at each of 3 coronal levels, from striatum in the 2 anterior-most sections, and from the ventral basal thalamus in the most posterior section. The measurements for cortex and striatum were averaged to give one value/region/animal. OD measurements were corrected for background staining by subtracting the OD in a contralateral structure with equal neuronal density but without evidence of injury. This correction for cell density plus the use of an average integrated OD over the entire sample should minimize any contribution of variation in size of area of interest to the results in relation to progression of injury, (i.e. edema or atrophy). Based on previous description of the present model (Towfighi et al., 1991) and present data, it was found that cavitary lesions develop in the parasagittal cortex at ≥ 72 hours, making it impossible to obtain relevant densitometry measurements. Therefore, we made no measurements in the cortical samples after 48 hours. The number of animals with cavitary cortical lesions was recorded separately.

Statistical Analysis:. Two-way ANOVA was used to compare OD measurements between control and experimental groups over time and between regions after hypoxia-ischemia.

ANOVA was used to compare apoptotic profile counts in the thalamus over time after hypoxia-ischemia. Post hoc testing for individual differences was performed with Fisher's analysis. A p value < 0.05 was used to determine significance.

Results

The onset of damage in the ipsilateral forebrain and thalamus is time-dependent and progressive, and it has an uneven distribution within regions: Forebrain neurodegeneration precedes thalamic neurodegeneration after neonatal hypoxic-ischemic brain injury (Fig. 1). Silver staining can be used as a marker for neurodegeneration. These silver depositions can represent degeneration of neuronal cell bodies and processes (axons, dendrites and terminals) (Du et al., 1998). In ipsilateral cerebral cortex and striatum silver staining was present by 3 hours after hypoxia-ischemia (p<0.05 vs control) (data are expressed as mean±SEM). Not until 24 hours after hypoxia-ischemia did optical density increase in the ventral basal thalamus. Eighty-three percent of rats exhibited cavitary cortical lesions by 72 hours after hypoxia-ischemia, therefore no further optical density measurements were obtained after 48 hours in the cerebral cortex. Injury progresses in the cortex at 48 hours and in the striatum and thalamus at 6 days (p<0.05 vs OD at time of first appearance of injury), suggesting ongoing neurodegeneration after initial injury.

The damage in cerebral cortex and striatum was discontinuous (Fig. 2). This pattern cannot be explained by tissue blood flow differences because of the close proximity of viable tissue to injured regions. This is notably evident in the patchy degeneration in the striatum. In figure 2 the arrows indicate neurodegeneration in the cortex and arrowheads indicate degeneration in the striatum. Silver deposition within cortical columns within the ipsilateral

forebrain is consistent with the columnar injury previously described in this model (Towfighi et al., 1997) and demonstrates that the present techniques identify the expected areas of injury and allows discrimination of injured from non-injured tissue within regions with a high degree of resolution. The interdigitation of injured and non-injured tissue is evident in the striatum (Fig. 2, panel B)

The validity of this model and the effect of the chosen duration of hypoxia (2.5 hours) to cause a consistent severe injury is supported by the finding of progression to cortical cavitation in 83% of brains obtained >48 hours after the end of hypoxia-ischemia and by the relatively small amount of variability in the measures of injury with OD.

In ipsilateral forebrain, neurodegeneration occurring immediately after hypoxia-ischemia is necrosis but delayed neurodegeneration is necrosis and apoptosis: Analysis of cresyl violet and silver stained sections allows identification of cells demonstrating clear light microscopic morphologic evidence of necrosis or apoptosis. Analysis of the ipsilateral cortex and striatum, shows predominant necrosis immediately after hypoxia-ischemia. At three hours, the major phenotypes of these neurons include irregularly condensed chromatin, argyrophillic cytoplasm, and disintegration of cellular membranes. (Figure 3, panel A-silver stain-ipsilateral striatum, three hours after hypoxia-ischemia, panel B- cresyl violet-ipsilateral cortex, three hours after hypoxia-ischemia, arrows indicate necrotic neurodegeneration)

In contrast to early ischemic necrosis seen in ipsilateral cortex and striatum after hypoxia-ischemia, morphology of injury within these regions at later time points is more varied. When examined at the time of the secondary phase of injury, neurons within upper and lower layers of parasagittal cortex and the striatum exhibit the light microscopic hallmarks of apoptosis and

those of a hybrid of apoptosis and necrosis previously described as part of the cell death

continuum in the immature cortex and striatum in response to excitotoxic injury (Portera-Cailliau

et al., 1997). Forty-eight hours after hypoxia-ischemia, apoptotic and continuum cells are seen in

the striatum in contrast to the predominant necrosis seen at three hours after hypoxia-ischemia.

The same is true in the cortex, with many apoptotic and continuum profiles found at delayed

time points (Figure 3, panel C, striatum - 48 hours after hypoxia-ischemia, silver stain, panel D,

cortex-48 hours after hypoxia-ischemia-CV, arrows indicate cells with apoptotic and hybrid

morphologies).

Damage occurs in remote locations after hypoxia-ischemia: Injury occurs in brain regions

remote from the areas of acute primary injury. This remote damage occurs in association with

damage to interconnected white matter pathways (Fig. 4). Between 24 and 72 hours, axonal

degeneration and neurodegeneration are identifiable in the mammillary tract and mammillary

nucleus, in corpus callosum and contralateral cortex, and in descending cortico-bulbar tracts and

brainstem and cranial nerve nuclei. Axonal degeneration is seen in the contralateral corpus

callosum and in the ipsilateral descending cortico-bulbar tracts (panels A and C) and in their

respective target areas, the contralateral cortex (panel B) and the nucleus of cranial nerve VII

(panel B) (injury indicated by areas of silver deposition, arrows). For comparison, no axonal

degeneration is seen in contralateral corpus callosum in controls (Fig 4, panel a).

Retrograde transport of flurogold identifies regions with efferent connections to the

ipsilateral cerebral cortex that are at risk for injury after hypoxia/ischemia: Injury within the

lateral geniculate and the ventral basal complex of thalamus occurs in association with columnar

cortical injury at 24 hours after hypoxia-ischemia (Fig 5, panel A). Posterior cortical injection of p4 rat pups demonstrates retrograde transport of flurogold to these same vulnerable areas of ipsilateral thalamus and to contralateral cortex (Fig 5, panels B, E, brown immunoreactivity). Retrograde axonal transport of the flurogold is confirmed by the presence of abundant immunoreactivity for flurogold filling the cell body and dendrites of thalamic neurons (Fig 5, panel C)

Injection of flurogold prior to hypoxia-ischemia combined with cresyl violet staining of tissue perfused at 48 hours after hypoxia/ischemia demonstrates death of neurons with connections to ipsilateral cortex (Fig 5, panel D, arrows). A cell labeled with flurogold (brown immunoreactivity) and with large chromatin clumps (cresyl violet) can be readily identified, demonstrating directly that cells with cortical connections die with an apoptotic morphology following neonatal hypoxia/ischemia.

Delayed and remote neurodegeneration in thalamus and brainstem is apoptosis: In contrast to the initial forebrain injury, initial injury in the thalamus and brainstem is apoptosis beginning 24 hours after hypoxia-ischemia (Fig 3, panel E-silver stain, LGN 24 hours after hypoxia-ischemia; panel F-silver stain, brainstem nuclei, 24 hours after hypoxia-ischemia). The light microscopic features displayed by these cells which are characteristic of apoptosis including large regular clumps of chromatin, condensation of cytoplasm, and preservation of cytoplasmic membrane.

Time of appearance of apoptotic profiles in the thalamus (Fig 6) is consistent with the delayed onset of injury in the diencephalon as compared to the forebrain. Utilizing the cresyl violet stained sections to count apoptotic profiles within the thalamus following hypoxia-ischemia, we find that for the first 6 hours after hypoxia-ischemia, the numbers of apoptotic

profiles are not increased above the baseline number found in age-matched controls or hypoxia only controls. From 24-72 hours after hypoxia-ischemia, a marked increase in number of cells with clearly identifiable apoptotic profiles occurs. By 6 days following the insult, number of apoptotic profiles is once again at control levels. The initial increase in apoptotic profiles in the thalamus coincides with the appearance of neurodegeneration in the thalamus at 24 hours, lags the onset of neurodegeneration in the cortex at 3 hours, and continues through the progression of injury in the cortex at 48 hours.

Remote but interconnected regions also exhibit terminal degeneration at delayed time points: In addition to apoptotic cell death in regions remote from the ipsilateral forebrain following neonatal hypoxia-ischemia, evidence of terminal degeneration is also found in remote regions at $\geq$ 24 hours after the end of hypoxia.   Within the respiratory centers of the medulla (Fig 3, panel G), the ipsilateral globus pallidus (Fig 3, panel H), and the contralateral cortex (Fig 3, panel I), primary and pyramidal neurons are found with fine silver deposits covering their surface indicating degenerating nerve terminals. In some cases, the silver deposits can be seen to decorate the surface of neuronal processes. In the contralateral cortex, cells with an apoptotic morphology are found in the same area as those with terminal degeneration (Fig 3, panel I).

Control experiments confirm the validity of this model and the lack of contribution of hypoxia alone to remote injury. In age matched control animals, no increase in optical density was found at any age (all control OD data combined, Figure 1). In control sections, occasional silver stained cells with apoptotic morphology were found as would be expected because of the previously demonstrated normal period of neuronal cell death that occurs in the first 2 weeks of

life in developing rats (Oppenheim, 1991). Neurodegeneration was also not found in animals

exposed to hypoxia alone nor ischemia without hypoxia (hypoxia only OD data-figure 1,

ischemia only OD data not shown). Lack of injury from either hypoxia or ischemia alone is

consistent with the original observations made in this model (Rice, 1981). Additionally, the lack

of injury in hypoxia only controls is evidence that injury found in remote regions following

hypoxia-ischemia is not the result of systemic hypoxemia.

Discussion

The most important findings of the present study are that following neonatal hypoxia-ischemia 1) brain regional vulnerability is dictated and organized along interconnected neural systems, 2) ipsilateral forebrain injury occurs as two fundamentally different time-dependant patterns: early neuronal necrosis and then delayed apoptotic neuronal death during a secondary injury phase, 3) delayed cell death can also exist as a hybrid of apoptosis and necrosis. 4) Injury to regions remote from the ipsilateral forebrain is associated with damage within interconnecting white matter pathways. 5) Cells in remote regions that have connections with ipsilateral cortex and are target deprived, die with a morphology consistent with apoptosis after hypoxia-ischemia.

In the present model of neonatal brain injury, the ipsilateral forebrain clearly represents the ischemic core of the lesion (Rice, 1981) (Nelson and Silverstein, 1994). Previous neuropathologic studies have demonstrated signs of ischemic necrosis evident as soon as the end of hypoxia within the ipsilateral cortex (Towfighi et al., 1995). Our results are in agreement with this observation and, for the first time, measurements of injury within the ipsilateral forebrain have been made with optical densitometry thereby demonstrating quantifiable injury in both cortex and striatum by 3 hours after the end of hypoxia. The simultaneous appearance of injury within ipsilateral cortex and striatum is evidence for the previously described role of hypoxia-ischemia in the initial phase of injury (Towfighi et al., 1991; Towfighi et al., 1995).

The injury evolves with a different time course in the cortex and striatum, suggesting that different mechanisms control the initial phase of injury versus the subsequent delayed phase of injury in these regions. The coexistence of injured and non-injured tissue within contiguous sub-regions of striatum and cortex and the different morphology of injury during the initial versus delayed phase (necrosis versus apoptosis) also supports the role for other mechanisms (in

addition to acute ischemia) in the overall resultant neuropathology. It is known that within the

developing cortex, interconnected neurons provide trophic support for each other (Miller and

Kuhn, 1997; Shatz, 1996). It is possible that the rapid necrotic death of an initial population of

cortical neurons results in the target deprivation death of connected neurons as is thought to

occur in the adult brain (Martin et al., 1998). Our data demonstrating a time dependant increase

in apoptotic cell death in the ipsilateral cortex is consistent with this possibility.

The previously reported effect of delayed administration of pan-caspase inhibitors to provide

neuroprotection (Cheng et al., 1998) within a region known to exhibit early necrotic

neurodegeneration (Rice, 1981; Towfighi et al., 1995) also suggests alternate mechanism of early

vs late injury.   Because many members of the caspase family are cytokine processors, caspase

inhibition may curtail a more delayed cytokine mediated cell death rather than solely blocking

delayed apoptosis (Wolf and Green, 1999). Regardless of the mechanism of caspase

neuroprotection, it is obvious that caspase inhibitors have an effect on the neurodegeneration

when administered 3 hours after hypoxia-ischemia, a time at which early necrosis is well

underway in the forebrain (Cheng et al., 1998).

A switch in the mechanism of cell death may also explain the neuropathology found in the

ipsilateral striatum. The patchy pattern of cell death may be the result of differential expression

patterns of neurotransmitter receptors in the striatal matrix (Martin et al., 1993) or may be the

result of heterogeneity of neuronal connectivity (Alloway et al., 1999). The initial columnar

neurodegeneration seen in the neocortex (Figure 2, and (Towfighi et al., 1997)) correlates with

areas of incomplete blood supply and patterns of altered NADH metabolism after hypoxia-

ischemia in the developing brain (Welsh et al., 1982)). It is known that cortical columns provide

afferent striatal input with specific areas of sensory-motor cortex being represented within

specific areas of the striatal matrix (Alloway et al., 1999) (Gerfen, 1992). The degeneration of specific cortical columns could lead to degeneration of specific areas within the striatal mosaic during the delayed phase of striatal injury. The more rapid progression of the secondary phase of injury in the cortex than in the striatum supports a temporal framework in which loss of cortical innervation and, thus a deafferentation, could result in striatal neurodegeneration in anatomically discrete regions. Although, no quantification of injury within the hippocampus was performed, qualitative analysis reveals timing and structure of injury very similar to that seen in the striatum. Specifically, early evidence of necrosis is abundant, followed by a secondary phase in which cells degenerate with the intermediate "continuum" phenotype (Portera-Cailliau et al., 1997), and with an apoptotic morphology.

The possibility that delayed cell death results from secondary mechanisms triggered by the early-occurring neurodegeneration is supported by the present data and previous experiments showing a prominent role for cortical connectivity in neuronal viability in immature thalamus, substantia nigra, and brainstem (Oo et al., 1995), (Kolb et al., 1986). Large cortical lesions created in the first week of life result in atrophy of the thalamus and brainstem (Kolb et al., 1986), while even selectively targeted cortical aspiration results in retrograde degeneration within thalamic nuclei (Al-Abdulla et al., 1998). Hypoxia-ischemia results in apoptosis of dopaminergic neurons in the substantia nigra, presumably secondary to loss of trophic support from their striatal inputs (Oo et al., 1995). This is the mechanism that we propose for the remote cell death seen in the present study. Evidence for this mechanism includes: 1) Injury in remote regions always occurs later than primary injury in ipsilateral forebrain. 2) Remote injury is accompanied by injury within interconnecting white matter pathways. 3) Neurons in thalamus that project to ipsilateral forebrain die via apoptosis following hypoxia-ischemia. 4) The

structure of the cell death in remote regions was most commonly apoptosis, consistent with target deprivation mediated injury. Apoptosis is present at significant amounts in the thalamus 21 hours following the first increase in injury detectable by OD in the cortex and it continues during the progression of cortical injury to cavitary lesions. 5) In addition to remote cell death, we also find evidence of terminal degeneration on viable principal neurons in remote regions that are known to receive inputs from ipsilateral forebrain (Carpenter, 1983).

Remote neurodegeneration has been reported in the present model and has most often been attributed directly to global ischemic injury (Towfighi et al., 1994; Towfighi et al., 1991). It is also possible that remote neurodegeneration occurs as the result of seizure activity. However, most evidence suggests that seizures do not exacerbate hypoxic-ischemic brain injury and that seizures may provide neuroprotection if they occur prior to the hypoxic-ischemic insult (Towfighi et al., 1999). Seizure-induced neurodegeneration would not be limited to the ipsilateral forebrain and could occur in the interconnected regions where injury was found in the present study.

If neuronal connectivity does participate in the propagation of neurodegeneration in regions outside of the vascular distribution of the right common carotid, then remote neurodegeneration should only be found in the presence of axonal degeneration in interconnecting white matter pathways between forebrain and contralateral cortex or brain stem. Because we do not find remote neurodegeneration in the absence of or preceding axonal degeneration, neuronal connectivity mediated neurodegeneration is possible. Absence of remote injury, in animals exposed to hypoxia only, also supports the hypothesis that neuronal connectivity dictates patterns of degeneration after hypoxia-ischemia. If systemic hypoxemia were the cause of injury to remote regions in the present model, these remote regions should sustain injury when the animals

are exposed to hypoxia alone. Neither previous investigators, nor we have found evidence of remote neurodegeneration as the result of systemic hypoxemia alone (Towfighi et al., 1994), (Towfighi et al., 1995). The presence of apoptotic neurodegeneration within specific brainstem nuclei also argues for our hypothesis that remote neurodegeneration after hypoxia-ischemia is the result of loss of trophic support from the primarily injured regions.

Neuronal cell death in this model of hypoxia-ischemia occurs as at least three different forms. These different forms of cell death coexist in different regions of brain and sometimes in the same regions. Other studies have revealed the occurrence of necrosis and apoptosis (Rice, 1981) (Towfighi et al., 1995) (Cheng et al., 1998). Support for our conclusion that apoptosis occurs through mechanisms possibly related to connectivity and target deprivation has been found elsewhere. (Oo et al., 1995). Our results are entirely consistent with these previous data and they extend our understanding of the neuropathology of neonatal hypoxia-ischemia to include neuroanatomical evidence for necrosis and apoptosis following hypoxia-ischemia and evidence for neurodegeneration within interconnecting axons and terminal projections. This study also shows for the first time, that after hypoxia-ischemia, apoptosis and necrosis may coexist within the same cell. This new finding is similar to the observation that a hybrid morpology of cell death, the 'continuum' cell, occurs in the forebrain, at delayed time points, in an immature model of glutamate receptor-mediated excitotoxic injury (Portera-Cailliau et al., 1997). The mechanism for the hybrid form of cell death is not yet understood but may relate to relative levels of ATP depletion as has been demonstrated in kidney cell culture *in vitro* (Feldenberg et al., 1999).

The methods utilized in the present study to evaluate neurodegeneration differ from the standard use of DNA end-labeling for identification of injury and cell death. We chose not to

use TUNEL because it does not differentiate between apoptosis, necrosis, and hybrids of apoptosis and necrosis (Martin et al., 1999) and does not provide any information about degeneration of axons or nerve terminals, and thus would not provide as much information as would silver staining. We chose to rely on silver staining for quantification of injury because its reliability has been validated and it allows identification of degeneration in both cell soma and processes (Du et al., 1998) and silver staining intensifies with progression of injury (Figure 1). Although, silver has been reported to label in the absence of cell death (Toth et al., 1998), the transient argyophlia reported on hippocampal neurons following febrile seizures may represent degenerating nerve terminals which are subsequently eliminated without death of their target neuron. This possibility is supported by our findings of degenerating nerve terminals contacting cells, which appear to be morphologically normal (Figure 3, panels I and J).

In conclusion, this study reveals differences in dell death patterns in ipsilateral forebrain over time following hypoxia-ischemia. Axonal and terminal degeneration occurring along with apoptotic cell death in remote regions after hypoxia-ischemia support the hypothesis that the distribution of neuronal connections dictates the presence of injury, as well as the structure of primary and remote neurodegeneration following neonatal hypoxia-ischemia. These findings have important implications for the development of appropriately timed and targeted therapies for the protection of the neonatal brain and rescue of neurons following hypoxic-ischemic insults.

Acknowledgements

Figure Legends

Figure 1 Neonatal hypoxia-ischemia causes neurodegeneration in ipsilateral cortex, striatum, and thalamus which can be measured densitometrically in silver-stained sections.   Optical density measurements from ipsilateral cortex (top panel), ipsilateral striatum (middle panel), and ipsilateral ventral basal thalamus (bottom panel) were obtained from coronal sections of brains perfused at 0, 1.5, 3, 6, 24, 48, 72 hours and 6 days following hypoxia-ischemia and stained with FD Neuro-silver kit.   Control groups included animals exposed to no manipulation or to hypoxia only.   Injury proceeds rapidly in ipsilateral forebrain (cortex and striatum), with an increase in silver deposition detectable by 3 hours after hypoxia-ischemia in both regions.   Initial evidence for neurodegeneration in thalamus is not found until 24 hours after hypoxia-ischemia.   Injury continues to progress in all three regions but at significantly different rates.   A secondary increase in neurodegeneration is detectable in cortex by 48 hours.   No further measurements were made in the cortex because by 72 hours cystic cavitary lesions were common in the posterior parieto-occipital cortex and precluded densitometric analysis.   Despite the similarity of time of first appearance of injury in cortex and striatum, secondary injury proceded much slower in the striatum with a difference not detectable until 6 days after hypoxia-ischemia.   A secondary increase in thalamic neurodegeneration also occurs at 6 days following hypoxia-ischemia.   In neither forebrain nor thalamus was there a detectable increase in neurodegeneration 24 hours after 2.5 hours of hypoxic exposure only.   The values are mean$\pm$ standard error of the mean from the regions at matched coronal levels.   A single asterisk indicates significant difference ($p<0.05$) from control and two asterisks indicate significant difference ($p<0.05$) from first appearance of detectable injury.

Figure 2 Forebrain injury after neonatal hypoxia-ischemia is discontinuous with areas of neurodegeneration immediately adjacent to non-injured tissue. (A) silver-stained coronal section of forebrain shows the previously reported columnar injury in cortex and discrete patches of injury in the adjacent striatum (arrows and arrowheads indicate areas of neurodegeneration, Scale bar= 1.1mm. (B) At greater magnification, the close approximation of injured (arrowheads) and non-injured areas of the striatum is apparent. Scale bar=300μm.

Figure 3 Structure of cell death following neonatal hypoxia-ischemia varies by region and time. Necrosis, apoptosis, and hybrids of apoptosis and necrosis revealing the cell death continuum are seen in both silver and cresyl violet stained sections (A-F). Immediately after hypoxia-ischemia, necrosis is most commonly seen in ipsilateral striatum (A-silver stain) and cortex (B-cresyl violet). These necrotic cells have numerous irregular small chromatin clumps (A, B), a loss of cytoplasmic integrity (A) or swelling of the cytoplasm (B). While necrotic cells can still be found in the forebrain at later time points, cells with fewer, larger, more regular chomatin clumps (C, D) and with pale cytoplasm contained within an apparently intact cellular membrane (D) are found in the stiatum (C) and cortex (D) at 48 hours. Cells of an intermediate morphology with more regularly defined chromatin condensation than that found in necrosis but with smaller and more numerous chromatin aggregates than is typical for apoptosis are also found in the forebrain after 24 hours (D, arrow). Ipsilateral thalamus (E) and brainstem (F) exhibit classic apoptosis following neonatal hypoxia-ischemia. Multiple rounded detached cells in both regions have 2 or 3 large sharply delineated, uniformly dense, smooth, round chromatin clumps contained within a dense, argyrophillic cytoplasm around which the cytoplasmic membrane is preserved. Cells which have progressed to the final stage of an extruded apoptotic body without apparent

cytoplasm are also found.   In addition to the neurodegeneration found in forebrain, thalamus and

brainstem following hypoxia-ischemia, terminal degeneration is found in regions that receive

efferent connections from these injured regions. Respiratory neurons in the medulla (G),

neurons in the ipsilateral globus pallidus (H), and layer III pyramidal neurons in the contralateral

cortex have multiple tiny silver grains deposisted on their surface consistent with silver labeling

of degenerating projections to the cell. In contrast to the injured neurons seen in ipsilateral

forebrain, thalamus, and brainstem, these neurons have maintained their normal cellular

architecture suggesting that they are intact, not primarily degenerating. For comparison, an

apoptotic layer III neuron is seen in (I). While multiple staining techniques allow adequate

visualization of nuclear and cytoplasmic structure, silver-staining allows the added ability to

visualize degenerating cellular projections. Scale bar= 11μm.

Figure 4 Neurodegeneration occurs in brain regions remote from the primary sites of injury in

association with damage to the interconnecting white matter pathways. Axonal degeneration

occurs in the contralateral corpus callosum (A) and ipsilateral descending cortico-bulbar tracts

(C) along with neurodegeneration in their respective targets, layer III of the contralateral cortex

(B) and the nucleus of cranial nerve VII (D). Injury in these target regions is much more focal

and circumscribed than that in the primary ipsilateral forebrain. For comparison, no injury is

seen in the contralateral corpus callosum of a control (a) or in the contralateral descending

cerebral pyramid (B). Scale bar for A, a, and B, = 81μm, for C and D= 371μm.

Figure 5 Retrograde transport of flurogold labels 2 regions which exhibit delayed

neurodegeneration following neonatal hypoxia-ischemia. Injection of flurogold into the

ipsilateral posterior parietal-cortex labels ipsilateral posterior and ventral basal thalamus and

lateral geniculate nucleus (B) and layer III neurons in the contralateral cortex (E).

Neurodegeneration occurs in these regions following hypoxia-ischemia in patterns similar to the

pattern of retrograde transport of flurogold (compare silver-staining of injured ipsilateral

thalamus (A) with flurogold immunoreactivity in thalamus (B) and layer III neurodegeneration in

contralateral cortex (Fig 4B) with flurogold immunoreactivity in layer III contralateral cortex

(E). Retrograde transport of flurogold occurs specifically to the cell soma and processes (C),

none is found in the surrounding neuropil. This specificity of retrograde transport allows

identification of neurons with cortical connection to be identified even in late stages of apoptosis

(D) when cellular morphology is disturbed. Scale bar A and B= 1mm, C and D= 11μm, E=

500μm.

Figure 6 Appearance of apoptotic profiles in ipsilateral thalamus coincides with initial

quantitative evidence of neurodegeneration in thalamus and follows neurodegeneration in

ipsilateral forebrain. Not until 24 hours after hypoxia-ischemia is there a significant increase in

the number of apoptotic profiles in the ipsilateral thalamus. A consistent increase in apoptotic

profiles persists at 48 and 72 hours. Counts at 0, 1.5, 3, 6 hours and 6 days are not different from

those found in age matched controls and hypoxia only controls (data not shown). Counts were

performed on cresyl violet stained sections of brains at similar coronal levels. The values are

mean± standard error of the mean for each group. A single asterisk indicates significant

difference in number of apoptotic profiles from (p<0.05) from control.

References

Al-Abdulla, N. A., Portera-Cailliau, C., and Martin, L. J. (1998). Occipital cortex ablation in adult rat causes retrograde neuronal death in the lateral geniculate nucleus that resembles apoptosis. Neuroscience *86*, 191-209.

Alloway, K. D., Crist, J., Mutic, J. J., and Roy, S. A. (1999). Corticostriatal projections from rat barrel cortex have an anisotropic organization that correlates with vibrissal whisking behavior . J Neurosci *19*, 10908-22.

Barks, J. D., and Silverstein, F. S. (1992). Excitatory amino acids contribute to the pathogenesis of perinatal hypoxic-ischemic brain injury. Brain Pathol 2, 235-43.

Bolz, J., Novak, N., Gotz, M., and Bonhoeffer, T. (1990). Formation of target-specific neuronal projections in organotypic slice cultures from rat visual cortex. Nature *346*, 359-62.

Carpenter, M. B., and Sutin, Jerome. (1983). Human Neuroanatomy (Baltimore: Williams and Wilkins), pp. 315-357, 579-611.

Cheng, Y., Deshmukh, M., D'Costa, A., Demaro, J. A., Gidday, J. M., Shah, A., Sun, Y., Jacquin, M. F., Johnson Jr, E. M., and Holtzman, D. M. (1998). Caspase Inhibitor Affords Neuroprotection with Delayed Adminstration in a Rat Model of Neonatal Hypoxic-Ischemic Brain Injury. J Clin Invest *101*, 1992-1999.

Du, F., Eid, T., and Schwarcz, R. (1998). Neuronal damage after the injection of aminooxyacetic acid into the rat entorhinal cortex: a silver impregnation study. Neuroscience *82*, 1165-78.

Eves, E. M., Boise, L. H., Thompson, C. B., Wagner, A. J., Hay, N., and Rosner, M. R. (1996). Apoptosis induced by differentiation or serum deprivation in an immortalized central nervous system neuronal cell line. J Neurochem *67*, 1908-1920.

Feldenberg, L. R., Thevananther, S., del Rio, M., de Leon, M., and Devarajan, P. (1999). Partial ATP depletion induces Fas- and caspase-mediated apoptosis in MDCK cells. Am J Physiol *276*, F837-46.

Gerfen, C. R. (1992). The neostriatal mosaic: multiple levels of compartmental organization. Trends Neurosci *15*, 133-9.

Hagan, P., Barks, J. D., Yabut, M., Davidson, B. L., Roessler, B., and Silverstein, F. S. (1996). Adenovirus-mediated over-expression of interleukin-1 receptor antagonist reduces susceptibility to excitotoxic brain injury in perinatal rats. Neuroscience *75*, 1033-45.

Kolb, B., Whishaw, I. Q., and van der Kooy, D. (1986). Brain development in the neonatally decorticated rat. Brain Res *397*, 315-26.

Kotak, V. C., and Sanes, D. H. (1997). Deafferentation weakens excitatory synapses in the developing central auditorysystem. Eur J Neurosci *9*, 2340-2347.

Levine, S. (1960). Anoxic-ischemic encephalopathy in rats. Am J Pathol *36*, 1-17.

Li, L., Prevette, D., Oppenheim, R. W., and Milligan, C. E. (1998). Involvement of specific caspases in motoneuron cell death in vivo and in vitro following trophic factor deprivation. Mol Cell Neurosci *12*, 157-167.

Liu, X. H., Eun, B. L., Silverstein, F. S., and Barks, J. D. (1996). The platelet-activating factor antagonist BN 52021 attenuates hypoxic- ischemic brain injury in the immature rat. Pediatr Res *40*, 797-803.

Lorenz, J. M., Wooliever, D. E., Jetton, J. R., and Paneth, N. (1998). A quantitive review of mortality and developmental disability in extremely premature newborns. Arch Pediatr Adolesc Med *152*, 425-435.

Martin, L. J., Al-Abdulla, N. A., Brambrink, A. M., Kirsch, J. R., Sieber, F. E., and Portera-Cailliau, C. (1998). Neurodegeneration in excitotoxicity, global cerebral ischemia, and target deprivation: A perspective on the contributions of apoptosis and necrosis. Brain Res Bull *46*, 281-309.

Martin, L. J., Blackstone, C. D., Huganir, R. L., and Price, D. L. (1993). The Striatal Mosaic in Primates: Striosomes and matrix are differentially enriched in ionotropic glutamate receptor subunits. Journal of Neuroscience *13*, 782-792.

Martin, L. J., Brambrink, A. M., Koehler, R. C., and Traystman, R. J. (1997). Primary Sensory and forebrain motor systems in the newborn brain are preferentially damaged by hypoxia-ischemia. The Journal of Comparitive Neurology *377*, 262-285.

Martin, L. J., Brambrink, A. M., Lehmann, C., Portera-Cailliau, C., Koehler, R. C., Rothstein, J., and Traystman, R. J. (1997). Hypoxia-ischemia causes abnormalities in glutamate transporters and death of astroglia and neurons in newborn striatum. Ann Neuro *42*, 335-348.

Martin, L. J., Kaiser, A., and Price, A. C. (1999). Motor neuron degeneration after sciatic nerve avulsion in adult rat evolves with oxidative stress and is apoptosis. J Neurobiol *40*, 185-201.

McDonald, J. W., Silverstein, F. S., and Johnston, M. V. (1988). Neurotoxicity of N-methyl-D-aspartate is markedly enhanced in developing rat central nervous system. Brain Res *459*, 200-3.

Miller, M. W., and Kuhn, P. E. (1997). Neonatal transection of the infraorbital nerve increases the expression of proteins related to neuronal death in the principal sensory nucleus of the trigeminal nerve. Brain Res *769*, 233-244.

Nelson, C., and Silverstein, F. S. (1994). Acute disruption of cytochrome oxidase activity in brain in a perinatal rat stroke model. Pediatr Res *36*, 12-9.

Nelson, K. B., and Grether, J. K. (1999). Causes of cerebral palsy. Curr Opin Pediatr *11*, 487-91.

Oo, T. F., Henchcliffe, C., and Burke, R. E. (1995). Apoptosis in substantia nigra following developmental hypoxic-ischemic injury. Neuroscience *69*, 893-901.

Oppenheim, R. W. (1991). Cell Death During Development of the Nervous System. Annu Rev Neurosci *14*, 453-501.

Portera-Cailliau, C., Price, D. L., and Martin, L. J. (1997). Excitoxic Neuronal Death in the Immature Brain Is an Apoptosis-Necrosis Morphological Continuum. The Journal of Comparitive Neurology *378*, 70-87.

Rice, J. E. (1981). The Influence of Immaturity on Hypoxic-Ischemic Brain Damage in the Rat. Ann Neuro *9*, 131-141.

Shatz, C. J. (1996). Emergence of order in visual system development. Proc Natl Acad Sci U S A *93*, 602-608.

Toth, Z., Yan, X. X., Haftoglou, S., Ribak, C. E., and Baram, T. Z. (1998). Seizure-induced neuronal injury: vulnerability to febrile seizures in an immature rat model. J Neurosci *18*, 4285-94.

Towfighi, J., Housman, C., Mauger, D., and Vannucci, R. C. (1999). Effect of seizures on cerebral hypoxic-ischemic lesions in immature rats. Brain Res Dev Brain Res *113*, 83-95.

Towfighi, J., Housman, C., Vannucci, R. C., and Heitjan, D. F. (1994). Effect of unilateral perinatal hypoxic-ischemic brain damage on the gross development of opposite cerebral hemisphere. Biol Neonate *65*, 108-18.

Towfighi, J., Mauger, D., Vannucci, R. C., and Vannucci, S. J. (1997). Influence of age on the cerebral lesions in an immature rat model of cerebral hypoxia-ischemia: a light microscopic study. Brain Res Dev Brain Res *100*, 149-60.

Towfighi, J., Yager, J. Y., Housman, C., and Vannucci, R. C. (1991). Neuropathology of remote hypoxic-ischemic damage in the immature rat. Acta Neuropathol *81*, 578-87.

Towfighi, J., Zec, N., Yager, J., Housman, C., and Vannucci, R. C. (1995). Temporal evolution of neuropathologic changes in an immature rat model of cerebral hypoxia: a light microscopic study. Acta Neuropathol *90*, 375-86.

Welsh, F. A., Vannucci, R. C., and Brierley, J. B. (1982). Columnar alterations of NADH fluorescence during hypoxia-ischemia in immature rat brain. J Cereb Blood Flow Metab *2*, 221-8.

Wolf, B. B., and Green, D. R. (1999). Suicidal tendencies: apoptotic cell death by caspase family proteinases. J Biol Chem *274*, 20049-52.
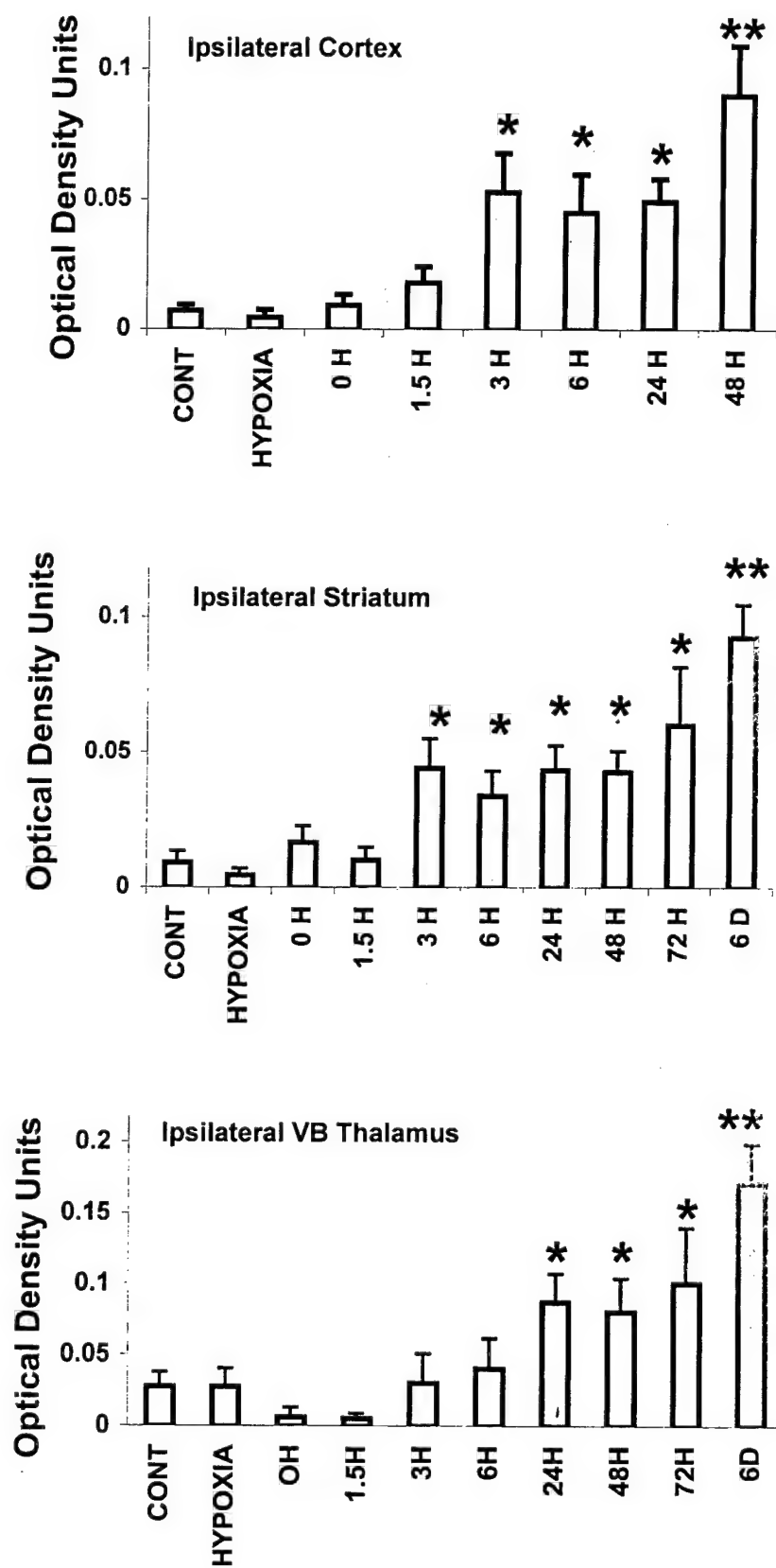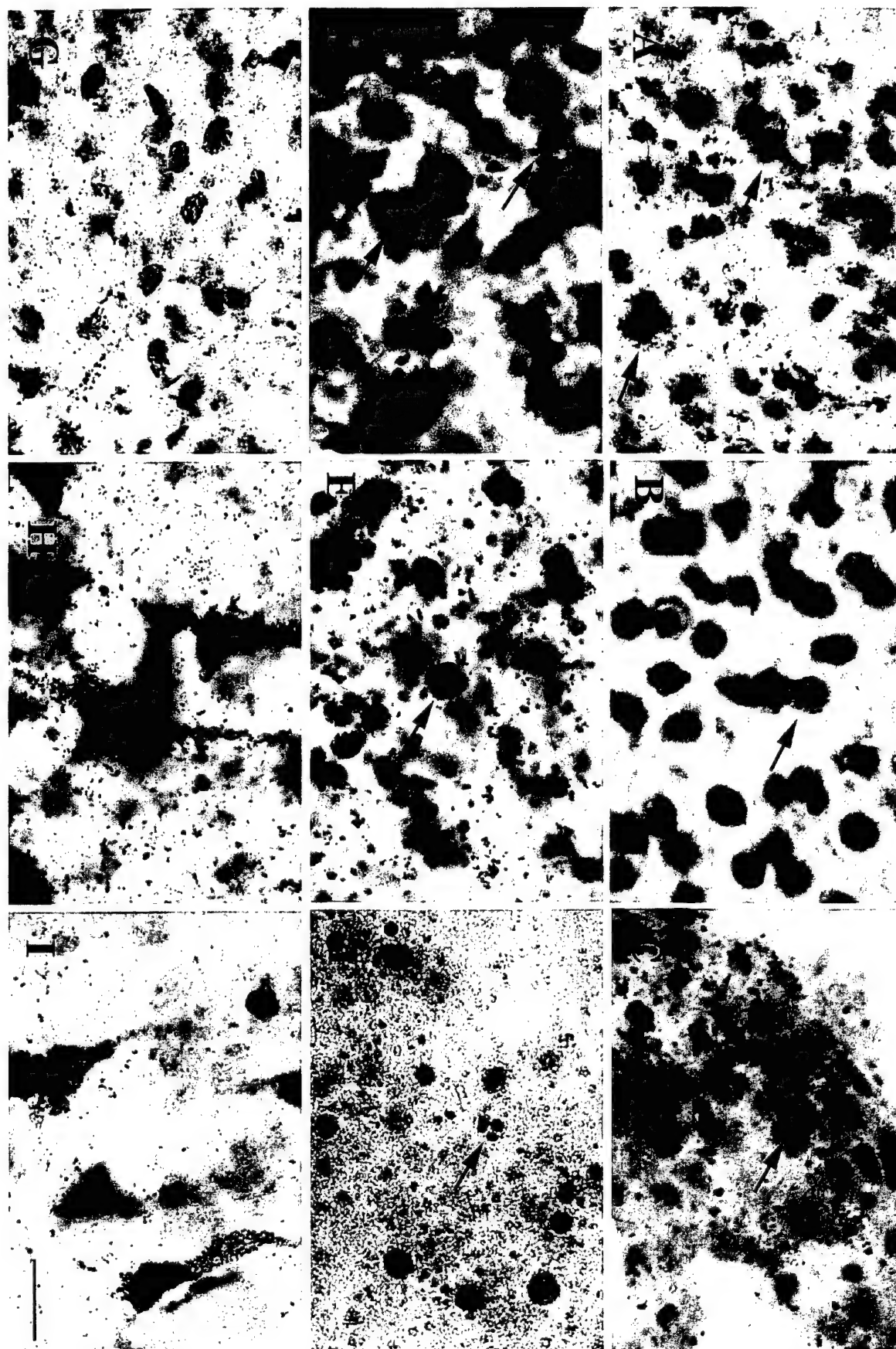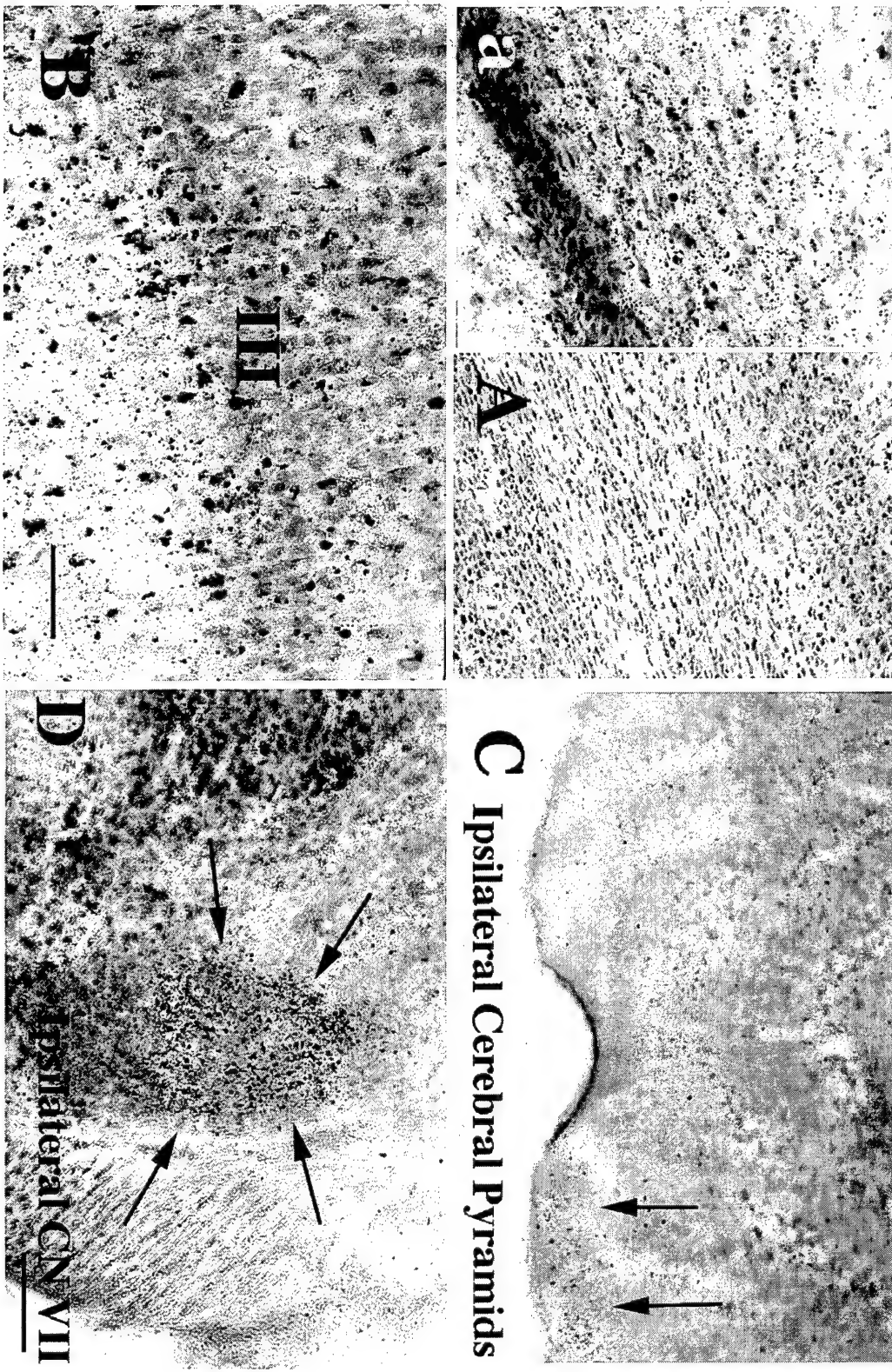
FIGURE 1

FIGURE 2

FIGURE 3

TOP

FIGURE 4
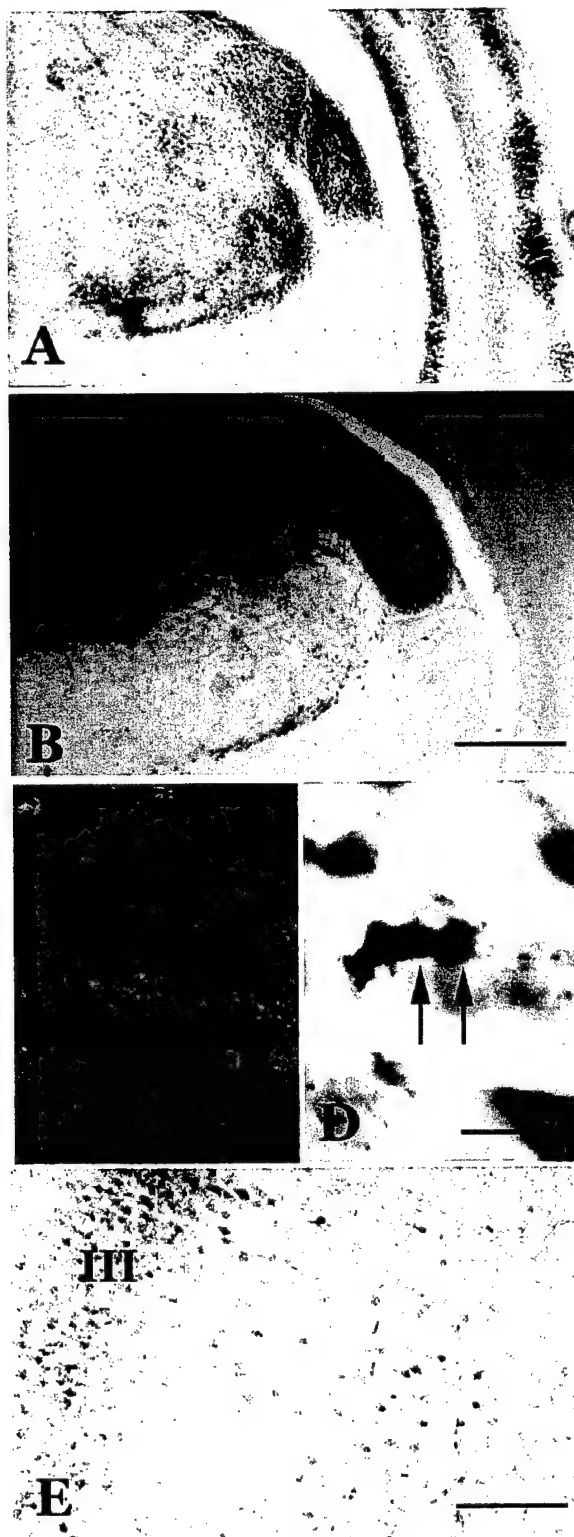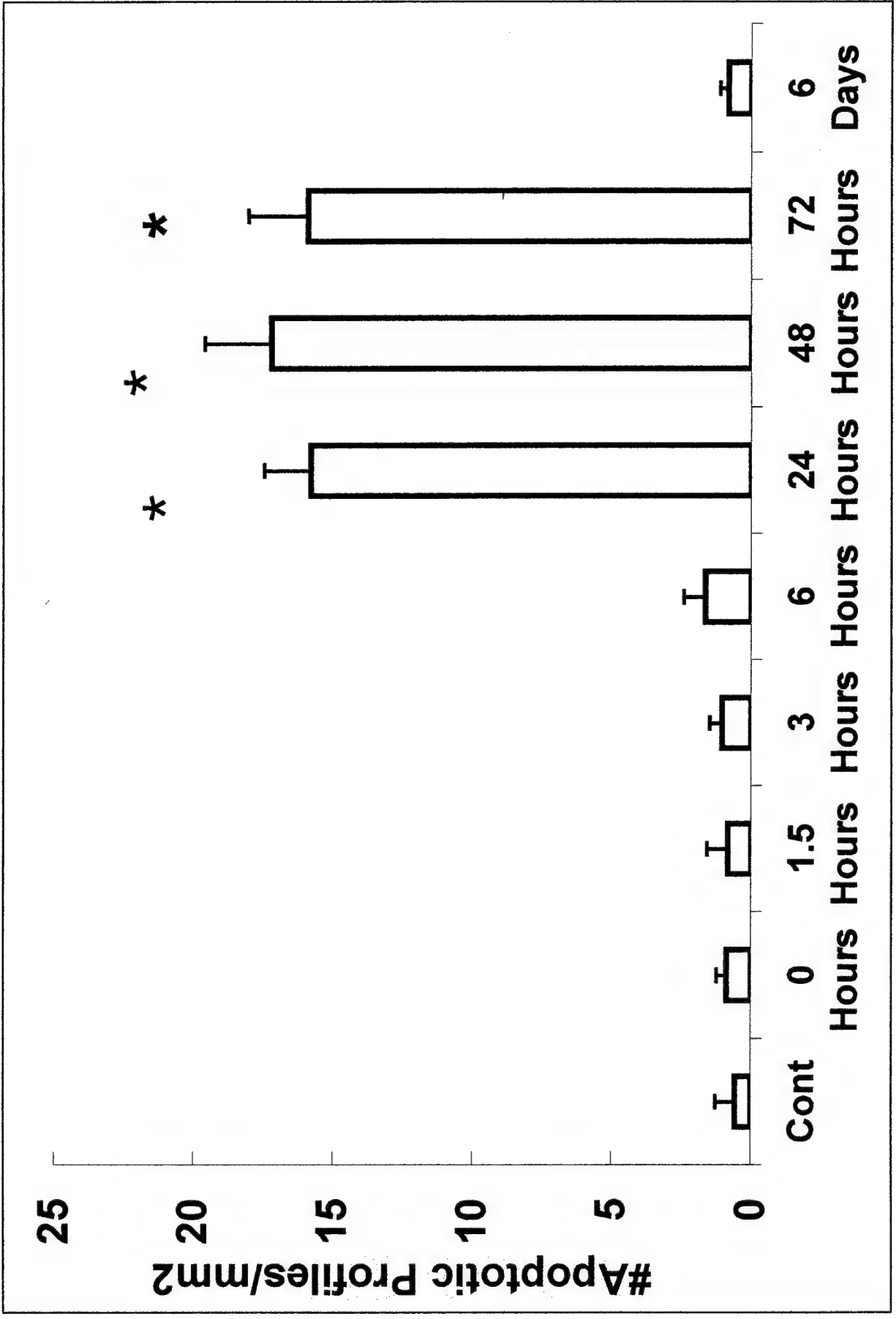
C Ipsilateral Cerebral Pyramids

Ipsilateral CN VII

FIGURE 5

FIGURE 6

DELAYED NEURODEGENERATION IN NEONATAL RAT THALAMUS AFTER

HYPOXIA-ISCHEMIA IS PROGRAMMED CELL DEATH

Frances J. Northington, M. D. [1], Donna M. Ferriero, M. D.[2], Debra L. Flock, B.A.[1], and
Lee J. Martin, Ph.D. [3]

Eudowood Neonatal Pulmonary Division, Departments of Pediatrics [1], and Pathology [3]. The
Johns Hopkins University School of Medicine, Baltimore, MD 21287. Departments of
Neurology and Pediatrics [2], University of California-San Francisco, San Francisco, CA 94143

Running head: Programmed cell death after neonatal hypoxia-ischemia

Text pages: 25   Figures: 7   Tables:0
Abstract: 188   Introduction: 413   Discussion: 1360

Corresponding Author:
Frances J. Northington, M.D.
Eudowood Neonatal Pulmonary Division
Department of Pediatrics,CMSC 210, Johns Hopkins Hospital
600 N. Wolfe Street
Baltimore, MD 21287
410-955-5259, 410-955-0298 fax
fnorthin@welchlink.welch.jhu.edu

Abstract

Brain injury in newborns can cause deficits in motor and sensory function. In most models of neonatal brain injury, thalamic damage often occurs. Using the Rice-Vannucci model of neonatal hypoxic-ischemic (H/I) brain injury, we have shown that neuronal degeneration in somatosensory thalamus is delayed in onset ($\approx$24 hours) compared to forebrain injury and exhibits prominent structural features of apoptosis. In the present study, we examined whether cell death in the thalamus has biochemical features of programmed cell death. Fas death receptor protein expression increased rapidly following neonatal hypoxia-ischemia, in concert with cleavage of pro-caspase 8 to its active form. Concurrently, the levels of Bax in mitochondrial-enriched cell fractions increase. Mitochondria accumulate in a perinuclear distribution by 6 hours after hypoxic-ischemia. Cytochrome oxidase subunit 1 protein levels also increase at 6 hours after hypoxia-ischemia. Increased levels of Fas death receptor and Bax, activation of caspase 8, and abnormalities in mitochondria in the thalamus significantly precede the activation of caspase 3 and appearance of neurodegeneration and apoptotic profiles at 24 hours. We conclude that the delayed neurodegeneration in neonatal rat ventral basal thalamus following H/I injury is programmed cell death.

Key Words

apoptosis, mitochondria, neonatal brain injury, Bax, Fas death receptor, caspase

Introduction

A large amount of investigation has focused on cytokine- and hypoxia/ischemia-mediated injury to the developing forebrain and periventricular white matter as the cause of the neurodevelopmental handicaps suffered by infants who have experienced perinatal brain injury. Energy failure, free radical, cytokine and excitatory amino acid release and caspase-dependant cell death are known to contribute to injury in the forebrain and periventicular white matter (Back et al., 1998; Barks and Silverstein, 1992; Cheng et al., 1998; Hagan et al., 1996; Liu et al., 1996; Martin et al., 1997b; McDonald et al., 1988). However, degeneration of non-forebrain structures after hiypoxia-ischemia is studied less frequently. Injury to somatosensory thalamus has been described in human newborns after hypoxia-ischemia (Barkovich, 1995; Roland et al., 1998), and may contribute to sensory-motor deficits in infants with neonatal brain injury and cerebral palsy. Sensory-motor deficits have been detected in neonatal rats subjected to the present model of hypoxic-ischemic injury (Bona et al., 1997). A few detailed neuropathologic studies of animal models have revealed injury to the developing diencephalon following neonatal hypoxia/ischemia (Towfighi et al., 1991), and we have recently demonstrated that injury to the diencephalon occurs in a delayed manner and exhibits prominent structural features of apoptosis when compared to the early necrotic cell death seen in the forebrain after hypoxia/ischemia (Northington et al., 1999).

The mechanisms of apoptotic neurodegeneration in the thalamus and other brain regions remote from the forebrain following neonatal hypoxia-ischemia are completely unknown. However, death receptor acitvated pathways, altered mitochondrial function and changes in expression of mitochondrial related *bcl-2* family proteins are likely important effectors of programmed cell death in the present model of neonatal brain injury (Felderhoff-Mueser et al.,

2000; Nelson and Silverstein, 1994; Silverstein, 1998). Fas death receptor protein expression is

increased in hippocampus bilaterally during the 24 hours immediately following neonatal

hypoxia-ischemia (Felderhoff-Mueser et al., 2000) and administration of cytokine antagonists

afford neuroprotection in the present model (Liu et al., 1996). In adult models of programmed

cell death, mitochondrial accumulation occurs during the critical chromatolytic phase prior to

apoptosis simultaneously with increased expression of the pro-apoptosis proteins BAX and BAK

(Martin, 1999; Martin et al., 1999).

In this study, we examine the possibility that a cascade of events including death receptor

activation, alteration in the ratio of pro- and anti-apoptosis regulating proteins in mitochondria,

altered mitochondrial activity and location, and cleavage of caspases into active subunits form a

pathway of delayed programmed cell death leading to apoptotic neurodegeneration in the

diencephalon following neonatal hypoxia-ischemia.

Methods

Hypoxia-ischemia in p7 rats: The Rice-Vannucci (Rice, 1981) neonatal adaptation of the

Levine procedure (Levine, 1960) was used to cause hypoxic ischemic brain injury in seven day

old (p7) rats. In brief, rat pups were anesthetized with 2.5% halothane, 15% nitrous oxide, in O_2.

The right common carotid artery was permanently ligated (in sham controls the ligature was

passed around the artery and removed). After the wound was sutured, the pups recovered from

anesthesia and were returned to the dam. Two hours later, pups were placed in an airtight

container in a 37^0 C water bath through which humidified 8% O_2, balance nitrogen flowed for

150 min. After hypoxia, pups were returned to the dam until sacrifice.

The animals were killed and the brains retrieved at 0, 1.5, 3, 6, and 24 hours following

the end of hypoxia for histological analysis (n=6 for each timepoint), or at 3, 6, and 24 hours

following the end of hypoxia for western blotting (n=4 or 5 samples/time point). Due to sample

size, 3 hemi-diencephalons and 2 hemi-cortexes per sample were required to generate adequate

tissue homogenate for immunoblot analysis. The multiple early time points were chosen because

our data, as well as that of others, showed a Faster progression of injury after hypoxia-ischemia

in neonates as compared to adults (Martin et al., 1997a; Northington et al., 1999; Towfighi et al.,

1995). Control groups consisted of sham operated littermates. Sham controls were sacrificed on

postnatal day 7, and 8 to control for developmental changes in protein expression or cytochome

oxidase activity.

All animal studies received prior approval from the Animal Care and Use Committee of

Johns Hopkins University School of Medicine and were performed in accordance with the NIH

"Guide for the Care and Use of Laboratory Animals", U.S. Department of Health and Human

Services 85-23, 1985.

Tissue preparation: Animals were killed with an overdose of pentobarbital, 65mg/kg IP, and

exsanguinated with cold 0.1 M PBS (pH7.4) via intra-cardiac perfusion. Brains were perfusion

fixed with 4% paraformaldehyde in PBS for 30m at 4ml/min. The brains were removed, post-

fixed in 4% paraformaldehyde overnight, cryoprotected in 30% sucrose and frozen in isopentane

($-30°$). 60μ coronal sections were cut on a sliding microtome for cresyl violet, and

immunohistochemical staining.

Immunoblotting: Samples of diencephalon and forebrain were obtained by rapid dissection

immediately after euthanasia and frozen on dry ice. 150-300 mg pooled samples were

homogenized in cold 20mM Tris HCl (pH7.4) containing (10% wt/vol) sucrose, 20μ/ml

aprotinin (Trayslol), 20µg/ml leupeptin, 20 µg/ml antipain, 20µg/ml pepstatin A, 20µg/ml

chymostatin, 0.1 mM phenylmethylsulfonyl fluoride, 10mM benzamidine, 1mM EDTA, and

5mM EGTA. Crude homogenates were centrifuged at 1000 gav X 10 min. The supernatant (S1

fraction) was then centrifuged at 114,000 gav X 20 min, and the resulting supernatant (S2

soluble fraction) collected. The pellet (P2 mitochondrial-enriched, membrane fraction) was

washed in homogenization buffer (without sucrose) 3 times by resuspension and centrifugation at

114,000 gav X 20 min. The P2 fraction was then re-suspended fully in homogenization buffer

supplemented with 20%(wt/vol) glycerol. This sub-cellular fractionation protocol has been

verified (Martin et al., 2000). Protein concentrations were measured by a Bio-Rad protein assay

with bovine serum albumin as a standard.

Samples of membrane or soluble proteins were subjected to SDS-PAGE and electro-

eluted onto nitrocellulose membranes. The reliability of sample loading and protein transfer was

evaluated by staining nitrocellulose membranes with Ponceau S before immonoblotting and by

quantification of commassie stained gels and ponceau stained blots with OD. Blots were

blocked with 2.5% non-fat dry milk with 0.1%Tween 20 in 50mM Tris-buffered saline (pH7.4)

and incubated overnight at 4^0C with antibody. After primary incubation, blots were washed,

incubated with peroxidase-conjugated secondary antibodies (0.2µg/ml) and developed with

enhanced chemiluminescence. To quantify cell death protein immuno-reactivity, films were

scanned using Adobe Photoshop and OD performed with IP Lab Gel H software. Protein levels

are expressed as relative OD measurements compared to control lanes in the same blot after

correcting for loading differences.

Antibodies: Anti-Fas death receptor antibody (Santa Cruz Biotechnology, Santa Cruz, CA) is a

rabbit polyclonal antibody generated against an epitope mapping to the carboxy terminus of human Fas and is non-cross reactive with other TNFR type 1 receptors. It recognizes a single band at 45kDa and higher molecular weight bands after SDS-PAGE. Jukrat cells known to express high levels of the Fas death receptor were used as a positive control. Anti-caspase 8 antibody (Santa Cruz Biotechnology, Santa Cruz, CA) is a rabbit polyclonal antibody raised against a recombinent protein corresponding to amino acids 217-350 of human caspase 8. Anti-Bax (Upstate Biotechnology, Lake Placid, NY) and anti-Bcl 2 antibodies (Santa Cruz Biotechnology, Santa Cruz, CA) are affinity purified rabbit polyclonal antibodies generated against a peptide corresponding to amino acids 1-21 of human Bax and a peptide mapping at the amino terminus of human Bcl-2, respectively. Anti-Bax antibody recognizes a single 23 kDa band, a faint band at 18.5 kDa representing the cleaved form of Bax and several less intense high molecular weight bands in P_2 protein fractions. Anti- Bcl-2 antibody recognizes a band at 26 kDa and several less intense high molecular weight bands in P_2 protein fractions. A second rabbit polycolonal anti-Bax antibody (Santa Cruz Biotechnology, Santa Cruz, CA) generated against a peptide homologous to amino acids 11-30 of human Bax, gave identical results to the Upstate antibody. Because these proteins were fractionated in denaturing gels, it is unlikely that the high molecular weight bands represent various Bax and Bcl-2 homo- and heterodimers. Anti-cytochrome oxidase subunit 1 (COX 1) antibody (Molecular Probes, Inc., Eugene, OR) is a mouse monoclonal antibody generated against subunit 1 of human cytochrome oxidase. The antibody recognizes only a single band ≈ 35 kDa in non-boiled P_2 protein samples subjected to SDS-PAGE. Anti-Caspase 3 antibody (Santa Cruz Biotechnology, Santa Cruz, CA) is a rabbit polyclonal antibody generated against amino acids 1-277 of full length human caspase-3, and it recognizes the 32 kDa pro-enzyme with an intense band of immunoreactivity and the 12, 17 and

20 kDa active fragments with less intense single bands. Because none of the antibodies except anti-cytochrome oxidase subunit 1 antibody recognized a single band with SDS-PAGE, they were considered unreliable for immunocytochemical studies.

Cytochrome Oxidase Histochemistry: To identify the levels of oxidative metabolism and intracellular distribution of oxidatively active mitochondria, we used the CO (cytochrome oxidase) histochemical method of Wong-Riley (Wong-Riley, 1979; Wong-Riley, 1989) as described previously for our laboratory (Martin et al., 1997a). Briefly, brain sections from control and hypoxic-ischemic rat pups were exposed to the assay simultaneously. The enzymatic reaction medium was prepared immediately prior to each experiment and consisted of 100mM phosphate buffer (pH 7.4), 0.1% horse heart cytochrome C (Sigma, St. Louis MO), 117mM sucrose, and 1.4mM diaminobenzidine tetrahydrochloride. In this histochemical reaction, in situ cytochrome oxidase catalyzes the transfer of electrons (donated by diaminobenzidine) from cytochrome C, provided as substrate, to O_2 to form H_2O. The donation of electrons from diaminobenzidine is a chromogenic reaction yielding the formation of an insoluble precipitate in the vicinity of CO activity thus revealing both the location of the mitochondria and relative metabolic activity of cytochrome oxidase (Wong-Riley, 1979). Sections were incubated for 2.5 hours at 37° in a Dubnoff metabolic shaker incubator. After the reaction, sections were rinsed in phosphate buffer, mounted on glass slides, and coverslipped.

Statistical Analysis: To quantify changes in expression of Fas death receptor protein, mitochondrial apoptosis regulating proteins, COX1 protein and caspase 8 and 3 active fragments, protein expression was corrected for loading differences and then expressed as percent of

control. In some blots, two different controls were used and the average optical density of the two bands was used for percent control calculations. Mean and standard deviation for protein expression in tissue obtained at similar time points was calculated and ANOVA was used to compare differences in protein expression over time. Post hoc testing for differences in expression at 3, 6, and 24 hours was performed with Fisher's analysis. A p value < 0.05 was used to determine significance.

Results

In the ipsilateral thalamus at 24 hours following neonatal hypoxia-ischemia, many degenerating neurons display light microscopic features of apoptosis (Figure 1, panel B, arrows) (Northington et al., 1999). This contrasts with the normal morphology of thalamic neurons from sham controls (Figure 1, panel A).

FAS receptor expression is induced in diencephalon rapidly following neonatal hypoxia-ischemia. By immunoblotting, Fas death receptor protein expression is increased in the diencephalon following neonatal hypoxia-ischemia (Figure 2). In membrane protein fractions of newborn rat diencephalon, Fas was detected at 45 kDa, corresponding to the known molecular weight of Fas death receptor protein in Jurkat cells (Felderhoff-Mueser et al., 2000). A comparison of diencephalic samples from sham-operated controls (SC) and p7 rat pups at 3, 6, and 24 hours after hypoxia-ischemia revealed a significant (p<0.05) increase in Fas levels after hypoxia-ischemia (Figure 2). This increase occurred as early as 3 hours after hypoxia-ischemia.

Caspase 8 is cleaved to its active subunits following neonatal hypoxia-ischemia. Procaspase 8 undergoes cleavage and activation in cell culture model systems of apoptosis (Dragovich et al., 1998; Nagata, 1999). Procaspase 8 is cleaved to its 30 and18 kDa subunits 8

in soluble protein from ipsilateral diencephalon following neonatal hypoxia-ischemia (Figure 3).
The levels of pro-caspase 8 in soluble fractions decrease as the cleaved subunits increase after
hypoxia-ischemia (Figure 3).

Ratio of mitochondrial apoptosis regulating proteins is altered rapidly following hypoxia-ischemia in the diencephalon prior to the appearance of prominent apoptosis. Following
neonatal hypoxia-iscemia, levels of the pro-apoptosis protein Bax rapidly increase in
mitochondrial enriched fractions of diencephalon (Figure 4, panel A). This increase in Bax
occurs without a concommitant change in the level of the anti-apoptosis Bcl-2 protein (Figure 4,
panel B). These alterations in level of expression of Bax and Bcl-2 proteins result in a marked
shift in protein abundance in favor of pro-apoptosis Bax (Figure 4, panel C). A significant
change in the relative abundance of Bax and Bcl-2 is evident as early as 3 hours following
neonatal hypoxia-ischemia.

Caspase-3 is cleaved into its active subunits at 24 hours after neonatal hypoxia-ischemia in the diencephalon. Caspases 3 and 8 are primary targets of death receptor mediated apoptosis
cascades (Nagata, 1999; Yamada et al., 1999). When cleaved from its 32kDa pro-enzyme form,
the active 12,17, and 20 kDa fragments have a central role in activating DNA fragmentation and
other irreversible steps in apoptosis (Du et al., 1997). Caspase-3 is cleaved to its active forms in
the diencephalon following neonatal hypoxia-ischemia (Figure 5, panel A), Interestingly this
activation is found only at 24 hours after hypoxia-ischemia (Figure 5, panel B).

Mitochondria accumulate at perinuclear locations in thalamic neurons following neonatal hypoxia-ischemia. Using a histochemical detection method for cytochrome oxidase activity to
identify mitochondria, we found that neurons in the ventral basal thalamus, following neonatal
hypoxia-ischemia, accumulate mitochondria (Figure 6). These changes occur prior to the

appearance of significant number of apoptotic profiles at 24 hours (Northington et al., 1999). In normal neurons, cytochrome oxidase activity is evenly distributed throughout the cell soma in ventral basal thalamic neurons (Figure 6, panel A). In contrast, by 3-6 hours following neonatal hypoxia-ischemia, mitochondria within neurons in the ipsilateral ventral basal thalamus exhibit intense cytochrome oxidase activity and form prominent perinuclear aggregates of mitochondria (Figure 6, panel B). These changes are most prominent in neurons in the chromatolytic stage of early neuronal apoptosis (Figure 6, panel C, cytochrome oxidase histochemistry and cresyl violet counterstaining) according to a recently proposed staging scheme for apoptosis of neurons (Al-Abdulla and Martin, 1998; Al-Abdulla et al., 1998; Martin et al., 1999). In these cells, dense cytochrome oxidase-positive aggregates cluster adjacent to peripherally displaced nuclei. By 24 hours, cells in late phases of apoptosis with tightly condensed chromatin aggregates have lost or are losing immunoreactivity for cytochrome oxidase (Figure 6, panel D, cytochrome oxidase histochemistry and cresyl violet counterstaining). This enhancement of cytochrome oxidase activity within the diencephalon following neonatal hypoxia-ischemia during the early phases of apoptotic neurodegeneration contrast strikingly with the rapid loss of cytochrome oxidase activity in the forebrain after neonatal hypoxia-ischemia. In agreement with previously published data, cytochrome oxidase immunoreactivity is decreased in the ipsilateral hippocampus (Nelson and Silverstein, 1994) and also in the parasagittal cortex (data not shown) by 1.5 –3 hours following neonatal hypoxia-ischemia.

The accumulation of mitochondria in the diencephalon following neonatal hypoxia-ischemia was confirmed indirectly by immunoblotting. By immunoblotting, levels of cytochrome oxidase subunit-1 protein (COX-1) increased after neonatal hypoxia-ischemia (Figure 7). Expression of this inner mitochondrial membrane protein increases in diencephalon (Figure 7,

panel A) and simultaneously decreases in forebrain (data not shown). In the diencephalon, a

significant increase in expression of COX-1 is evident at 6 hours following hypoxia-ischemia

(Figure 7, panel B) coincident with the peak of cytochrome oxidase activity in neurons in early

phases of apoptotic neurodegeneration.

Discussion

We have found that neuronal degeneration in the neonatal thalamus after hypoxia-ischemia is apoptosis (Northington et al., 1999). We explored the mechanisms for this apoptosis and based on these experiments, we conclude that delayed neuronal degeneration in neonatal rat thalamus after hypoxia-ischemia is programmed cell death. The findings that support this conclusion are 1) increased Fas death receptor levels, 2) an imbalance in the levels of Bax and Bcl-2 favoring apoptosis promoting Bax, 3) intracellular redistribution of active mitochondria, and 4) cleavage of caspases 8 and 3 to active forms. This cascade of biochemical and structural events is consistent with Fas mediated, mitochondrial amplified, programmed cell death as a major mechanism of delayed neurodegeneration following neonatal hypoxia-ischemia.

Thalamic damage after hypoxia-ischemia in newborns has long been recognized, and is particularly important in infants with extrapyramidal cerebral palsy (Malamud, 1950; Volpe, 1995). Human neuroimagining and neuropathological studies have revealed that the thalamus, especially the ventral tier nuclei, is among the selectively vulnerable brain regions in the human newborn (Barkovich, 1995; Yokochi et al., 1991). Despite recognition of injury to the thalamus in children with cerebral palsy, the contribution of delayed injury and injury to non-forebrain regions to the development of cerebral palsy has been less well studied. The ventral basal thalamus contains both afferent and efferent connections to the ipsilateral cortex, and functions prominently in sensory-motor integration (Erzurumlu and Jhaveri, 1990). Injury to these circuits interrupts cortical sensory function and the integration of sensory information into volitional movement (White, 1989). Damage to motor relay nuclei in the thalamus may lead to movement disorders such as ataxia or dystonia (White, 1989) and when this injury occurs in the immature brain, may contribute to the motor and sensory handicaps suffered by children with cerebral

palsy.

In the model of neonatal brain injury used in these studies, the ipsilateral forebrain is the major vulnerable region and clearly represents the ischemic core of the lesion (Rice, 1981), However, the thalamus is damaged in this model and in most other models of neonatal brain injury (present data and (Martin et al., 1997a; Myers, 1975; Northington et al., 1999; Towfighi et al., 1991; Towfighi et al., 1995)). We wanted to understand the possible mechanisms for thalamic neuronal apoptosis. We identified increased Fas death receptor protein levels in the ventral basal thalamus following neonatal hypoxia-ischemia, providing an additional link between cytokine and hypoxia-ischemia mediated neonatal brain injury. Despite previous studies demonstrating activation of interleukins (Szaflarski et al., 1995), neuroprotection with cytokine antagonists and in the absence of IL-1ß converting enzyme (Liu et al., 1996; Liu et al., 1999), the mechanism of hypoxia-ischemia induced, cytokine mediated cell death in the developing brain has not been clearly defined. The present study demonstrates that hypoxia-ischemia induces a cytokine death receptor that functions in programmed cell death (Nagata, 1999). Although, we have not yet shown directly that Fas is induced in thalamic neurons (because the antibodies are not suitable for immunocytochemistry), the rapid induction (by 3 hours) and the sustained elevation over the relevant time preceeding thalamic apoptosis make Fas death receptor induction unlikely to be the result of inflammation.

An elevation in Fas death receptor is a link to multiple pathways of cell death. Fas is a member of the tumor necrosis factor receptor (TNFR) family. Oligomerization of Fas death receptor and recruitment of FADD/MORT1 and procaspase 8 create the death inducing signal complex (DISC). DISC is a potent apoptosis stimulus in multiple cell culture models. When pro-caspase 8 is bound by the DISC, auto-cleavage to its active fragments occurs. Cleaved

caspase 8 then acts directly and indirectly to cleave caspase 3 depending on cell type and injury stimulus (Dragovich et al., 1998; Nagata, 1999). Cleavage of caspase 3 is generally considered one of the irreversible steps immediately responsible for the execution of apoptosis in which the cell develops the morphologic features recognizable as late stage apoptosis (Petit et al., 1996). Our data demonstrate early Fas death receptor elevation, early and progressive cleavage of caspase 8 to its active form, followed by delayed caspase 3 cleavage just at the time of appearance of significant apoptosis in the thalamus following neonatal hypoxia-ischemia. We have not yet shown activation of caspase 8 and caspase 3 specifically in thalamic neurons due to the lack of specific reagents. Fas death receptor protein and downstream caspase 3 cleavage likely bracket an important signaling cascade for apoptotic neurodegeneration in the thalamus.

Direct caspase 8 cleavage of caspase 3 is the original model of Fas mediated apoptosis signaling (Dragovich et al., 1998), however mitochondria and mitochondrial apoptosis regulating proteins of the *bcl-2* family are now known to greatly amplify cell death signals (Susin et al., 1997). Most of the *bcl*-2 family of genes that regulate rate of programmed cell death are normally present within mitochondrial membranes. Several *in vivo* and *in vitro* systems have shown the ratio of the pro-apoptosis protein Bax and the anti-apoptosis proteins Bcl-2 and Bcl-x(l) to be critical in determining cell survival (Almeida et al., 2000; Antonawich et al., 1999; Isenmann et al., 1998; Krajewski et al., 1995; Martin, 1999; Shimizu et al., 1999; Vekrellis et al., 1997).

We find a marked alteration in the balance of pro and anti-apoptosis *bcl-2* proteins in the mitochondrial fraction of diencephalon after hypoxia-ischemia. This accumulation of mitochondrial Bax occurs before caspase 3 cleavage and appearance of large numbers of apoptotic profiles (present data and (Northington et al., 1999)). A four-fold increase in the

amount of pro-apotosis protein Bax in the mitochondrial fraction was detected by three hours following injury, while Bcl-2 in the mitochondria is not changed during the first 24 hours after hypoxia-ischemia. Bax normally exists as a cytosolic protein and is translocated to the mitochondria upon ligation of Fas receptor. This translocation is inhibited by Bcl-2 (Murphy et al., 2000). The present data suggest active mitochondrial translocation of BAX greatly in excess of the steady state amount of Bcl-2. This is consistent with a strong death signal and may participate in mitochondrial amplification of Fas mediated apoptosis. Cleavage of Bax to an18 kDa isoform also enhances its programmed cell death potency` [Wood DE, 2000 #415]. Although neither antibody used in the present study was designed to detect the 18 kDa isoform, there is weak expression of an 18 kDa Bax band in the diencephalon at 24 hours following neonatal hypoxia-ischemia. The late appearance of this isoform in mitochondrial enriched fractions is consistent with published reports of calpain mediated Bax cleavage after translocation of Bax to the mitochondria (Wood and Newcomb, 1999).

Changes in mitochondrial morphology and membrane potential function precede caspase 3 activation in *in vitro* model systems (Vander Heiden et al., 1997; Zamzami et al., 1996). In axotomy models of neuronal apoptosis, mitochondrial trafficking is altered with peri-nuclear accumulation of mitochondria in neurons as they undergo apoptosis (Al-Abdulla and Martin, 1998; Martin et al., 1999), a finding very similar to that of the present study. These previous *in vitro* and *in vivo* observations support our conclusions described here. Within 3-6 hours following neonatal hypoxia-ischemia, neurons in the ventral basal thalamus exhibit marked accumulation of mitochondria (as revealed by intense cytochrome oxidase activity) and simultaneously display altered morphology. The mitochondria assume a prominent punctate appearance and concentrate in a perinuclear location. As thalamic neurons enter late stages of

apoptosis, the cytoplasm becomes progressively devoid of COX activity. These data are consistent with immunoblotting for cytochrome oxidase subunit-1 protein, which shows maximal levels at 6 hours following neonatal hypoxia-ischemia in the diencephalon. These findings are in contrast to the early and sustained loss of both cytochrome oxidase activity and COX-1 protein expression in the forebrain. Taken together these data provide evidence for the participation of mitochondria in thalamic neurodegeneration following neonatal hypoxia-ischemia.

In summary, these experiments provide the first evidence for the presence of crucial components of Fas-mediated, mitochondrial amplified, programmed cell death in the thalamus following neonatal brain injury. These findings are important for the further understanding of the mechanisms of neuronal apoptosis in the immature brain. Eventually, these studies may be important for development of appropriately timed and targeted therapies for the protection of the neonatal brain and rescue of neurons following hypoxic-ischemic insults.

References

Al-Abdulla, N.A., and L.J. Martin. 1998. Apoptosis of retrogradely degeneration neurons occurs in association with the accumulation of perkaryal mitochondria and oxidative damage to the nucleus. *Am J Pathol*. 153:447-456.

Al-Abdulla, N.A., C. Portera-Cailliau, and L.J. Martin. 1998. Occipital cortex ablation in adult rat causes retrograde neuronal death in the lateral geniculate nucleus that resembles apoptosis. *Neuroscience*. 86:191-209.

Almeida, O.F., G.L. Conde, C. Crochemore, B.A. Demeneix, D. Fischer, A.H. Hassan, M. Meyer, F. Holsboer, and T.M. Michaelidis. 2000. Subtle shifts in the ratio between pro- and antiapoptotic molecules after activation of corticosteroid receptors decide neuronal fate. *Faseb J*. 14:779-790.

Antonawich, F.J., H.J. Federoff, and J.N. Davis. 1999. BCL-2 transduction, using a herpes simplex virus amplicon, protects hippocampal neurons from transient global ischemia. *Exp Neurol*. 156:130-137.

Back, S.A., Y. Li, X. Gan, P.A. Rosenberg, and J.J. Volpe. 1998. Maturation-dependent vulnerability of oligodendrocytes to oxidative stress-induced death caused by glutathione depletion. *J Neurosci*. 18:6241-6253.

Barkovich, A. 1995. Profound asphyxia in the premature infant: image findings. *AJNR Am J Neuroradiol*. 95:1837-1846.

Barks, J.D., and F.S. Silverstein. 1992. Excitatory amino acids contribute to the pathogenesis of perinatal hypoxic-ischemic brain injury. *Brain Pathol*. 2:235-243.

Bona, E., B.B. Johansson, and H. Hagberg. 1997. Sensorimotor function and neuropathology five to six weeks after hypoxia-ischemia in seven-day-old rats. *Pediatr Res*. 42:678-683.

Cheng, Y., M. Deshmukh, A. D'Costa, J.A. Demaro, J.M. Gidday, A. Shah, Y. Sun, M.F. Jacquin, E.M. Johnson Jr, and D.M. Holtzman. 1998. Caspase Inhibitor Affords Neuroprotection with Delayed Adminstration in a Rat Model of Neonatal Hypoxic-Ischemic Brain Injury. *J Clin Invest*. 101:1992-1999.

Dragovich, T., C.M. Rudin, and C.B. Thompson. 1998. Signal transduction pathways that regulate cell survival and cell death. *Oncogene*. 17:3207-3213.

Du, Y., K.R. Bales, R.C. Dodel, E. Hamilton-Byrd, J.W. Horn, D.L. Czilli, L.K. Simmons, B. Ni, and S.M. Paul. 1997. Activation of a caspase 3-related cysteine protease is required for glutamate-mediated apoptosis of cultured cerebellar granule neurons. *Proc Natl Acad Sci USA*. 94:11657-11662.

Erzurumlu, R.S., and S. Jhaveri. 1990. Thalamic axons confer a blueprint of the sensory periphery onto the developing rat somatosensory cortex. *Brain Res Dev Brain Res*. 56:229-234.

Felderhoff-Mueser, U., D.L. Taylor, K. Greenwood, M. Kozma, D. Stibenz, U.C. Joashi, A.D. Edwards, and H. Mehmet. 2000. Fas/CD95/APO-1 can function as a death receptor for neuronal cells in vitro and in vivo and is upregulated following cerebral hypoxic- ischemic injury to the developing rat brain. *Brain Pathol*. 10:17-29.

Hagan, P., J.D. Barks, M. Yabut, B.L. Davidson, B. Roessler, and F.S. Silverstein. 1996. Adenovirus-mediated over-expression of interleukin-1 receptor antagonist reduces susceptibility to excitotoxic brain injury in perinatal rats. *Neuroscience*. 75:1033-1045.

Isenmann, S., G. Stoll, M. Schroeter, S. Krajewski, J.C. Reed, and M. Bahr. 1998. Differential regulation of Bax, Bcl-2, and Bcl-X proteins in focal cortical ischemia in the rat. *Brain Pathol*. 8:49-62; discussion 62-43.

Krajewski, S., J.K. Mai, M. Krajewska, M. Sikorska, M.J. Mossakowski, and J.C. Reed. 1995. Upregulation of bax protein levels in neurons following cerebral ischemia. *J Neurosci*. 15:6364-6376.

Levine, S. 1960. Anoxic-ischemic encephalopathy in rats. *Am J Pathol*. 36:1-17.
Liu, X.H., B.L. Eun, F.S. Silverstein, and J.D. Barks. 1996. The platelet-activating factor antagonist BN 52021 attenuates hypoxic- ischemic brain injury in the immature rat. *Pediatr Res*. 40:797-803.

Liu, X.H., D. Kwon, G.P. Schielke, G.Y. Yang, F.S. Silverstein, and J.D. Barks. 1999. Mice deficient in interleukin-1 converting enzyme are resistant to neonatal hypoxic-ischemic brain damage. *J Cereb Blood Flow Metab*. 19:1099-1108.

Malamud, N. 1950. Status Marmoratus: A form of birth injury following either bith injury or inflammation of the central nervous system. *J. Pediatr*. 37:610.

Martin, L.J. 1999. Neuronal death in amyotrophic lateral sclerosis is apoptosis: possible contribution of a programmed cell death mechanism. *J Neuropathol Exp Neurol*. 58:459-471.

Martin, L.J., A.M. Brambrink, R.C. Koehler, and R.J. Traystman. 1997a. Primary Sensory and forebrain motor systems in the newborn brain are preferentially damaged by hypoxia-ischemia. *The Journal of Comparitive Neurology*. 377:262-285.

Martin, L.J., A.M. Brambrink, C. Lehmann, C. Portera-Cailliau, R.C. Koehler, J. Rothstein, and R.J. Traystman. 1997b. Hypoxia-ischemia causes abnormalities in glutamate transporters and death of astroglia and neurons in newborn striatum. *Ann Neuro*. 42:335-348.

Martin, L.J., A. Kaiser, and A.C. Price. 1999. Motor neuron degeneration after sciatic nerve avulsion in adult rat evolves with oxidative stress and is apoptosis. *J Neurobiol*. 40:185-201.

Martin, L.J., A.C. Price, A. Kaiser, A.Y. Shaikh, and Z. Liu. 2000. Mechanisms for neuronal degeneration in amyotrophic lateral sclerosis and in models of motor neuron death (Review). *Int J Mol Med*. 5:3-13.

McDonald, J.W., F.S. Silverstein, and M.V. Johnston. 1988. Neurotoxicity of N-methyl-D-aspartate is markedly enhanced in developing rat central nervous system. *Brain Res*. 459:200-203.

Murphy, K.M., U.N. Streips, and R.B. Lock. 2000. Bcl-2 inhibits a Fas-induced conformational change in the Bax N- terminus and Bax mitochondrial translocation. *J Biol Chem*. in press.

Myers, R.E. 1975. Four patterns of perinatal brain damage and their conditions of occurrence in primates. *Adv Neurol*. 10:223-234.

Nagata, S. 1999. Fas ligand-induced apoptosis. *Annu Rev Genet*. 33:29-55.

Nelson, C., and F.S. Silverstein. 1994. Acute disruption of cytochrome oxidase activity in brain in a perinatal rat stroke model. *Pediatr Res*. 36:12-19.

Northington, F.J., D.M. Ferriero, R.J. Traystman, and L.J. Martin. 1999. Early neurodegeneration in forebrain after neonatal hypoxia-ischemia is necrosis while delayed neuronal death in thalamus and remote brain regions is apoptosis. *Society for Neuroscience Abstracts*. 25:755.

Petit, P.X., S.A. Susin, N. Zamzami, B. Mignotte, and G. Kroemer. 1996. Mitochondria and programmed cell death: back to the future. *FEBS Lett*. 396:7-13.

Rice, J.E. 1981. The Influence of Immaturity on Hypoxic-Ischemic Brain Damage in the Rat. *Ann Neuro*. 9:131-141.

Roland, E.H., K. Poskitt, E. Rodriguez, B.A. Lupton, and A. Hill. 1998. Perinatal hypoxic-ischemic thalamic injury: clinical features and neuroimaging [see comments]. *Ann Neurol*. 44:161-166.

Shimizu, S., M. Narita, and Y. Tsujimoto. 1999. Bcl-2 family proteins regulate the release of apoptogenic cytochrome c by the mitochondrial channel VDAC [see comments]. *Nature*. 399:483-487.

Silverstein, F.S. 1998. Can inhibition of apoptosis rescue ischemic brain? *J Clin Invest*. 101:1809-1810.

Susin, S.A., N. Zamzami, M. Castedo, E. Daugas, H.G. Wang, S. Geley, F. Fassy, J.C. Reed, and G. Kroemer. 1997. The central executioner of apoptosis: multiple connections between protease activation and mitochondria in Fas/APO-1/CD95- and ceramide- induced apoptosis. *J Exp Med*. 186:25-37.

Szaflarski, J., D. Burtrum, and F.S. Silverstein. 1995. Cerebral Hypoxia-Ischemia Stimulates Cytokine Gene Expression in Perinatal Rats. *Stoke*. 26:1093-1100.

Towfighi, J., J.Y. Yager, C. Housman, and R.C. Vannucci. 1991. Neuropathology of remote hypoxic-ischemic damage in the immature rat. *Acta Neuropathol*. 81:578-587.

Towfighi, J., N. Zec, J. Yager, C. Housman, and R.C. Vannucci. 1995. Temporal evolution of neuropathologic changes in an immature rat model of cerebral hypoxia: a light microscopic study. *Acta Neuropathol*. 90:375-386.

Vander Heiden, M.G., N.S. Chandel, E.K. Williamson, P.T. Schumacker, and C.B. Thompson. 1997. Bcl-xL regulates the membrane potential and volume homeostasis of mitochondria [see comments]. *Cell*. 91:627-637.

Vekrellis, K., M.J. McCarthy, A. Watson, J. Whitfield, L.L. Rubin, and J. Ham. 1997. Bax promotes neuronal cell death and is downregulated during the development of the nervous system. *Development*. 124:1239-1249.

Volpe, J.J. 1995. Neurology of the Newborn. W. B. Saunders Co., Philadelphia. 314-369.
White, E. 1989. Cortical Circuits: Synaptic Oganization of the Cerebral Cortex: Structure, Function, and Theory. Birkhauser, Boston.

Wong-Riley, M. 1979. Changes in the visual system of monocularly sutured or enucleated cats demonstrable with cytochrome oxidase histochemistry. *Brain Res*. 171:11-28.

Wong-Riley, M.T. 1989. Cytochrome oxidase: an endogenous metabolic marker for neuronal activity. *Trends Neurosci*. 12:94-101.

Wood, D., Newcomb EW. 2000. Cleavage of bax enhances its cell death function. *Experimental Cell Research*. 256:375-382.

Wood, D.E., and E.W. Newcomb. 1999. Caspase-dependent activation of calpain during drug-induced apoptosis. *J Biol Chem*. 274:8309-8315.

Yamada, H., S. Tada-Oikawa, A. Uchida, and S. Kawanishi. 1999. TRAIL causes cleavage of bid by caspase-8 and loss of mitochondrial membrane potential resulting in apoptosis in BJAB cells. *Biochem Biophys Res Commun*. 265:130-133.

Yokochi, K., K. Aiba, M. Kodama, and S. Fujimoto. 1991. Magnetic resonance imaging in athetotic cerebral palsied children. *Acta Paediatr Scand*. 80:818-823.

Zamzami, N., S.A. Susin, P. Marchetti, T. Hirsch, I. Gomez-Monterrey, M. Castedo, and G. Kroemer. 1996. Mitochondrial control of nuclear apoptosis [see comments]. *J Exp Med*. 183:1533-1544.

Figure Legends

Figure 1: Thalamic neurons die by apoptosis following neonatal hypoxia-ischemia. A) Compared to sham controls, B) at 24 hours after hypoxia-ischemia, many apoptotic profiles are found in cresyl violet stained sections of the ventral basal thalamus (arrows).

Figure 2: Fas death receptor protein levels increase in diencephalon following neonatal hypoxia-ischemia. A) Immunoblot showing increased Fas death receptor protein in membrane fractions from diencephalic homogenates obtained 3, 6, and 24 hours following neonatal hypoxia-ischemia compared to non-injured control samples. Jurkat cell lysates were used as a positive control, becauase they express high levels of Fas as detected at 45 kDa. Corresponding bands in controls and injured diencephalon were used for quantification. The corresponding comassie stained gel is shown as a loading control for normalizing protein levels. B) Graph represents changes in Fas death receptor protein levels in diencephalon over time following neonatal hypoxia-ischemia. Results are shown as mean $\pm$ standard deviation of 4-5 samples /time point. *=$p<0.05$ compared to control.

Figure 3: Pro-caspase 8 is cleaved to active fragments in diencephalon following neonatal hypoxia-ischemia. A) Immunoblot showing procaspase 8 levels decrease concurrently with an increase in the levels of the 30 and18 kDa active fragments of caspase 8 in cytosolic fractions from diencephalon at 3, 6, and 24 hours following neonatal hypoxia-ischemia. There is no cleaved caspase 8 in controls and a progressive increase in expression of the active subunits during the first 24 hours after hypoxia-ischemia. Jurkat cells (Jk), which are highly sensitive to Fas mediated apoptosis, express both procaspase 8 and the active subunits.

The corresponding ponceau stained blot is shown as a loading control. B) Graph represents changes in abundance of the 18 kDa active subunit of caspase 18 in diencephalon over time

following neonatal hypoxia-ischemia. After correcting for protein loading differences and comparing to control, results are shown as mean $\pm$ standard deviation of 4-5 samples /time point. *=p<0.05 compared to control.

Figure 4: Neonatal hypoxia-ischemia causes an elevation in pro-apoptosis Bax protein levels in mitochondrial fraction but does not alter levels of anti-apoptotic Bcl-2. A) Immunoblot showing increased Bax protein levels in mitochondrial membrane fractions from diencephalon from homogenates obtained 3, 6, and 24 hours following neonatal hypoxia-ischemia compared to non-injured control samples. Anti-Bax antibody recognizes the expected 21kDa band corresponding to Bax protein. Faint expression of an 18kDa band (panel A, arrow) is seen in the injured samples, perhaps corresponding to the cleaved Bax protein (Wood, 2000). The corresponding ponceau stained blot is shown as a loading control. B) In comparison Bcl-2 protein expression is not changed in mitochondrial membrane fractions from diencephalon homogenates obtained 3, 6, and 24 hours following neonatal hypoxia-ischemia compared to non-injured control samples. Anti- Bcl-2 antibody recognizes the expected 26kDa band corresponding to Bcl-2 protein. The corresponding comassie stained gel is shown as a loading control. C) Graph represents alteration in relative amounts of Bax and Bcl-2 protein in mitochondrial membrane fraction in diencephalon over time following neonatal hypoxia-ischemia. By 3 hours, there is a significant shift in the Bax/ Bcl-2 ratio favoring pro-apoptosis Bax. After correcting for protein loading differences and comparing to control, results are shown as mean $\pm$ standard deviation of 4-5 samples /time point. *=p<0.05 compared to control.

Figure 5: Cleavage of pro-caspase 3 to active fragments occurs at 24 hours after neonatal hypoxia-ischemia. A) Immunoblot showing levels of 32kDa pro-caspase 3 and its lower molecular weight cleavage products in diencephalon cytosolic fractions from homogenates
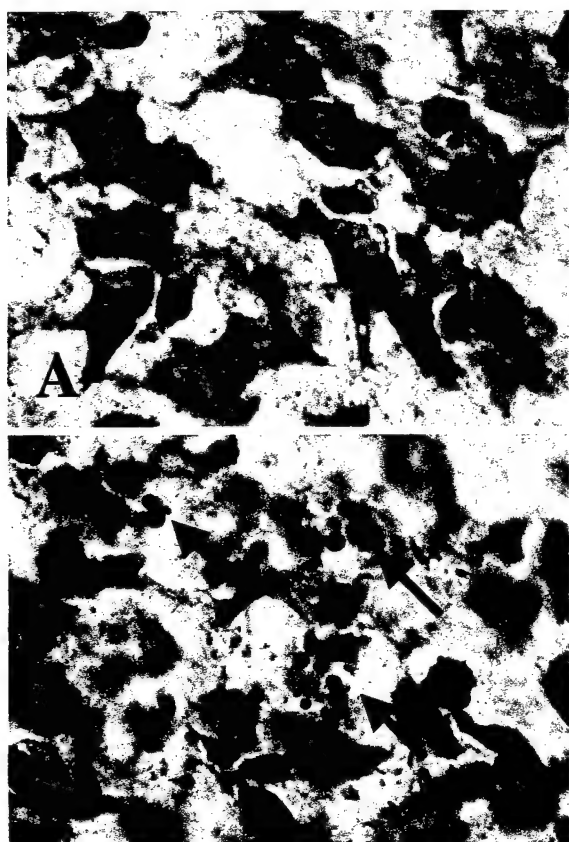
obtained 3, 6, and 24 hours following neonatal hypoxia-ischemia compared to non-injured

control samples. The corresponding ponceau stained blot is shown as a loading control. B)

Graph represents changes in expression of the12kDa cleavage product in diencephalon over time

following neonatal hypoxia-ischemia. Not until 24 hours is there a significant increase in the

amount of the 12kDa fragment. After correcting for protein loading differences and comparing

to control, results are shown as mean $\pm$ standard deviation of 4-5 samples /time point. *=p<0.05

compared to control.

Figure 6: Mitochondria accumulate in a perinuclear location in ventral basal thalamic neurons

after neonatal hypoxia-ischemia. Histochemistry for cytochrome oxidase activity in

diencephalon following neonatal hypoxia-ischemia shows intense cytochrome oxidase activity in

mitochondria and alteration in appearance and intracellular location of mitochondria following

neonatal hypoxia-ischemia. At 6 hours, mitochondria are densely immunoreactive for

cytochome oxidase assuming a punctate appearance and clustering near nuclei which are in the

chromatolytic phase of apoptosis (top right and bottom left panels, cytochrome oxidase

histochemistry and cytochrome oxidase histochemisty counterstained with cresyl violet,

respectfully). By 24 hours, (bottom right) cytochrome oxidase immunoreactivity is dissipating in

thalamic neurons undergoing late stages of apoptotic degeneration. Three cells with densely

condensed chromatin are shown with variable but decreasing levels of cytochrome oxidase

activity. Scale bar for both top panels and the bottom left panel = 12μm. Scale bar for bottom
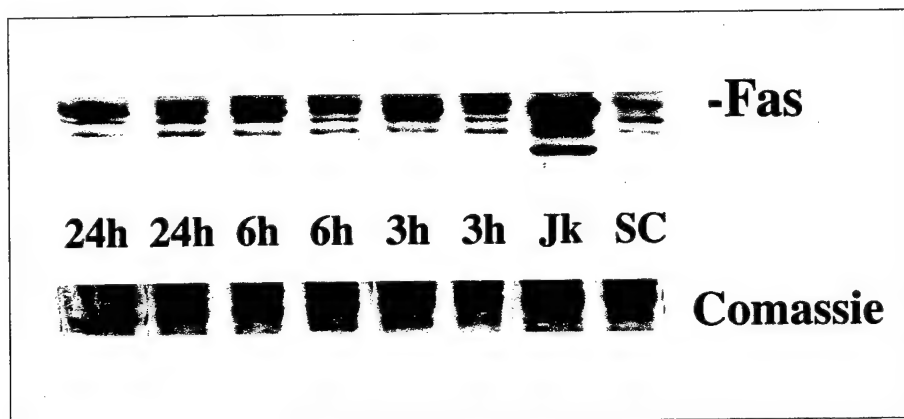
right panel = 6μm.

Figure 7: COX1 protein increases in thalamic mitochondrial protein fractions coincident with

mitochondrial accumulation following neonatal hypoxia-ischemia. A) Immunoblot showing

increase in COX1 protein in mitochondrial membrane fractions from diencephalon from

homogenates obtained 3, 6, and 24 hours following neonatal hypoxia-ischemia compared to non-injured control samples. Anti-COX1 antibody recognizes a single ≈35kDA band in non-boiled samples. The corresponding ponceau stained blot is shown as a loading control. B) Graph represents changes in COX1 protein levels in diencephalon over time following neonatal hypoxia-ischemia. The maximal increase at 6 hours corresponds nicely with the peak in mitochondrial accumulation seen at 6 hours in figure 6. After correcting for protein loading differences and comparing to control, results are shown as mean ± standard deviation of 4-5 samples /time point. *=$p<0.05$ compared to control.

FIGURE 1

A
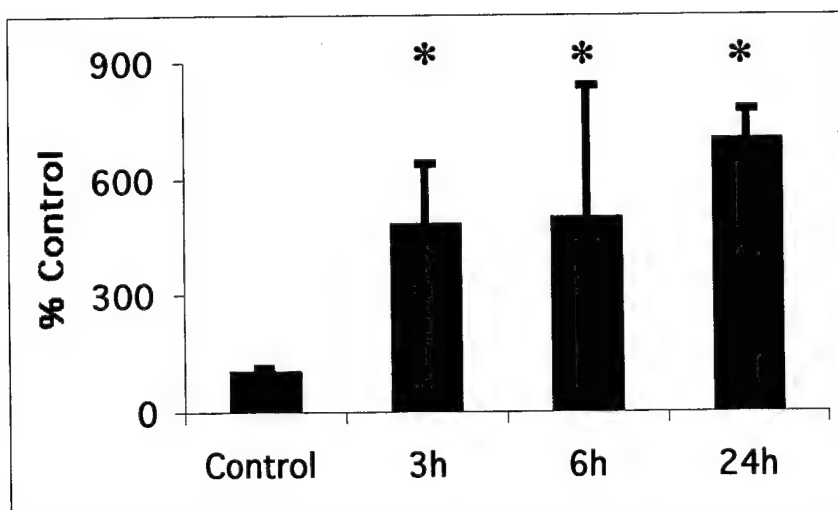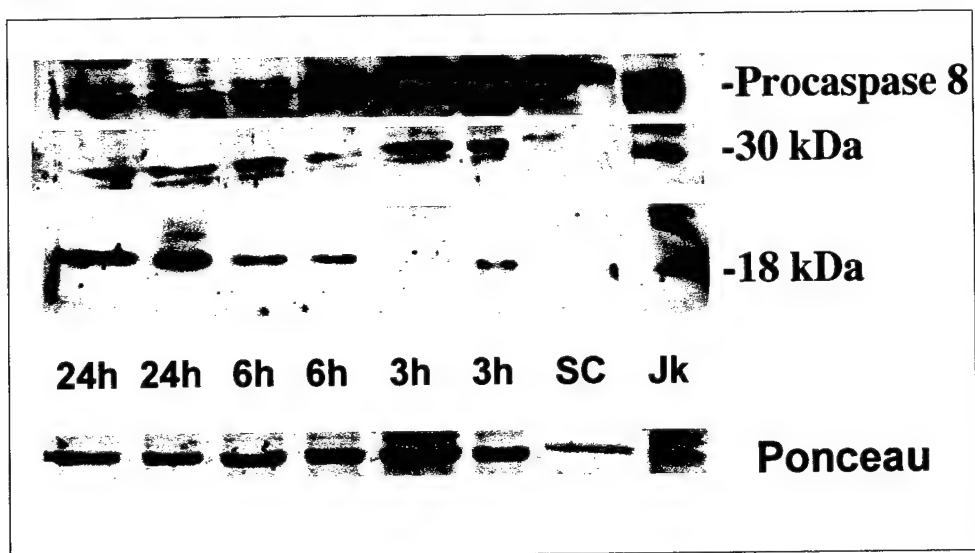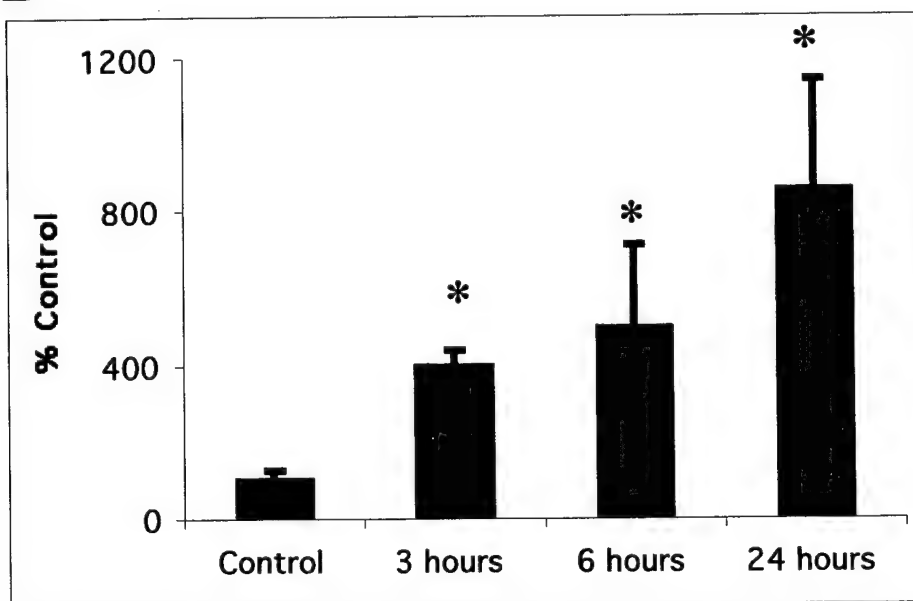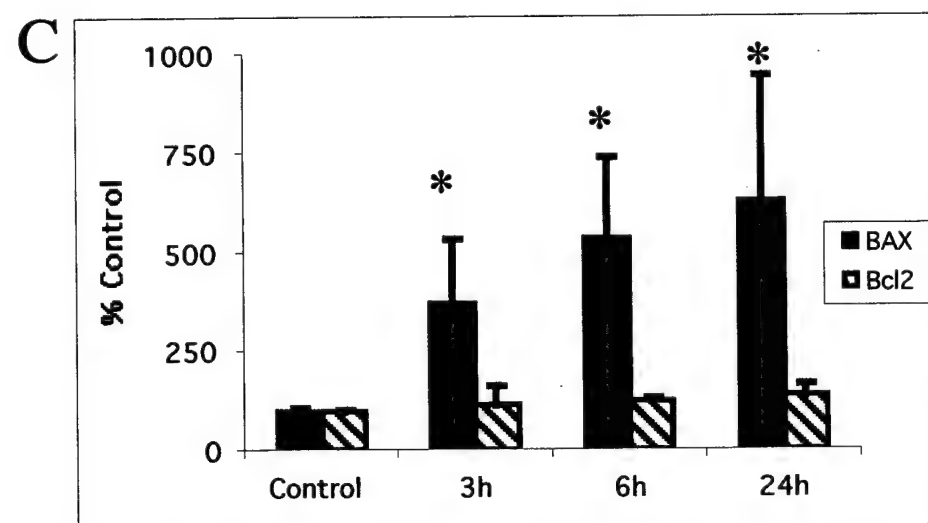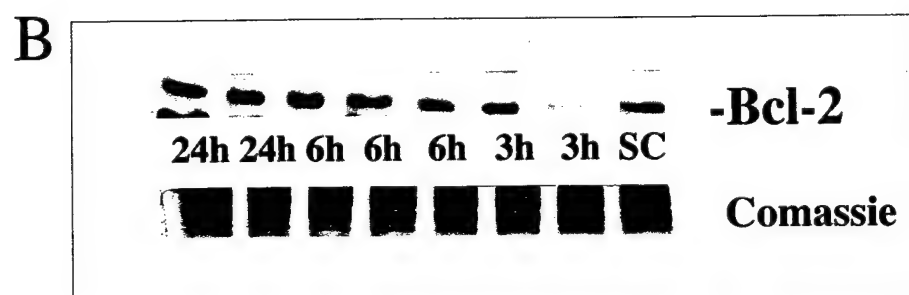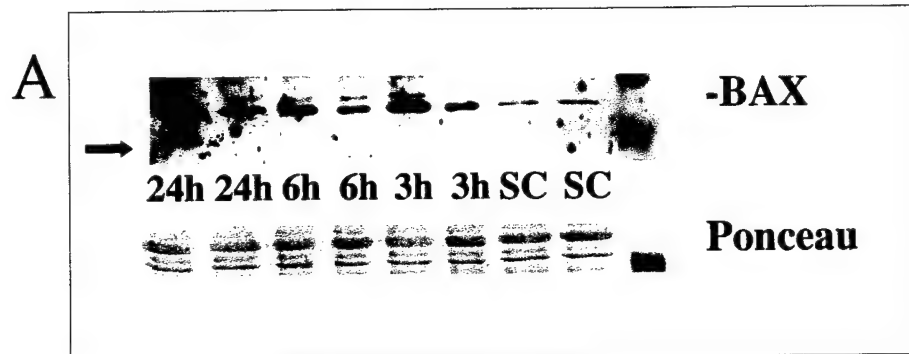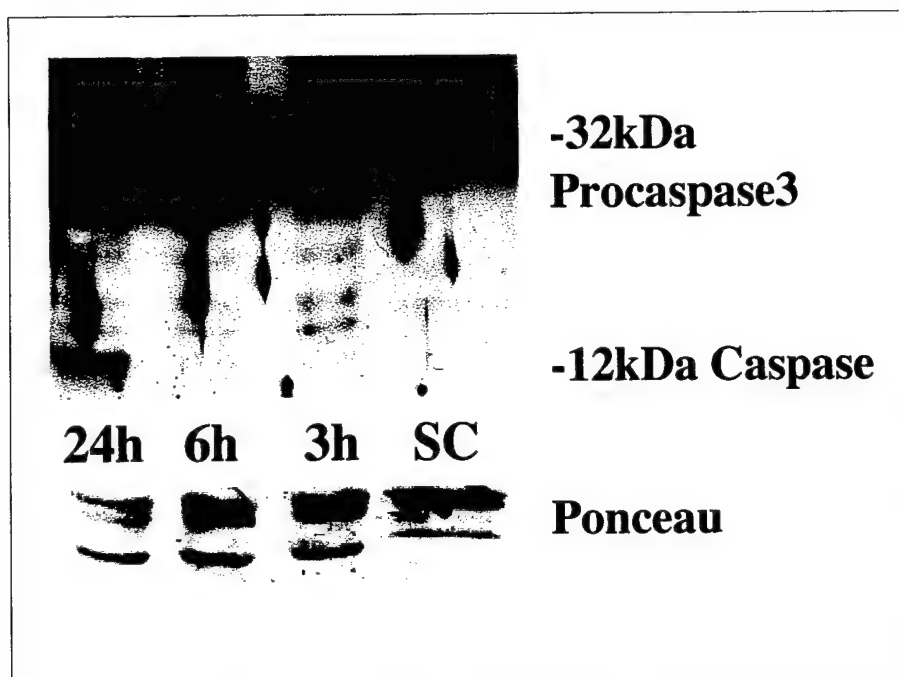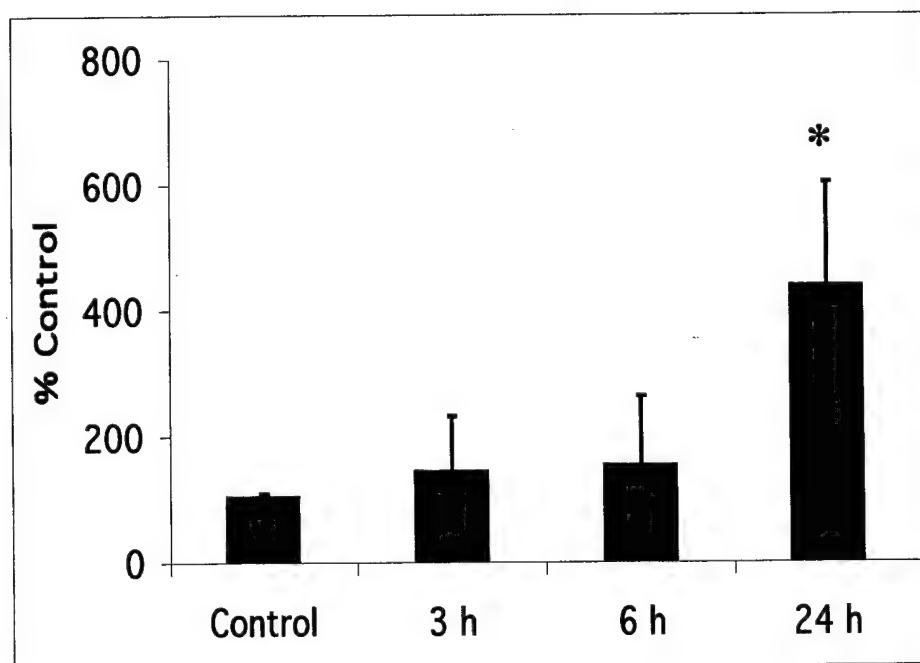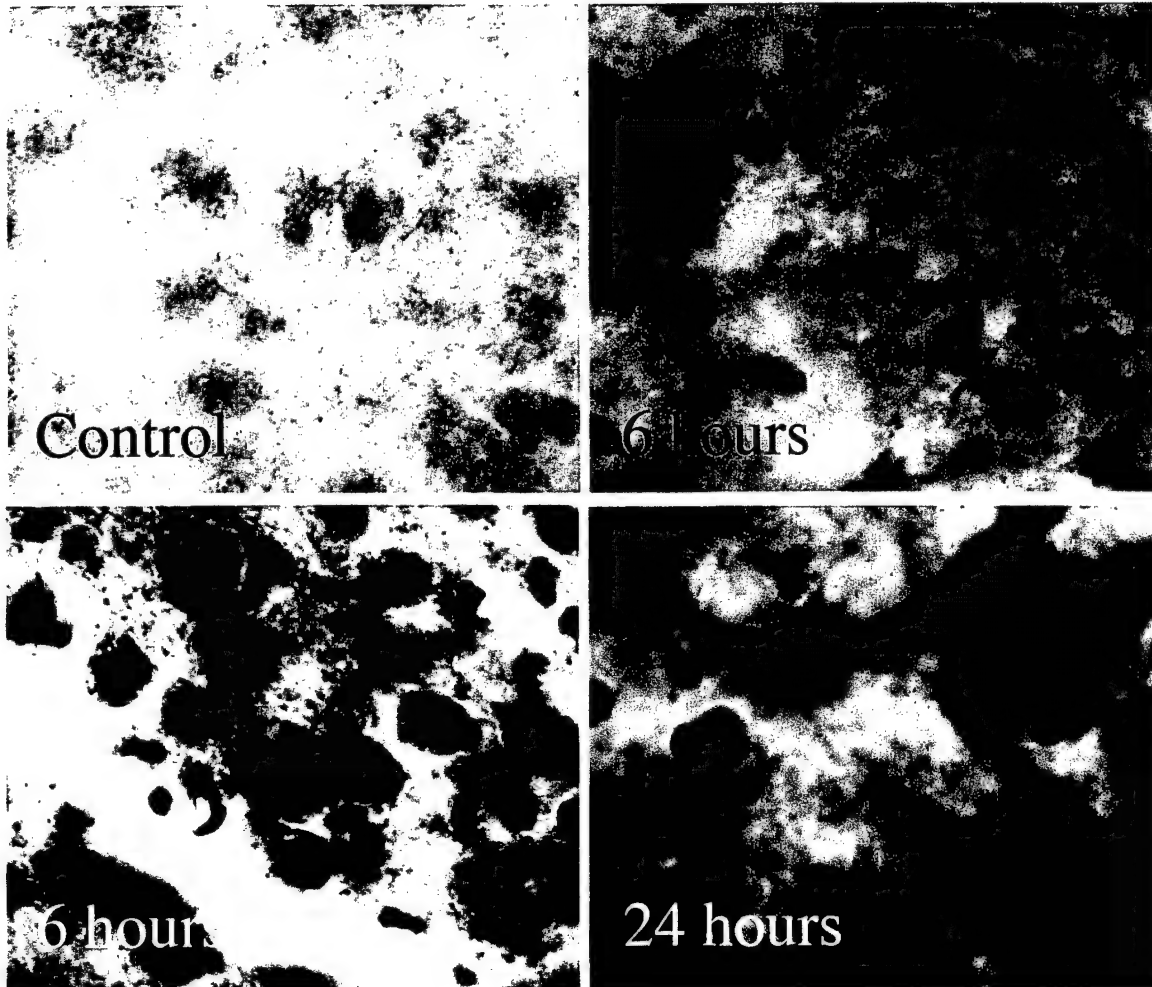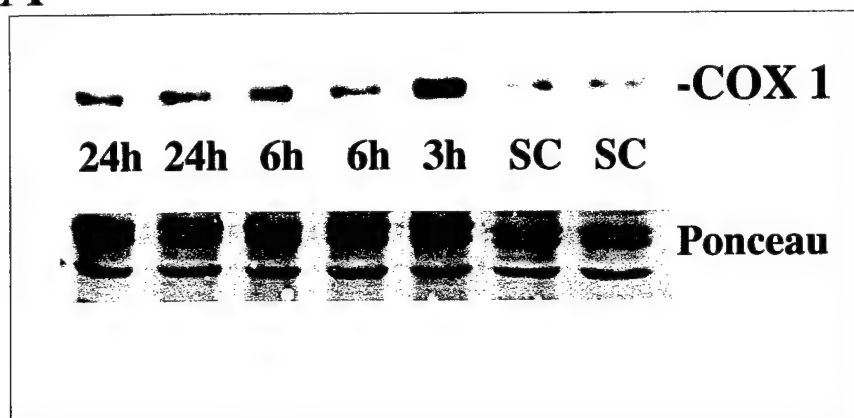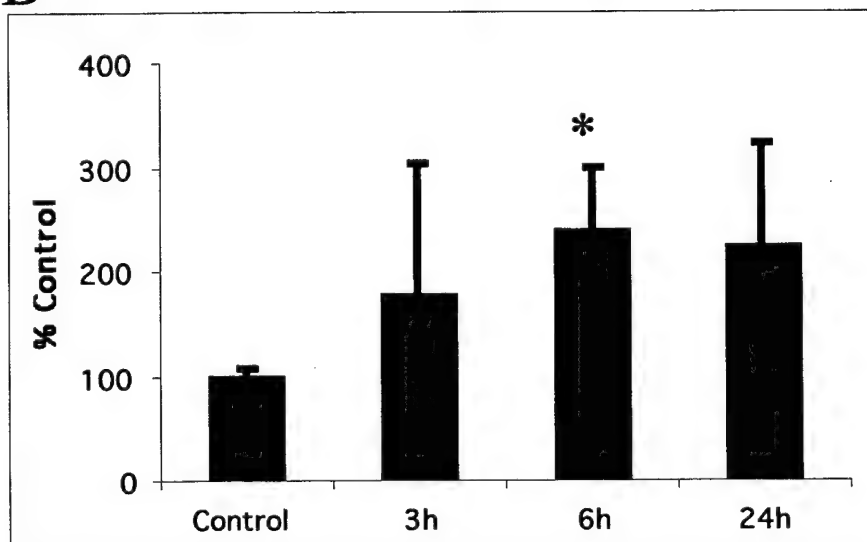
-Fas

24h 24h 6h 6h 3h 3h Jk SC

Comassie

B

FIGURE 2

A

-Procaspase 8

-30 kDa

-18 kDa

24h 24h 6h 6h 3h 3h SC Jk

Ponceau

B

FIGURE 3

FIGURE 4

A

-32kDa
Procaspase3

-12kDa Caspase

24h 6h 3h SC

Ponceau

FIGURE 5

B

FIGURE 6

Control

6 hours

6 hours

24 hours

FIGURE 7

SOCIETY FOR NEUROSCIENCE
2000 ABSTRACT FORM

Read all instructions before typing abstract.
See *Call for Abstracts* and reverse of this sheet.
Complete abstract and **all boxes at left and below.**
(Please type or print in black ink.)

Lee J. Martin, Ph.D.
DAMD17-99-1-9553

Appendix

First (Presenting) Author

Provide full name (no initials), address, and phone numbers *of first author on abstract. You may present (first author) only one abstract.* (Please type or print in black ink.)

JOANNE ELIZABETH NATALE, MD, PHD
DEPT. OF ANESTHESIOLOGY AND CCM
JOHNS HOPKINS UNIV., BLALOCK 904B
BALTIMORE, MD 21287

Fax: (410) 502-5312

Office: (410) 614-1130 Home: (301) 779-8089

E-mail: jnatale@jhmi.edu

SMALLEST RECOMMENDED TYPE SIZE: 10 POINT

SAMPLE:
2000 Annual Meeting
New Orleans, La.
November 4–9, 2000

POSTMARK DEADLINE:

MONDAY, APRIL 24, 2000

An asterisk must be placed after the sponsor's (signing member) name on the abstract.

MANDATORY: The present scientific work may involve a real or perceived financial conflict of interest. (See page 4, item 11.)
☐ yes ☒ no If yes: _____

Presentation Preference

Check one: ☐ poster only ☒ slide/poster

Themes and Topics

See list of themes and topics, pp. 17–18. Indicate below a first and second choice appropriate for programming and publishing your paper.

1st theme title: DISORDERS OF THE NERVOUS SYSTEM theme letter: J
1st topic title: TRAUMA
topic number: 137

2nd theme title: DISORDERS OF THE NERVOUS SYSTEM theme letter: J
2nd topic title: DEGENERATIVE DISEASE: OTHER topic number: 132

Special Requests (for example, projection, video, or computer requirements)

Include nonrefundable **abstract handling fee** of **$50.** Fill out payment information form below. Purchase orders will not be accepted. Submission of abstract handling fee does not include registration for the Annual Meeting.

ABLATION OF OCCIPITAL CORTEX IN IMMATURE MOUSE BRAIN INDUCES P53 AND NEURONAL APOPTOSIS IN THE LATERAL GENICULATE NUCLEUS. J.E. Natale[1]* and L.J. Martin[2,3]. Depts. of [1]Anesthesiology & Critical Care Medicine, [2]Pathology and [3]Neuroscience, Johns Hopkins School of Medicine, Baltimore, MD, 21287.

Traumatic brain injury (TBI) is the leading cause of acquired brain damage, producing persistent functional disability in children. After TBI the loss of neurotrophic support from the damaged cortex may cause degeneration of thalamic neurons. Unilateral ablation of the occipital cortex, a model of axotomy/target deprivation in the adult CNS, induces neuronal apoptosis in the lateral geniculate nucleus (LGN). We hypothesized that in the immature CNS, occipital cortex ablation causes (1) neuronal apoptosis in the LGN, (2) p53 induction in the LGN prior to neuronal apoptosis, and (3) accelerated apoptosis in the LGN compared to adult mice. Ten-day-old and adult C57BL6 mice were anesthe-tized, the right occipital cortex aspirated, and recovered for up to 7 days. In immature mice, this lesion caused selective neuronal apoptosis in the dorsal LGN ipsilateral (ipsi LGN) to the cortical ablation. These apoptotic cells are neurons based on (1) structural characteristics, (2) labeling of apoptotic cells with the retrograde tracer fluorogold, and (3) the absence of apoptotic features in cells expressing glial markers. Internucleosomal DNA fragmentation is evident in the ipsi LGN at 18-24 hours after cortical ablation. Neuronal apoptosis in the LGN progressed through chromatolysis by 12-24 hours, followed by cytoplasmic and nuclear condensation by 48 hours. At 12, 24, 36, and 48 hours after cortical ablation, counts of apoptotic profiles in the ipsi LGN are 1.2 ± 0.7, 0.7 ± 0.3, 110 ± 18, 64 ± 27, respectively. p53 immunoreactivity is induced at 24 hours in ipsi LGN neurons after occipital cortex ablation in the immature brain. In adult mice, occipital cortex ablation also causes p53 induction and neuronal apoptosis in the LGN; however this progression occurs over six to seven days. We conclude that axotomy/target deprivation-induced neuronal apoptosis is induced more rapidly in immature CNS compared to adult CNS, although both may be mediated by p53.
Supported by AG16282 and DAMD17-99-1-9553.

Key Words: (see instructions p. 4)

1. AXOTOMY
2. DEGENERATION
3. HEAD INJURY
4. TRAUMA

Signature of Society for Neuroscience member required below. *No member may sign more than one abstract. The signing member must be an author on the paper and an asterisk must be placed after the sponsor's (signing member) name on the abstract.*

JoAnne E. Natale
Society for Neuroscience member's signature

JOANNE E. NATALE
Printed or typed name

100004219
Member ID number (mandatory)

(410) 614-1130
Telephone number

TARGET-DEPRIVED LATERAL GENICULATE PROJECTION NEURONS IN THE ADULT RAT UNDERGO DNA DAMAGE AND APOPTOSIS WHILE INTERNEURONS TRANSIENTLY ATROPHY

N.A. Al-Abdulla* and L.J. Martin. Department of Pathology, Johns Hopkins School of Medicine, Baltimore, MD 21205.

The mechanisms of *in-vivo* apoptosis in the CNS remain poorly understood. We have developed a unilateral occipital cortex ablation model in the adult rat to test the hypothesis that target-deprived projection neurons in the lateral geniculate nucleus (LGN) selectively undergo DNA damage and apoptosis, while interneurons in the LGN are spared. Dying LGN projection neurons enter apoptosis from chromatolysis. During the late chromatolytic and early apoptotic stages, mitochondria in injured projection neurons significantly accumulate, appear normal ultrastructurally, and retain cytochrome C oxidase activity, assessed by enzymatic histochemistry and quantified by densitometry. During this transitional stage, these projection neurons exhibit oxidative damage to nuclear DNA, observed by antibodies to 8-hydroxy-2$'$-deoxyguanosine, a marker of oxidative damage to DNA. In contrast, interneurons, identified by their particular nuclear morphology and glutamic acid decarboxylase (GAD) staining, undergo an atrophic, vacuolar degeneration starting early during LGN degeneration and peaking immediately after the projection neuron apoptosis is complete. Very few interneurons [< 1:100 interneurons and < 1:100 apoptotic cells] undergo apoptosis concurrently with projection neurons. We conclude that retrograde degeneration of geniculocortical neurons in adult brain occurs by apoptosis that is engaged during chromatolysis, possibly in response to mitochondrial abnormalities and oxidative damage to DNA. Unlike the selectively vulnerable projection neurons, most interneurons undergo transient transsynaptic atrophy and recovery rather than cell death.

SOCIETY FOR NEUROSCIENCE
2000 ABSTRACT FORM

Read all instructions before typing abstract.
See *Call for Abstracts* and reverse of this sheet.
Complete abstract and **all** boxes at left and below.
(Please type or print in black ink.)

_____ Check here if this is a **REPLACEMENT** of abstract submitted earlier. Remit a nonrefundable $50 for each replacement abstract. Replacement abstracts must be **RECEIVED** by Wednesday, May 3, 2000.

First (Presenting) Author

Provide full name (no initials), address, and phone numbers *of first author on abstract. You may present (first author) only one abstract.* (Please type or print in black ink.)

Zhiping Liu, M.D., Ph.D., M.S.

558 Ross Bldg/720 Rutland Ave.

Neuropathology Lab, The Johns Hopkins

Medical Institutions, Baltimore,

MD, 21205   Fax: (4)0-955-9777

Office: (4)0 955-5632 Home: (41) 882-8884

E-mail: dul@welch.jhu.edu

SMALLEST RECOMMENDED TYPE SIZE: 10 POINT

SAMPLE:
2000 Annual Meeting
New Orleans, La.
November 4–9, 2000

POSTMARK DEADLINE:

MONDAY, APRIL 24, 2000

An asterisk must be placed after the sponsor's (signing member) name on the abstract.

MANDATORY: The present scientific work may involve a real or perceived financial conflict of interest. (See page 4, item 11.)
❑ yes ❑ no If yes: _____

Presentation Preference

Check one: ☒ poster only ❑ slide/poster

Themes and Topics

See list of themes and topics, pp. 17–18. Indicate below a first and second choice appropriate for programming and publishing your paper.

1st theme title: Development and Regeneration theme letter: A
1st topic title: Neuronal Death
_____ topic number: 17

2nd theme title: Disorders of the Nervous system theme letter: J
2nd topic title: Degenerative Disease: other topic number: 132

Special Requests (for example, projection, video, or computer requirements)

Include nonrefundable **abstract handling fee** of $50. Fill out payment information form below. Purchase orders will not be accepted. Submission of abstract handling fee does not include registration for the Annual Meeting.

DNA SINGLE-STRAND BREAKS OCCUR RAPIDLY IN MOTOR NEURONS IN VITRO AND IN VIVO AFTER OXIDATIVE STRESS AND AXOTOMY. Z-P. Liu* and L.J. Martin. Dept. of Pathology, Johns Hopkins Univ. Sch. Med., Baltimore, MD 21205.

DNA damage can initiate apoptosis. DNA single-strand breaks (SSB) are a major form of early DNA damage that can be induced by oxidative stress. Reactive oxygen species (ROS) can directly damage genomic DNA and are involved in the pathogenesis of motor neuron apoptosis in animal models and in patients with amyotrophic lateral sclerosis. We tested the hypothesis that DNA-SSB occur in adult motor neurons subjected to oxidative stress *in vitro* and axotomy *in vivo*. We used single-cell gel electrophoresis (comet assay) that detects mainly DNA-SSB under alkaline elution conditions. We developed and characterized a motor neuron enriched cell suspension from adult rat spinal cord ventral horns. This cell suspension is ~84% neurons (determined by NeuN immunophenotyping), 86% of these neurons being motor neurons (determined by CAT immunoreactivity), and 72% of these motor neurons are α-motor neurons with axons in the sciatic nerve (determined by retrograde tracing). The viability of adult motor neurons in suspension was ~61% after 12 h incubation. Exposure of these cells to nitric oxide (NO) donor sodium nitroprusside (SNP), H_2O_2, or SNP plus H_2O_2 induced very rapid DNA damage that was dose- and time-related, as represented by comet formation and cell loss. H_2O_2 at a nontoxic concentration potentiated the toxicity of SNP. Different forms of ROS left different DNA damage fingerprints, indicating different target domains of chromatin and different severities of DNA damage. By applying the comet assay to an *in vivo* model of motor neuron apoptosis (unilateral sciatic nerve avulsion), we found that DNA-SSB accumulate very slowly in injured motor neurons *in vivo* and that the comet fingerprint is similar to that caused by NO toxicity. Supported by grants NS34100, AG16282 and DAMD17-99-1-9553.

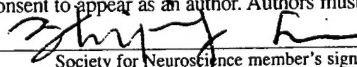## Key Words: (see instructions p. 4)

1. SPINAL CORD INJURY
2. APOPTOSIS
3. DNA DAMAGE
4. NITRIC OXIDE

Signature of Society for Neuroscience member required below. *No member may sign more than one abstract. The signing member must be an author on the paper and an asterisk must be placed after the sponsor's (signing member) name on the abstract.*

The signing member certifies that any work with **human or animal subjects** related in this abstract complies with the guiding policies and principles for experimental procedures endorsed by the Society. This signature acknowledges that each author on this abstract has seen and approved the final version of the abstract and has given consent to appear as an author. Authors must comply with ethical guidelines for human and animal research, and may be asked to supply added documentation.

Society for Neuroscience member's signature

Zhiping Liu
Printed or typed name

000164964
Member ID number (mandatory)

(410)955-5632
Telephone number

SOCIETY FOR NEUROSCIENCE
2000 ABSTRACT FORM

Read all instructions before typing abstract.
See *Call for Abstracts* and reverse of this sheet.
Complete abstract and **all boxes at left and below.**
(Please type or print in black ink.)

_____ Check here if this is a **REPLACEMENT** of abstract submitted earlier. Remit a nonrefundable $50 for each replacement abstract. Replacement abstracts must be **RECEIVED** by Wednesday, May 3, 2000.

First (Presenting) Author

Provide full name (no initials), address, and phone numbers *of first author on abstract. You may present (first author) only one abstract.* (Please type or print in black ink.)

CHRISTIAN LESUISSE
Dpt of Pathology, Johns
Hopkins University, 720 Rutland
Av. Baltimore, MD 21205

Fax: (410) 9559777
Office: (410) 9555632 Home: (410) 337272C
E-mail: LESUISSE@MAIL.JHMI.EDU

SMALLEST RECOMMENDED TYPE SIZE: 10 POINT

SAMPLE:
2000 Annual Meeting
New Orleans, La.
November 4–9, 2000

POSTMARK DEADLINE:

MONDAY, APRIL 24, 2000

An asterisk must be placed after the sponsor's (signing member) name on the abstract.

MANDATORY: The present scientific work may involve a real or perceived financial conflict of interest. (See page 4, item 11.)
☐ yes ☒ no If yes: _____

Presentation Preference

Check one: ☒ poster only ☐ slide/poster

Themes and Topics

See list of themes and topics, pp. 17–18. Indicate below a first and second choice appropriate for programming and publishing your paper.

1st theme title: DEVELOPMENT AND REGENERATION theme letter: A
1st topic title: NEURONAL DEATH topic number: 17

2nd theme title: DISORDERS OF THE N.S. AND Aging theme letter: J
2nd topic title: DEGENER. dis. : OTHER topic number: 132

Special Requests (for example, projection, video, or computer requirements)

Include nonrefundable **abstract handling fee of $50.** Fill out payment information form below. Purchase orders will not be accepted. Submission of abstract handling fee does not include registration for the Annual Meeting.

NEURONAL MATURITY INFLUENCES THE PROGRESSION OF NEURONAL APOPTOSIS INDUCED BY DNA DAMAGE. C. Lesuisse* and L.J. Martin. Departments of Pathology and Neuroscience, Johns Hopkins Univ. Sch. Med., Baltimore, MD 21205.

Neuronal apoptosis contributes to the neurodegeneration in individuals with amyotrophic lateral sclerosis, Alzheimer's disease, Parkinson's disease, and Huntington's disease, and after cerebral ischemia and CNS trauma. DNA damage occurs in these neurological disorders and may be related to this neurodegeneration by signaling the induction of apoptosis. However, the mechanisms for DNA damage-induced apoptosis in neurons are not understood. We have established a mouse cortical culture system to study the mechanisms for DNA damage-induced apoptosis of neurons. These neuronal cultures can be maintained for long term, for at least 60 days *in vitro* (DIV60). During this maturational time course, the levels of apoptosis regulatory proteins undergo prominent changes. Between DIV5 and DIV60, Bcl-2 increases, Bax decreases, Bak increases, and p53 decreases. When neurons are exposed to DNA damaging agent, apoptosis is induced more rapidly at DIV25 than at DIV5, as demonstrated by internucleosomal fragmentation of DNA. In apoptotic cortical neuron cultures, the levels of proapoptotic and antiapoptotic proteins change differentially in older versus younger cortical neuron cultures. These results demonstrate that the maturational state of neurons has a prominent influence on the progression, and possibly the mechanisms, of neuronal apoptosis induced by DNA damage.

Key Words: (see instructions p. 4)

1. AGING
2. PROGRAMMED CELL DEATH
3. DEVELOPMENT
4. NEUROTOXICITY